Investigations on Some Compact Wideband Fractal Antennas

Yogesh Kumar Choukiker

Department of Electronics and Communication Engineering
National Institute of Technology Rourkela
Rourkela-769 008, Odisha, India

Investigations on Some Compact Wideband Fractal Antennas

Thesis submitted in partial fulfillment
of the requirements for the degree of

Doctor of Philosophy

in

Electronics and Communication Engineering

by

Yogesh Kumar Choukiker
(Roll: 509EC604)

under the guidance of

Dr. Santanu Kumar Behera

Department of Electronics and Communiation Engineering
National Institute of Technology Rourkela
Rourkela-769 008, Odisha, India

2013

Dedicated to my Dada-Dadi,
Papa-Mummy with Love...

Department of Electronics and Communication Engg.
National Institute of Technology Rourkela
Rourkela-769 008, Odisha, India.

October 16, 2014

CERTIFICATE

This is to certify that the thesis titled ***Investigations on Some Compact Wideband Fractal Antennas*** by ***Yogesh Kumar Choukiker*** is a record of an original research work carried out under my supervision and guidance in partial fulfillment of the requirements for the award of the degree of Doctor of philosophy in ***Electronics and Communication Engineering*** during the session 2013-2014. I believe that the thesis fulfills part of the requirements for the award of degree of Doctor of Philosophy. Neither this thesis nor any part of it has been submitted for any degree or academic award elsewhere.

Dr. Santanu Kumar Behera
Asso. Professor
Dept. of ECE
National Institute of Technology, Rourkela
Odisha, India - 769 008

Acknowledgement

"The will of God will never take you where Grace of God will not protect you."
Thank you God for showing me the path...

It is my pleasure and privilege to thank the many individuals who made this thesis possible. First and foremost I offer my sincere gratitude towards my supervisor, Prof. S. K. Behera. He is not only a great teacher/professor with deep vision but also and most importantly a kind person. In addition to science, I learned many valuable things on other important fields of life from him.

Many thank to Prof. S. K. Sarangi, Director, NIT Rourkela. It was his vision that gave birth to such a wonderful establishment with international facilities.

I thank from bottom of my heart Prof. R. K. Mishra, Dept. of Electronic science, Berhampur University, Orissa, for his support and good will through all my years. I thank Prof. S. Meher, Head, Dept. of ECE, NIT Rourkela for his support during the process of writing this dissertation. I take this opportunity to thank Prof. S. K. Patra for his vision in setting up communication group in Department of ECE at NIT Rourkela.

I whole heartily thank to Prof. S. K. Sharma, Dept. of ECE, SDSU, USA, for introducing me to the joy of learning antennas, and electromagnetics theory during my days at San Diego, USA. His easily approachable character and his remarkable skill of solving problems was greatly helpful during my research.

Many thanks to ISRO, Govt. of India for providing financial support, for which I have pursued my PhD work as a Senior Research Fellow (SRF). Thank to Mr. Rajiv Jyoti and Mr. B. Pandey at SAC, ISRO facilitating the same.

I would also like to acknowledge TEQIP-II, NIT Rourkela to extending financial support for my visit to SDSU, USA, for research work.

My sincere thank to members of Doctoral Scrutiny Committee (DCS). Also, thank to my teachers Prof. K. K. Mahapatra, Prof. U. C. Pati, Prof. S. K. Das, Prof. A. K. Sahoo, Prof. A. Swain, Prof. D. P. Acharya., Prof. P. K. Tiwari, Prof. U. K. Sahoo, Prof. H. M. Hiramath, for providing a solid background for my studies and research

thereafter. They have been great sources of inspiration to me and thank them from bottom of my heart.

I thank to all the non-teaching staff and technical staff at the Dept. of ECE especially Mr. Kujur and Mr. B. Das for their support.

I remember with appreciation Mr. S. Natarajamani and Mrs. Runa Kumari, Research scholar, Dept. of ECE, on the supreme rapport and care and for technical & scientific talks we shared together.

I take this opportunity to thank Gaurav, Rajib, Arun, Prashant sir, Sujeet, Kapil, Pallab, Ramkrishna, Akhilesh, Sambhu, Arvind, Nihar, Tom, Venkatratnam, Ashish, Pyari, Ayaskant, for all the thoughtful and mind stimulating discussion we had, which prompted us to think beyond the obvious. I have enjoyed their companionship so much during my stay at NIT Rourkela.

Thank to Prof. K J Vinoy, IISc, Banglore for providing measurement facility in his antenna and microwave lab. Also, thanks to Ms. Vijayshree and Ms. Anushruti for their support during the measurement of antenna.

I would like to thank Mr. Pradeep Kumar, VIT Vellore, India, for his valuable help fruitful discussion and constant engorgement.

Thank to B. Babakhani, S. Fernandez, Anusha and Bhakti, for their support during stay in San Diego, USA.

My deepest gratitude goes to my family for their unflagging love and support throughout my life. My father Shri M. L. Choukiker and mother Smt. Radhika Choukiker, who thought me the value of hard work by their own example. I thank my younger brother Guddu, he is always with me for support, love and faith forwards me. I specially thank to my Dada-Dadi for inspiring me with simple yet righteous lives.

Finally, I would like to thank everybody who was important to the successful realization of thesis as well as expressing my apology that i could not mention personally one by one.

Yogesh Kumar Choukiker

Abstract

Today's small handheld and other portable devices challenge antenna designers for ultrathin, and high performances that have the ability to meet multi standards. In the context, fractal geometries have significant role for antenna applications with varying degree of success in improving antenna characteristics.

In this thesis, we have investigated several wideband fractal monopole antennas. This work starts with design and implementation of Koch fractal, hybrid fractal, sectoral fractal, semi-circle fractal monopole antennas with discussion, covering their operations, electrical behavior and performances. The performances of these designs have been studied using standard simulation tools used in industry/academia and are experimentally verified.

Frequency reconfigurable Koch snowflake fractal monopole antenna is also introduced. The present antenna can be used as an array element and has a wideband frequency of operation.

A square Sierpinski monopole antenna has been designed, which is suitable for use in indoor UWB radio system and outdoor base station communication systems. Technique for obtaining a band stop function in the 5-6 GHz frequency band is numerically and experimentally presented. In addition to examining the performance of UWB system, the transfer function and waveform distortion are discussed.

Finally, fractal antenna for array with MIMO environment is developed for mobile communication devices. Aim of this work is to achieve the acceptable performances in terms of isolation, envelope correlation coefficient, capacity loss, radiation patterns and efficiency. Furthermore, a wideband feed network prototype based on a modified Wilkinson power divider is designed. The designed feed network has been used in constructing 2-element and 4-element linear antenna arrays for high gain. This research work has addressed the effectiveness of fractal geometries in antenna and to bring-out the true advantages of their in antenna engineering.

BIO-DATA

Yogesh Kumar Choukiker

Date of Birth: 21^{st} June, 1984

Correspondence:

PhD Scholar, Department of Electronics and Communication Engineering,

National Institute of Technology Rourkela, India – 769 008.

Ph: +91 9439427181 (M)

e-mail: yogesh.ku.84@gmail.com

Qualification

- Ph.D. (Continuing)
  National Institute of Technology Rourkela, India
- M.Tech. (Electronics and Communication Engineering)
  National Institute of Technology Rourkela, India [First division]
- B.E.
  Globus Engineering College, Bhoapl, India [First division]
- 12th (Science)
  Board of Secondary Education, Madhya Pradesh, Bhopal, India [First division]
- 10th
  Board of Secondary Education, Madhya Pradesh, Bhopal, India[First division]

Publications

- 3 Journal articles;
- 6 Journal articles are communicated;
- 8 Conference articles.

Contents

Certificate ii

Acknowledgement iv

Abstract vi

Contents viii

List of Figures xii

List of Tables xx

List of Abbreviations xxii

List of Symbols xxiv

1 Introduction 1

1.1 Characteristics of Fractal Geometry 2

1.2 Generating of Fractal 4

1.3 Examples of Fractal 6

1.3.1 Koch Curve 6

1.3.2 Koch Snowflake 7

1.3.3 Cantor Set 8

1.3.4 Sierpinski Gasket 9

1.3.5 Sierpinski Carpet 10

1.4 Fractal Antenna Technology 10

1.5 Motivation 13

1.6 Problem Statement 13

1.7 Organization of Thesis 14

1.8 Summary 15

2 Planar Wideband Antennas: A state-of-the-art **16**

2.1 Introduction 16

2.2 Wideband Antenna Technology 18

2.3 Wideband Antenna Designs 19

2.4 Reconfigurable Microstrip Antennas 23

2.5 Ultra-Wideband Antenna Technology 28

2.6 Antennas with Multiple Input Multiple Output 33

2.7 Wideband Linear Antenna Arrays 37

2.8 Summary 39

3 Fractal Monopole Wideband Antennas **40**

3.1 Introduction 40

3.2 Koch Curve Fractal Monopole Antenna 41

3.2.1 Antenna Geometry and Simulation Results 41

3.2.2 Experimental Verification 46

3.3 Hybrid Fractal Monopole Antenna 47

3.3.1 Antenna Geometry and Simulation Results 48

3.3.2 Experimental Verification 52

3.4 Sectoral Fractal Monopole Antenna 53

3.4.1 Antenna Geometry and Simulation Results 54

3.4.2 Experimental Verification 58

3.5 Modified Sectoral Fractal Monopole Antenna 61

3.5.1 Antenna Geometry and Simulation Results 61

3.5.2 Experimental Verification 65

3.6 Semi-Circle Fractal Monopole Antenna 68

3.6.1 Antenna Geometry and Simulation Results 68

3.6.2 Experimental Verification 73

3.7 Summary 76

4 Wideband Frequency Reconfigurable Fractal Antenna **77**

4.1 Introduction 77

4.2 Frequency Reconfigurable Monopole Antenna 78

4.2.1 Koch Snowflake Antenna Geometry 78
4.2.2 RF PIN Diodes in Antenna Design 80
4.2.3 Antenna Geometry and Simulation Results 81
4.2.4 Experimental Verification 85
4.3 Summary 88

5 Fractal Antenna for UWB Applications 90
5.1 Introduction 90
5.2 UWB Square Sierpinski Monopole Antenna 91
5.2.1 Antenna geometry and simulation results 92
5.2.2 Experimental verification 99
5.3 Summary 103

6 Fractal Antenna Array for MIMO Environment 104
6.1 Introduction 104
6.2 Hybrid Fractal Antenna with MIMO Implementation 105
6.2.1 2-Element Hybrid Fractal Antenna 105
6.2.2 4-Element Hybrid Fractal Antenna 115
6.3 Modified 3-Section 2-way Wilkinson power divider 125
6.3.1 Circuit structure and Design 125
6.4 Wideband Sectoral Fractal Linear Antenna Array 128
6.4.1 2-Element sectoral fractal antenna array 130
6.4.2 4-Element sectoral fractal antenna array 134
6.5 Summary 138

7 Conclusions and Future Work 141
7.1 Conclusions 141
7.2 Suggestion for Future Work 144

A Design Methodology 146
A.1 Introduction 146
A.1.1 Numerical and Analytical approaches 146
A.1.2 Finite Element Method using Ansoft HFSS 148
A.1.3 Finite Integration Technique using CST 150

A.1.4 Antenna Fabrication 153
A.1.5 S-Parameter Measurement 153
A.1.6 Anechoic Chamber 154
A.1.7 Radiation pattern Measurement 155
A.1.8 Antenna Gain Measurement 155

Bibliography **157**

Disseminations **173**

List of Figures

1.1 Futuristic vision of a tree. Every arm can be considered a scaled down copy of the whole tree. 4
1.2 The affine transform. 5
1.3 Iteration level of Koch curve. 6
1.4 Iterations of a Koch snowflake. 8
1.5 Construction of the first five iterations of a Cantor set. 9
1.6 Iteration of the Sierpinski gasket composed of full triangles. 9
1.7 Iteration of the Sierpinski gasket composed of sides of triangles. . . . 9
1.8 Iteration of a Sierpinski carpet. 10

3.1 Geometry of ACS-Fed Koch fractal monopole antenna (a) Front view (b) Top view (c) Prototype (b) 3D view. 42
3.2 Reflection coefficients of ACS-fed Koch fractal monopole antenna for different iteration levels. 43
3.3 Reflection coefficients of ACS-fed Koch fractal monopole antenna for different sizes of Koch curve, 'a'. 43
3.4 Reflection coefficients of ACS-fed Koch fractal monopole antenna for various feed gap, 'g'. 44
3.5 Reflection coefficients of ACS-fed Koch fractal monopole antenna for ground plane width, 'W_g'. 44
3.6 3D radiation patterns and surface current distributions of proposed ACS-fed Koch fractal monopole antenna at (a) 3.07 GHz (b) 7.3 GHz. 45
3.7 Simulated and measured reflection coefficients of proposed ACS-fed Koch fractal monopole antenna. 46

3.8 Measured radiation patterns for proposed ACS-fed Koch fractal monopole antenna (a) 3.1 GHz (b) 7.3 GHz. 47
3.9 Recursive procedure for (a) Self-affine fractal and (b) Koch curve fractal. 48
3.10 Geometry of proposed hybrid fractal monopole antenna. 49
3.11 Reflection coefficients of proposed hybrid fractal monopole antenna at different iteration levels. 50
3.12 Reflection coefficients of proposed hybrid fractal monopole antenna for different heights, 'L_1'. 50
3.13 3D radiation patterns of proposed hybrid fractal monopole antenna at (a) 1.9 GHz (b) 2.7 GHz (c) 3.07 GHz. 51
3.14 Photograph of proposed hybrid fractal monopole antenna (a) Front view (b) Rear view. 51
3.15 Simulated and measured reflection coefficients of proposed hybrid fractal monopole antenna. 52
3.16 Measured radiation patterns of hybrid fractal monopole antenna at (a) 1.9 GHz (b) 3.1 GHz. 53
3.17 Stages of the IFS that generates the sectoral fractal geometry (a) Basic geometry (b) First iteration (c) Second iteration. 54
3.18 Geometry of sectoral fractal monopole antenna (a) Front view (b) Top view (c) 3D view. 55
3.19 Reflection coefficients of triangular antenna, Sierpinski fractal antenna and proposed sectoral fractal antenna. 56
3.20 Reflection coefficients of proposed sectoral monopole antenna at different iteration levels. 56
3.21 Reflection coefficients of proposed sectoral monopole antenna at different feed gap widths, 'g'. 57
3.22 3D radiation patterns and simulated surface current distributions on sectoral fractal monopole antenna at (a) 3.5 GHz, (b) 4.5 GHz, (c) 5.5 GHz and (d) 6.5 GHz. 57

3.23 Photograph of fabricated sectoral fractal monopole antenna (a) Front view (b) Rear view. 59
3.24 Simulated and measured reflection coefficients of proposed sectoral fractal monopole antenna. 59
3.25 Measured radiation patterns of sectoral fractal monopole antenna at (a) 3.5 GHz, (b) 4.5 GHz, (c) 5.5 GHz and (d) 6.5 GHz. 60
3.26 Basic antenna design procedure (a) Basic triangle (b) Sectoral shape (c) Sectoral inscribing a circular gap. 61
3.27 Geometry of modified sectoral fractal monopole antenna (a) Front view (b) Top view (c) 3D view. 62
3.28 Reflection coefficients of Sierpinski fractal antenna, sectoral fractal antenna, and proposed modified sectoral fractal antenna. 63
3.29 Reflection coefficients of proposed modified sectoral monopole antenna with different diameters of inscribing circle, 'D'. 63
3.30 Reflection coefficients of proposed modified sectoral monopole antenna with different feed gap widths, 'g'. 64
3.31 3D radiation patterns and simulated surface current distributions on sectoral fractal planar monopole antenna at (a) 1.7 GHz (b) 3.0 GHz (c) 5.8 GHz. 65
3.32 Photograph of proposed modified sectoral fractal monopole antenna. . 66
3.33 Simulated and measured reflection coefficients of proposed modified sectoral fractal antenna. 67
3.34 Measured radiation patterns of proposed modified sectoral fractal monopole antenna at (a) 1.72 GHz (b) 3.07 GHz (c) 5.82 GHz. 68
3.35 Recursive procedure for designing of semi-circle fractal geometry. . . . 70
3.36 Geometry of proposed semi-circle fractal monopole antenna (a) Front view (b) 3D view. 70
3.37 Reflection coefficients of proposed semi-circle fractal monopole antenna for different iteration levels. 71

3.38 Reflection coefficients of proposed semi-circle fractal monopole antenna for different feed gaps, 'g'. 72
3.39 Reflection coefficients of proposed semi-circle fractal slot antenna for gap, 'S', between feed line and ground plane. 72
3.40 3D radiation patterns and surface current distributions of proposed semi-circle fractal monopole antenna at (a) 2.45 GHz (b) 5.5 GHz. . . 73
3.41 Simulated and measured reflection coefficients of proposed semi-circle fractal monopole antenna. 74
3.42 Measured radiation patterns of proposed semi-circle fractal monopole antenna at (a) 2.45 GHz (b) 5.5 GHz. 74

4.1 Recursive procedure for Koch snowflake fractal geometry. 78
4.2 Simulated reflection coefficients of Koch snowflake fractal monopole antenna for different iterations. 79
4.3 Circuit model of series switch using RF PIN Diode 80
4.4 Geometry of proposed Koch snowflake fractal monopole antenna (a) Front view (b) Top view (c) Top view zoomed (d) PIN diode circuit. . 82
4.5 Geometry for different cases (a) Case I (b) Case II (c) Case III. . . . 82
4.6 Simulated reflection coefficients of proposed frequency reconfigurable Koch snowflake fractal monopole antenna 83
4.7 Surface current distributions (a) Case I at 3.9 GHz (b) Case II at 2.8 GHz d) Case III at 3.0 GHz. 84
4.8 Simulated 3D radiation pattern figs (a), (b) & (c) for case I at 3.2 GHz, 3.9 GHz & 4.4 GHz, figs (d), (e) & (f) for case II at 2.2 GHz, 2.8 GHz & 3.4 GHz, figs (g), (h) & (i) for case III at 2.0 GHz, 3.0 GHz & 4.0 GHz 84
4.9 Photograph of fabricated frequency reconfigurable Koch snowflake monopole antenna (a) Front view (b) Rear view. 86
4.10 Simulated and measured reflection coefficients of proposed frequency reconfigurable Koch snowflake fractal monopole antenna for case I, case II & case III. 86

4.11 Measured radiation patterns for figs (a) at 3.2 GHz (b) at 3.9 GHz (c) at 4.4 GH, figs (d) at 2.2 GHz (e) at 2.8 GHz (f) at 3.4 GHz , figs (g) at 2.0 GHz (h) at 3.0 GHz (i) at 4.0 GHz. 87
4.12 Gain curves of the proposed frequency reconfigurable Koch snowflake fractal monopole antenna for case I, case II & case III. 88

5.1 Stages of the IFS that generates the square Sierpinski. 92
5.2 Geometry of proposed MSSF antenna (a) Front view (b) Rear view (c) Photograph. 92
5.3 MSSF geometry and its different stages (a) Basic geometry (b) First iteration (c) Second iteration (d) Third iteration (e) Modified geometry. 92
5.4 Simulated reflection coefficients of proposed MSSF antenna for different iterations. 94
5.5 Simulated reflection coefficients of proposed MSSF antenna for different configuration of grooved ground plane. 95
5.6 Simulated reflection coefficients of proposed MSSF antenna for length t_l of band notch slot. 96
5.7 Simulated reflection coefficients of proposed MSSF antenna for width t_s of band notch slot. 96
5.8 Simulated reflection coefficients of proposed MSSF antenna for width t_w of band notch slot. 97
5.9 Simulated reflection coefficients of proposed MSSF antenna for with and without notch 97
5.10 Simulated 3D radiation patterns for proposed MSSF antenna at (a) 4 GHz (b) 5.5 GHz (c) 6.2 GHz (d) 8.7 GHz 99
5.11 Simulated and measured reflection coefficients of proposed UWB MSSF antenna (a) Without band-notch (b) With band-notch characteristics. 100
5.12 Simulated and measured reflection coefficients of proposed UWB MSSF antenna (a) Without band-notch (b) With band-notch characteristics. 100

5.13 Measured radiation pattern of proposed MSSF antenna (a) at 4 GHz (XZ and YZ Co- and Cross- pol.), (b) at 6.2 GHz (XZ and YZ Co- and Cross- pol.), (c) 8.7 GHz (XZ and YZ Co- and Cross- pol.). 101
5.14 Measured peak realized gain of proposed UWB MSSF antenna with and without band notch 101
5.15 Phase responses for different identical pairs (a) Reference antenna (b) Band-notch antenna 102
5.16 Transmission characteristics and group delay of proposed MSSF antenna 103

6.1 Recursive procedure if the hybrid fractal antenna (a) Initial geometry (b) First iteration (c) Second iteration 106
6.2 Geometry of 2-element hybrid fractal antenna (a) Front view (b) Top view (c) Hybrid fractal design dimensions 107
6.3 Simulated reflection and isolation coefficients of proposed hybrid fractal antenna with different iterations 108
6.4 Simulated reflection and isolation coefficients of proposed hybrid fractal antenna with different configuration of grooved area. 109
6.5 Simulated reflection and isolation coefficients of proposed hybrid fractal antenna with different configuration of T-shape strip. 109
6.6 Simulated surface current distribution of the MIMO antenna (a) Antenna 1 at 1.75 GHz and 4.5 GHz (b) Antenna 2 at 1.75 GHz and 4.5 GHz. 111
6.7 Simulated 3D gain radiation patterns for the antenna 1 & antenna 2; Figs. (a) and (b) are at 1.75 GHz , Figs. (c) and (d) are at 3 GHz, Figs. (e) and (f) are at 4.5 GHz, and finally, Figs. (g) and (h) are at 6 GHz. 111
6.8 Photographs of the fabricated hybrid fractal MIMO antenna (a) Front view (b) Rear view. 112
6.9 Simulated and measured reflection and isolation coefficients of proposed hybrid fractal antenna 112

6.10 Simulated and measured (a) Envelope correlation coefficient (ECC) (b) Capacity loss of the proposed MIMO antenna. 115
6.11 Measured radiation pattern for the antenna 1 and antenna 2; Figs. (a) and (e) at 1.75 GHz, Figs. (b) and (f) at 3 GHz, Figs. (c) and (g) at 4.5 GHz, and finally, Figs. (d) and (h) at 6 GHz. 116
6.12 Geometry of proposed 4-element hybrid fractal antenna. 117
6.13 Simulated reflection and isolation coefficients of proposed 4-element antenna. 118
6.14 Simulated surface current distribution of the MIMO antenna (a) Antenna 1 at 1.75 GHz and 4.5 GHz (b) Antenna 2 at 1.75 GHz and 4.5 GHz (c) Antenna 1 at 1.75 GHz and 4.5 GHz (d) Antenna 2 at 1.75 GHz and 4.5 GHz 119
6.15 Simulated 3D radiation patterns for the antenna 1, 2, 3 & 4; Figs. (a),(e),(i) and (m) at 1.75 GHz, Figs. (b),(f),(j) and (n) at 3 GHz, Figs. (c),(g),(k) and (o) at 4.5 GHz, and finally, Figs. (d),(h),(l) and (p) at 6 GHz. 120
6.16 Photographs of the fabricated hybrid fractal MIMO antennas (a) Front view (b) Rear view. 121
6.17 Measured reflection and isolation coefficients of proposed 4-element hybrid fractal antenna 121
6.18 Measured and simulated envelope correlation coefficient (ECC) and capacity loss of 4-element MIMO antenna (a) Envelope correlation Coefficient (ECC) (b) Capacity loss. 122
6.19 Measured radiation patterns for the antennas 1, 2, 3 & 4; Figs. (a),(e),(i) and (m) at 1.75 GHz, Figs. (b),(f),(j) and (n) at 3 GHz, Figs. (c),(g),(k) and (o) at 4.5 GHz, and finally, Figs. (d),(h),(l) and (p) at 6 GHz. . . 124
6.20 Coupled line Wilkinson power divider 126
6.21 Simplified equivalent circuit of the Wilkinson power divider (a) even- (b) odd-mode excitations 127
6.22 Geometry of modified Wilkinson power divider. 128

6.23 Simulated results of proposed modified Wilkinson power divider (a) Reflection coefficients (b) Group delay. 129
6.24 Measured S-parameters of modified Wilkinson power divider. 129
6.25 Geometry of proposed 2-element linear antenna array (a) Front view (b) Top view (c) Photograph of fabricated antenna 131
6.26 Simulated reflection coefficients of proposed 2-element linear antenna array for different grooved areas in ground plane 132
6.27 Simulated 3D radiation patterns and surface current distribution at (a) 3.5 GHz (b) 5.5 GHz (c) 6.5 GHz. 132
6.28 Simulated and measured reflection coefficients of proposed 2-element linear antenna array. 133
6.29 Measured radiation patterns of proposed 2-element linear antenna array at (a) 3.5 GHz (b) 5.5 GHz (c) 6.5 GHz. 134
6.30 Geometry of proposed 4-element linear antenna array (a) Front view (b) Rear view (c) Photograph of fabricated antenna 135
6.31 Simulated reflection coefficients of proposed 4-element linear antenna array for different grooved area in ground plane. 136
6.32 Simulated 3D radiation patterns and surface current distribution at (a) 3.5 GHz (b) 5.5 GHz (c) 6.5 GHz. 136
6.33 Simulated and measured reflection coefficients of proposed 4-element linear antenna array 137
6.34 Measured radiation patterns of proposed 4-element linear antenna array at (a) 3.5 GHz (b) 5.5 GHz (c) 6.5 GHz 138

A.1 Meshing of an antenna structure in Ansoft HFSS. 149
A.2 A single mesh shape used in Ansoft HFSS 149
A.3 A single (a) hexahedral, (b) tetrahedral and (c) surface mesh element used in CST MW Studio 151
A.4 Meshing of an antenna structure in CST MW studio. 151
A.5 Setup for measurement of reflection coefficients and radiation patterns. 153

List of Tables

1.1 General Comparison of Euclidean and Fractal Geometries 10

3.1 Dimensions of proposed ACS-fed Koch fractal monopole antenna. . . 41
3.2 Measured gain and simulated total antenna efficiency of proposed Koch fractal monopole antenna. 46
3.3 Dimensions of proposed hybrid fractal monopole antenna. 49
3.4 Measured gain and simulated total antenna efficiency of proposed hybrid fractal monopole antenna. 53
3.5 Dimensions of the proposed sectoral fractal monopole antenna. 55
3.6 Measured gain and simulated total antenna efficiency of proposed sectoral monopole antenna. 61
3.7 Dimensions of proposed modified sectoral fractal monopole antenna. . 62
3.8 Measured gain and simulated total antenna efficiency of proposed modified sectoral fractal monopole antenna. 68
3.9 Dimensions of proposed semi-circle fractal monopole antenna. 71
3.10 Measured gain and simulated total antenna efficiency of proposed semi-circle fractal monopole antenna. 75
3.11 Comparison among different monopole wideband antenna design prototypes. 75

4.1 Simulated gain, measured gain and total antenna efficiency of proposed Koch reconfigurable antenna 85

5.1 Dimensions of proposed MSSF antenna 91

5.2 Simulated gain, measured gain and simulated total antenna efficiency of MSSF antenna 98

6.1 Dimensions of 2-element hybrid fractal MIMO antenna 107
6.2 Gain and simulated total antenna efficiency of 2-element MIMO antenna 115
6.3 Gain and simulated total antenna efficiency of 4-element MIMO antenna 123
6.4 Comparison of 2-element & 4-element MIMO antenna 123
6.5 Dimensions of modified Wilkinson power divider 128
6.6 Dimensions of proposed 2-element linear antenna array 130
6.7 Measured gain and simulated total antenna efficiency of proposed 2-element linear antenna array. 134
6.8 Dimensions of proposed 4-element linear antenna arrays 135
6.9 Measured gain and simulated total antenna efficiency of proposed 4-element linear antenna array. 138
6.10 Comparison of 2-element and 4-element linear antenna array with single element 139

List of Abbreviations

ACS	Asymmetric Coplanar Waveguide
ANN	Artificial Neural Network
AR	Axial Ratio
AUT	Antenna Under Test
BA	Bees Algorithm
BW	Bandwidth
CAD	Computer Aided Design
CDR	Cylindrical Dielectric Resonator
CPW	Coplanar Waveguide
CP	Circular Polarization
CST	Computer Simulation Technology
DC	Descarts Circle theorem
DCS	Defense Communication System
DECT	Digital Enhanced Cordless Telecommunications
DGS	Defected Ground Structure
DSRC	Dedicated Short Range Communication
DTV	Direct Television
dB	Decibel
dBi	Decibel isotropic
ECC	Envelope Correlation Coefficient
EIRP	Effective Isotropic Radiated Power
EM	Electromagnetic
FCC	Federal Communication Commission
FDTD	Finite Differentiation Time Domain
FEM	Finite Element Method
FIT	Finite Integration Technique
GA	Genetic Algorithm
GPS	Global Position System
GPRS	General Packet Radio Services

GSM	Global System for Mobile Communication
IE	Integral Equations
IFS	Iterative Function System
LTE	Long Term Evolution
LHCP	Left Hand Circular Polarization
MEMS	Micro-Electro-Mechanical Systems
MIMO	Multiple Input Multiple Output
MoM	Method of Moment
OLRs	Open Loop Resistors
PCS	Personal Communication System
PD	Power Divider
PDA	Personal Digital Assistant
PSO	Particle Swarm Optimization
RF	Radio Frequency
RFID	Radio Frequency Identification
RHCP	Right Hand Circular Polarization
RL	Return Loss
SC	Short Circuit
SDMB	Satellite Digital Multimedia Broadcasting
SLL	Side Lobe Level
T/R	Transmitter and Receiver
UHF	Ultra High Frequency
UMTS	Universal Mobile Telecommunication System
UWB	Ultra Wide Band
VSWR	Voltage Standing Wave Ratio
VNA	Vector Network Analyzer
WiMax	Worldwide Interoperability for Microwave Access
WiBro	Wireless Broadband
WLAN	Wireless Local Area Network

List of Symbols

ϵ_r	Dielectric constant
ζ_n	Fixed unit length
ρ_e	Envelope correlation coefficient
λ	Wavelength
$tan\delta$	Loss tangent
c	Speed of light in free space
ψ_R	Envelope correction coefficient
ρ	Receiving antenna correlation matrix
$\tau_g(\omega)$	Group delay
φ_f	Phase of radiated signal
$W(A)$	Hutchinson operator.
$\vec{E}$	Electric field intensity
$\vec{H}$	Magnetic field intensity
$\vec{D}$	Electric flux density
$\vec{B}$	Magnetic flux density
φ_E	Scalar quantities of electric flux
φ_B	Scalar quantities of magnetic flux
$\bar{x}$	Electric field vector
Δt	Maximum time step
f_c	Centre frequency
G_t	Gain of the transmitting antenna
G_r	Gain of the receiving antenna
P_t	Transmitted power
P_r	Received power

CHAPTER 1

Introduction

"***Everybody wants to go wireless***": this statement actually describes the trend of modern wireless communications. At the end of nineteenth century James clark Maxwell had laid the initial foundation for electromagnetic radiation [1]. He said, "***the energy, by the engagement of electric and magnetic waves could be transported through materials and space at a finite velocity.***" [2]. In 1888, Maxwell theory was supported by the experiments of Heirich Hertz. He proved that the light and electromagnetic waves travel with same velocity. His experiment with these electromagnetic waves led to the development of wireless telegraph and the radio [3]. Later in 1901, Gulilmo Marconi had performed the remarkable Translatic Equipment, transmitting the letter 'S' (three dots in Morse code), over a distance of 1.8 miles [4]. With the effort of these great scientists, the users have obtained a much stronger freedom to communicate. This initial success of wireless communications shortly began to be a reality and further exploration was made towards today's booming area of personal communication systems.

In past years the evolution of wireless communications has the major significant interest in antenna design. Specifically, due to market demand, design of small antennas for new mobile terminals is currently receiving a lot of attention [5–8]. However, designing a hand-held antenna is not an easy task, as this type of antenna is subjected to very tough specifications [9]. Compact structure, light weight, flexibility, robustness and low profile are some of the key considerations for conventionally design of small antennas [10]. In addition, as new mobile handsets are required to operate at multiple standards, their antennas are expected to grab as much spectrum as possi-

ble, requiring multi-band or broadband operation [11]. Unfortunately, as the antenna geometries are complicated, more often than not, there is no close formulation to analyze them, and the use of numerical methods [12–14] becomes imperative. In consequence, design of modern antennas relies on the use of self-developed numerical codes or commercial electromagnetic simulators, such as IE3D [15], FEKO [16], CST MW Studio [17], HFSS [18], etc., to evaluate antenna performance before a physical prototype is fabricated. Even with these simulators, the success of the final design depends on the intuition and previous experience of the designer. In most cases, the final optimization is in fact made by trial and error methods.

On the other hand, an alternative and certainly in prevalence approach to design antennas consists of using optimization techniques based on pseudo-random search algorithms [19]. The typical examples based on these techniques are particle swarm optimization (PSO) [20], artificial neural networks (ANN) [21, 22] genetic algorithms (GA) [23, 24], bees algorithms [25], etc. The main advantage with them is that once the optimized algorithm is developed and coded, a little intervention of the designer is required due to independent procedures.

Now a days small hand-held devices challenge antenna designers for portable and high performance devices that have the ability to meet multi standards. This has initiated antenna research in various directions, one of which is by using fractal shaped antenna elements. In recent years, several fractal geometries have been introduced for antenna applications with varying degrees of success in improving antenna characteristics. Some of these geometries are particularly useful in reducing the size of the antenna, while other designs aim at inclusion of multi-band/wideband characteristics.

1.1 Characteristics of Fractal Geometry

Recent endeavors by researchers around the world to combine fractal geometry with electromagnetic theory have led to an opulence of new and attractive antenna designs [26, 27]. In this chapter, we provide a comprehensive overview of recent developments in the rapidly growing field of fractal antenna engineering, which has been primarily focused in two areas: the design and analysis of fractal antenna elements,

and the application of fractal concepts to the design of antenna arrays. Several fractal geometries have been explored for antennas with special characteristics, in the context of both antenna elements and spatial distribution functions for elements in antenna arrays. Till now there have been no concrete efforts to design antennas using fractal shaped elements. In many fractal antennas [28–31], the self-similarity and space-filling nature of fractal geometries are often qualitatively linked to its frequency characteristics.

Fractals may be found from nature or generated using a mathematical technique. The word "*fractal*" was named by Benoit Mandelbrot [32]. Sometimes he is referred to as the father of fractal geometry. He said, "I coined *fractal* from the Latin adjective".

To date, there exists no clearcut definition of a fractal object. Mandelbrot also said, "A fractal is by definition a set for which the Hausdorff dimension strictly exceeds the topological dimension", which he later withdrew and replaced with: "A fractal is a shape made of parts similar to the whole in some way".

The simplest way to define a fractal is as an object that appears self-similar under varying degrees of magnification, and in effect, possessing symmetry across scale, with each small part of the object replicating the structure of the whole. This is perhaps the loosest of definitions; however, it captures the essential, defining characteristic, that of self-similarity. The four major properties of fractals have:

1. Self-Similarity/self-affinity property.
2. Scaling property.
3. Space filling/fractal dimensions property.
4. Statical property.

Among the several properties that characterize fractals, two are of interest in terms of antenna design: self-similarity/self-affinity and space-filling/fractal-dimension properties. We are going to briefly define these properties in the next section and we will relate such geometrical properties to the antenna field.

Some fractals are self-similar which can be roughly understood as there being copies of the whole structure within the structure at different scales. For example,

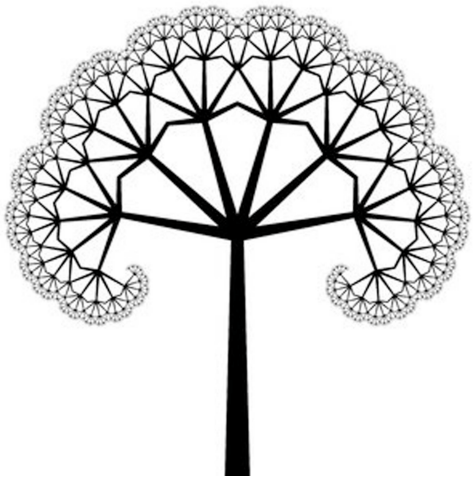

Figure 1.1: Futuristic vision of a tree. Every arm can be considered a scaled down copy of the whole tree.

the futuristic tree of Figure. 1.1 can be understood in a loose sense to be self-similar. If we cut one branch, we will see that it is a reduced simplified copy of the whole structure. If such a scale factor is different for several directions, the structure is no longer self-similar but self-affine. Some mathematical foundations are explained in [33]. They are useful to relate the geometrical properties of the antenna and its electromagnetic behavior to obtain multi-frequency antennas.

Another interesting feature of fractals is their property of filling the space. In order to characterize such space-filling properties, the concept of fractal dimension is used. There are several definitions of fractal dimension [34]. A fractal object can have a fractional dimension or a larger dimension than its topological one. Some examples are presented in Section 1.3.

1.2 Generating of Fractal

Iterated function systems (IFSs) represent an extremely versatile method for conveniently generating a wide variety of useful fractal structures. This IFS is based on the application of a series of affine transformations, w [26, 27].

$$w.\begin{pmatrix} x \\ y \end{pmatrix} = \begin{pmatrix} a & b \\ c & d \end{pmatrix} \times \begin{pmatrix} x \\ y \end{pmatrix} + \begin{pmatrix} e \\ f \end{pmatrix} \tag{1.1}$$

or, equivalently, by

$$w(x, y) = (ax + by + e, cx + dy + f) \tag{1.2}$$

where $a, b, c, d, e,$ and f are real numbers. Hence, the affine transformation, w is represented by six parameters as given below.

$$\begin{pmatrix} a & b \\ c & d \end{pmatrix} \begin{pmatrix} e \\ f \end{pmatrix} \tag{1.3}$$

where $a, b, c,$ and d control rotation and scaling, while e and f control linear translation (Figure 1.2).

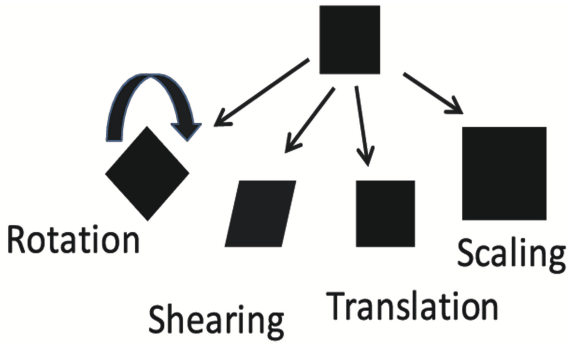

Figure 1.2: The affine transform.

Now suppose, we consider w_1, w_2, ..., w_N as a set of affine linear transformations, and let A be the initial geometry. Then a new geometry produced by applying the set of transformations to the original geometry, A, and collecting the results from $w_1(A)$, $w_2(A)$, $w_N(A)$, can be represented by

$$W(A) = \bigcup_{n=1}^{N} w_n(A) \tag{1.4}$$

where W is known as the Hutchinson operator.

A fractal geometry can be obtained by repeatedly applying W to the previous geometry. For example, if the set A_0 represents the initial geometry it is written as:

$$A_1 = W(A_0); A_2 = W(A_1); \ldots A_{k+1} = W(A_k) \tag{1.5}$$

An iterated function system generates a sequence that converges to a final image, A_α in such a way that

$$W(A_\infty) = A_\alpha \tag{1.6}$$

This image is called the attractor of the iterated function system, and represents a "fixed point" of W. The affine transformation matrix equation 1.1 is used for designing of Koch fractal curve, Sierpinski gasket, fractal tree, etc.

1.3 Examples of Fractal

Deterministic fractals

Some fractal structures are constructed simply by using an iterative process consisting of an initiator (initial state) and a generator (iterative operation).

1.3.1 Koch Curve

Koch curve has an infinite length and it was generated by Helge von Koch in 1904. Each segment of length ϵ is replaced by a broken line (generator), composed of four segments of length $\epsilon/3$, according to the following recurrence relation (Figure 1.3):

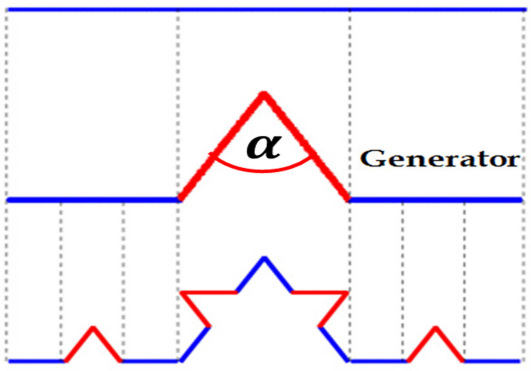

Figure 1.3: Iteration level of Koch curve.

At iteration zero, we have an initiator which is a segment in the case of the triadic Koch curve, or an equilateral triangle in the case of the Koch island. If the initiator is a segment of horizontal length L, at the first iteration (the curve coincides with the generator) the base segments will have length $\epsilon_1 = \mathrm{L}/3$;

At the second iteration they will have length $\epsilon_2 = \mathrm{L}/9$, as each segment is again replaced by the generator, then $\epsilon_3 = L/27$ at the third iteration and so on. The relations giving the length L of the curve are thus

$\epsilon_1 = L/3 \rightarrow \mathrm{L}_1 = 4\ \epsilon_1$

$\epsilon_2 = L/9 \rightarrow \mathrm{L}_2 = 16\ \epsilon_2$

...

...

$\epsilon_n = L/3^n \rightarrow \zeta_n = 4^n\ \epsilon_n$

by eliminating n from the two equations in the last line, the length ζ_n may be written as a function of the measurement unit ϵ_n

$$\zeta_n = L^D \left(\epsilon_n\right)^{1-D} \tag{1.7}$$

where,

$$D = \frac{\log 4}{\log 3} = 1.261\ldots \tag{1.8}$$

For a fixed unit length ϵ_n, ζ_n grows as the D^{th} power of the size L of the curve. Here, the exponent ρ = D-1 of ϵ_n, which is based on Richardson's law and it shows the divergence of ζ_n as $\epsilon_n \rightarrow 0$.

1.3.2 Koch Snowflake

A Koch snowflake is constructed by starting with an equilateral triangle and then altering each line segment recursively.

The previous expression is the first example given of a scaling law which may be written as:

$$\zeta_n/\epsilon_n = f\left(L/\epsilon_n\right) = \left(L/\epsilon_n\right)^D \tag{1.9}$$

A scaling law is a relation between different dimensionless quantities describing the system, (here the relation is a simple power law). Such a law is generally possible only when there is a single independent unit of length in the object (here ϵ_n). A structure associated with the Koch curve is obtained by choosing an equilateral triangle as initiator. The structure generated in this way is the well known Koch island or Koch

snowflake shown in Figure 1.4.

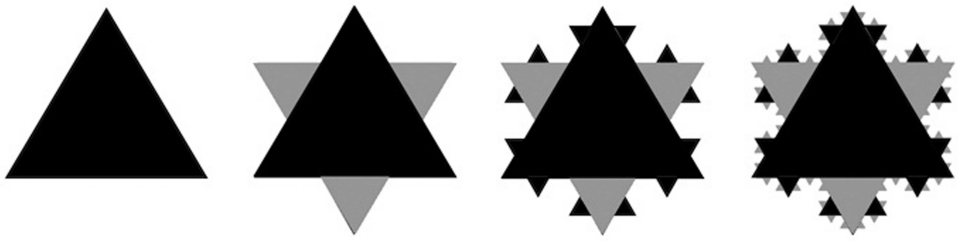

Figure 1.4: Iterations of a Koch snowflake.

Simply by varying the generator, the Koch curve may be generalized to give curves with fractal dimension $1 \leq \mathrm{D} \leq 2$. A straightforward example is provided by the modified Koch curve whose generator with angle α shown in Figure 1.3. The fractal dimension is given by

$$D = log4/log\left[2 + 2sin\left(\alpha/2\right)\right] \tag{1.10}$$

It is noticed that in the limit $\alpha = 0$ we have $\mathrm{D} = 2$, that is a curve which fills a triangle. It is not exactly a curve as it has an infinite number of multiple points. But the construction can be slightly modified to eliminate them.

1.3.3 Cantor Set

In mathematics, the Cantor set is a set of points lying on a single line segment that has a number of remarkable and deep properties. It was discovered in 1874 by Henry John Stephen Smith and introduced by German mathematician George Cantor in 1883. This is another example of objects which had been much studied before the idea of fractals was introduced. The following Cantor set is obtained by iteratively deleting the central third portion of each segment:

First five iterations are shown in Figure. 1.5. The fractal dimension of this set is given by:

$$D = \frac{\log 2}{\log 3} = \log_3\left(2\right) = 0.6309\ldots \tag{1.11}$$

For Cantor sets we have $0 \leq \mathrm{D} \leq 1$: it is said to be a "dust". As it is composed only of points, its *t*opological dimension is $d_T = 0$.

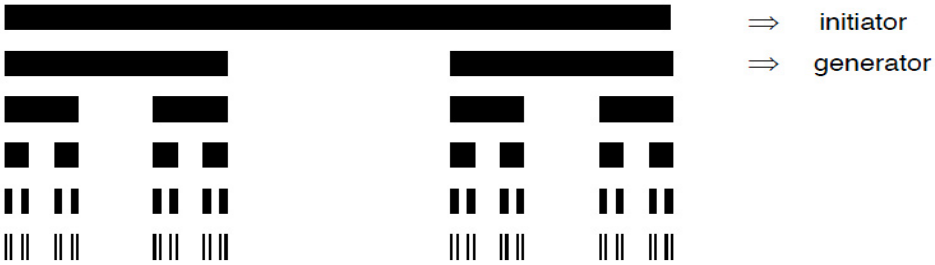

Figure 1.5: Construction of the first five iterations of a Cantor set.

1.3.4 Sierpinski Gasket

The Sierpinski triangle or Sierpinski gasket or the Sierpinski Sieve is a fractal and attractive fixed set. It was introduced by Polish mathematician Waclaw Sierpinski in 1915.

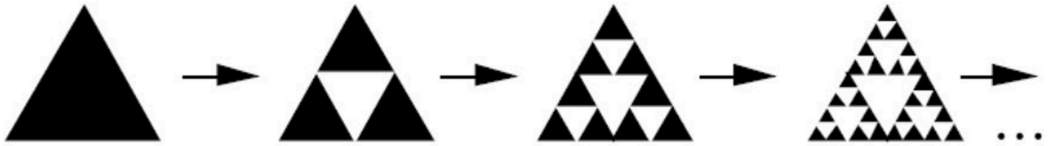

Figure 1.6: Iteration of the Sierpinski gasket composed of full triangles.

The scaling factor of the iteration is 2, while the mass ratio is 3 (Figure 1.6). The corresponding fractal dimension is given in (1.12)

$$D = \frac{\log 3}{\log 2} = 1.585 \tag{1.12}$$

The Sierpinski gasket generated by the edges is also often used (Figure 1.7). It clearly has the same fractal dimension $\mathrm{D} = \log 3/\log 2 = 1.585\ldots$

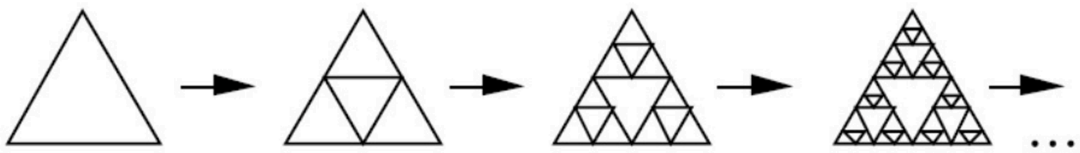

Figure 1.7: Iteration of the Sierpinski gasket composed of sides of triangles.

The two structures can be shown to "converge" asymptotically towards one other, in the sense of the Hausdorff distance.

1.3.5 Sierpinski Carpet

The Sierpinski carpet is a plane fractal. It was also described by Waclaw Sierpinski in 1916. The carpet is a generalization of the Cantor set to two dimensions (another is *Cantor dust*).

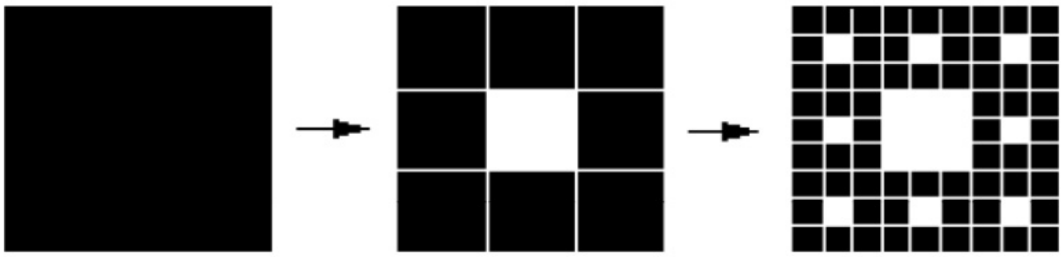

Figure 1.8: Iteration of a Sierpinski carpet.

The scaling factor is 3 and the mass ratio (black squares) is 8 (Figure 1.8). Hence,

$$D = \frac{\log 8}{\log 3} = 1.8928\ldots \tag{1.13}$$

1.4 Fractal Antenna Technology

Traditional approaches to the design and analysis of antenna systems have their foundation in Euclidean geometry. There has been a considerable amount of recent interest, however, in the possibility of developing antennas that employ fractal geometry in their design. The general comparison of Euclidean geometry and fractal geometry is shown in Table 1.1.

Table 1.1: General Comparison of Euclidean and Fractal Geometries

Euclidean Versus Fractal Geometry	
Euclidean Geometry	**Fractal Geometry**
Often defined by formula	Often defined by iterative rule
Applicable for artificial objects	Applicable for natural objects
Shapes change with scaling	Invariant under scaling, self-similar
Objects defined by analytical equations	Objects defined by recursive algorithms
Locally smooth, differentiable	Locally rough, not differentiable
Elements: vertices, edges, surfaces	Elements: iteration of functions

In the field of antenna theory, first application of fractals was reported by Kim and

D.L. Jaggard [35]. They introduced a methodology for designing low-side-lobe arrays based on the theory of random fractals. To explore the multi-frequency properties of fractals as a radiating structure was proposed by Carles Puente Baliarda [28,29,36,37]. In those studies, Sierpinski monopole antennas were introduced. This monopole antenna has multiband behavior over five operating bands. Such behavior is based on the self-similarity property of the antenna's fractal shape. Fractal shaped dipole antennas with Koch curves are generally fed at the center of the geometry. By increasing the fractal iteration, the length of the curve increases thereby reducing the resonant frequency of the antenna. The resonance of monopole antennas using these geometries below the small antenna limit has been reported by Puente et al. [31]. C. Borja et al. [38] have introduced a simple and fast numerical model to predict the input parameters of a network with the topology of the Sierpinski gasket fractal shape. A Sierpinski fractal antenna and several modifications in this geometry were investigated in [39–50]. Dual-band and wideband antennas, based on variation of the Sierpinski fractal monopole, were presented in [46–50]. The multiband properties of fractal monopoles based on the generalized family of mod-p Sierpinski gaskets were investigated by Castany et al. [51]. The advantage of this approach is that it provides a high degree of flexibility in choosing the number of bands and the associated band spacing for a candidate antenna design. In order to overcome the problem of miniature microstrip antennas (i.e., small bandwidth and radiation efficiency), parasitic techniques have been combined with fractal techniques to obtain miniature and wideband antennas with improved efficiency [33]. A novel configuration of a fractal square Sierpinski gasket antenna was presented and discussed in [52].

It has already been an important characteristic of many fractal geometries is their space filling nature. Antenna size is a critical parameter because its behavior depends on dimensions in terms of free space wavelength (λ_0). An antenna is said to be small when its larger dimension is less than twice the radius of the radian sphere; its radius is $\lambda/2\pi$. Wheeler and Chu were first to investigate the fundamental limitations of such antennas. The Hilbert and Koch fractal curves have also been useful in designing small microstrip patch antennas [27, 41, 53–57]. An additional facet of the reduction

in size of the resonant antenna is that the input resistance of small loops can be increased using fractals. One problem with a small loop is that the input resistance is very low, making it difficult to couple power to the antenna. By using a fractal loop, the antenna can be brought closer to resonance, which raises the input impedance. A Koch island was used as a loop antenna to increase the input resistance [54, 55]. The process is similar to the formation of the Minkowski fractal loop, except that the generator is comprises of only four segments of equal length, instead of five segments of two different scales. For comparison, a circular loop with equal radius was also constructed, which circumscribes the fractal loop [27, 58, 59].

Fractals can be used to miniaturize patch elements as well as wire elements. The same concept of increasing the electrical length of a radiator can be applied to a patch element [60]. The patch antenna can be viewed as a microstrip transmission line. Therefore, if the current can be forced to travel along the convoluted path of a fractal instead of a straight Euclidean path, the area required to occupy the resonant transmission line can be reduced. This technique has been applied to patch antennas in various forms [61–66]. Recently, new forms of fractal antennas (Combination of fractal geometry) are proposed for miniaturization, WLAN, UWB applications [67–72]. A novel technique to reduce the size of microstrip patch antennas is proposed [67]. Here, by etching the patch edges according to Koch curves as inductive loading, and inserting the Sierpinski carpets into the patch as slot loading, it is experimentally found that the resonant frequency of the patch can be sufficiently lowered. In addition, the higher iteration order of the fractal shapes resulting lowering the resonant frequency. This property can be utilized to reduce the size of the microstrip patch antennas. Another hybrid fractal antenna is proposed for UWB applications [68]. In this study two fractal geometries are used. First, Giusepe Peano fractal are applied on the edges of a square patch, and second, a Sierpinski Carpet fractal is formed on its surface.

1.5 Motivation

The motivation for the proposed work comes from the need for compact, highly efficient, low cost antenna suitable for use in multi-band, dual-band, dual polarized and broadband/wideband operations with the possibility of embedding with Microwave Integrated Circuits (MICs). Moreover, as emerging wireless systems need to handle large amount of data in a very short time, Multiple Input Multiple Output (MIMO) and wideband array antenna techniques are also important. Recently, Federal Communication Commission (FCC) has licensed a spectrum designated Advanced Wireless Services (AWS) that offers a variety of wireless services including the broadband 3G mobile. Leading mobile telephone manufacturers are integrating features like satellite radio and TV to the hand held devices. To meet some of these challenging demands, novel shaped fractal antennas are investigated. Therefore, the aim of the thesis is to understand the effect of fractal geometries in antennas, and to explore their usage in antenna engineering.

1.6 Problem Statement

With the motivation, mentioned in Section 1.5, we take up a problem, for the doctoral research, which is stated as follows.
To design and develop fractal antennas for:

- Wideband wireless applications,
- Dual wideband wireless applications,
- Wideband frequency reconfigurability,
- Ultra-wide band (UWB) applications,
- MIMO implementations,
- Array applications,

using fractal geometries.

1.7 Organization of Thesis

The **FIRST** chapter of this thesis is devoted to the background of fractal geometries, literature review and development of fractal antennas for wireless communication. The motivation and problem statement are also included in this chapter. Finally, the chapter is summarized.

The **SECOND** chapter of this thesis is dedicated to the literature on the present work. Recent development of wireless technology, review on wideband technology, UWB technology, reconfigurable microstrip antenna, MIMO antennas, wideband linear arrays are studied. Finally, the chapter is summarized.

The **THIRD** chapter contributes to the fundamental ideas used to design wideband fractal monopole antennas. The proposed antennas are simulated and experimentally verified. However, due to the varied nature of fractal geometries studied antenna design using them differs in their performances and appearances. This chapter is arranged with different types of antennas based on fractal geometries. The antennas are microstrip feed and CPW feed for easy fabrication and better integration with monolithic microwave circuits (MICs). The surface current and field distribution on the antenna resonant mode and their corresponding radiation patterns are analyzed in detail. Finally, the chapter conclusions are outlined.

The **FOURTH** chapter deals with frequency reconfigurable Koch snowflake wideband monopole antenna. Here, frequency reconfigurability is observed by using a PIN diode in proposed Koch fractal antenna. This antenna provides a continuous coverage for three wide frequency bands.

The **FIFTH** chapter is based on the Sierpinski square fractal monopole antenna for UWB applications. The proposed antenna performs well in terms of its impedance match and gain, over wideband and easily complies with the FCC UWB frequency band 3.1 GHz to 10.6 GHz. The $\bigcap$-slot is introduced in feed line without changing the patch size for narrow band frequency notched. Finally, the chapter is summarized.

The **SIXTH** chapter is divided into two parts. In first part, hybrid fractal antenna is designed with 2×2 MIMO implementation for hand-held devices. The diversity performance of the proposed antenna evaluated by envelope correlation coefficient

computed from the reflection coefficient values. Furthermore, all the performances are presented for 4×4 MIMO antenna system in hand-held devices. The second part of this chapter is based on feeding network for wideband fractal antenna using modified Wilkinson power divider. The designed wideband feed network is then integrated with previously designed wideband antenna in chapter 3 (Sectoral) to construct two- and four- element antenna arrays. The proposed antennas are designed fabricated and experimentally verified. The surface current and field distribution on the antenna resonant mode and their corresponding radiation patterns are analyzed in details. Finally, the chapter conclusions are outlined.

Finally thesis is concluded in **SEVENTH** chapter by compiling the overall work and their results along with a brief description on the scope for future work.

A detailed description of design methodology used for designing wideband antenna elements are described in the **APPENDIX A**. Here, Electromagnetic (EM) numerical modeling techniques for both Ansoft High Frequency Structure Simulator (HFSS) and Computer Simulation Technology Microwave Studio (CST MWS) simulation programs are discussed.

1.8 Summary

This chapter provides a brief introduction to fractal geometries and fractal antenna technology. It also systematically outlines, the motivation which resulted in the investigation and the problem statement of the thesis. A concise presentation of research work has been carried out in each chapter and the contribution made by the candidate have also been dealt. In essence this chapter provides a complete overview of the total thesis in a condensed manner.

CHAPTER 2

Planar Wideband Antennas: A state-of-the-art

2.1 Introduction

Wireless is a term used to describe telecommunications in which electromagnetic waves carry the signal over a part or the entire communication path. Common examples of wireless equipment in use today include: cell phones, pagers, global positioning systems (GPS), cordless computer peripherals, satellite televisions, wireless local area network (WLAN) and wireless personal area network (WPAN), etc. Wireless technology is rapidly evolving and playing a vital role in the lives of people throughout the world. In addition, larger number of people are relying on wireless technology, either directly or indirectly. More recent examples of wireless communications include the following technologies:

— *Global System for Mobile Communication (GSM)*: a digital mobile telephone system commonly used in Europe and Asia;

— *General Packet Radio Service (GPRS)*: a packet-based wireless communication service that provides continuous connection to the internet for mobile phone and computer users;

— *Enhanced Data GSM Environment (EDGE)*: a faster version of the Global System for Mobile (GSM) wireless service designed to deliver data at rates up to 384 Kbps and to enable the delivery of multimedia and other broadband applications to mobile phones and computer users;

— *Universal Mobile Telecommunications System (UMTS)*: a broadband packet based system offering an integrated set of services to mobile computers and phone users no matter where they are located in the world;

— *Wireless Application Protocol (WAP)*: a set of communication protocols to standardize the way that wireless devices, such as cellular telephones and radio transceivers can be used for internet access.

Wireless can be divided into three categories: fixed, mobile, and portable. Fixed wireless refers to the operation of wireless devices or systems in fixed locations such as homes and offices. Mobile wireless applications refer to devices or systems on moving vehicles. Examples include the automotive cell phone and on-board GPS system. Portable wireless applies to the operation of autonomous, battery-powered wireless devices or systems outside the office, home, or vehicle; examples include hand-held cell phones and personal communication system (PCS) units.

Recent technologies enable wireless communication devices to become physically smaller in size. Antenna size is obviously a major factor that limits miniaturization. Antenna physical size is inversely proportional to its operating frequency. However, reducing the antenna physical size also means reducing its electrical size since the operating frequency of these devices does not change. Electrical size is expressed as a fraction of wavelength, λ. Examples of antennas of quarter-wavelength electrical size that are used include monopole antennas, helical antennas, and planar inverted-F antennas (PIFAs).

In the past few years, new designs of low-profile antennas for hand-held wireless devices have been developed. The major drawback of many low-profile antenna designs is their narrow impedance bandwidth. Some designs can barely cover the bandwidth requirement, hence, may not be used because there is no margin in the bandwidth for potential detuning effects due to the presence of a human operator.

In this chapter, the background information and literature review related to the design of antennas for wideband communication applications are discussed. This chapter is organized as follows: Section 2.2 presents a brief introduction on wideband technology as well as its potential applications. Different wideband antennas are

investigated in Section 2.3. The UWB antenna technology is described in Section 2.4. Section 2.5 gives detail information related to the reconfigurable antennas. Various MIMO antennas are reviewed in Section 2.4. Then, Section 2.5 introduces the background information about wideband linear antenna array and its advantages followed by summary in Section 2.9

2.2 Wideband Antenna Technology

In order to increase the bandwidth of an antenna, several methods such as using thick and low permittivity substrates, stacked and suspended structures, aperture or L-probe coupling, parasitic resonators and planar designs with different shapes (circular, triangular, etc.) can be considered. Wideband antennas normally occupy larger space than multiband antennas in the applications and the profile can be even higher with possible array configurations to obtain higher gain. Therefore, wideband antennas are mostly preferred in indoor or outdoor base station applications rather than mobile handset applications. VSWR (or reflection coefficient) requirement within the desired frequency bands is responcible for mobile applications. Similiarly, additional criteria such as high gain and high isolation between the antenna elements should be satisfied for wideband antennas in base station applications. The commonly used wideband antennas in mobile communication systems are described as follows.

Wideband antenna concept was reported in 1947 [73] by U.S. Radio Research Laboratory of Harvard University. The concept of a wideband antenna evolves from a transmission line that gradually diverges while keeping the inner and outer conductor ratio constant. They have developed several concepts, such as sleeve antenna, the teardrop antenna and inverted trapezoidal antenna etc.

In 1950, the spiral antenna was introduced in the class of frequency independent antennas. The equiangular spiral and Archimedean spiral antennas are the most well-known spiral antennas. Spiral antenna has about a 10:1 bandwidth, providing circular polarization in low-profile geometry [74].

In 1982, R.H. Duhamel had invented the sinuous antenna, which provides dual-linear polarization plus wide bandwidth in a compact, low-profile geometry [75]. The

sinuous antenna is more complicated than the spiral antenna. However, it provides dual orthogonal linear polarizations so that it can be used for polarization diversity or for transmit/receive operation. Also, the two 2-arm pair outputs can be combined to produce LHCP and RHCP simultaneously [76]. Several monopole disc antennas were invented since 1992 [77–81].

2.3 Wideband Antenna Designs

The technologies for wireless communication have been developed very quickly in recent years. It can be seen that there have been more and more wireless devices available in the market such as mobile phones, GPS navigation systems, Bluetooth earphones, and PS3 game pads etc. All these devices need antennas for transmitting and receiving wireless signals to the base station. Without antennas, wireless communication would be impossible. A good antenna design can improve the quality of the wireless signal transmission and enhance the performance of the wireless system. Portable wireless devices normally are small in size. This implies that the size of antennas should be small enough for embedding into the devices. Among different types of antennas, patch antennas are suitable for this purpose because of their light weight, simple structure, low profile, and ease of fabrication.

M. Sindou et al. [82] have designed a novel structure based on the fractal branches for wideband/multi-band applications. The multiband behavior is generated by the elements of successive iteration levels. A wideband response is produced by the large number of element in the last iteration.

E. Lee, P.S. Hall and P. Garder [83] have designed co-axial feed planar monopole wideband antenna. In this study, a shorting pin technique is used to get an additional mode below the fundamental mode for the proposed antenna. Here, 50 % size reduction is gained as compared to an equivalent planar monopole without a shorting post.

CPW-fed wide slot antenna is investigated by A.U. Bhobe et al. [84]. This antenna achieves impedance bandwidth of 49 % about the design frequency of 4.8 GHz. The cross polarization in both the principal planes is at least -20 dB below entire

bandwidth.

A novel E-Shaped patch antenna for wideband applications is presented by Fan Yang et al. [85]. Here, two parallel slots are incorporated to the patch of a microstrip antenna to expand its bandwidth. This antenna gives the inpedance bandwidth of 30.3 % at wireless frequency band of 1.9-2.4 GHz.

A new technique for bandwidth enhancement of microstrip fed annular ring slot antenna is proposed by N. Behdad and K. Sarabandi [86]. Using this technique, significant improvement in the bandwidth is obtained. The bandwidth of 6 % for single-element ring antenna is attained, whereas for double element antenna, it is about 36 %.

A stubby antenna fed by a coaxial probe and tuning technique is proposed by D.U. Sim et al. [87]. The impedance matching and bandwidth of this antenna are mainly affected by the length of the ground patch at bottom of a small substrate. For this antenna, the impedance bandwidth is found to be 59.7 %. The proposed antenna is capable of covering the Korean PCS/IMT-200, Bluetooth bands and provides omnidirectional radiation patterns.

T. Sudha et al. [88] have designed a circularly polarized (CP) wideband antenna. The proposed design has a reduced antenna size compared to the conventional CP microstrip antenna. Here, CP bandwidth of 18.85 % (determined from 3 dB) and impedance bandwidth of 22.13 % centered at 1.99 GHz are obtained.

M. Joseph et al. [89] have designed a compact wideband antenna at 2.4 GHz frequency for WLAN applications. This antenna has low profile dimensions of $15\times15\times1.6$ mm^3 and impedance bandwidth of 18.6 % with an average gain of 5 dBi.

A simple and successful design method that yields a wideband and compact antenna without ground plane is proposed by S. Tanaka et al. [90]. In this study, the bandwidth of 53 % is obtained for loop antenna. Here, volume reduction of 50 % is achieved by selecting strip width and element gap.

A novel CPW-fed wideband planar monopole antenna design is suggested by J.Y. Jan and T.M. Kou [91]. Here, using a symmetrically slope ground plane, wideband operation is obtained. This antenna provides an impedance bandwidth of 51 %.

The design of a planar monopole square-ring patch antenna with wideband operation is illustrated by J.S. Row and S.H. Chen [92]. This antenna consists of a parasitic square-ring radiating patch antenna that is shorted with the ground plane through two shorting walls and is excited by a top-loaded coaxial probe. This antenna provides an impedance bandwidth more than 50 %.

An asymmetrical slot CPW-fed wide-band planar antenna is proposed by J.Y. Jan and C.Y. Hsiang [93]. The asymmetrical slots are square-like structure with the same width but different length at the sides. Broadband operation can be obtained by choosing suitable length of this asymmetrical slots. The impedance bandwidth of 82 % is gained with respect to center frequency of 2.16 GHz for the same antenna.

S.H. Wi et al. [94] have intended a wideband ⋃-shaped parasitic patch antenna. Here, two parasitic elements are incorporated into the radiating edges of a rectangular patch, in order to achieved a wide bandwidth with relatively small size. Here, an impedance bandwidth of 27.3 % at 5.5 GHz center frequency is obtained.

A compact dual wideband printed wire antenna for application in wireless communications is proposed by Y.F. Ruan [95]. This antenna offers two separate measured impedance bandwidth of 25.92 % (2.35-3.05 GHz) and 42.78 % (3.95-6.1 GHz), for a -10 dB reflection coefficient.

T.P. Wong [96] has designed a wideband vertical patch antenna (VPA). It is devised from fractal antenna technology. An impedance bandwidth of 42 % and 8 dBi gain at the center frequency is achieved by using a dual-Koch loop structure.

The Wideband fractal antenna in the shape of Koch snowflake is proposed by B. Mirzapour [97]. Here, with the use of Koch snowflake, the impedance bandwidth of 49 % is achieved. Also, a reduction of about 70 % in patch surface size compared to an ordinary Koch snowflake is obtained by using an air filled substrate and capacitive feed.

D.D. Krishna et al. [98] have investigated a dual wide-band modified Koch fractal antenna. Here, the operating frequency of a triangular slot antenna is lowered by the Koch iteration technique. The proposed antenna has an impedance bandwidth of 40 % from 2.38-3.95 GHz and 20 % from 4.95-6.05 GHz covering 2.4/5.2/5.8 GHz

WLAN bands and the 2.5/3.5/5.5 GHz WiMAX bands.

The microstrip line fed Penta-gasket Koch antenna for wideband applications is introduced by N.J. Mahdi [99]. In this study, the design acquires a good input impedance match and linear phase of $S_{11}\leq$-10 dB throughout the passband (1.5-20 GHz).

A compact wideband Koch snowflake printed slot antenna suitable for WLAN and WiMAX applications is proposed by D.D. Krishna et al. [100]. Here, the antenna size inclusive of the ground plane is compact and has a wide operating bandwidth. This antenna covers impedance bandwidth of 90.61 % from 2.33-6.19 GHz for the second iteration Koch.

W.L. Chen et al. [64] have designed microstrip line fed printed wide-slot antenna with a fractal shaped slot for bandwidth enhancement. By etching the wide slot as fractal shapes, it is experimentally found that the impedance bandwidth of 56.2 % is obtained with respect to the center frequency at 3.825 GHz.

A microstrip planar monopole antenna using the geometry of the fractal binary tree is presented by R. Guo [101]. In this study, to get a wide impedance bandwidth, the fractal antenna is optimized in an automated design, making use of the genetic algorithm with the full-wave electromagnetic simulation and cluster parallel computation. Here, good agreement is obtained between numerically calculated and measured results. It shows that the proposed fractal antenna gains a quite promising impedance bandwidth of 42.8 % (2.46-3.80 GHz).

Recently, a compact wideband unidirectional antenna with a reflector connected to the ground using a stub is investigated by G.M. Zhang et al. [102]. This antenna consists of a pair of stepped-structure patches and a coplanar waveguide feeding line. The proposed antenna provides an impedance bandwidth of 38.30 % from 3.82-5.63 GHz. The optimized size of the proposed antenna is 20×20 mm^2, which is much smaller than most of the current wideband unidirectional antennas.

2.4 Reconfigurable Microstrip Antennas

Recently, reconfigurability in antenna systems has received significant attention in developing novel multifunctional antenna designs. Compared to conventional antennas, reconfigurable antennas provide the ability to dynamically adjust various antenna parameters. They can reduce any unfavorable effects resulting from co-site interference and jamming. In addition, they have a remarkable characteristic of achieving diversity in operation, i.e one or multiple parameters, including operating frequency, radiation pattern, gain and/or polarization, can be reconfigured with a single antenna. The use of reconfigurability in coordination with a self-similar antenna leads to a considerable improvement in antenna performance. This is because not only a wider selection of frequencies is achieved, but also similar radiation properties for all designed frequency bands are obtained.

With multiband and wideband capability, reconfigurable antennas can utilize more efficiently the radio frequency spectrum, facilitating better access to wireless services in modern radio transceivers. Reconfigurable antennas are generally divided into two main categories: frequency tunable and pattern diversity antennas. Furthermore, the selection of electronic switches is of paramount importance. Depending on the type of antennas, switches such as RF MEMS, varactor and PIN diodes can be used. The choice is governed by electrical specifications, fabrication complexity, bias requirement, switching time, and price.

Reconfigurable antennas come in a large variety of different shapes and forms. Their operation can largely be analyzed through existing design principles [103, 104] by utilizing well defined antennas as the base design and a point of reference for the desired operation.

E.R. Brown [105] presents a paper on RF-MEMS Switches for Reconfigurable Integrated Circuits. This work deals with radio-frequency (RF) technology based on micro-electro mechanical systems (MEMS). It provids superior high-frequency performance relative to conventional (usually semiconductor) devices which enable new system capabilities. Here, the only device addressed is the electrostatic micro-switch perhaps the paradigm RF-MEMS device. Through its superior performance char-

acteristics, the micro-switch is being developed in a number of existing circuits and systems, including radio front-ends, capacitor banks, and time-delay networks.

A novel architecture for reconfigurable multiband, multifunctional planar antenna is demonstrated by Y. Qian et al. [106]. In this study, a microstrip based leaky-mode antenna array can easily be reconfigured to patch antenna (operating at multiple frequency bands) as well as monopulse radars by employing either conventional or MEMS switches. This design provides promising solution to the problem of antenna congestion in modern communications and radar platforms.

F. Yang et al. [107] have designed a microstrip patch antenna with switchable slots, to achieve circular polarization diversity. Here, two orthogonal slots are incorporated into the patch and two pin diodes are utilized to switch the slots ON and OFF. By turning the diodes ON or OFF, this antenna can radiate with either right hand circular polarization (RHCP) or left hand circular polarization (LHCP) using the same feeding probe.

J.S. Petko et al. [108] have introduced a design methodology for miniaturized multiband as well as reconfigurable antennas that exploits the self-similar branching structure of three-dimensional (3-D) fractal trees. It is found, through a series of systematic MOM simulations, that the two most critical factors inciting the successful design of miniaturized 3-D fractal tree antennas.

D. Peroulis et al. [109] have developed the design of a compact, efficient and electronically tunable antenna. A single-fed resonant slot loaded with a series of PIN diode switches constitutes the fundamental structure of the antenna. In this antenna, tuning is realized by changing its effective electrical length, which is controlled by the bias voltages of the solid state shunt switches along the slot antenna. Here, theoretical results for significant antenna parameters are validated experimentally.

N. Jin, et al. [110] have proposed patch antenna with switchable concept. In this study, a reconfigurable antenna with both frequency and polarization diversities are implemented. Using only one switch and a single patch, the antenna operates at 4.20 GHz and 4.55 GHz with RHPC and LHPC respectively. The fabricated antenna has an acceptable reflection coefficient and a broadside axial ratio (AR) lower than 2

dB for both frequency operations. The frequency and polarization diversities of this design could potentially improve the reliability of wireless communication systems.

An effective design of a reconfigurable patch antenna with a broad bandwidth for wireless communication and radar systems is investigated by B.Z. Wang et al. [111]. The proposed antenna possesses an E-shaped structure and its operating frequency can be changed by integrated switches. The operating frequency of the antenna can cover an octave frequency range by utilizing only two switch states. In state 1, the antenna operates from 9.2-15.0 GHz and, in state 2, from 7.5-10.7 GHz. Its impedance bandwidths of 48 % and 35 % are achieved for state-1 and state-2 respectively.

S.L.S. Yang and K.M. Luk [112] have presented a wideband circularly polarized reconfigurable microstrip patch antenna fed by L-shaped probes. Here, RHPC and LHPC are excited by L-shaped probe feeding perturbed square patch. The L-shaped probe is connected to a switch which is fabricated underneath the ground plane, such that circularly polarized radiation pattern reconfiguration could be realized. Measured results of this antenna attain a bandwidth of over 10 % with both SWR ≤ 2 and axial ratio < 3 dB.

A radiation pattern reconfigurable antenna is proposed by W.S. Kang [113]. By controlling the switch states, the antenna can be worked as a monopole antenna with an omnidirectional radiation pattern or a dipole antenna with reflector, which has directional radiation pattern. This antenna is designed to cover the 2.3 GHz wireless broadband internet (WiBRO) band at the switch OFF state, since a WIBRO receiver antenna needs an omnidirectional pattern. It covers 2.6 GHz satellite digital multimedia broadcasting (SDMB) band at the switch ON state since an SDMB receiver antenna needs a directional pattern.

S.J. Wu and T.G. Ma [114] have proposed a slotted bow-tie antenna with pattern reconfigurability. This antenna consists of a pair of reconfigurable CPW-to-slot line transitions, a pair of Vivaldi-shaped radiating tapered slots, and four PIN diodes. The proposed antenna demonstrates reconfigurable radiation patterns in the frequency range from 3.5-6.5 GHz for suitable arrangement of the bias networking. A broadside radiation with fairly omnidirectional pattern and two end-fire radiations whose main

beams are directed to exactly opposite directions are achieved.

Y. Tawk and C.G. Christodoulou [115] have designed a reconfigurable antenna for cognitive radio application. It consists of two structures incorporated together into the same substrate. The first structure is an UWB antenna covering the spectrum from 3.1-11 GHz for channel sensing. The second structure is a frequency reconfigurable triangular-shaped patch for establishing communication with another RF device. The antenna reconfigurability is achieved via a rotational motion.

A simple reconfigurable slot antenna with a wide bandwidth is proposed by Hui Li et al. [116]. In this study, an open slot of size 0.125λ at higher frequency is etched at the edge of the ground. To achieve the tunability, a PIN diode and a varactor diode are used. By switching the PIN diode placed at the open end of the slot, the slot antenna can resonate as a standard slot (switch ON) or a half slot (switch OFF). A varactor diode is used to provide continuous tuning over some wider frequency range.

An antenna with reconfigurable polarization for wireless local area network (WLAN) applications is demonstrated by P.Y. Qin et al. [117]. In this study, PIN diodes are used to change the length of the U-slot arms, which switches the antenna's polarization state. Two antenna prototypes with identical dimensions are designed, fabricated and experimentally verified. The first antenna prototype enables switching between linear and circular polarization by using a PIN diode. The second antenna prototype uses two PIN diodes to use as a switch between the two circular polarization senses. A good impedance match for both linear and circular polarization is achieved from 5.725-5.85 GHz. The 3 dB axial ratio bandwidth of this antenna is greater than 2.8 %.

A planar inverted-F reconfigurable antenna using a switchable PIN-diode and a fine-tune varactor is investigated by J.H. Lim et al. [118] for mobile communication applications. Here, selection of operating modes is achieved by switching ON the PIN-diode, which is placed between radiators. In mode I, with the PIN-diode OFF and tuning the varactor, the antenna operates for USPCS (1.85-1.99 GHz), WCDMA (1.92-2.18 GHz), and WLAN (5.15-5.825 GHz). In mode II, with the PIN diode ON and the fixed 0-Volt varactor antenna operates for USPCS and m-WiMAX (3.4-3.6

GHz). Furthermore, equivalent models of a PIN diode and a varactor are presented for accurate prediction of antenna performances which are also analyzed by varying diode parameters. The peak gains are 2.84, 2.81, 1.25, and 1.49 dBi at USPCS, WCDMA, m-WiMAX, and WLAN, respectively.

A reconfigurable loop antenna for mobile handheld devices is proposed by Y. Li et al. [119]. Here, two operating states with different frequencies are obtained by switching the shorting pins of the loop. The bandwidth of the proposed antenna has been increased by adopting a matching bridge. The proposed antenna operates in hepta-band, including GSM 850/900, UMTS, GPS, DCS, PCS, and WLAN, with the reflection coefficient lower than -6 dB.

A reconfigurable antenna using two PIN diodes is presented by Y.K. Park and Y. Sung [120] for quad-band (GSM900/GSM1800/GSM1900/UMTS) mobile handset applications. In this study, by independently adjusting the ON/OFF states of the two PIN diodes located on the radiating element, the proposed structure is operated in the PIFA and loop mode, respectively. The PIN diodes are replaced with conducting tape in order to verify the concept. In regard to the fabricated reconfigurable antenna, when operating in the PIFA mode, the measured results show that -7 dB impedance bandwidth is 8.62%, which covers the GSM900 (880-960 MHz) band. When operating in the loop mode, the measured results show that the -7 dB impedance bandwidth is 26.36%, which covers the GSM1800 (1710-1880 MHz), GSM1900 (1850-1990 MHz), and UMTS (1920-2170 MHz) bands, respectively.

A frequency reconfigurable wideband/multiband C-slot patch antenna with dual-patch elements is proposed by H.F. Abutarboush et al. [121]. In this study, the antenna is operated in two dual-band modes and a wideband mode. Two parallel C-slots on the patch elements are employed to perturb the surface current paths for excitation of the dual-band and the wideband modes. Two switches, implemented using PIN diodes are placed on the connecting lines of a simple feed network to the patch elements. Dual-band modes are achieved by switching "ON" either one of the two patch elements, while the wideband mode with an impedance bandwidth of 33.52 % is obtained by switching "ON" both patch elements. The frequencies in the dual-band

modes can be independently controlled using positions and dimensions of the C-Slots without affecting the wideband mode. The main advantages of the proposed antenna include low profile, lightweight and easy to fabricate, simple structure targeting future smaller wireless communication devices.

Recently, a frequency-reconfigurable spirograph planar monopole antenna (SPMA) operating in the Ultra High Frequency (UHF) band using RF PIN diodes is investigated by J.T. Rayno and S.K. Sharma [122]. The radiating element is compact and is used as an array element. It has three measured frequency bands with VSWR$<$ 2: case 1, impedance bandwidth of 43.0 % (2.17-3.36 GHz); case 2, impedance bandwidth of 69.5 % (1.21-2.50 GHz); and case 3, impedance bandwidth of 92.7 % (1.07-2.92 GHz). Cases 1 and 2 provide contiguous coverage, and case 3 covers almost the entire range of cases 1 and 2. Thus, this antenna provides continuous coverage of 103.4 % (1.07-3.36 GHz). This antenna has acceptable omnidirectional radiation patterns with relatively low cross polarization.

E. Erfani et al. [123] have designed a new incorporated planar UWB/reconfigurable slot antenna for cognitive radio applications. A slot resonator is precisely embedded in the disc monopole radiator to achieve an individual narrow band antenna. A varactor diode is also deliberately inserted across the slot, providing a reconfigurable frequency function in the range of 5-6 GHz. The slot is fed by an off-centered microstrip line that creates the desired matching across the tunable frequency band.

2.5 Ultra-Wideband Antenna Technology

UWB technology is considered to be attractive by many researchers, scientists and engineers and a promising technology for high-speed, high data rates and short-range indoor wireless communications. This is especially true when the Federal Communication Commission (FCC) permitted using the frequency band from 3.1 to 10.6 GHz for UWB radio applications in 2002 [124]. Currently, there is a great interest in UWB system design and implementation in both academic research and industry areas. The concept of UWB radio was first developed several decades ago in the late 1960's. The U.S. Department of Defense first founded the term 'ultra-wideband' in 1989 [125].

In the beginning, UWB was mainly for military purposes such as radar applications. It employed wideband signals in frequency domain or very short duration pulses in the time domain to get fast, reliable and accurate information about moving targets such as missiles. Recently, UWB systems use a very short duration pulse to transmit data over a large absolute bandwidth of up to 7.5 GHz. The FCC has allowed uses of the the unlicensed frequency band of 3.1-10.6 GHz with a limited transmitted power of -41.3 dBm/MHz for use in commercial wireless applications. It has been shown to be of increasingly great research interest especially in the field of personal and commercial wireless communications.

Since 1992, several microstrip, slot and planar monopole antennas with simple structure have been reported [77–80, 126]. They produce very wide bandwidth with a simple structure such as circular, elliptical or trapezoidal shapes. The radiating elements are mounted orthogonal to a ground plane and are fed by a coaxial cable. The large ground plane mounted orthogonal to the patch made these antennas bulkier and are difficult to fit into small devices.

Guillanton et al. [127] had proposed a new balanced antipodal Vivaldi antenna for UWB application in 1998. The authors extended the tapers of the balanced antipodal vivaldi to make the vivaldi antenna work as a dipole in lower frequency. Here, the slot cannot radiate to extend low frequency limit. However, the bandwidth of the antenna is limited by the transition from the feed line to the slot line of the antenna.

K. Chung has investigated UWB antenna with notched band characteristics [128]. This antenna is made insensitive to particular frequencies. This technique is useful for creating UWB antennas with narrow frequency notches, or for creating multiband antenna. Since then, many researchers have extended their research to investigate the possibility interference between UWB system and existing wireless communication systems such as HIPERLAN/WLAN systems. The common technique used is adding a half wavelength slot to the patch antenna. The slot is intended to reject the required frequencies [129–138].

In 2006, many researchers had proposed UWB with band notch characteristics antennas. Young Jun Cho et al. [139] have designed a planar monopole antenna with

a staircase shape and small volume ($25\times26\times1$ mm^3). Here, half-bowtie radiating element, the staircase-shape and a modified ground plane structure are used for very wide impedance bandwidth. The measured results indicate that the impedance bandwidth is about 11.6 GHz (2.9-14.5 GHz) which include the WLAN band notched in the vicinity of 5 GHz. A coplanar waveguide-fed uniplanar log-periodic slot antenna suitable for use in the ultra-wideband radio systems is presented by S.Y. Chen et al. [140]. The in-band impedances and radiation performances are quite stable and satisfactory. A band-notched UWB antenna is presented by S.W. Qua et al. [141]. Here, the notched-band characteristic is realized by a compact CPW resonant cell (CCRC). T.G. Ma et al. [142] have proposed a new coplanar waveguide-fed tapered ring slot antenna for UWB applications. This antenna consists of a 50Ω coplanar waveguide feeding line, wideband coplanar waveguide-to-slot line transition, and a pair of curved radiating slots. This antenna offers an impedance bandwidth from 3.1-12 GHz.

In 2007, K. Bahadori et al. [143] had designed elliptic-card UWB planar antenna. It consists of an elliptic radiating element and a rectangular ground plane. Here, a novel feeding mechanism is proposed to feed the antenna by using a microstrip line on the other side of the substrate and connecting the line to the elliptic element by a via. The proposed antenna provides a band rejection at the WLAN band (5.1-5.8 GHz) by adding two slits within the elliptic element. C.Y. Hong et al. [144] designed a novel planar UWB antenna with band-notched function. This antenna consists of a radiation patch that has an arc-shaped edge and a partially modified ground plane. Printed elliptical monopole antenna configurations, which give larger bandwidth than circular configuration, have been investigated for UWB applications by K.P. Ray and Y. Ranga [145]. Approximate formula to calculate lower band edge frequency and frequency dependent design curve for the critical microstrip feed line length have been presented in their work.

In 2008, M.E. Bialkowski and A.M. Abbosh [146] had described a method to improve the cutoff capability of an UWB planar antenna at the out-of-band frequencies using a meandered slot. In this study, an UWB band is formed using a semi circle

shaped radiating patch and ground plane. Here, the meandered shape slot is made in radiating patch to get notched frequency. O. Ahmed et al. [147] have presented a printed monopole antenna for UWB and band notch characteristics. This antenna consists of a half circular disc and a rectangular patch with two steps. Here, an arc shaped slot is cut away from the radiating patch to achieve band notched characteristics. A novel printed antenna for UWB applications is presented by M.E. Chen and J.H. Wang [67]. Here, an open annulus strip as a ground plane and an open crescent patch in the inner space of the annulus as a radiating element is used. This antenna is fed by a coplanar waveguide with a central strip connected to the crescent patch.

J.W. Jang and H.Y. Hwang [148] have designed a new antenna for UWB applications with band notched characteristics. Here, an UWB characteristic is formed by using two parasitic patch and a parasitic slot. The proposed antenna has an excellent band rejection characteristic. N. Choi et al. [149] have designed a compact UWB antenna with a band-notch function for laptop applications. The band-notch function is realized by a half-wavelength parasitic element printed on the rear side of the substrate. M. Ojaroudi et al. [150] have investigated a novel printed monopole antenna for UWB applications. This antenna consists of a square radiating patch with two rectangular slots and a ground plane with inverted T-shaped notch, which provides a wide usable fractional bandwidth of more than 120% (3.12-12.73 GHz).

A compact planar monopole antenna with standard band-notched characteristic suitable for UWB applications is presented by H.W. Liu et al. [151]. This antenna consists of a square slot patch with a vertical coupling strip. The proposed antenna is very compact. Here, the band notch is achieved using vertical coupling strip. A miniaturized hook-shaped monopole antenna is presented by H.W. Liu and C.F. Yang [152] for UWB applications. K. Shambavi and Z.C. Alex [153] have designed and measured the performance of a printed dipole antenna with band rejection characteristics for UWB applications. The proposed antenna operates in the frequency range 3.656 GHz to 15.64 GHz with impedance bandwidth of 11.027 GHz and maximum gain of 6.046 dBi. It consists of five dipole strips of different resonant length combined orthogonally for effective signal reception. Here, inverted L-shaped slots are introduced in

the ground plane for WLAN band rejection.

R. Azim et al. [154] have investigated a compact microstrip line-fed UWB tapered-shape slot antenna. This antenna comprises a tapered-shape slot and rectangular tuning stub. A compact UWB antenna with sharp band-notched characteristics is presented by Q.X. Chu and T.G. Huang [155]. Here, the sharp band-notched characteristic is realized by inserting a half wavelength C-shaped slot in the patch and adding two half wavelength stepped impedance resonators around the feed-line. A simple and compact UWB printed monopole antenna with filtering characteristic is presented by A. Nouri and G.R. Dadashzadeh [156]. In this study, a radiating patch with arc-shape is responsible for UWB operations. Here, a modified shovel-shaped defected ground structure is used for creating a band notch frequency.

T. Li et al. [157] have proposed a compact UWB antenna with an electronically tunable notched band for UWB communication applications. This antenna utilized a C-shaped ground to realize miniaturization and a pair of open-loop resonators (OLRs) to create notched band. The center frequency of the notched band can be electronically tuned by changing the effective electrical length of the OLRs, which is achieved by employing varactor diodes. A trapezoid monopole antenna with a band-notched performance for UWB is presented by Y.S. Seo et al. [158]. J.H. Lu et al. [159] have designed a novel broadband design of planar arc-shaped monopole antenna with a rectangular parasitic patch for UWB systems. With the use of rectangular parasitic patch, multi resonant modes are excited to meet the specifications of UWB systems.

Recently, A.K. Gautam et al. [160] have designed a novel coplanar waveguide (CPW)-fed compact UWB microstrip antenna for ultra-wideband applications. This antenna possesses a method to minimize the monopole antenna by loading of inverted L-strip over the conventional monopole patch antenna to lower the height of the antenna. The ground is vertically extended toward two sides of the single radiator.

2.6 Antennas with Multiple Input Multiple Output

A technology that promises to bring all the advantages of spatial multiplexing to point-to-point communications is MIMO. It is advised as one of the most advanced technologies in wireless communications up to date. The MIMO system is a communication system using multiple antennas on both sides of communications. It is taking an advantage of the multipath propagation, synthesizing a number of independent communication sub-channels by means of a proper handling of the signals at the transmitting and at the receiving antennas. An angular diversity in Space Division Multiple Access (SDMA) requires an angular separation of the users which is provided by the multiple paths where the electromagnetic waves follow from the transmitting array to the receiving one.

The earliest concepts regarding the capacity of MIMO communication systems were published in the seventies by Kaye and George [161] and Van Etten [162]. In 1987 J.H Winters [163], had proposed MIMO systems. He investigated the data rates of multiple antenna systems. In 1994, Paulraj and Kailath patented a system employing a "distributed transmission and a directional reception" [164]. Finally, in 1998, Foschini and Gans had stated the limits on the performances of MIMO systems [165]. A prototype of MIMO systems was first demonstrated at Bell Laboratories. Recently, theoretical and experimental published articles confirm the superior data rate, multipath fading reduction and co-channel interferences suppression. Moreover, nowadays, the trend for mobile terminals is to accommodate the increased number of wireless communication applications.

A printed diversity monopole antenna for 2.4 GHz (WLAN) band is investigated by T.Y. Wu [166]. Here, two orthogonal linear monopole antennas are placed symmetrically between T-shaped ground plane. This antenna has the isolation (S_{21}) $\leq$ -20 dB. It is capable of combating the multipath interference problem for WLAN operation.

An UWB diversity monopole antenna is presented by K.L. Wong [167]. The proposed antenna consists of two truncated square monopoles, orthogonally and symmet-

rically printed on the two sides of a T-shaped protruded ground plane. It is capable of operating in a very wide bandwidth, defined by a -10dB reflection coefficient, of about 108 % (about 2.3-7.7 GHz). Across the operating bandwidth, the antenna also shows good port isolation (S_{21}≤-20 dB) and can provide spatial diversity to combat the multipath fading problem. To compute the envelope correlation of an antenna diversity system, a simple formulation is derived by S. Blanch et al. [168]. Here, the envelope correlation is computed from the S-parameter description. This approach does not require the computation or the measurement of the radiation pattern of the antenna system. This technique provides a clear understanding of the effects of isolation and input match on the diversity performance of the antenna system.

M.A. Jensen et al. [169] have described a review for MIMO wireless communications systems. They have considered issues including channel capacity computation, channel measurement & modeling approaches, and the impact of antenna element properties for array configuration on system performance.

G. Chi et al. [170] have designed dual-band printed diversity antenna for WLAN 2.4/5.2 GHz operations. Here, two orthogonal C-shaped monopoles are placed symmetrically with respect to a protruding T-shaped ground plane. The antenna has the isolation (S_{21})≤-25 dB. The proposed antenna is capable of combating the multipath interference problem for WLAN operation.

A simple closed-form equation to calculate the envelope correlation between any two receiving or transmitting antennas in a MIMO system of an arbitrary number of elements is derived by J.Thaysen et al. [171]. The equation uses the scattering parameters obtained at the antenna feed point to calculate the envelope correlation coefficient.

A dual-band printed diversity antenna is designed by Y. Ding et al. [172]. This antenna consists of two back-to-back monopoles with symmetric configuration. A prototype of the antenna operated at UMTS (1920-2170 MHz) and 2.4-GHz WLAN (2400-2484 MHz) bands is provided to demonstrate the usability of the methodology in dual-band diversity antenna for mobile terminals. The measured bandwidths are 1.86-2.19 GHz and 2.40-2.49 GHz with acceptable isolation over the bandwidths.

S. Hong et al. [173] have designed a two-element diversity planar antenna for MIMO applications. This antenna provides wideband impedance matching characteristics over the desired frequency band by adopting two Y-shaped radiators. In order to reduce the mutual coupling between two radiating elements, three stubs are inserted in the ground plane. Its measured impedance bandwidth over 2.27-10.2 GHz for a reflection coefficient of less than -10dB is obtained.

A quad-band monopole antenna array for MIMO enabled wireless communication is presented by R.A. Bhatti et al. [174]. Here, a C-shaped slot and a T-shaped slit are used to excite three current modes for proposed antenna. It exhibits quite low isolation coefficient and reflection coefficient at the desired four frequency bands. The proposed dual-element antenna array operates at the following frequency bands: 2.4-2.5 GHz, 3.4-3.6 GHz, 5.15-5.35 GHz, and 5.75-5.875 GHz.

S. Zhang. et al. [175] have proposed a compact printed UWB MIMO/diversity antenna system (of two elements) with a size of 35×40 mm^2 operating at a frequency range of 3.1-10.6 GHz. The wideband isolation can be achieved through a tree-like structure on the ground plane.

S.W. Su [176] has proposed a high-gain, three-antenna systems suitable to be concealed inside wireless access points for MIMO applications in the WLAN 2.4/5.2/5.8 GHz bands. Here, the port isolation can be obtained together with high-gain and directional radiation characteristics. The calculated envelope correlation for this proposed antenna is less than 0.007 within the bands of interest.

A compact dual-band MIMO antenna with high port isolation is proposed by S. Cui et al. [177]. This antenna is basically composed of two folded monopoles and is designed to operate at 2.4/5.6 GHz frequency band. The high isolation is achieved by introducing two transmission lines on the top surface of the substrate and etching two slots on the ground.

J.F. Li et al. [56] have designed a compact wideband MIMO antenna. Here, two symmetric monopoles with edge-to-edge separation of nearly $0.083\lambda_0$ at 2.5 GHz and two bent slits are etched out from the ground plane. At the lower frequencies, the bent slits are used for reducing the mutual coupling and have slight effect on the

reflection coefficient. At the higher frequencies, the slits are used as slit antennas to enhance the impedance bandwidth because the two slits are couple-fed with two 50Ω microstrip lines.

Tri-band four-element MIMO antenna with high isolation is presented by J.F. Li et al. [178]. It consists of four symmetrical antenna elements. In this study, four rectangles have cut from the four corners of the ground plane to improve the operational bandwidth of the antenna. In addition, two kinds of isolation structures are introduced to reduce the isolation for the four antenna elements.

C.H. See et al. [179] have proposed a novel printed diversity monopole antenna for WiFi/WiMAX applications. This antenna comprises two crescent shaped radiators placed symmetrically with respect to a defected ground plane. A neutralization line is connected between them to achieve good impedance matching and low mutual coupling. Theoretical and experimental characteristics of this antenna exhibit an impedance bandwidth of 54.5% (over 2.4-4.2 GHz) with a reflection coefficient $<$ -10 dB and mutual coupling $<$ -17 dB.

A compact printed MIMO antenna for tetra band (GSM900/1800/1900/UMTS) mobile handset application is presented by Q. Zeng et al. [180]. It consists of two couple-fed loop antennas with symmetrical configuration. The edge-to-edge spacing between the two elements is only $0.03\lambda_0$ of 920 MHz. A slot and a dual inverted L-shaped ground branch are added in the ground plane to decrease the mutual coupling between the antenna elements. The measured isolation of the proposed antenna is better than -15dB among the four operating frequency bands.

Recently, frequency reconfigurable microstrip antenna operating at Digital TV and LTE bands with MIMO implementation is designed. This antenna is matched from 496-862 MHz (DTV) and LTE bands 3 & 7 from 1710-1880 MHz and 2500-2700 MHz, respectively for all considering S_{11}=-6dB matching criterion. The proposed antenna is designed by A.N. Kulkarni and S.K. Sharma [181].

2.7 Wideband Linear Antenna Arrays

A high gain antenna system is needed especially in certain applications such as microwave imaging, localization and/or radar applications. A single element antenna has relatively low gain of order of 3 or 4 dBi across the frequency band of operation. This can be improved using antenna arrays instead of just a single element. One important and critical problem in designing an antenna array system is the grating lobes. They appear, when the inter element spacing among antenna elements exceeds approximately the wavelength at the operating frequency. In order to avoid grating lobes at higher frequencies, this space should be kept smaller than a half wavelength at higher frequency.

A.A. Eldek et al. [182] have designed a wideband 16 × 4 element array of a microstrip-proximity-fed rectangular-slot antenna for marine radar systems operating in the X-band. A wideband corporate feed network is designed to feed the proposed array. The new design has a small size, a wide bandwidth of 52%, and good radiation characteristics in the entire operating band.

H.Z. Liu et al. [183] have designed a 2-element elliptical patch antenna array with a bidirectional radiation pattern for UWB communications. In this study, the array is constructed by feeding two elliptical patch elements using a 3-section hybrid power divider. The proposed antenna has a stable radiation pattern and a low return loss over a broad bandwidth of 64 % (3.1-6 GHz). Its measured gain is 2-3dB higher than that of the single element.

A 4-element antenna array for UWB application with satisfactory performances is proposed by P. Li et al. [184]. The array gain and radiation patterns are heavily dependent on the separation between the two adjacent elements. A gain of 13 dBi is obtained when the element separation is properly selected.

A 4-element cylindrical dielectric resonator (CDR) array is proposed by D. Guha et al. [185]. The impedance matching bandwidth of 29 % (S_{11}≤-10 dB) with monopole-like radiation pattern over the entire band are achieved with 4 dBi peak gain from a prototype occupying a very compact space measuring $0.6\lambda_0$ by $0.1\lambda_0$ approximately.

The measured results of a 2×2 microstrip line fed U-slot rectangular antenna array

are presented by H. Wang et al. [186]. An impedance bandwidth of 18% (VSWR<2) ranging from 5.65-6.78 GHz is achieved. The radiation performance including radiation pattern, cross polarization, and gain is also satisfactory within this bandwidth.

A novel planar antenna array based on four identical antenna elements for UWB applications is presented by Y.Y. Yang et al. [112]. This antenna array yields an impedance bandwidth of 3.1-10.6 GHz with VSWR<2. Over the entire bandwidths, it has constant high gain, which is about 6.5-10.5 dBi and a 60^0 beamwidth within the operational band.

A study of a UWB array antenna is presented by Y. Ito et al. [187], which is composed of leaf-shaped bowtie radiating elements printed on a dielectric substrate. With the use of a flat reflector, the presented antenna has unidirectional radiation characteristics and higher directivity in comparison with omnidirectional UWB antennas. The proposed antenna has the actual gain of 10.3-13.3 dB over the frequency range of 4.1-10.0 GHz.

The 2-element and 4-element planar antenna arrays with bidirectional radiation patterns based on identical antenna elements for UWB communication applications are proposed by O.M.H. Ahmed et al. [188]. The calculated gain of the 2-element and 4-element array is quite stable with about 3 and 6 dB higher than that of the single element, respectively. They also have stable radiation patterns with 60°, 3 dB beam-width through the entire UWB frequency spectrum.

C.H. Weng et al. [189] have investigated planar 2×2 microstrip array antenna with dual circular polarization (CP). This array can be reconfigured and operated with either the right-handed (RH) or left-handed (LH) CP by controlling the input state of the branch-line coupler. Good radiation properties across the operating band are also obtained so that the proposed array antenna is suitable for WLAN and WiMAX applications.

R.K. Mishra et al. [190] have proposed a 3-element planar antenna array with uniform and non-uniform spacing. In this study, the antenna with non uniform spacing uses the golden ratio with 2:1:1 corporate feeding.

An innovative 4-element array topology of microstrip E shaped patches for use in

WLAN applications is revisited and optimized using a novel PSO implementation by Z. Ma et al. [191]. In this study, the operating frequency range is from 3.4-3.8 GHz and the gain of the array is more than 13 dBi. Here, the main beam direction is normal to the ground plane.

R. Bayderkhani and H.R. Hassani [192] have investigated two unique techniques to increase the impedance bandwidth and reduce the sidelobe level (SLL) of printed antenna arrays. In the first, a printed tapered wide-slot antenna array fed by an array of printed patch elements placed above a metal reflector is introduced. The impedance bandwidth of this antenna array is 10.3-23.1 GHz, i.e, 76.6 %. By tapering the width, each of the slot elements, a very low SLL of 233.5 dB is obtained. The proposed antenna has stable radiation pattern over the range 14.7-17 GHz. The 3 dB gain bandwidth is 14.5 % with the front-to-back ratio (F/B) level of -40 dB. A low cross-polar component 245 dB at broadside and 235dB off-broadside direction is achieved. In the second technique, the length of the slot array elements is tapered in the form of an arc-shape to achieve further improvement in the SLL of the antenna array. This array is leading to an antenna array with very low SLL of 235 dB at a center frequency of 16.26 GHz, a wide bandwidth of 78.8 %, 20 dB SLL bandwidth of 8.8 %, and high F/B of 38 dB.

2.8 Summary

In this chapter, the state-of-art of wideband planar monopole antennas has been presented. It is started by describing the introduction of wideband technology and its advantages over future wireless communication system. It is followed by investigated research work related to wideband antenna design. The chapter also presents several research works related to UWB technology, reconfigurable antenna, MIMO antennas and wideband linear antenna arrays. It is found that the present communication systems need more compact and wideband antennas. Therefore, it motivates us to design and develop wideband fractal antennas.

CHAPTER 3

Fractal Monopole Wideband Antennas

3.1 Introduction

Wideband antennas are gaining prominence and becoming very important in modern wireless and mobile communication systems. These antennas avoid multiple band designs of narrow band elements and hence are simpler. Monopole antennas are popular in the area of wireless & mobile communication due to their simple structure and merits such as wide impedance bandwidth, omni-directional radiation patterns and moderate gain.

This chapter deals with the outcome of some experimental investigations performed on different types of fractal monopole antennas for wideband applications. The important design considerations throughout this study are reduction of effective patch area, frequency tuning by varying the antenna parameters to obtain wide impedance bandwidth.

This chapter is organized as follows. Section 3.2 presents the simulated and experimental results of a compact ACS-fed Koch curve fractal monopole antenna. A Hybrid fractal monopole antenna with combination of two fractal geometries (Koch curve and self-affine fractals) is presented in Section 3.3. Section 3.4 studies, a sectoral fractal monopole antenna. Modified sectoral fractal and semi-circle fractal monopole antennas are proposed in Section 3.6 and Section 3.6, respectively. Finally, conclusions and summary are in Section 3.7. Parametric studies are carried out for all proposed antennas to observe the effect of parameters on their performances investigated in the different subsections.

3.2 Koch Curve Fractal Monopole Antenna

An antenna structure based on Koch curve fractal geometry and Asymmetric Coplanar Waveguide (ACS) feeding technique for wideband wireless applications is studied in this Section. The ACS feeding technique [193, 194] is used to design a compact antenna. This feeding mechanism is analogous to the coplanar wave guide feed expect that the ACS feed has a single lateral ground strip compared with twin lateral strip in the CPW feeding. The Koch curve structure is applied to the upper side of the rectangular patch. The impedance bandwidth of 100.7 % from 2.6-7.88 GHz (2:1 VSWR) is observed.

Table 3.1: Dimensions of proposed ACS-fed Koch fractal monopole antenna.

L	W	a	W_f	α
37.5 mm	25.2 mm	24.3 mm	2.4 mm	60°
L_f	W_g	L_g	g	
15 mm	8.0 mm	13.0 mm	0.8 mm	

3.2.1 Antenna Geometry and Simulation Results

The graphical representation of Koch curve is shown in Figure 1.3 (chapter 1). It is based on IFS model (Section 1.2). The geometry of the proposed antenna is shown in Figure 3.1 and corresponding optimized parameters are listed in Table 3.1. Here, Koch fractal is considered on simple rectangular patch edges to achieve high impedance as well as to expand the antenna bandwidth. The proposed antenna is built on one side of a FR-4 dielectric substrate (thickness h_s=1.58 mm and relative permittivity (ϵ_r)= 4.4) of L×W with the ground size of W_g and L_g. It is fed by a 50Ω ACS feeding technique with the length (L_f) and width (W_f).

In Figure 3.1, the upper edge of the rectangular geometry is replaced by a Koch curve with iteration factor of 3. This is the first iteration of Koch fractal geometry. As the iteration number increases, the average electrical length of the patch also increases. However, after 2^{nd} iterations, the antenna design becomes quite complicated and its fabrication becomes difficult.

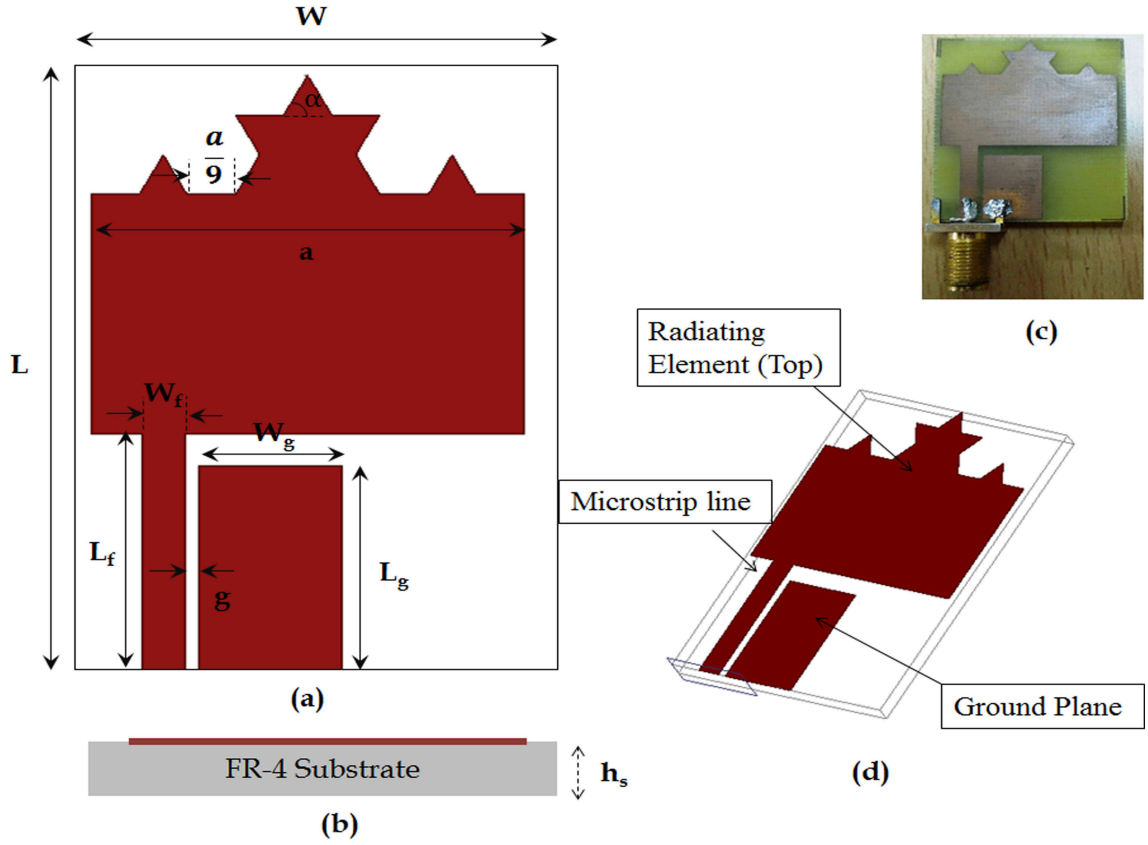

Figure 3.1: Geometry of ACS-Fed Koch fractal monopole antenna (a) Front view (b) Top view (c) Prototype (b) 3D view.

Figure 3.2 shows the simulated reflection coefficients of proposed antenna for different stages of iteration levels. It is observed from Figure 3.2 that when the number of iterations increase, the resonant frequency of the antenna slightly decreases and the antenna matches well for 2^{nd} iteration. The number of iterations of the Koch curve has been chosen after parametric analysis, i.e, the enough number of iterations in order to get high input impedance for wideband of frequency operations. Figure 3.3 shows the simulated reflection coefficients of the equilateral triangle size of Koch fractal shape, 'a'. As per expectation, the resonant frequency and the antenna reflection coefficients are changed with increase in the shape. It is noticed that the Koch fractal geometry improves the reflection coefficients at lower frequency along with the bandwidth enhancement when the size 'a' decreases. This observation shows that the reflection coefficient is improved with Koch size, $a = 24.3\ mm$.

Figure 3.4 explains the reflection coefficients of feed gap (g) between feed line. At

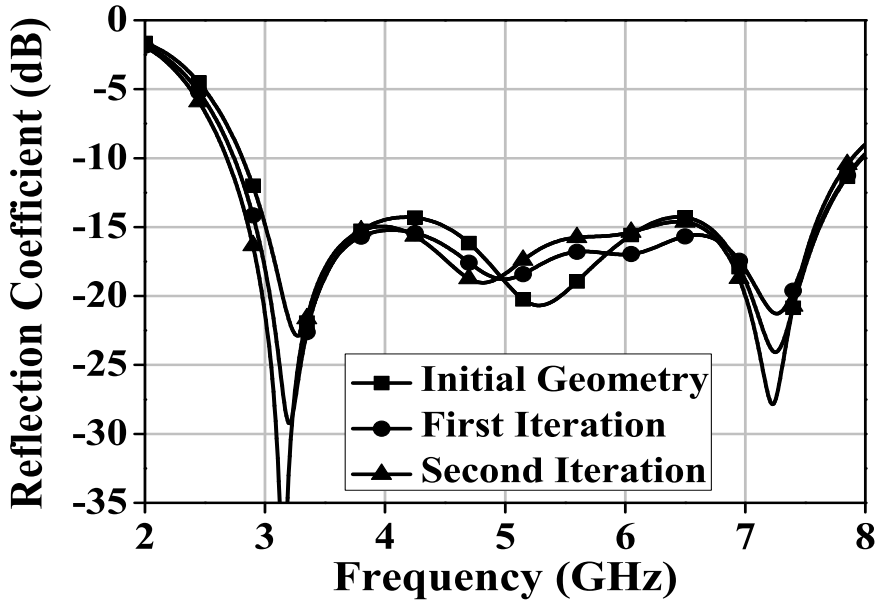

Figure 3.2: Reflection coefficients of ACS-fed Koch fractal monopole antenna for different iteration levels.

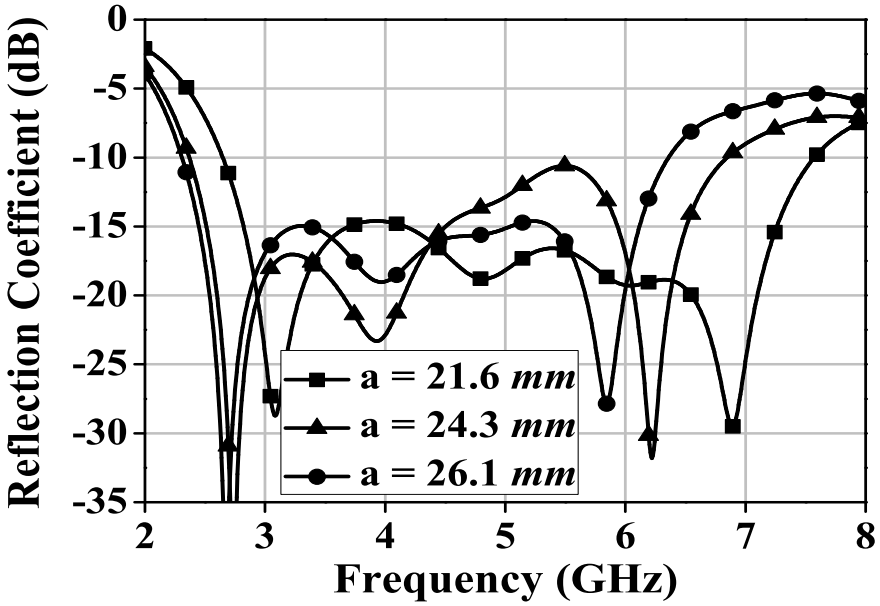

Figure 3.3: Reflection coefficients of ACS-fed Koch fractal monopole antenna for different sizes of Koch curve, 'a'.

$g = 0.8\ mm$ the impedance bandwidth is well matched to below -10 dB. Figure 3.5 shows the simulated reflection coefficients performance for ground size width, 'W_g'.

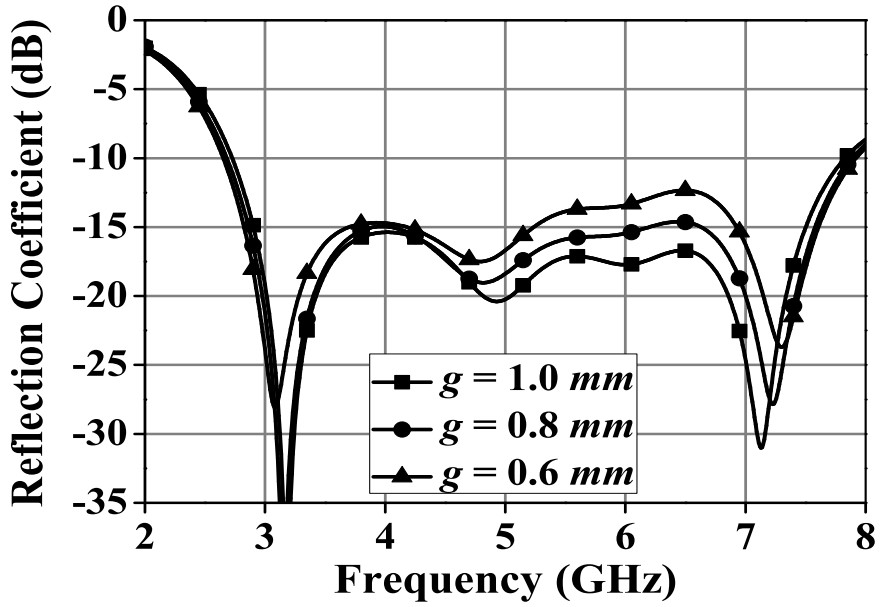

Figure 3.4: Reflection coefficients of ACS-fed Koch fractal monopole antenna for various feed gap, 'g'.

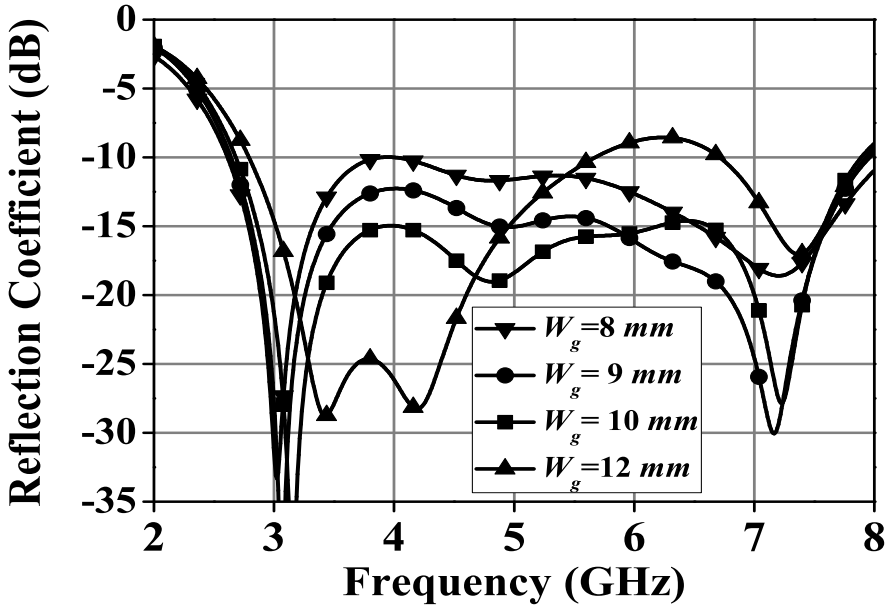

Figure 3.5: Reflection coefficients of ACS-fed Koch fractal monopole antenna for ground plane width, 'W_g'.

The width (W_g) has a prominent effect on the wideband operation of the proposed fractal antenna. As length (L_g) has almost negligible effect, therefore the length, L_g

= 13 mm, is fixed for this operation. It is observed that while increasing the width of ground plane, the resonant frequency decreases. At W_g= 10 mm the impedance bandwidth covers desired operating frequency bands. The above parametric studies show that the proposed antenna provides simulated impedance bandwidth from 2.6-7.88 GHz and resonant at 3.07 GHz and 7.30 GHz.

The reflection coefficient or the input impedance can only describe the behaviour of an antenna as a lumped load at the end of a feeding line. The surface current distributions show the different modes of propagation as well as variation of resonant frequencies. Similiary, the 3D radiation pattern describes the behaviour of antenna direction and gain. Figure 3.6 illustrates the simulated 3D radiation patterns and surface current distributions of proposed antenna at 3.07 GHz and 7.30 GHz. It shows that the patterns are omnidirectional in nature for wide band frequency. The current distribution in lower frequency covers feed line and left part of the Koch fractal curve whereas for higher frequency the current moves towards the right side of radiating element as well as covers whole radiating element.

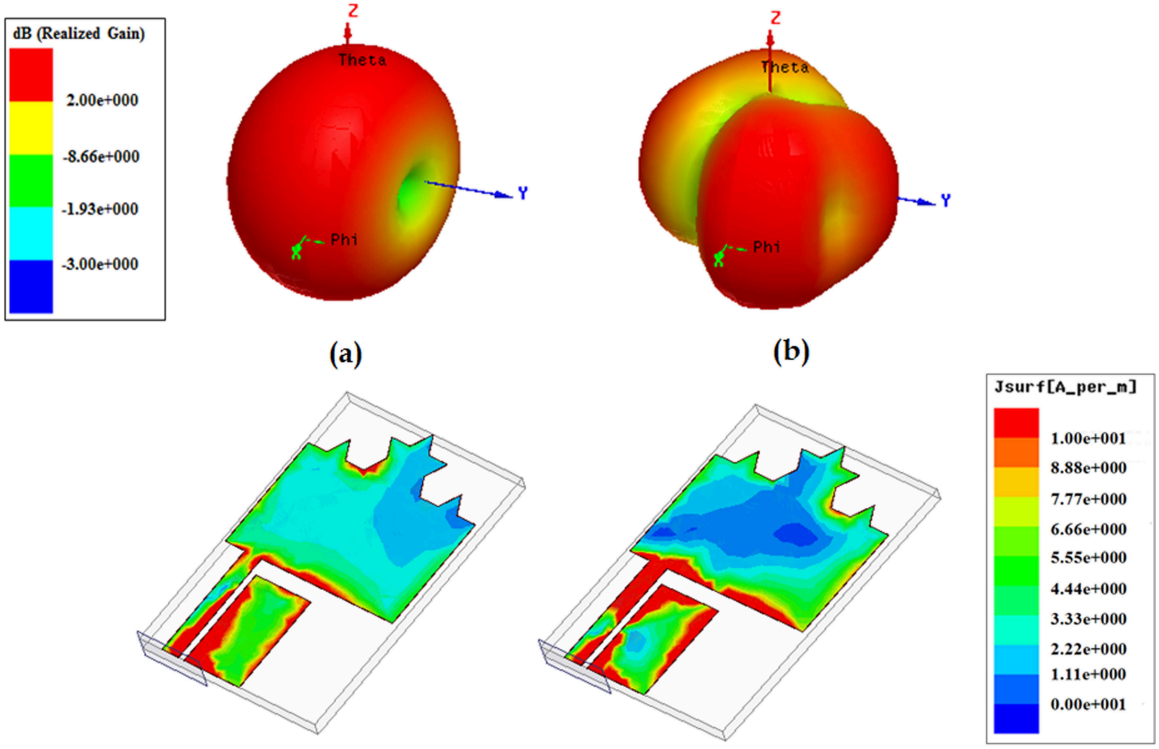

Figure 3.6: 3D radiation patterns and surface current distributions of proposed ACS-fed Koch fractal monopole antenna at (a) 3.07 GHz (b) 7.3 GHz.

3.2.2 Experimental Verification

A photograph of fabricated ACS-fed Koch fractal monopole antenna is shown in Figure 3.1 (c). The simulated and measured reflection coefficients of proposed antenna are plotted in Figure 3.7. The measured impedance bandwidth is well matched with simulated ones. The measured impedance bandwidth is of 100.7 % from 2.6-7.88 GHz with resonances at 3.1 GHz and 7.3 GHz. It covers several wireless bands like Wi-Fi 802.11y (3.6-3.7 GHz), WiMAX (3.4-3.6 GHz and 3.7-4.2 GHz) and WLAN 802.11 a (5.0-6.0 GHz). The antenna is tested experimentally in the Space Applications Center (SAC), ISRO, Ahmadabad, India. All measurements are carried out using Agilent vector network analyzer (model no. E8363B).

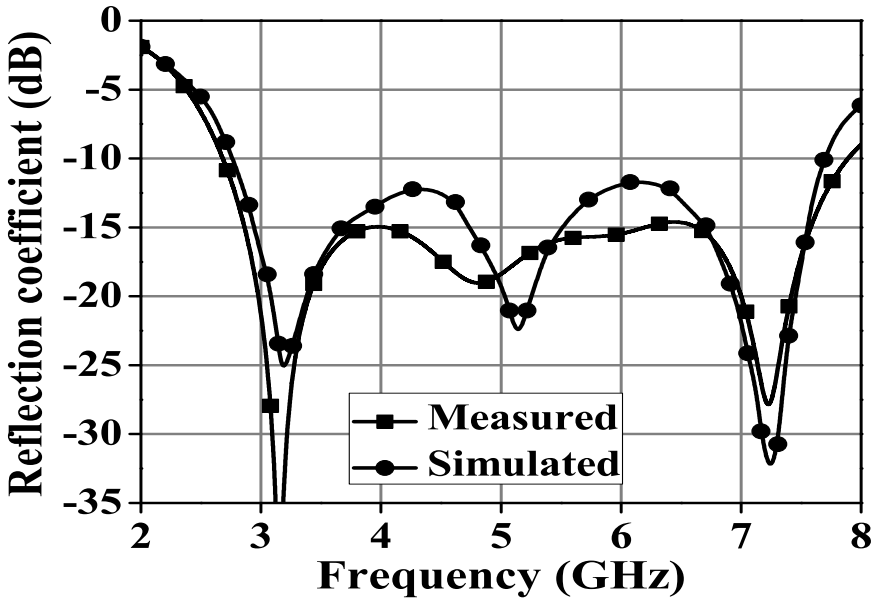

Figure 3.7: Simulated and measured reflection coefficients of proposed ACS-fed Koch fractal monopole antenna.

Table 3.2: Measured gain and simulated total antenna efficiency of proposed Koch fractal monopole antenna.

Frequency (GHz)	3.0	3.5	4.0	4.5	5.0	5.5	6.0	6.5	7.0
Gain (dBi)	0.81	2.58	2.85	3.18	3.45	3.70	4.42	4.18	2.36
Efficiency (%)	97.29	97.33	97.45	97.47	97.11	95.97	94.22	94.12	94.94

The measured E- and H- planes radiation patterns at 3.1 GHz and 7.3 GHz are

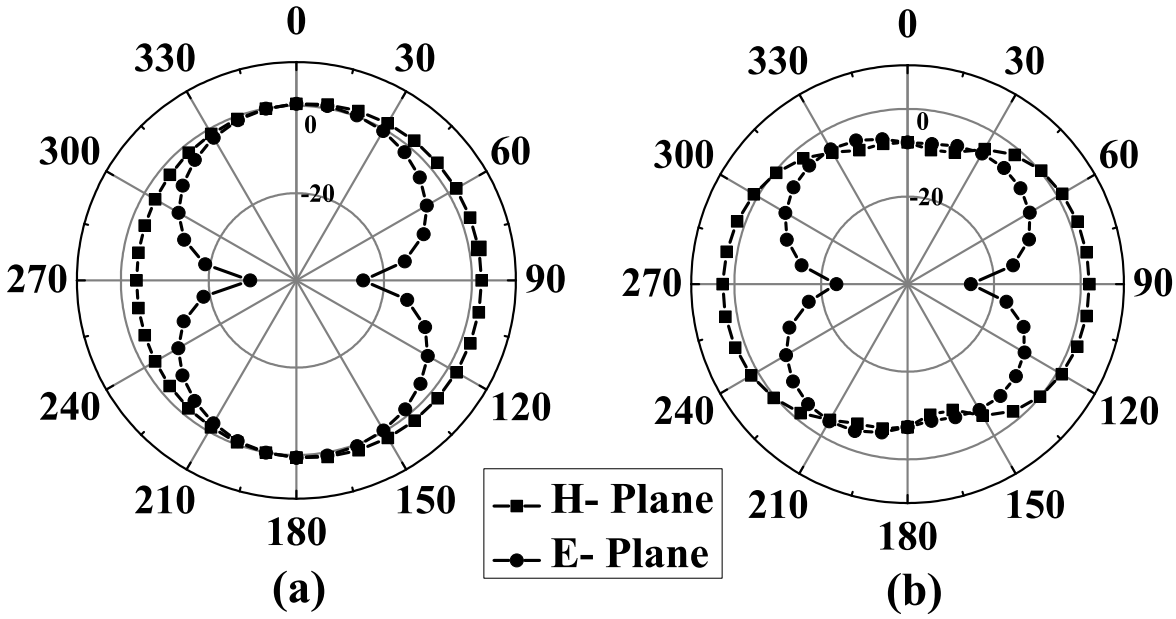

Figure 3.8: Measured radiation patterns for proposed ACS-fed Koch fractal monopole antenna (a) 3.1 GHz (b) 7.3 GHz.

shown in Figure 3.8. It can be noticed that in H-plane, the proposed antenna has fairly good omnidirectional radiation patterns. Similiary, in E-plane, the radiation patterns are like a small dipole leading to bidirectional patterns in the wide frequency band. Table 3.2 shows the measured gain and simulated total antenna efficiency at different frequencies. The measured peak realized gain of proposed antenna is 4.42 dBi at 6 GHz. The total antenna efficiency is observed more than 95 % throughout the band.

3.3 Hybrid Fractal Monopole Antenna

This Section presents a new antenna structure based on two fractal geometries for wideband applications, which are realized by the combination of Koch curve [31] and self-affine fractals shapes [61]. Basic antenna structure is a rectangular shape, fed by microstrip line [195]. The Koch curve structure is applied to the down edge of basic antenna shape and the self-affinity fractal property is implemented by cutting slot on the upper side of the patch respectively. The proposed model exhibits measured impedance bandwidth of 72.37 % over resonance in 1.6-3.4 GHz (VSWR=2:1) frequency band.

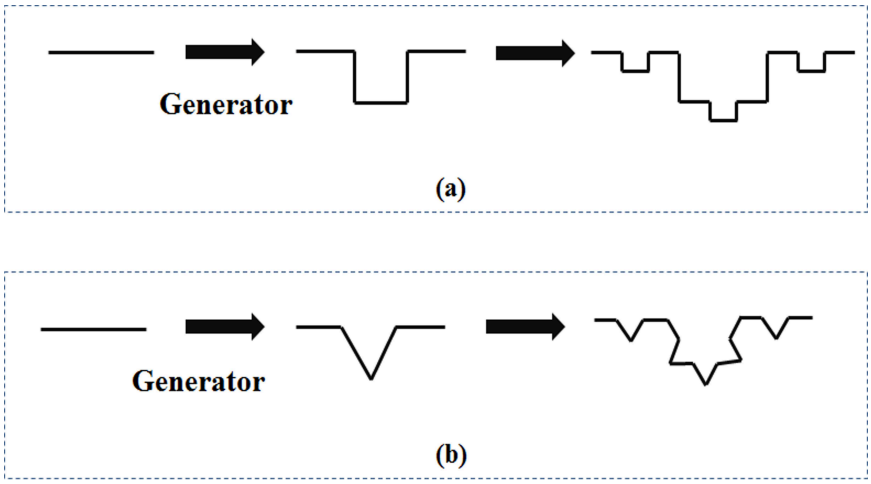

Figure 3.9: Recursive procedure for (a) Self-affine fractal and (b) Koch curve fractal.

3.3.1 Antenna Geometry and Simulation Results

The recursive procedure of Koch curve fractal and self-affine fractal is shown in Figure 3.9, which is applied to the edge of rectangular patch. The structure of the proposed hybrid fractal monopole antenna for wideband operation is shown in Figure 3.10 with corresponding optimized parameters, listed in Table 3.3.

Here, in order to expand the antenna bandwidth, two fractal properties are combined in a simple rectangular patch edges and fed by a 50 Ω microstrip line of width W_f. The proposed antenna is built on one side of a FR-4 dielectric substrate (thickness h_s=1.58 mm and relative permittivity (ϵ_r)= 4.4) of 66×27mm size. On the other side of the substrate, a rectangular ground plane of length 39 mm and width 27 mm is used as reflector element. As shown in Figure 3.10, for obtaining the proposed hybrid fractal antenna geometry, lower edge of the rectangular geometry is replaced by a Koch curve with iteration factor of 3. Upper edge of the geometry is replaced by cutting the self-affine fractal with scaling factor of 3 in the horizontal direction as well as by a factor of 2 in the vertical direction. This becomes the first iteration of hybrid geometry. As the iteration number increases, the average electrical length of the patch also increases, just like the inductive loading and slot loading techniques reported in [196, 197]. Hence, it lowers the resonant frequency of the proposed patch antenna. However, for iterations more than 2^{nd}, the reduction of operating frequency is not achieved. The configuration of proposed hybrid fractal geometry becomes quite

unwieldy for more than 2^{nd} iteration. This procedure is known as iterated function system (IFS) (Section 1.2).

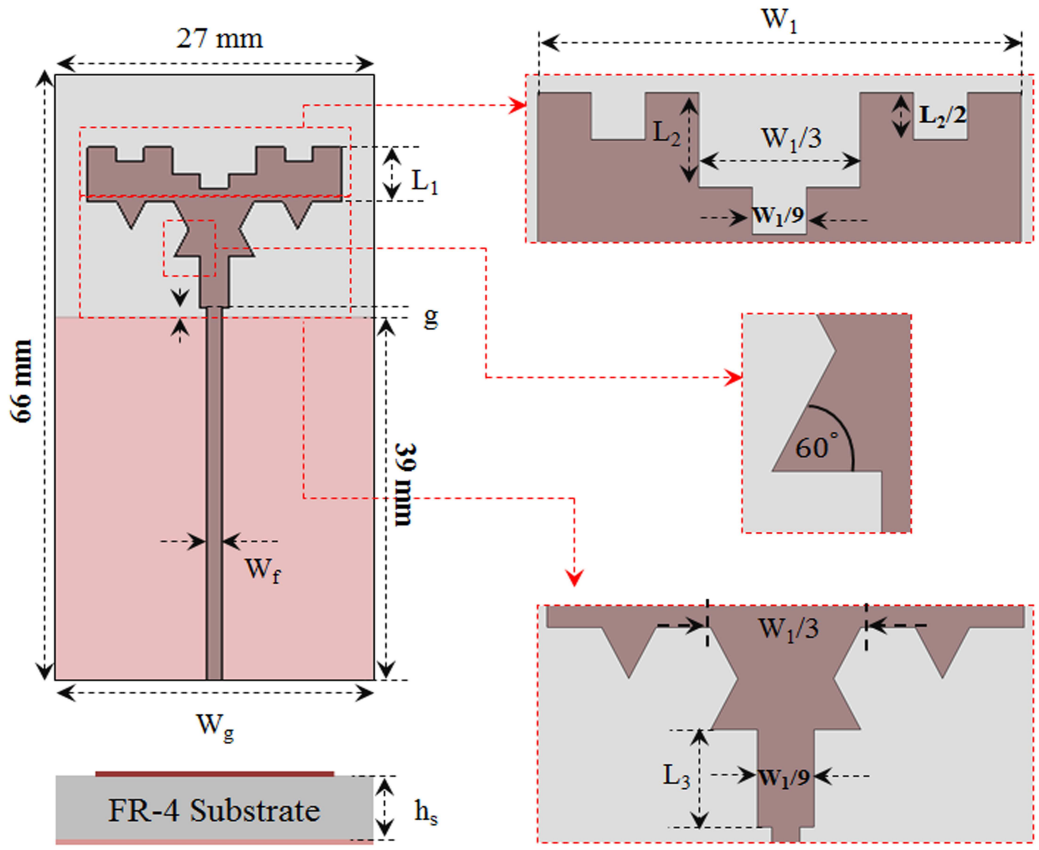

Figure 3.10: Geometry of proposed hybrid fractal monopole antenna.

Table 3.3: Dimensions of proposed hybrid fractal monopole antenna.

L_1	L_2	L_3	W_1
5.8 mm	2.9 mm	5.5 mm	25.4 mm
W_g	W_f	h_s	g
27 mm	1.5 mm	1.58 mm	1.0 mm

Figure 3.11 shows the simulated reflection coefficients of hybrid fractal monopole antenna for different iteration levels. It is perceived that when the number of iteration increases upto 2, the impedance matching and bandwidth are proper as compared to iteration 0 and 1. It creates resonances at 1.9 GHz and 3.1 GHz frequency. Figure 3.12 shows the simulated reflection coefficients for different sizes of the radiating element (L_1). It is found that when the size of the radiating element (L_1) decreases, the

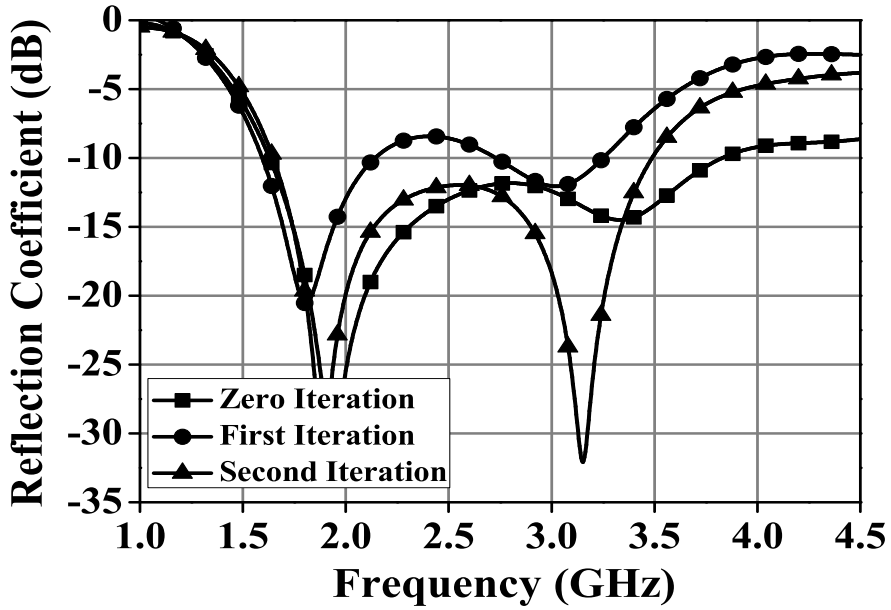

Figure 3.11: Reflection coefficients of proposed hybrid fractal monopole antenna at different iteration levels.

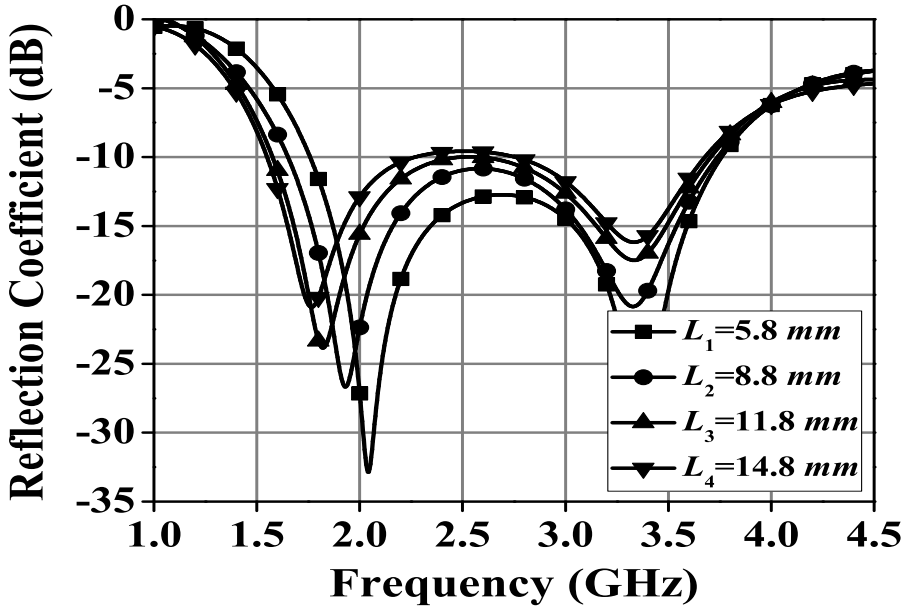

Figure 3.12: Reflection coefficients of proposed hybrid fractal monopole antenna for different heights, 'L_1'.

impedance matching at the lower frequencies improve. For L_1=5.8 mm the bandwidth of hybrid fractal antenna is 72 % over 1.6-3.4 GHz frequency range. Optimum per-

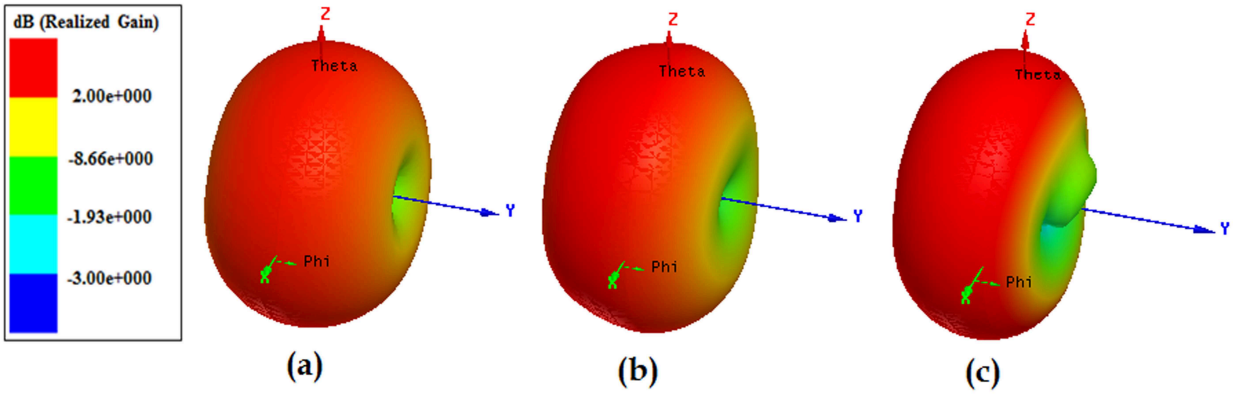

Figure 3.13: 3D radiation patterns of proposed hybrid fractal monopole antenna at (a) 1.9 GHz (b) 2.7 GHz (c) 3.07 GHz.

formance is obtained in terms of compact size and broad bandwidth of the proposed antenna, keeping other parameters fixed.

Figure 3.13 shows the simulated 3D radiation patterns at 1.9 GHz, 2.7 GHz and 3.07 GHz for the proposed antenna. It has been observed that the antenna is showing omnidirectional property with gain more than 2 dBi for wide frequency band.

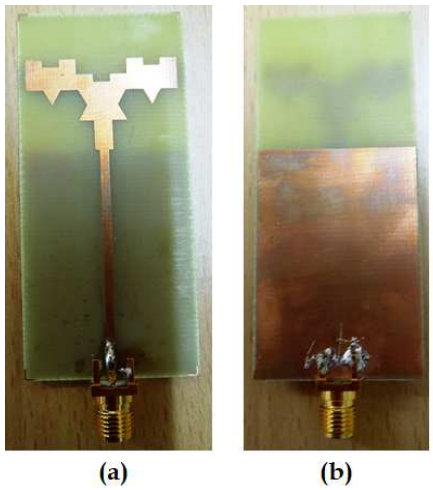

Figure 3.14: Photograph of proposed hybrid fractal monopole antenna (a) Front view (b) Rear view.

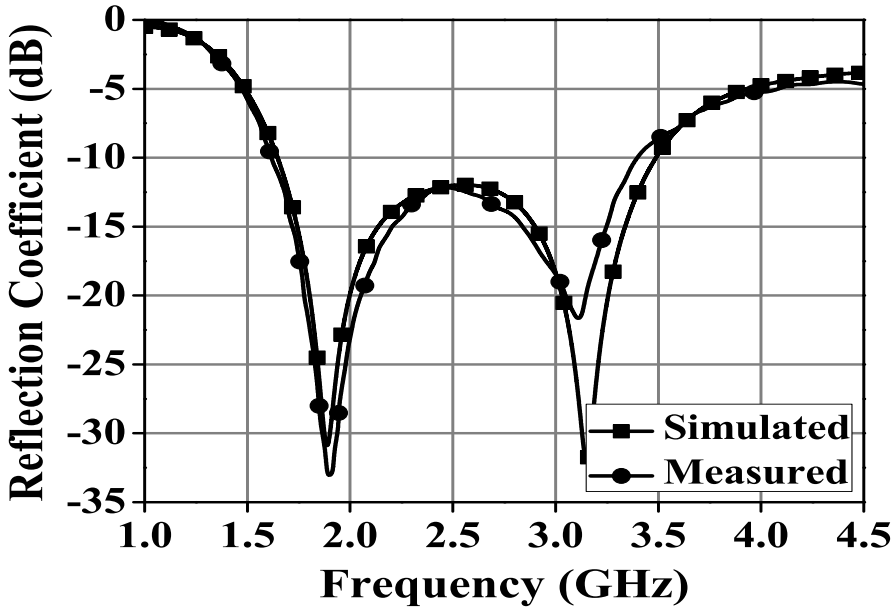

Figure 3.15: Simulated and measured reflection coefficients of proposed hybrid fractal monopole antenna.

3.3.2 Experimental Verification

The photographs of the proposed hybrid fractal monopole antenna are shown in Figure 3.14. The antenna reflection coefficients are plotted in Figure 3.15. It shows a good agreement between simulated and measurement results. The -10 dB measured impedance bandwidth is spans 1.6-3.4 GHz with resonances at 1.9 GHz and 3.1 GHz. Thus the antenna covers wireless bands like DCS-1800 (1.71-1.88 GHz), PCS-1800 (1.80-1.99 GHz), UMTS (1.92-2.17 GHz), IMT-2000 (1.9-2.2 GHz), WiBro (2.3-2.4 GHz), Bluetooth (2.4-2.48 GHz), WLAN 802.11 (2.4-2.485 GHz) and WiFi. The proposed antenna is tested experimentally in the Space Applications Center (SAC), ISRO, Ahmadabad, India.

The measured E- plane (XZ, Co-pol. and Cross-pol.)and H-plane (YZ, Co-pol. and Cross-pol.)radiation patterns at three frequencies, 1.9 GHz and 3.1 GHz are shown in Figure 3.16. The antenna radiation patterns are omnidirectional in lower resonant frequency band and nearly omnidirectional in higher resonant frequency band. The distortion of radiation pattern in higher frequency is caused by unequal phase distribution of electric field on the fractal slot and the magnitudes of higher order modes.

In addition, it can be observed that the cross polar component is quite low. At the beam peak, the designed antenna has maximum co-pol. gain within operating bandwidth. Table 3.4 shows the measured gain and total efficiency at different frequencies. The maximum peak realized gains in the two resonant frequencies are 2.58 dBi (at 1.9 GHz) and 4.18 dBi (at 3.1 GHz). The simulated total antenna efficiency is found to be more than 75 % throughout the band.

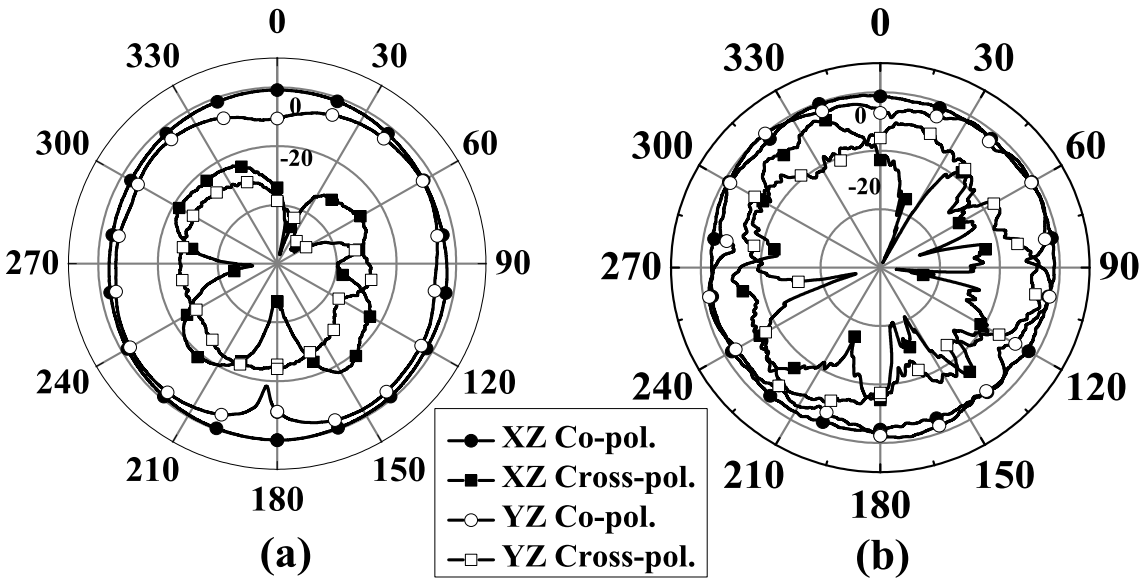

Figure 3.16: Measured radiation patterns of hybrid fractal monopole antenna at (a) 1.9 GHz (b) 3.1 GHz.

Table 3.4: Measured gain and simulated total antenna efficiency of proposed hybrid fractal monopole antenna.

Frequency (GHz)	1.6	2.0	2.5	3.0	3.5
Gain (dBi)	0.67	2.67	3.56	4.48	4.35
Efficiency (%)	75.2	89.56	87.90	86.34	84.26

3.4 Sectoral Fractal Monopole Antenna

The sectoral fractal monopole antenna is derived from Sierpinski fractal antenna [27, 29, 40]. Sierpinski is one of the earliest reported fractal antenna geometry with multiband characteristics and gradual tapering of the inner and outer conductors of a

coaxial transmission lines. Theoretically, the monopole antennas can be of any shape for broad operating bandwidth [7]. Small and gradual discontinuities are desired for a reflection less transducer action over wide frequencies. The proposed fractal antenna in this section operates efficiently over a wide frequency band. For better understanding of the antenna characteristics, the reflection coefficient (S_{11}) curves are plotted in decibel or dB scale, i.e. (S_{11} dB = 20 log$|S_{11}|$ = -Return loss (RL). A parametric study is carried out to investigate the effect of physical parameters on antenna.

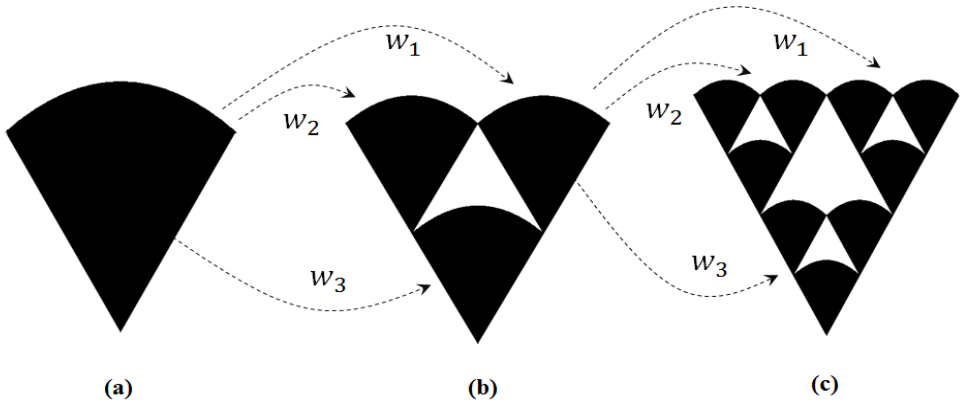

Figure 3.17: Stages of the IFS that generates the sectoral fractal geometry (a) Basic geometry (b) First iteration (c) Second iteration.

3.4.1 Antenna Geometry and Simulation Results

The overall graphical representation of recursive procedure for proposed sectoral geometry is shown in Figure 3.17. The proposed geometry is based on IFS model (Section 1.2). The scale factor in transformation is identical leading to geometrically identical copies of original.

The geometry of the proposed sectoral fractal monopole antenna is shown in Figure 3.18 and corresponding optimized parameters are listed in Table 3.5. The antenna is printed on an 27×35 mm^2 dielectric substrate. The radiating element is fed by a 50Ω microstrip feed line with the width W_f=1.5 mm. The substrate used in the proposed design is FR-4 with thickness, h_s=1.58 mm, relative permittivity, ϵ_r = 4.4 and loss tangent, tanδ = 0.005. A finite ground plane of length 20.84 mm and width 27 mm

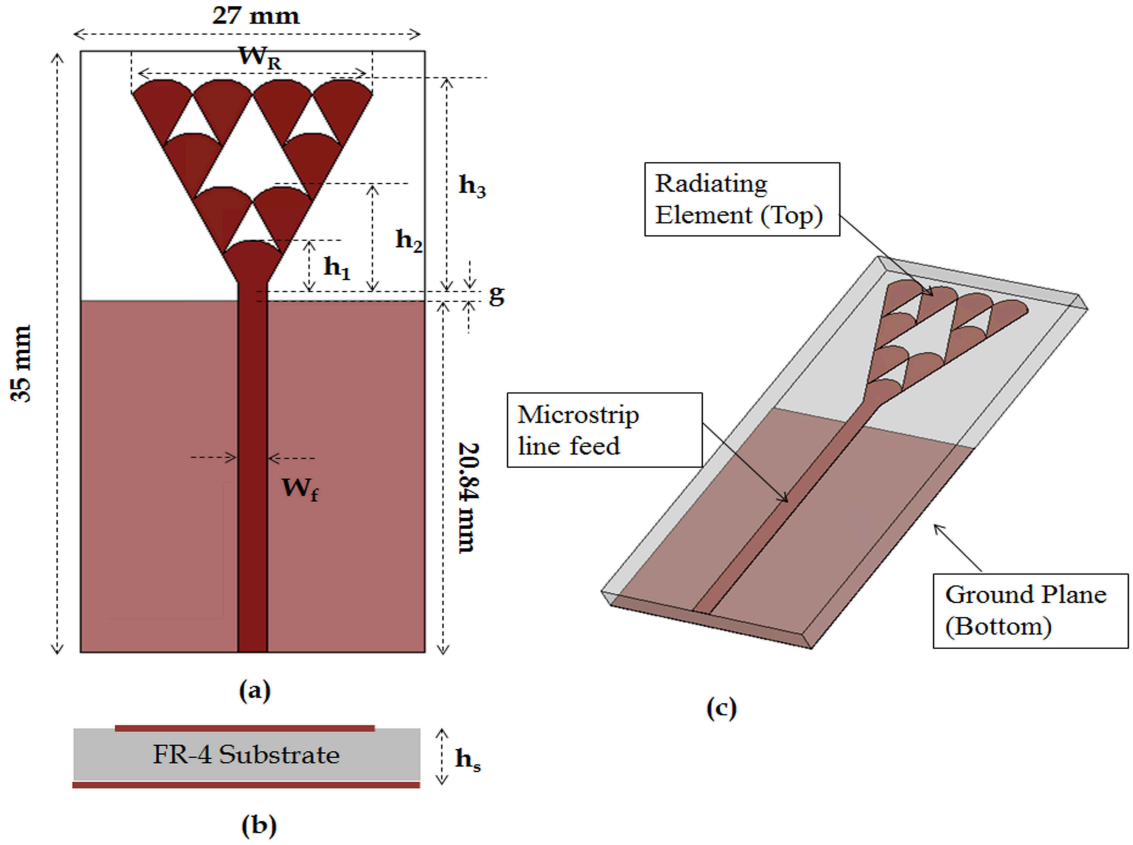

Figure 3.18: Geometry of sectoral fractal monopole antenna (a) Front view (b) Top view (c) 3D view.

is printed on the other side of the substrate. The feed gap width between the ground plane and the radiating patch 'g', is a very critical parameter for impedance matching purposes.

Figure 3.19 shows the simulated antenna reflection coefficients (20 log $|S_{11}|$) curves for basic Sierpinski fractal antenna, triangular antenna and the proposed sectoral fractal antenna. It can be noticed, that in case of Sierpinski and triangle antenna, the reflection coefficient is $\geq$ -10 dB. However, in case of the sectoral fractal antenna it covers bandwidth from 3.2-6.5 GHz ($S_{11}\leq$-10dB).

Table 3.5: Dimensions of the proposed sectoral fractal monopole antenna.

h_1	h_2	h_3	W_f	W_R	g
4 mm	7.12 mm	13.36 mm	1.5 mm	12.47 mm	0.16 mm

Figure 3.20 shows the simulated reflection coefficients for different iteration levels

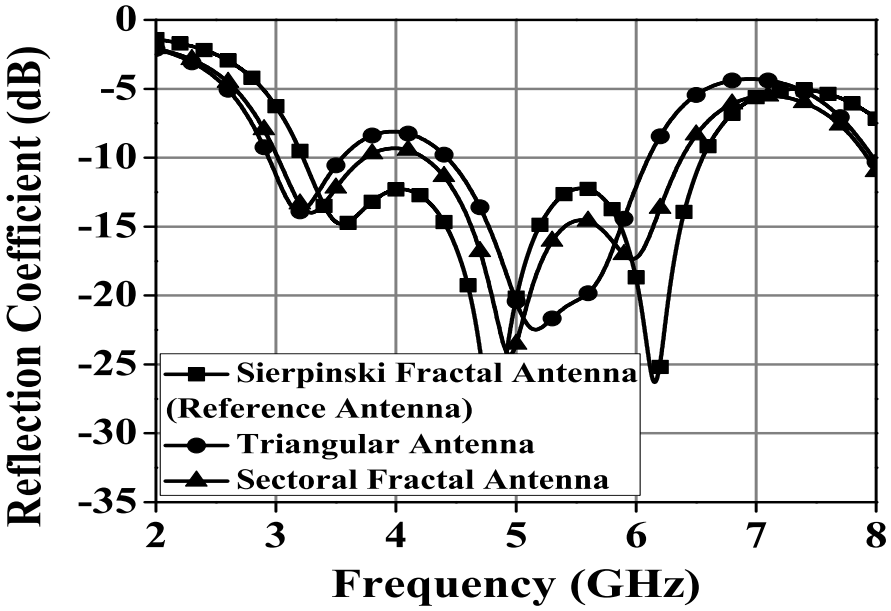

Figure 3.19: Reflection coefficients of triangular antenna, Sierpinski fractal antenna and proposed sectoral fractal antenna.

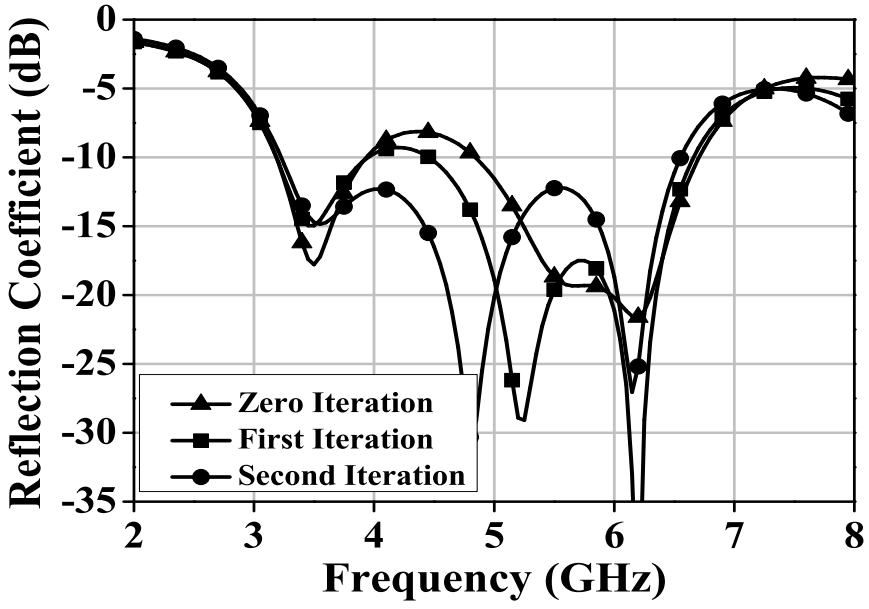

Figure 3.20: Reflection coefficients of proposed sectoral monopole antenna at different iteration levels.

of the proposed antenna. It can be found that, with increase in number of iterations (up to second) the resonant frequency shifts towards the lower resonance whereas the

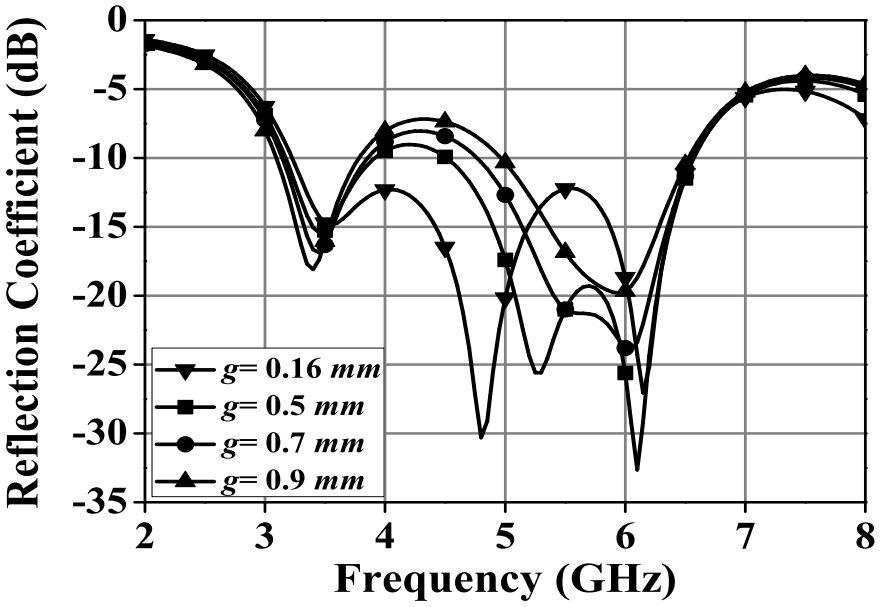

Figure 3.21: Reflection coefficients of proposed sectoral monopole antenna at different feed gap widths, 'g'.

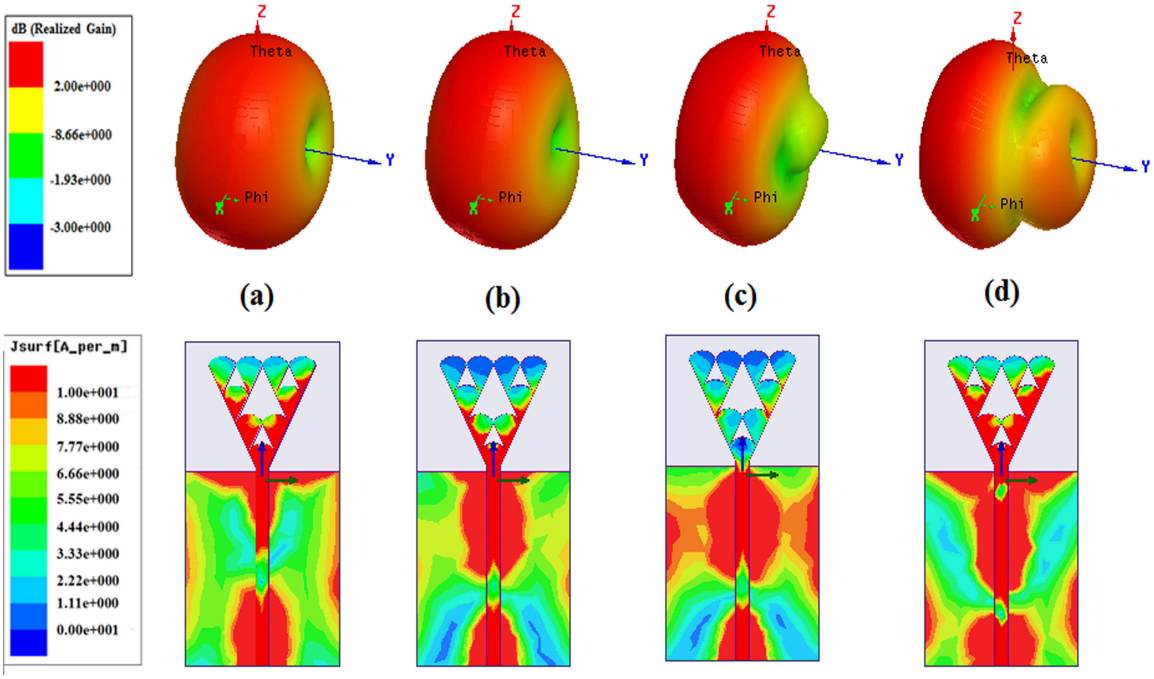

Figure 3.22: 3D radiation patterns and simulated surface current distributions on sectoral fractal monopole antenna at (a) 3.5 GHz, (b) 4.5 GHz, (c) 5.5 GHz and (d) 6.5 GHz.

impedance matching as well as impedance bandwidth improves. However, more than 2^{nd} iteration, the operating frequency can not be achieved since the antenna becomes quite complicated. Figure 3.21 shows the simulated reflection coefficients for effect of feed gap, 'g'. It is clear from the Figure 3.21 that maximum impedance bandwidth can be achieved by tuning the feed gap, g. At g=0.16 mm, the reflection coefficient is well below -10 dB.

The surface current distribution and simulated 3D radiation patterns are plotted in Figure 3.22. Here, surface current is mainly distributed on the conductor edges of the radiator and rectangular ground, which gives an indication about the dependence of antenna geometry on the resonant frequencies. At 3.5 GHz and 4.5 GHz resonance frequencies, the distributions are nearly similar. The antenna has a dipole like behavior whereas the current is oscillating and a pure standing wave pattern along most part of the sectoral edges. This is ascertained by their doughnut shaped radiation patterns. However, the distribution is more confined in the gap between radiator and ground edges near the feed at the second resonance. The distributions at 5.5 GHz and 6.5 GHz indicate the fundamental resonating modes. Animations at 5.5 GHz shows that the current is travelling along the feed line and in the ground plane, but oscillating at the top edge. The radiation patterns also appear to loose its omni-directionality in the XY plane at 5.5 GHz and 6.5 GHz. It can be concluded from these observations that the gain of proposed antenna is more than 2 dBi. The 3D radiation patterns are omnidirectional at the lower side of the operating band whereas nearly omnidirectional at higher frequencies.

3.4.2 Experimental Verification

A prototype of the microstrip line feed sectoral monopole antenna with optimized dimensions is fabricated and shown in Figure 3.23. It is tested experimentally in the Space Applications Center (SAC), ISRO, Ahmadabad, India. All scattering parameters measurement are carried out using Agilent vector network vnalyzer (model no. E8363B). Figure 3.24 shows the simulated and measured reflection coefficient plots of the proposed antenna. It is observed that the simulation and measurement results are in good agreement with wide impedance bandwidth. Here, the measured

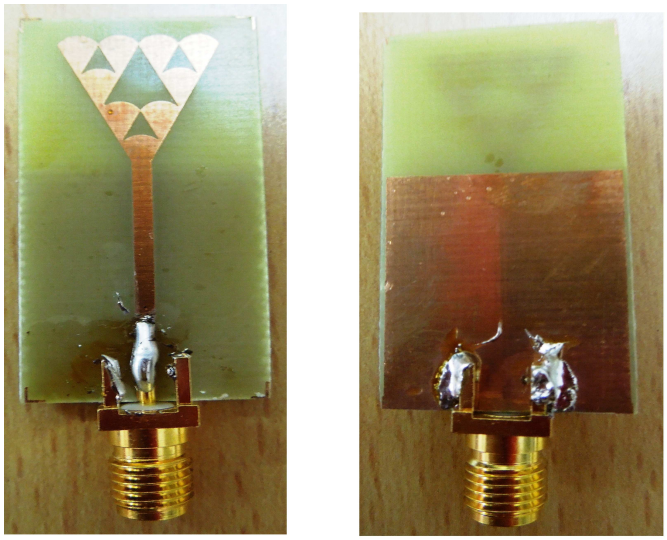

Figure 3.23: Photograph of fabricated sectoral fractal monopole antenna (a) Front view (b) Rear view.

-10 dB impedance bandwidth of 68.04% (3.22-6.55 GHz) is observed. The measured bandwidth meets the requirements of many commercial bands such as Wi-Fi 802.11y (3.6-3.7 GHz), WiMAX (3.4-3.6 GHz and 3.7-4.2 GHz) and WLAN 802.11 (5.31-6.32 GHz).

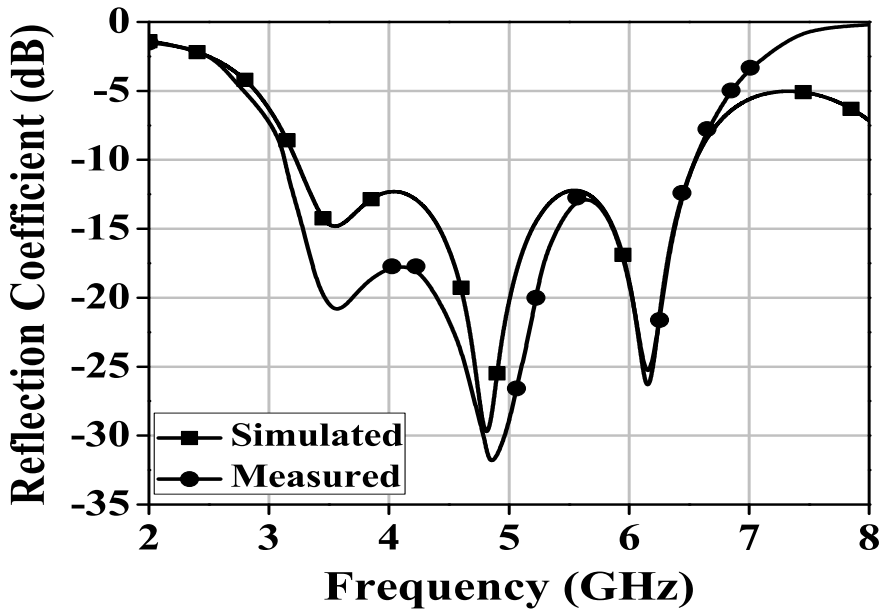

Figure 3.24: Simulated and measured reflection coefficients of proposed sectoral fractal monopole antenna.

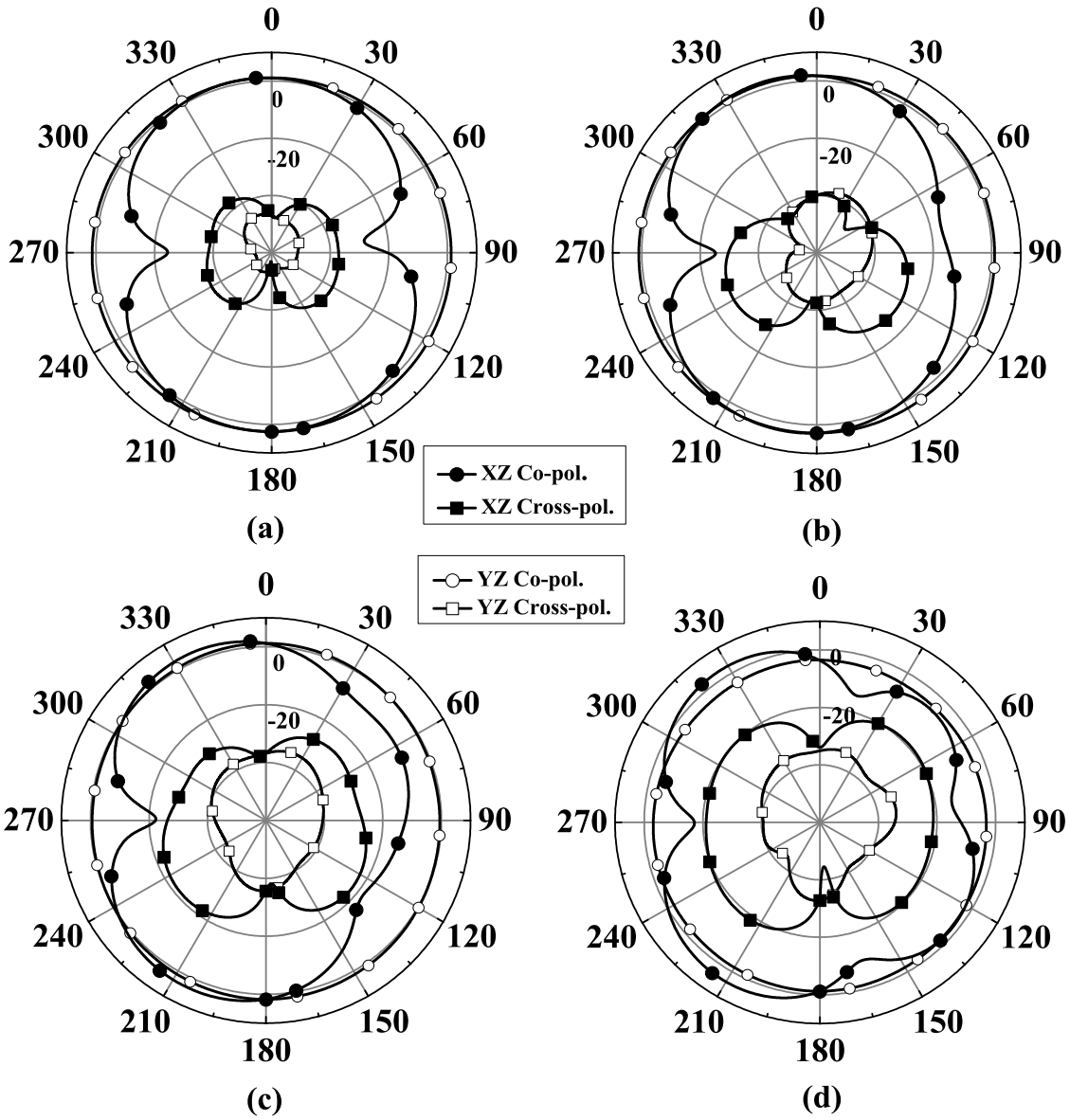

Figure 3.25: Measured radiation patterns of sectoral fractal monopole antenna at (a) 3.5 GHz, (b) 4.5 GHz, (c) 5.5 GHz and (d) 6.5 GHz.

Figure 3.25 shows the measured E- and H- planes radiation patterns at 3.5 GHz, 4.5 GHz, 5.5 GHz and 6.5 GHz. The radiation patterns are like stable monopole and almost omnidirectional in XZ (Co-pol. and Cross-pol.) and YZ (Co-pol. and Cross-pol.) planes. However, there are some ripples and discrepancies in the measured radiation patterns, especially at the higher frequencies. This discrepancies may be due to sensitivity and accuracy of the measuring devices at higher frequencies or the difference in current distributions on the sectoral patch element. Table 3.6 shows the

measured peak realized gain and simulated total efficiency at different frequencies. The maximum peak realized gains at two resonant frequencies are 2.60 dBi (at 3.55 GHz) and 4.35 dBi (at 6.15 GHz). The total simulated antenna efficiency including all losses is found to be more than 80 % throughout the band.

Table 3.6: Measured gain and simulated total antenna efficiency of proposed sectoral monopole antenna.

Frequency (GHz)	3.5	4.0	4.5	5.0	5.5	6.0	6.5
Gain (dBi)	2.58	2.85	3.18	3.45	3.70	4.42	4.18
Efficiency (%)	90.63	87.93	90.61	91.83	87.23	90.33	80.34

3.5 Modified Sectoral Fractal Monopole Antenna

In this section, a microstrip line fed modified sectoral fractal monopole antenna operating over dual wideband frequencies is investigated. The proposed antenna model exhibits resonances impedance bandwidth of 76.6 % (1.51-3.39 GHz) for band 1 and 17.3 % for band 2. This antenna is compact and is suitable for wireless communication devices owing to its features like easy fabrication and circuit integration.

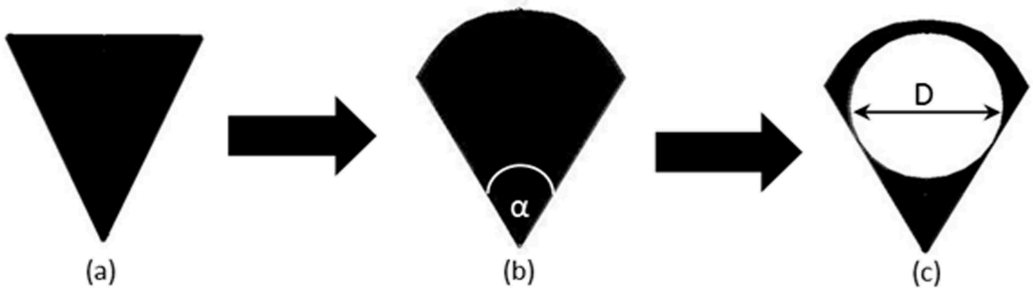

Figure 3.26: Basic antenna design procedure (a) Basic triangle (b) Sectoral shape (c) Sectoral inscribing a circular gap.

3.5.1 Antenna Geometry and Simulation Results

The design procedure of sectoral geometry is discussed in previous section. Graphical representation of modification in the sectoral geometry and configuration of the modified sectoral fractal monopole antenna for dual-wideband band operation is illustrated in Figure 3.26 and Figure 3.27 respectively. The corresponding optimized parameters are listed in Table 3.7.

Table 3.7: Dimensions of proposed modified sectoral fractal monopole antenna.

h_1	h_2	h_3	h_s	W_f
8 mm	13.74 mm	25.24 mm	1.58 mm	1.5 mm
W_R	S	D	g	
26.56 mm	26.55 mm	2.5 mm	0.3 mm	

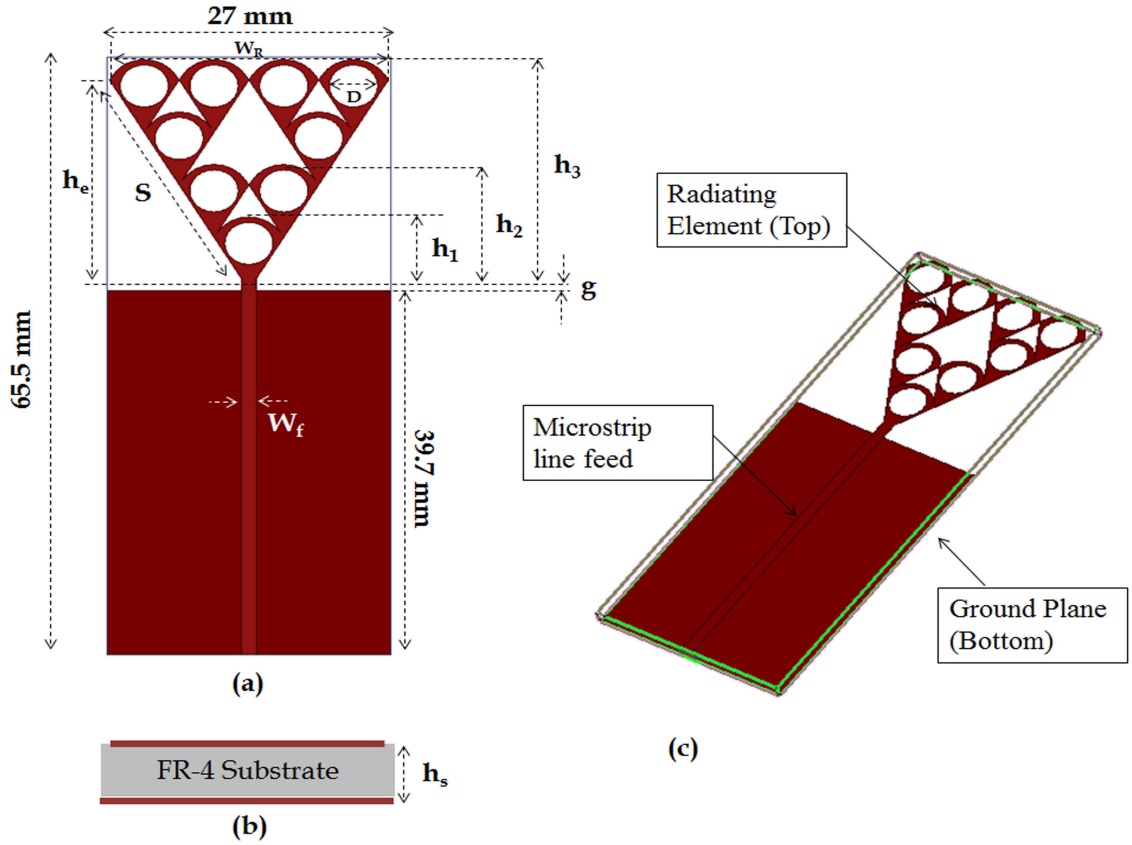

Figure 3.27: Geometry of modified sectoral fractal monopole antenna (a) Front view (b) Top view (c) 3D view.

The proposed antenna consists of two metallic layers with the radiating element printed on top side and fed by 50 Ω microstrip line, which is over the ground plane and bottom of the substrate. The selected substrate is FR-4 with dielectric constant ϵ_r= 4.4. The thickness of the substrate is h_s=1.58 mm, and tanδ=0.005.

Figure 3.28 shows the reflection coefficients for different stages of fractal geometries (Sierpinski, sectoral and modified sectoral). It is perceived that the Sierpinski fractal antenna shows multi-resonance behavior. When all the triangles of perturbed fractal antenna are converted into sectoral shapes, multi-resonances occur at 1.76 GHz, 3.18

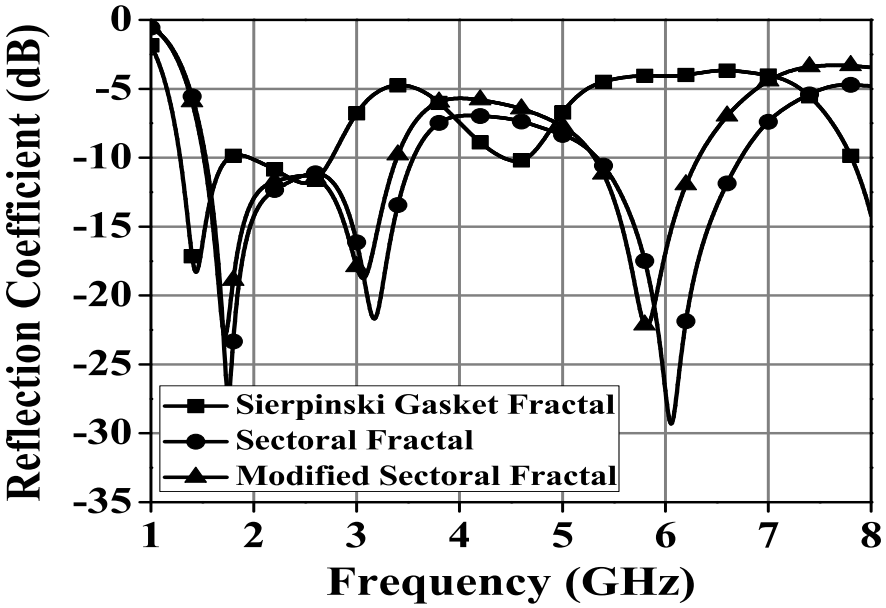

Figure 3.28: Reflection coefficients of Sierpinski fractal antenna, sectoral fractal antenna, and proposed modified sectoral fractal antenna.

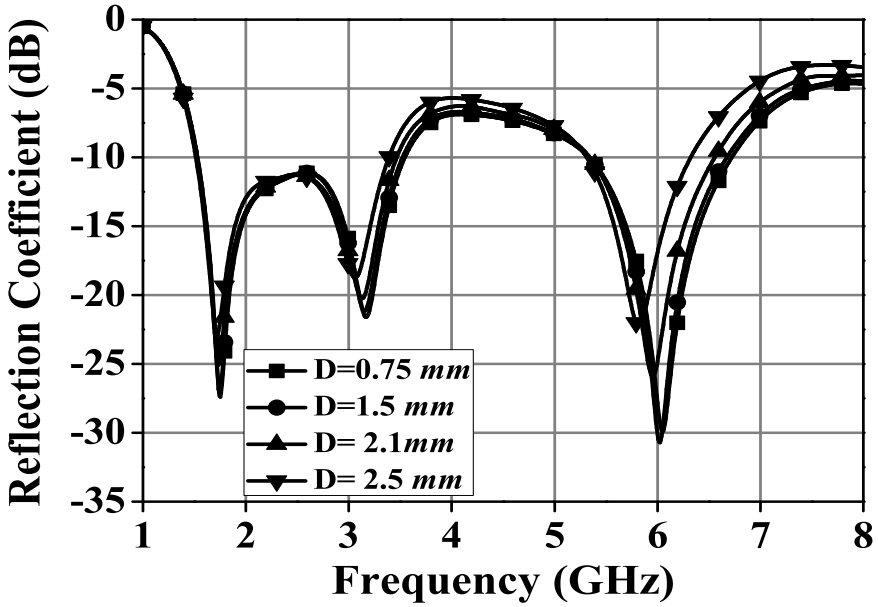

Figure 3.29: Reflection coefficients of proposed modified sectoral monopole antenna with different diameters of inscribing circle, 'D'.

GHz, and 6.06 GHz. However, 6.06 GHz is not approved by FCC for WLAN and needs to be notched out. Finally, circles are etched out from the center of all sectoral

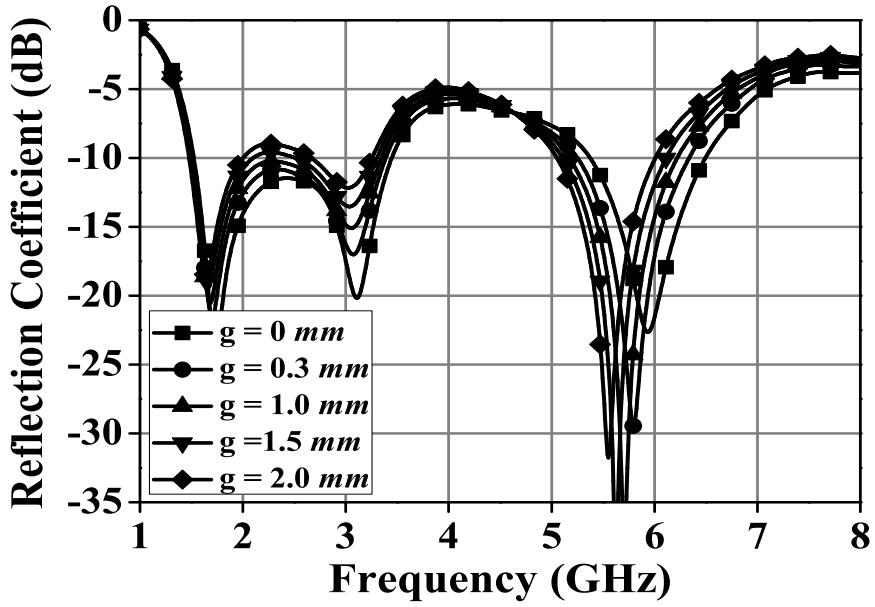

Figure 3.30: Reflection coefficients of proposed modified sectoral monopole antenna with different feed gap widths, 'g'.

fractal shaped geometries and resonant frequencies are shifted to 1.72 GHz, 3.07 GHz, and 5.8 GHz. It is observed that the downward shift in resonant frequency for initial structure is more comparable with the modified antenna structure.

Figure 3.29 demonstrates the parametric study of circle with different diameters 'D'. It is found that when the diameter of the circle is increased upto the optimum point (D=2.5 mm), upper frequency shifts from 6.06 GHz to 5.8 GHz and impedance bandwidth of 17.3% is observed at 5.8 GHz frequency. Similiary, Figure 3.30 demonstrates the parametric study with different values of feed gap 'g'. The feed gap (g) plays an important role for determining the characteristics impedance of the antenna. It is observed that resonance frequency is shifted towards lower frequency band and impedance matching occurs. This is due to coupling between the feed gap and radiating element.

Circular slots are etched out from the radiating element as a result of which surface area of the element reduces. This is a challenging task to the antenna engineers. This can be done by analyzing the antenna surface current distributions. Figure 3.31 shows the current distribution and simulated 3D radiation patterns at 1.7 GHz, 3.07

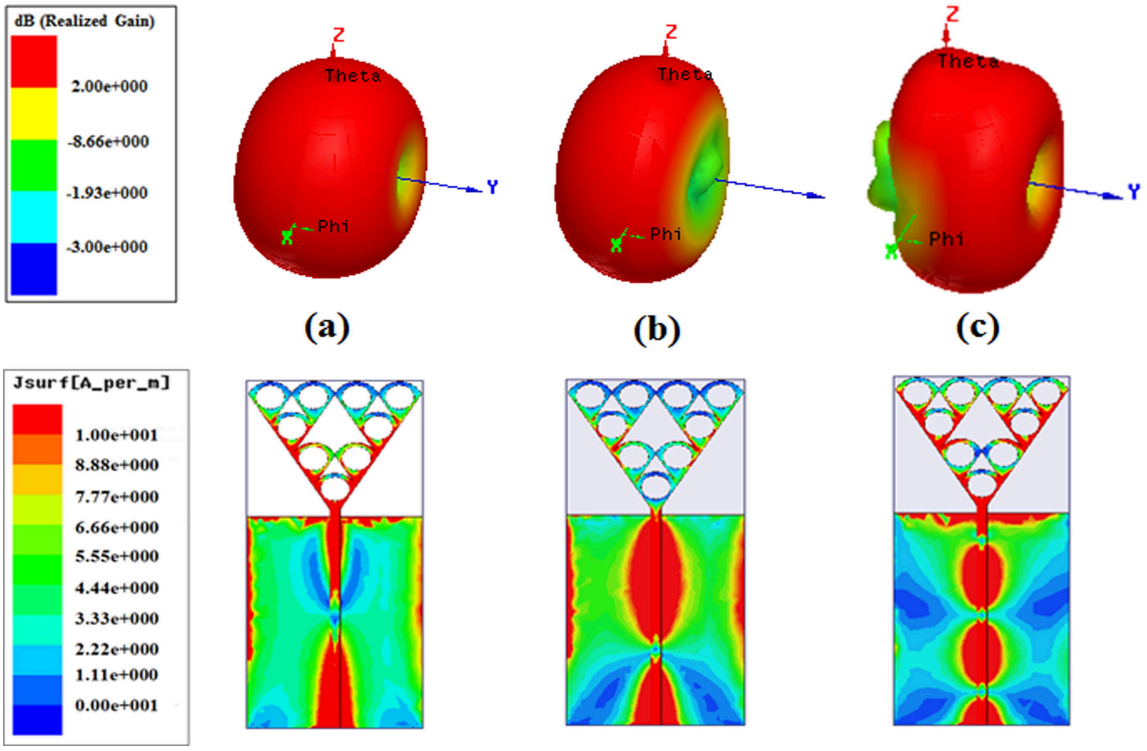

Figure 3.31: 3D radiation patterns and simulated surface current distributions on sectoral fractal planar monopole antenna at (a) 1.7 GHz (b) 3.0 GHz (c) 5.8 GHz.

GHz and 5.82 GHz for the modified sectoral fractal planar monopole antenna. It is noticed that the proposed geometry supports a multiple resonant modes. Mainly the distribution of current in lower frequency comes down side of the radiating element whereas in higher frequency current moves towards the tip of the radiating element. The proposed antenna is having omni-directional property at lower frequency band. However, it is nearly omnidirectional when operating frequency increases.

3.5.2 Experimental Verification

A prototype of the microstrip line fed modified sectoral planar monopole antenna with optimized dimensions is fabricated, shown in Figure 3.32 and tested experimentally in the Space Applications Center (SAC), ISRO, Ahmadabad, India. All scattering parameters are measured using Agilent vector network analyzer (model no. E8363B). Figure 3.33 shows the simulated and measured reflection coefficient plots of the proposed antenna. It is perceived that the simulation and measurement re-

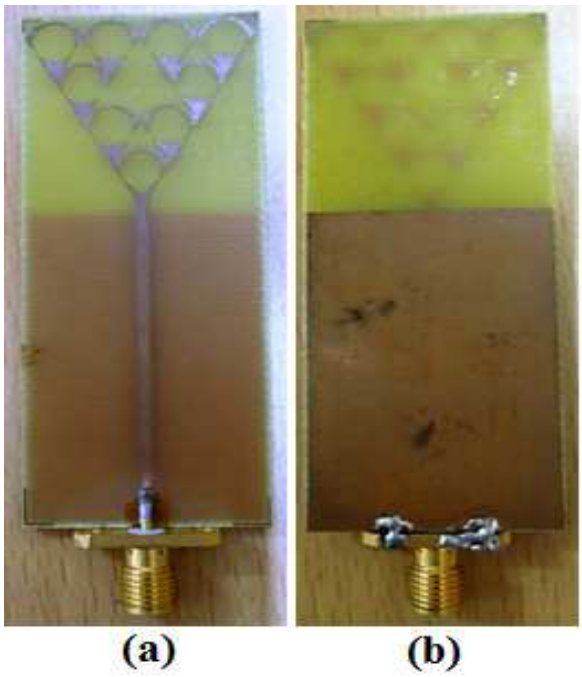

Figure 3.32: Photograph of proposed modified sectoral fractal monopole antenna.

sults are well matched and exhibit dual wideband resonances. The measured -10 dB impedance bandwidths are found as 76.7 % for lower band (1.51-3.39 GHz) and 17.3% for upper band (5.31-6.32 GHz). The measured bandwidth meets the requirements of many commercial bands such as GPS (1.51-2.6 GHz), DCS-1800 (1.71-1.88 GHz), PCS-1800 (1.80-1.99 GHz), UMTS (1.92-2.17 GHz), IMT-2000 (1.9-2.2 GHz), Wi-Bro (2.3-2.4 GHz), Bluetooth (2.4-2.48 GHz), and WLAN (802.11b/g/a) (2.4-2.485 GHz and 5.31-6.32 GHz). It can be seen that the proposed antenna matched approximately at frequencies (f_r) [198] as given below.

$$f_r = \begin{cases} (0.15345 + 0.34\rho x)\,\frac{c}{h_e}\,(\xi^{-1}) & \text{for } n = 0 \\ 0.26\frac{c}{h_e}\delta^n & \text{for } n > 0 \end{cases}, \tag{3.1}$$

where c is the speed of light, n is the band number (n=0, i.e., band 1 and $n = 1$, i.e., band 2), h_e is the effective height of the sectoral, $\xi = \frac{h_n}{h_{n+1}}$ is the ratio of the height of the gasket in the n^{th} iteration to that in the $(n+1)$ iteration, δ is the scale factor $\frac{1}{\xi}$, $x = \begin{cases} 0 & k = 0 \\ 1 & k > 0 \end{cases}$, and k is the number of iteration. For this proposed modified sectoral antenna, the

effective height, h_e of the Sierpinski gasket is given as:

$$h_e = \frac{\sqrt{3}S_e}{2} \tag{3.2}$$

where

$$S_e = S + h_s\,(\epsilon_r)^{-0.5} \tag{3.3}$$

with h_s being the thickness of the substrate and S the side length of proposed modified Sectoral antenna.

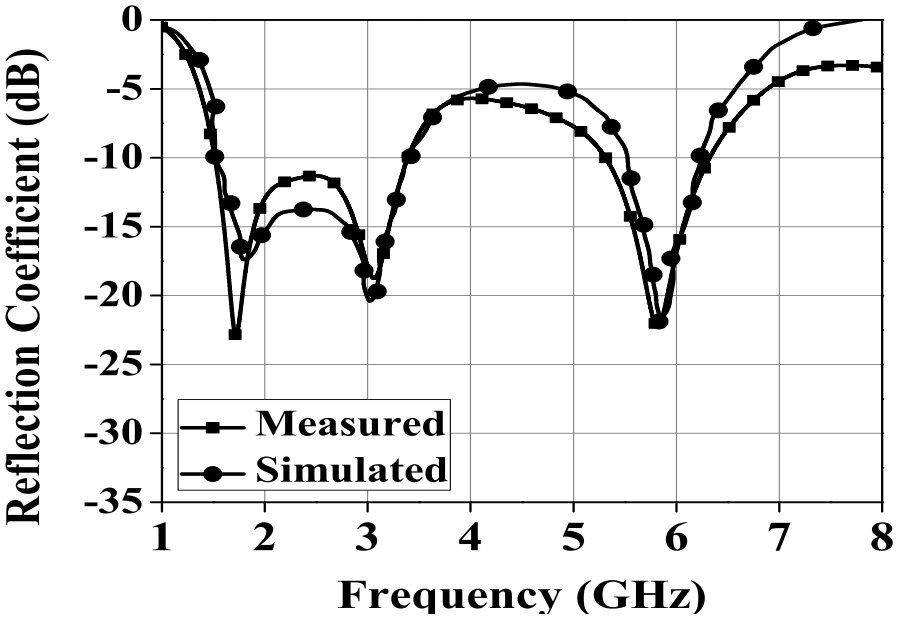

Figure 3.33: Simulated and measured reflection coefficients of proposed modified sectoral fractal antenna.

The measured radiation patterns at 1.72 GHz, 3.07 GHz, and 5.82 GHz are shown in Figure 3.34. It is observed that the patterns at different frequencies are similar, winch is expected for both the frequency bands. In addition, the cross pol. levels are very small for all measured patterns. Specifically, a co-pol./cross-pol. ratio better than 40-50 dB is observed at boresight direction for all measured radiation patterns. The cross pol. level at other direction is also very small, indicating excellent polarization purity. As can be concluded that the proposed antenna has symmetrical radiation patterns, which are omnidirectional in XZ (Co-pol. and Cross-pol.) and YZ (Co-pol. and Cross-pol.) planes. Table 3.8 shows the measured peak realized gain

and simulated total efficiency at different frequencies. The peak realized gains in the two resonant bands are 2.35 dBi at 1.72 GHz and 4.79 dBi at 5.8 GHz. The total antenna efficiency is found as more than 80 % for band 1 and band 2.

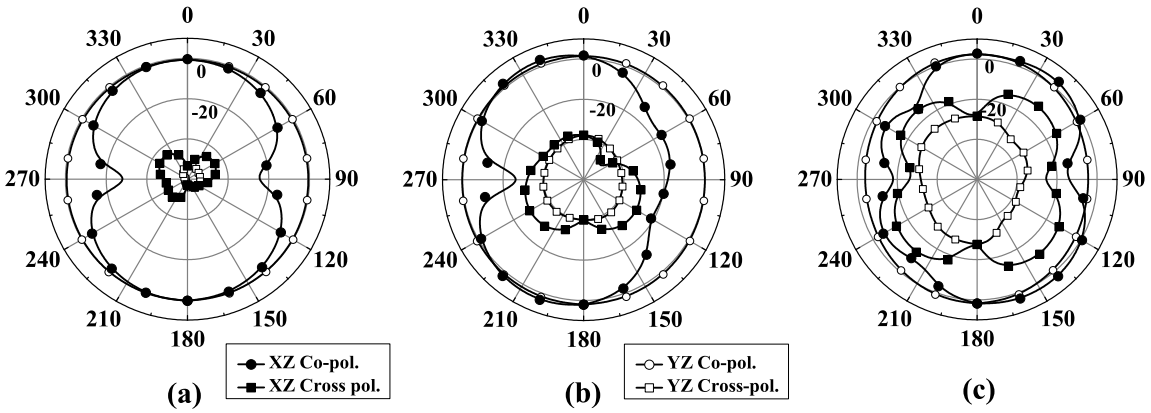

Figure 3.34: Measured radiation patterns of proposed modified sectoral fractal monopole antenna at (a) 1.72 GHz (b) 3.07 GHz (c) 5.82 GHz.

Table 3.8: Measured gain and simulated total antenna efficiency of proposed modified sectoral fractal monopole antenna.

Frequency (GHz)	1.15	1.72	2.42	3.07	3.39	5.31	5.82	6.32
Gain (dBi)	2.15	2.35	3.23	4.48	4.68	4.08	4.79	5.51
Efficiency (%)	81.66	96.16	92.68	90.12	91.62	93.11	95.35	93.6

3.6 Semi-Circle Fractal Monopole Antenna

In this section a semi-circle fractal monopole antenna is developed for dual wideband wireless applications. The proposed structure is used semi-circle fractal patch as a radiating element with Co-planar waveguide (CPW) feed. The proposed antenna model exhibits resonances in 2.0-2.45 GHz and 4.50-6.60 GHz bands. Here, CPW-feeding method is considered for better impedance matching, lower radiation loss and easy application with active integrated antenna.

3.6.1 Antenna Geometry and Simulation Results

The recursive procedure of semi-circle fractal slot antenna is presented in Figure 3.35. The construction of circular fractal pattern is based on iterative processes and the

Descartes Circle theorem.

Descartes Circle Theorem

The Descartes circle theorem is an ancient theorem about four mutually tangent circles in the Euclidean plane, asserting that their curvatures satisfy the quadratic relation as given in (3.4) [199].

$$(a_i + b_i + c_i + d_i)^2 = 2(a_i^2 + b_i^2 + c_i^2 + d_i^2) \tag{3.4}$$

where the reciprocals of these curvatures are (or bend) $a_i = 1/R_{ai}, b_i = 1/R_{bi}, c_i = 1/R_{ci}, d_i = 1/R_{di}$ and radii of the circles are $R_{ai}, R_{bi}, R_{ci}, R_{di}$. This theorem can be used to construct a four circle tangent for three given mutually tangent circles.

Iterative Design

The circular conductor is constructed in initial stage to obtain circular fractal patterns using Descartes Circle (DC) theorem. For first stage, two inner circles are obtained with equal radius, then fourth circle is obtained using equation 3.4. Hence, at the second stage , a set of four circles is selected from initial five circles obtained in first stage to determine six circles. Similarly, this process is continued to determine the n number of circles, as shown in Figure 3.35. Details of the iterative model which satisfies the curvature is reported in [199]. For modification of the proposed geometry, the circle is miniaturized by D/2 height; where the full circle height is 'D'.

The geometry of the proposed semi circle fractal monopole antenna is shown in Figure 3.36 with corresponding optimized parameters listed in Table 3.9. The proposed antenna is printed on FR-4 substrate ($\epsilon_r = 4.4$) of size $44 \times 48\ mm^2$ with height 1.58 mm and loss tangent, tanδ=0.005. Figure 3.37 describes the simulated reflection coefficients of proposed antenna for different stages of iteration levels. It is observed that, when the number of iteration increases, the resonant frequency of proposed antenna decreases. In sixth iteration, the proposed geometry is modified as in Figure 3.35 (g) and is resonating at two frequencies. First resonance frequency is 2.4 GHz for -10 dB impedance bandwidth in the range of 2.0-2.85 GHz. Similiary, the second resonance frequency is 5.2 GHz, -10 dB impedance bandwidth in the range

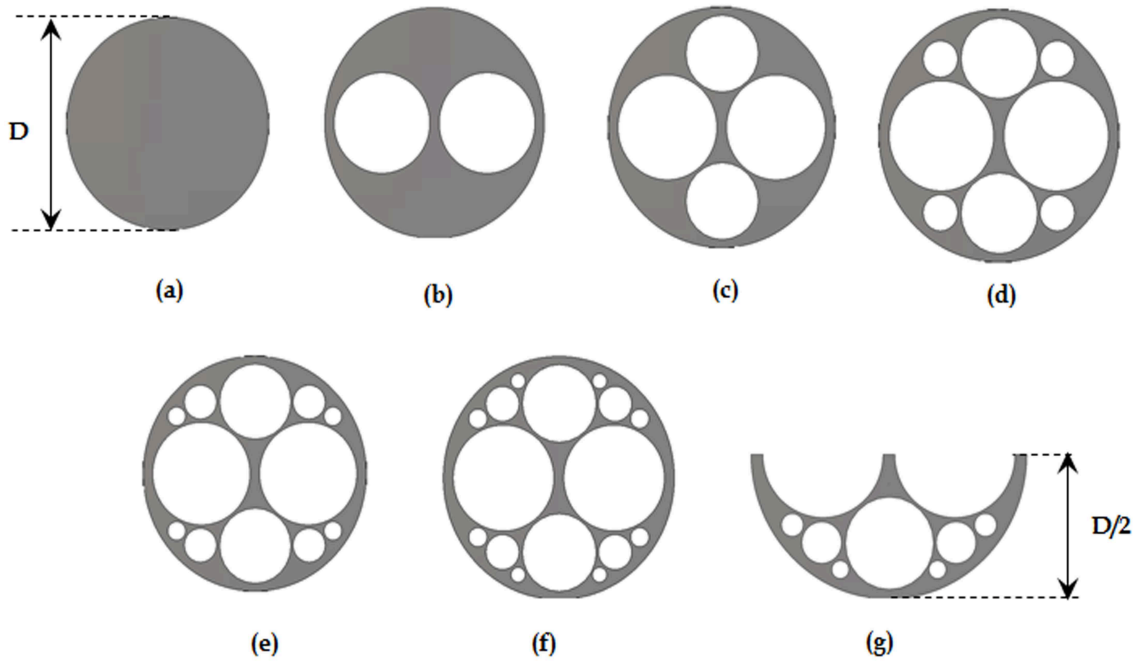

Figure 3.35: Recursive procedure for designing of semi-circle fractal geometry.

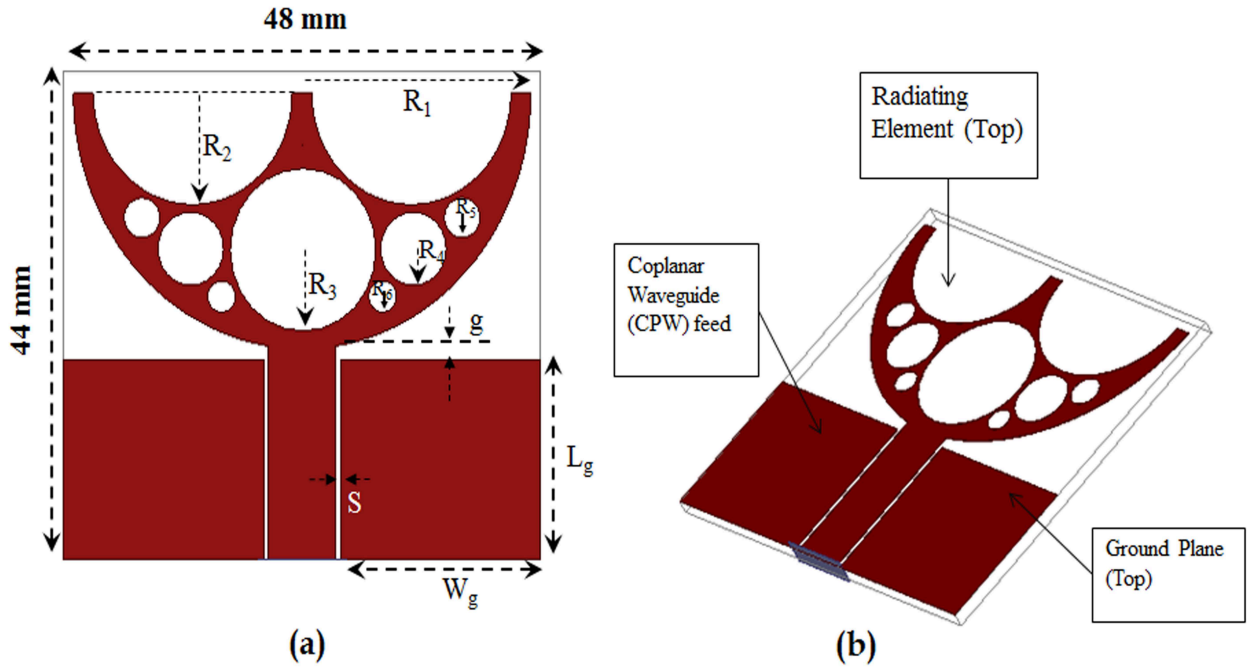

Figure 3.36: Geometry of proposed semi-circle fractal monopole antenna (a) Front view (b) 3D view.

of 4.5-6.6 GHz. Both resonating frequencies cover the IEEE standard 802.11b/g and 802.11 a, for WLAN (2.4/5.4 GHz) applications. Figure 3.38 and Figure 3.39 illustrate the reflection coefficients plots of gap (g) and the fed gap (S). Here, 'g' is the

gap between the radiating element and ground plane and 'S' is the gap between feed line and ground plane. They play an important role in determining the characteristics impedance of the antenna. Figure 3.38 shows the reflection coefficients for feed gap, 'g'. It is seen that when the gap between radiating element and ground plane increases, more variations occur in higher band whereas less variation in lower band. This is due to coupling between the feed gap and radiating element. Figure 3.39 explains the reflection coefficients of proposed antenna for feed gap, 'S'. In this study, it is found that with increase in feed gap the resonant frequency decreases. At S=0.5 mm, the -10 dB impedance bandwidth is well matched covering the desired operating bandwidth.

Table 3.9: Dimensions of proposed semi-circle fractal monopole antenna.

R_1	R_2	R_3	R_4	R_5
23.0 mm	10.0 mm	7.33 mm	3.3 mm	1.8 mm
R_6	g	W_g	L_g	S
1.4 mm	1.25 mm	19.3 mm	18.0 mm	0.5 mm

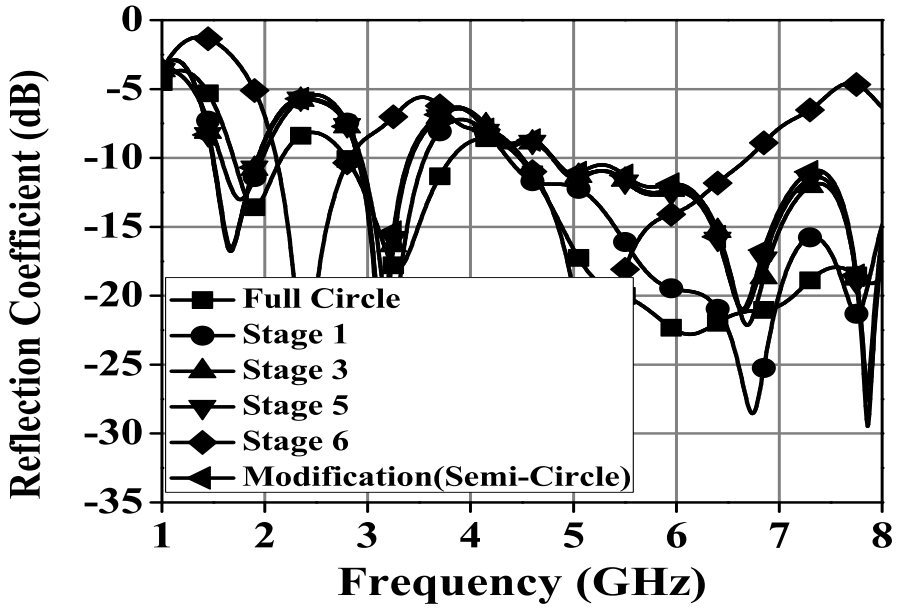

Figure 3.37: Reflection coefficients of proposed semi-circle fractal monopole antenna for different iteration levels.

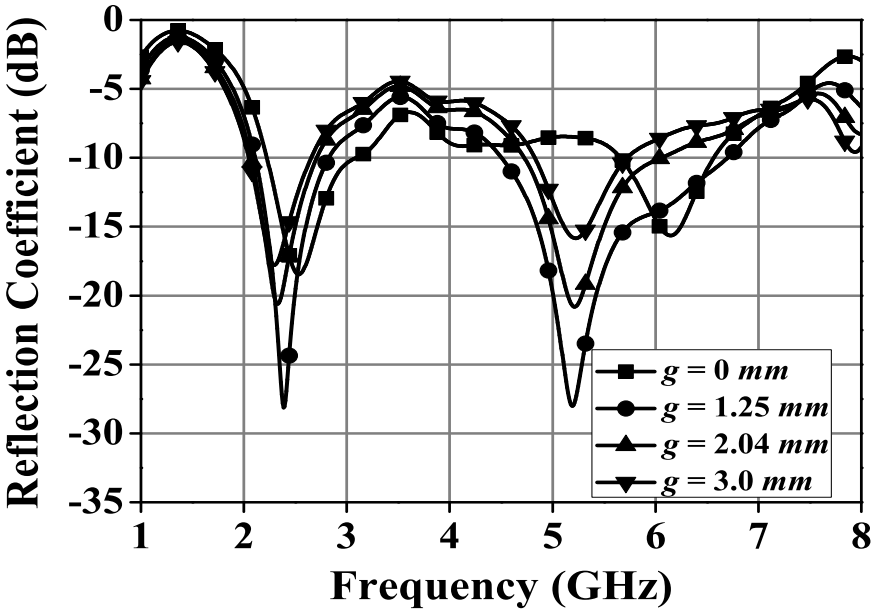

Figure 3.38: Reflection coefficients of proposed semi-circle fractal monopole antenna for different feed gaps, 'g'.

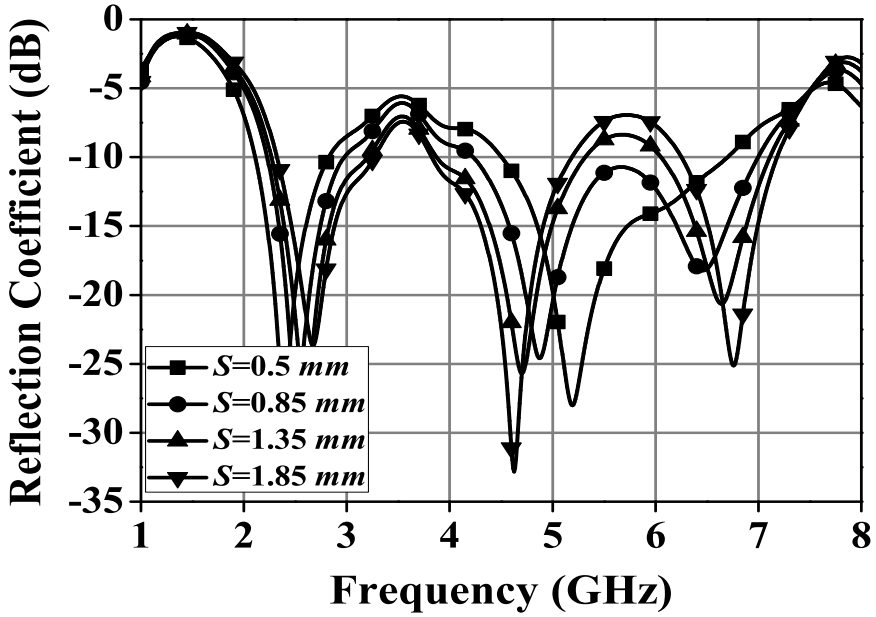

Figure 3.39: Reflection coefficients of proposed semi-circle fractal slot antenna for gap, 'S', between feed line and ground plane.

Figure 3.40 shows the simulated 3D radiation patterns and surface current distributions at 2.45 GHz and 5.5 GHz for the proposed semi circle fractal monopole

antenna. It is noticed from 3D radiation patterns that the proposed antenna has omnidirectional property for both the frequency bands. The surface current of proposed antenna is mainly distributed on the edges of the radiator. This is also distributed on the ground plane and feed line for lower frequency band, which gives an indication about the dependence of antenna geometry on the resonant frequencies. In addition, for higher resonant frequency, the current travels toward the tip of the antenna and covers whole of the radiating element.

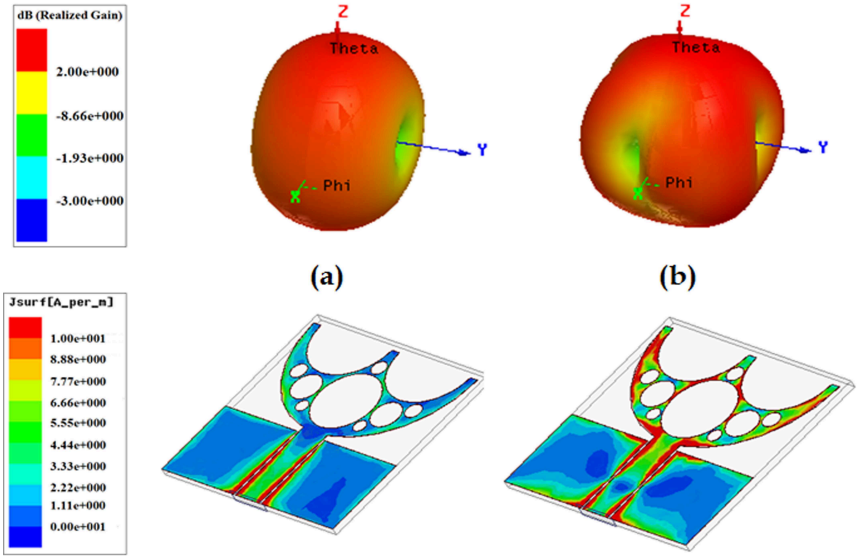

Figure 3.40: 3D radiation patterns and surface current distributions of proposed semi-circle fractal monopole antenna at (a) 2.45 GHz (b) 5.5 GHz.

3.6.2 Experimental Verification

The proposed semi-circle fractal monopole antenna is also tested experimentally in the Space Applications Center (SAC) ISRO, Ahmadabad, India. All scattering parameters are measured using Agilent Network analyzer (model no. E8363B).The measured and simulated reflection coefficients of proposed semi-circle fractal monopole antenna are plotted in Figure 3.41. It is observed that the simulation and measurement results are well matched and exhibit dual wideband resonances. The measured -10 dB impedance bandwidth for lower band is 33.3% (2.0-2.8 GHz) and for upper band, 39.28% (4.5-6.7 GHz). The measured impedance bandwidth confirms the requirements of many commercial bands such as Wi-Bro (2.3-2.4 GHz), Bluetooth (2.4-2.48

GHz), and WLAN (802.11b/g/a) (2.4-2.485 GHz and 5.0-6.0 GHz).

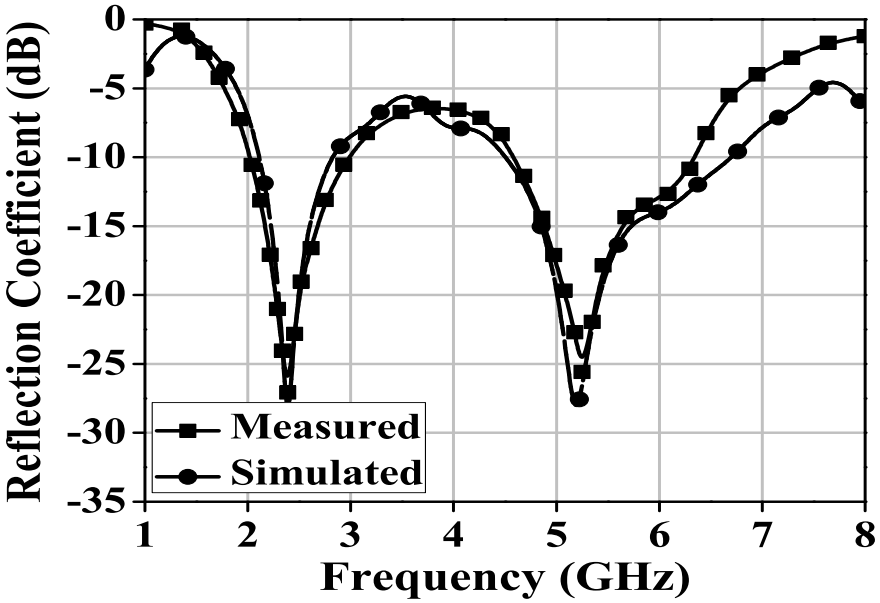

Figure 3.41: Simulated and measured reflection coefficients of proposed semi-circle fractal monopole antenna.

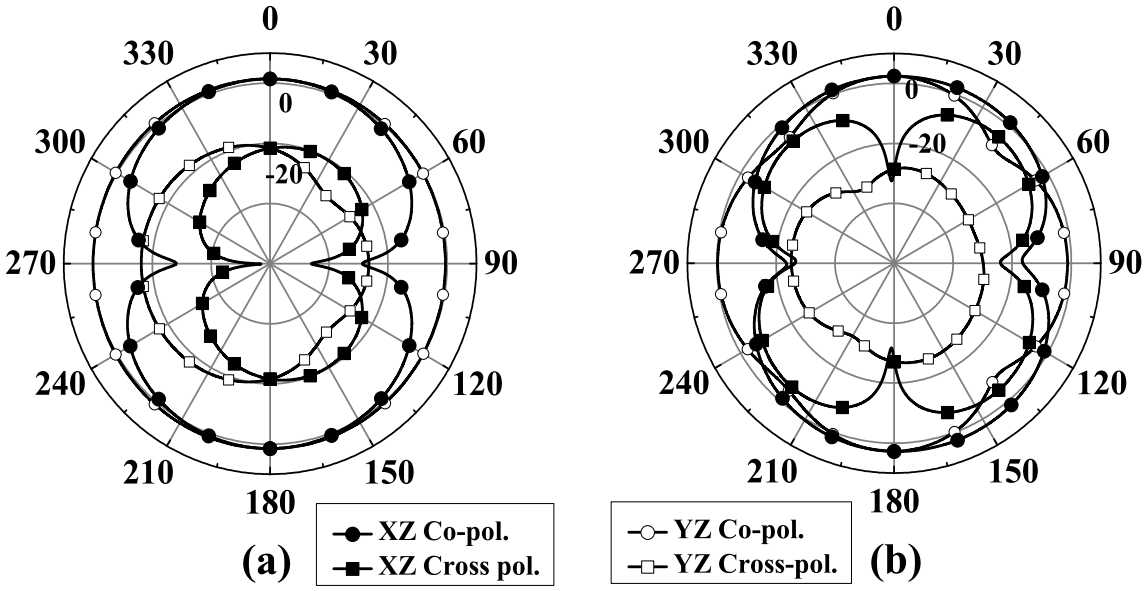

Figure 3.42: Measured radiation patterns of proposed semi-circle fractal monopole antenna at (a) 2.45 GHz (b) 5.5 GHz.

The radiation patterns of the antenna in E- and H-planes, at 2.45 GHz and 5.5 GHz frequency over the operating frequency band are measured in an anechoic chamber and

shown in Figure 3.42. It is noticed that the antenna has nearly good omnidirectional patterns at both the frequencies in XZ (Co-pol. and Cross-pol.) and YZ (Co-pol. and Cross-pol.) planes. These patterns are suitable for application in most of the wireless communication equipments. Table 3.10 shows the measured gain and total efficiency at different frequencies. The measured peak realized gain for lower band is 1.99 dBi at 2.45 GHz whereas 3.01 dBi at 5.5 GHz. The simulated total antenna efficiency as more than 75 % for the proposed antenna.

Table 3.10: Measured gain and simulated total antenna efficiency of proposed semi-circle fractal monopole antenna.

Frequency (GHz)	2.0	2.5	3.0	4.5	5.0	5.5	6.0	6.5
Gain (dBi)	1.51	2.02	2.01	2.67	2.77	3.01	2.55	2.61
Efficiency (%)	84.6	91.0	92.0	78.07	83.47	91.96	87.27	81.33

Table 3.11: Comparison among different monopole wideband antenna design prototypes.

Parameters	**ACS-fed Koch fractal antenna**	**Hybrid fractal antenna**	**Sectoral fractal antenna**	**Modified sectoral fractal antenna**	**Semi-circle fractal antenna**
Dimensions (mm)	25.2×37.5×1.58	27×66×1.58	25×37×1.58	27×65.5×1.58	48×44×1.58
10dB Impedance bandwidth (GHz)	2.6-7.88	1.6-3.4	3.22-6.55	(Dual Band) 1.51-3.39, 5.31-6.32	(Dual Band) 2.2-2.8 4.5-6.7
10dB Impedance bandwidth (%)	100.7 %	72 %	68.04 %	76.37%, 17.3 %	33.3%, 39.28 %
Realized gain (dB)	2.61-4.42 ± 1.8	2.51-4.35 ± 1.8	3.11-4.42 ± 1.8	2.15-5.51 ± 1.68	2.26-4.42 ± 0.75
Efficiency (%)	> 95 %	> 75 %	> 70 %	> 80 %	> 80 %

3.7 Summary

In this chapter, different wideband fractal planar monopole antennas have been developed to achieve low profile and ease of integration. The Koch fractal curve monopole antenna is designed for wideband wireless application. It covers measured impedance bandwidth of 100.7 % (2.62-7.88 GHz). A peak realized gain of 4.42 dBi is observed with the total antenna efficiency of 95 %. Hybrid fractal and sectoral fractal monopole antennas are also investigated for wideband frequency range. For hybrid fractal monopole antenna, the two fractal geometries are used in simple rectangular patch. The measured impedance bandwidth of 72.37 % for 1.6-3.4 GHz frequency range is observed. The sectoral fractal monopole antenna is covering the impedance bandwidth of 68.04% from 3.22-6.55 GHz. Therefore, for dual wideband wireless operation, modified sectoral and semi-circle fractal antennas are investigated. The modified sectoral fractal antenna is covering 76.37 % impedance bandwidth for band 1 (1.51-3.39 GHz) and 17.3 % impedance bandwidth for band 2 (5.31-6.32). The semi-circle fractal antenna is constructed using a Descartes Circle (DC) theorem. It is noticed that the impedance bandwidth of 33.3 % for band 1 (2.2-2.45 GHz) and 39.28 % for band 2 (4.5-6.6 GHz) are observed. The parametric studies have been performed to observe the effect of antenna parameters. For further understanding the behavior of the proposed antennas, the surface current distributions and 3D radiation patterns are presented. Experimental as well as the simulated results confirm the wideband/dual wideband property of the proposed antennas with nearly stable omni-directional radiation patterns over the entire frequency band of interest. A comparison among all different types of wideband fractal antenna prototypes is summarized in Table 3.11. These features make them attractive for future communication system.

CHAPTER 4

Wideband Frequency Reconfigurable Fractal Antenna

4.1 Introduction

In previous chapter, several wideband and dual-wideband monopole antennas were investigated. These designs are based on fractal geometries. In this chapter, a frequency reconfigurable antenna is designed using Koch snowflake fractal antenna for wideband applications.

Wireless communication systems are evolving toward multi-functionality. This multi-functionality provides users with options of connecting to different kinds of wireless services for different purposes at different times. Large numbers of antennas are mounted on ships, aircrafts or other vehicles. It is highly desirable to develop single radiating element having capabilities of performing different functions and/or multi-band operation in order to minimize the antenna's weight and area. Antennas with reconfiguration capabilities (frequency, bandwidth, radiation pattern, polarization) have the potential to open up a world of new possibilities for system performance, flexibility, and robustness. In current wireless networks reconfigurable antennas can be utilized to improve the system robustness in today's harsh and time varying electromagnetic environments. The goal of this chapter is to explore antenna structures suitable for wideband communications. Here, Koch snowflake fractal reconfigurable monopole antenna is developed for wideband operations. This fractal antenna can be used as an array element.

This chapter is organized as follows; Section 4.2 introduces frequency reconfig-

urable monopole antenna. Subsections describe the Koch snowflake fractal antenna, simulation results and experimental verifications. The proposed antenna provides three wide frequency bands. Finally, conclusions are summarized in Section 4.3.

4.2 Frequency Reconfigurable Monopole Antenna

Today's communication systems demand both increased performance and reduced size. The present section deals with the contributions towards the compact frequency reconfigurable antenna that can be used as an array element and have a wideband frequency band option. The proposed antenna is based on Koch snowflake fractal geometry and used in frequency reconfigurability. It provides three wideband configurations for impedance bandwidth of 100% (1.5-4.5 GHz). Besides, a frequency reconfigurable multi-functionality provides users with options of connecting to different kinds of wireless services. Moreover, the proposed antennas is capable of achieving selective polarization, radiation patterns as well as gain.

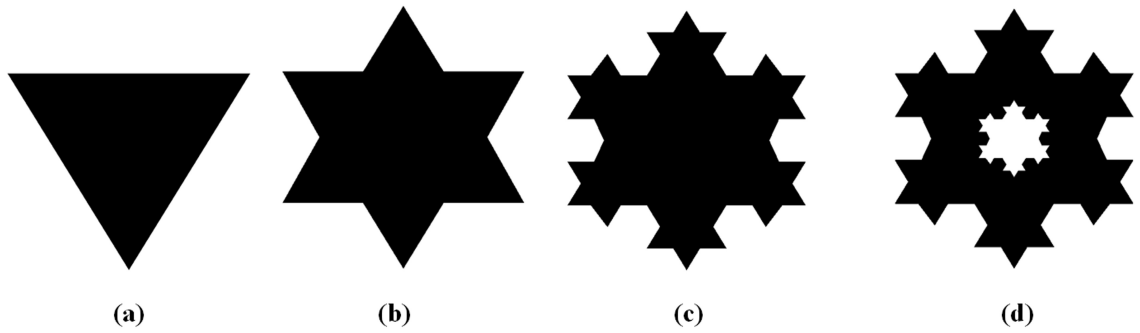

Figure 4.1: Recursive procedure for Koch snowflake fractal geometry.

4.2.1 Koch Snowflake Antenna Geometry

The overall pictorial representation of recursive procedure for Koch snowflake is presented in Figure 4.1. It is based on IFS model and formed by repeating 'n' numbers of iterations (Section 1.3). The proposed antenna is implemented on a substrate FR-4 of relative permittivity ϵ_r=4.4 and thickness h=1.58 mm and loss tangent $\tan\delta$=0.005. A Koch snowflake fractal slot antenna is fed by a 50Ω microstrip line, width of W_f=3.2 mm. It is printed on 40×80 mm^2 substrate and the maximum side length of Koch

snowflake is around 28.8 mm. The antenna is elevated from the ground plane (40×47 mm^2) with a sizable air gap to achieve wide bandwidth. For modification, another Koch snowflake is etched scaling down by factor of three from the basic Koch snowflake geometry. The modified geometry is shown in Figure 4.1 (d). The purpose of etching Koch snowflake is to get space for bias line without changing the patch dimensions. Figure 4.2 describes the simulated reflection coefficients for Koch snowflake and modified Koch snowflake antenna at different iteration levels. It is observed that the value of reflection coefficient in case of 2^{nd} iteration is well below -10 dB for wide impedance bandwidth. Moreover, another observation from Figure 4.2 is that after 2^{nd} iteration, the modified geometry maintains the same reflection coefficient as before. Hence, in both the cases the Koch snowflake and the modified Koch snowflake provide the same reflection coefficients as before. It is concluded that the proposed modified geometry is useful for creating bias line into the element for frequency reconfigurability.

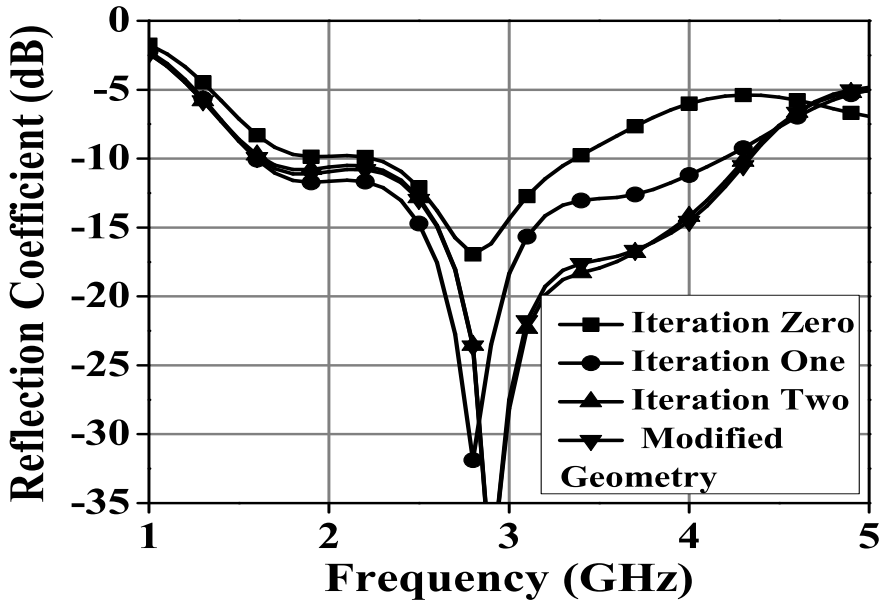

Figure 4.2: Simulated reflection coefficients of Koch snowflake fractal monopole antenna for different iterations.

4.2.2 RF PIN Diodes in Antenna Design

RF PIN diodes are used as 'switches' in the proposed frequency reconfigurable antenna. The PIN diode behaves as a variable resistor and it is shown in Figure 4.4 (d). For ON and OFF states, a package inductance L is used. The equivalent circuit for the ON state (forward biased) has a low resistance R_s which contributes to the insertion loss. Similiary for the OFF state (reverse biased) the circuit has the parallel combination of the parallel reverse bias resistance R_P and the total capacitance C_T, which contributes to the isolation. The OFF state resistance is determined by $R_P = V_R/I_R$, where I_R is the reverse leakage current when a test voltage of V_R is applied. All values necessary for the circuit models are given in standard RF PIN diode data sheet. The RF PIN diode used as a series switch for frequency reconfigurable antenna is shown in Figure 4.3. The PIN diode is connected with two DC bias lines. The first DC bias line is connected with a positive voltage V and the other connected to ground. A resistor 'R' is used to obtain the ON state current. When a positive voltage is applied the diode turns ON, and when both are connected to ground, the diode turns OFF. To keep the RF signal out of the DC bias lines, RF choke inductors (L_C) are used. To keep the DC out of the RF portion of the circuit, DC blocking capacitors (C_B) are used.

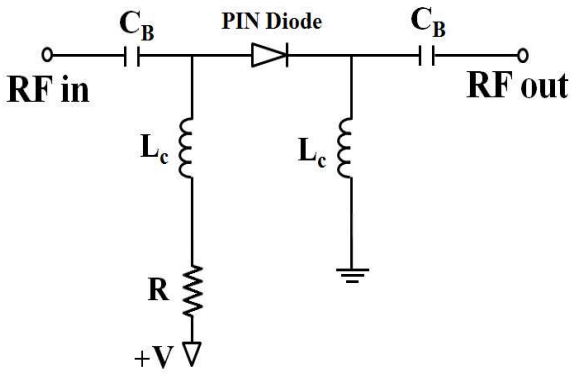

Figure 4.3: Circuit model of series switch using RF PIN Diode

4.2.3 Antenna Geometry and Simulation Results

The configuration of the proposed Koch snowflake frequency reconfigurable fractal antenna for wideband operation is illustrated in Figure 4.4. The antenna performance is analyzed using Ansoft HFSS v14.

There are four PIN diodes used as switches in the proposed frequency reconfigurable antenna. They are placed in 1.6 mm gap, etched segment with the angle of 30°, 90°, 180° & 240°. The position of PIN diodes and the capacitor on the antenna are optimized so that the maximum tunable range with independent control can be accomplished. Surface mount chip capacitors C_1 & C_2 are used for blocking DC signal in series with PIN diodes. These capacitors are preventing the DC signal from flowing to the antenna and allowing the radio frequency (RF) signal pass through. Similiary, the inductors L_1 & L_2 are used as RF choke. They are providing low impedance for the DC signal and high impedance for the RF signal. The resistors R_1 & R_2 are used to provide extra protection to the PIN diode. The RF choke inductors L_1=L_2=2 nH, the DC blocking capacitors C_1=C_2=0.14 pF and the bias line regulation resistors R_1=R_2=47 Ω are used in the proposed geometry(assuming a bias voltage +1.5 V).

The PIN diode model BAR50 from Infineon is used for reconfigurable operation. It is difficult to model the packing of the capacitor in a full wave solver, so the PIN diodes are modeled using the resistance, capacitance and inductance (RLC) boundaries (Figure 4.4(c)) to create the equivalent circuit shown in Figure 4.4 (d). The inductance, L=0.6 nH and resistance, R_S=45 Ω are considered as a PIN diode, for the ON state (forward biased), which contributes to insertion loss. The total capacitance, C_T=0.15 pF (contributes to the isolation) and reverse biased resistance R_P=5 KΩ are in parallel combination with inductance in series. The above circuit combination is for OFF state (zero or reverse biased).

The proposed frequency-reconfigurable antenna is using four PIN diodes. They can provide three possible combinations. Switch 1 & 2 are connected with DC blocking capacitance in series for second & third segment . Switch 3 & 4 are used for connecting fourth segment . Bias line 1 & 3 are used for positive voltage and bias line 2 is used for ground plane.

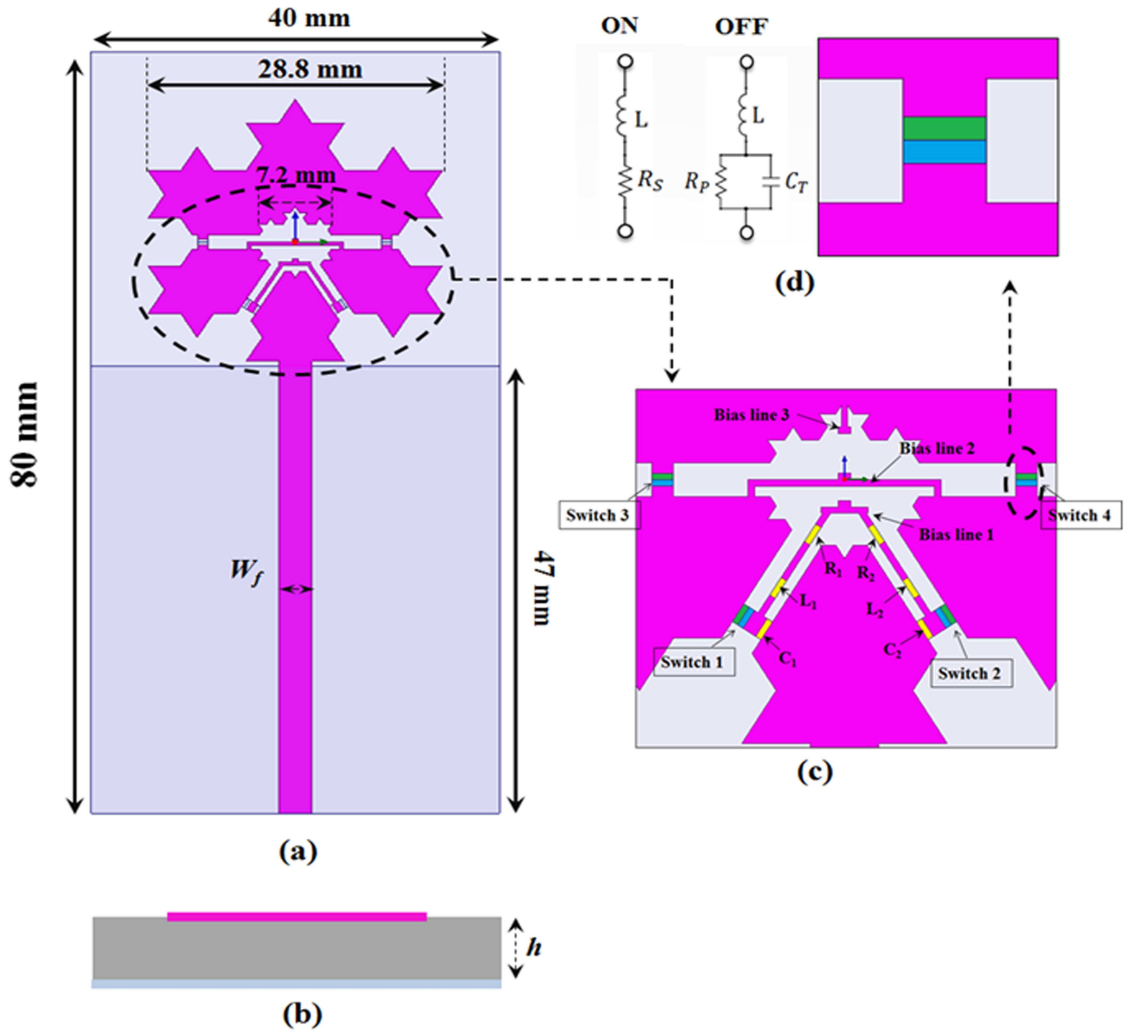

Figure 4.4: Geometry of proposed Koch snowflake fractal monopole antenna (a) Front view (b) Top view (c) Top view zoomed (d) PIN diode circuit.

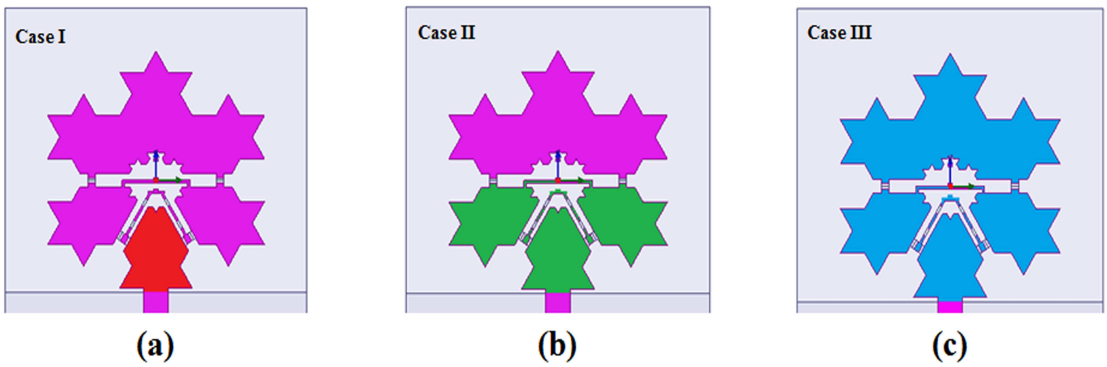

Figure 4.5: Geometry for different cases (a) Case I (b) Case II (c) Case III.

Figure 4.5 shows three possible combinations of proposed antenna. Figure 4.5 (a) shows the case I, when all PIN diodes are OFF. In this case, first segment (red) of the proposed Koch snowflake is connected to feed line. Figure 4.5 (b) shows the case II, when switches 1 & 2 are ON, and three segments (green) are connected to the feed line. Figure 4.5 (c) shows case III, when all PIN diodes are ON, so that all segments (blue) of the proposed Koch snowflake reconfigurable antenna are connected to feed line.

Figure 4.6 shows the simulated reflection coefficients for cases I, II & III. In case I, the reflection coefficient (-10 dB) covers the impedance bandwidth of 35 % for 3.24-4.5 GHz frequency band. In case of II & III, the reflection coefficients cover the impedance bandwidth of 45 % and 92 % for 2.13-3.28 GHz and 1.55-4.14 GHz respectively.

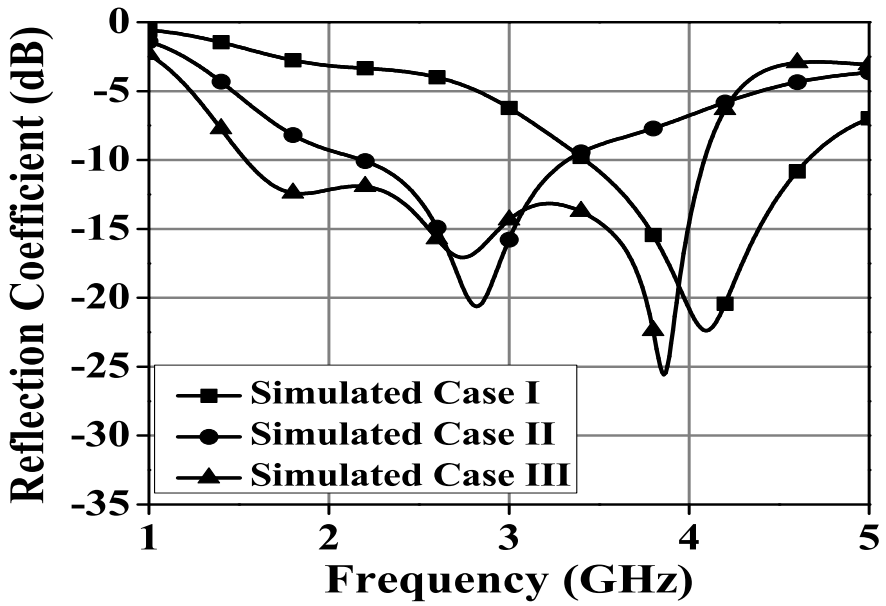

Figure 4.6: Simulated reflection coefficients of proposed frequency reconfigurable Koch snowflake fractal monopole antenna

Figure 4.7 shows the simulated surface current distribution of proposed Koch snowflake reconfigurable fractal monopole antenna for cases I, II & III. For case I, all switches are OFF, only first segment is connected to feed line, therefore the current flows in this segment. In case II, switch 1 & 2 are in ON state, the current flows in segment first, second & third. Finally, in case III, since all the PIN diodes are switched

ON the distribution of current found at the tip of the Koch snowflake geometry.

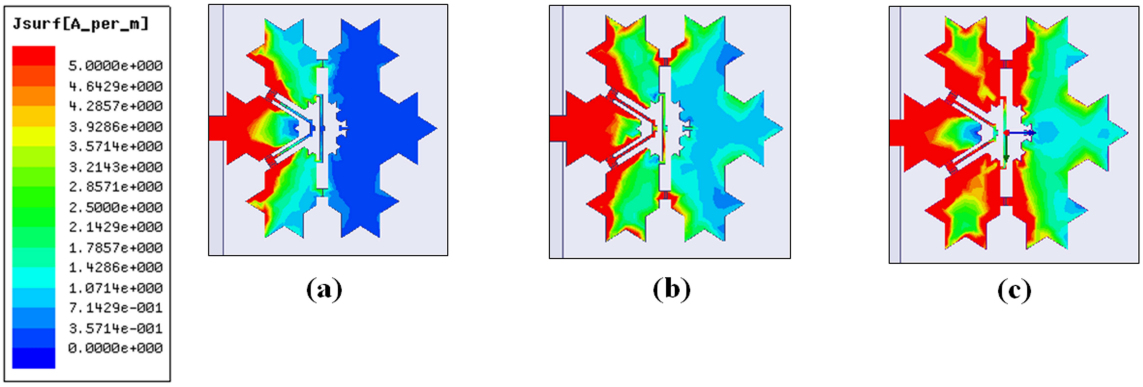

Figure 4.7: Surface current distributions (a) Case I at 3.9 GHz (b) Case II at 2.8 GHz d) Case III at 3.0 GHz.

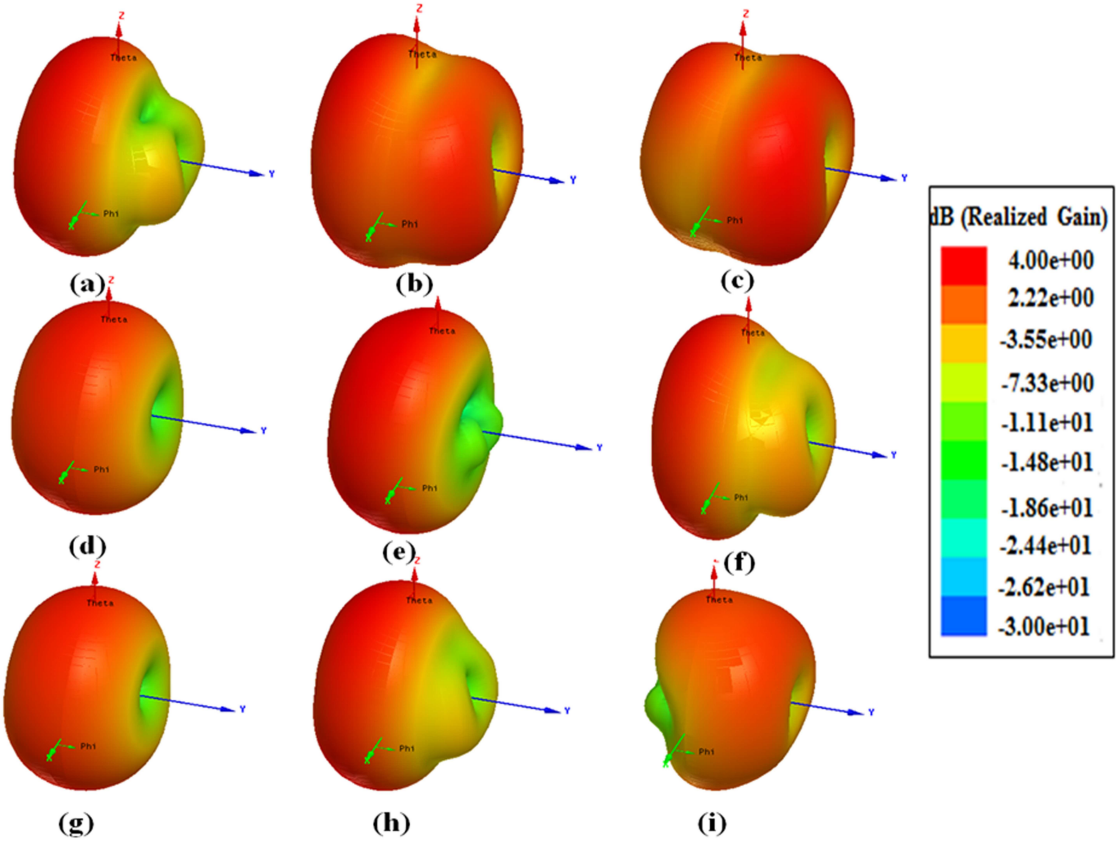

Figure 4.8: Simulated 3D radiation pattern figs (a), (b) & (c) for case I at 3.2 GHz, 3.9 GHz & 4.4 GHz, figs (d), (e) & (f) for case II at 2.2 GHz, 2.8 GHz & 3.4 GHz, figs (g), (h) & (i) for case III at 2.0 GHz, 3.0 GHz & 4.0 GHz

Figure 4.8 illustrates the 3D radiation patterns for the proposed Koch snowflake reconfigurable fractal monopole antenna for cases I, II & III. The radiation patterns

at 3.2 GHz, 3.9 GHz & 4.4 GHz (case I), 2.2 GHz, 2.8 GHz & 3.4 GHz (case II) and 2.0 GHz, 3.0 GHz & 4.0 GHz (case III) are omni-directional and gain is more than 2 dBi. Table 4.1 illustrates the measured gain, simulated gain and total antenna efficiency for the cases I, II & III. From the table, it is observed that, some variation occurs in measured and simulated gain of the antenna. The difference in variation of results is not consistent in nature. This may be attributed to fabrication tolerances associated with fractal shape, scattering effects due to the feed cable and antenna under test (AUT). However, simulated total antenna efficiency is found to be more than 70 % for all the cases.

Table 4.1: Simulated gain, measured gain and total antenna efficiency of proposed Koch reconfigurable antenna

Cases	**Frequency (GHz)**	**Simulated Gain (dBi)**	**Measured Gain (dBi)**	**Total Antenna Efficiency (%)**
Case I	3.2	2.65	3.12	70.64
	3.9	2.15	2.36	79.08
	4.4	1.70	1.93	65.23
Case II	2.2	1.52	1.87	76.31
	2.8	2.71	3.30	79.35
	3.4	2.27	2.77	63.62
Case III	2.0	1.48	2.23	79.39
	3.0	2.66	2.91	71.48
	4.0	1.39	2.42	61.14

4.2.4 Experimental Verification

Photographs of proposed Koch snowflake frequency reconfigurable fabricated antenna are shown in Figure 4.9. The measurement has been carried out using Agilent vector network analyzer (model no.N5230A) and radiation patterns are measured in an anechoic chamber in Microwave Lab, IISc Bangalore, India. Measured values of the reflection coefficients are plotted in Figure 4.10 for case I, II & III. For case I, battery (+1.5V) is not connected with the antenna. In this case, the impedance bandwidth of 30 % (3.34-4.52 GHz) is observed. In case II, bias line 1 is connected to a positive voltage and bias line 2 is connected to ground. As can be seen from Figure, the measured impedance bandwidth is 43 % (2.2-3.4GHz). In case III, the bias line 1 and bias

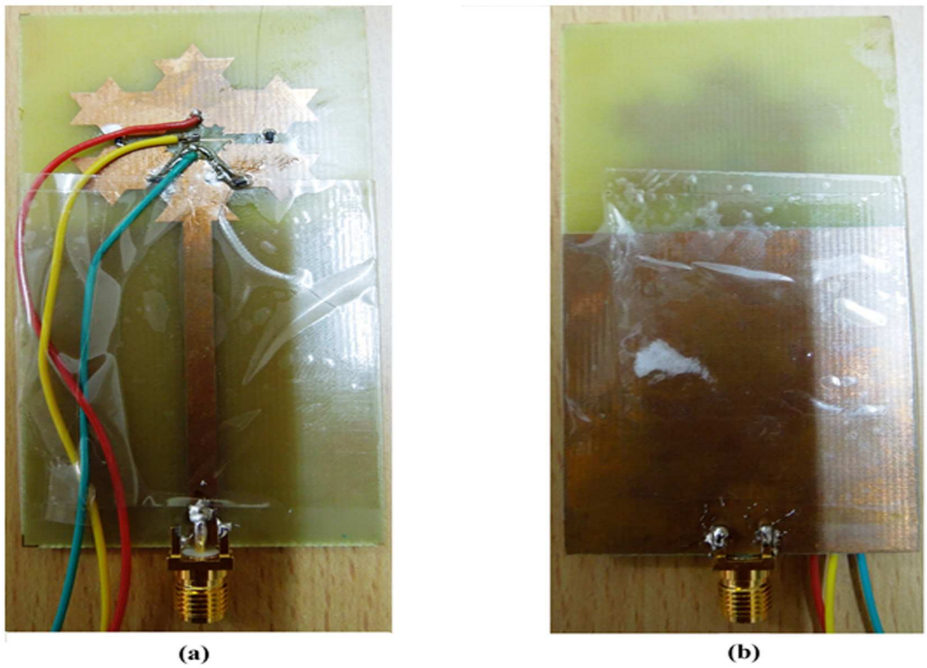

Figure 4.9: Photograph of fabricated frequency reconfigurable Koch snowflake monopole antenna (a) Front view (b) Rear view.

line 3 are connected to positive voltage and bias line 2 connected to ground plane. It is observed that the impedance bandwidth is 95.49% from 1.45-4.1GHz.

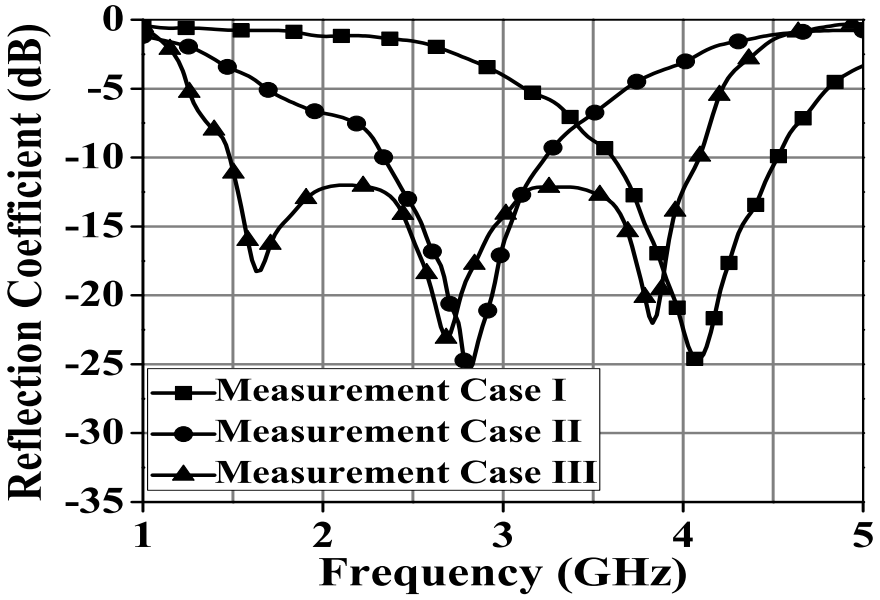

Figure 4.10: Simulated and measured reflection coefficients of proposed frequency reconfigurable Koch snowflake fractal monopole antenna for case I, case II & case III.

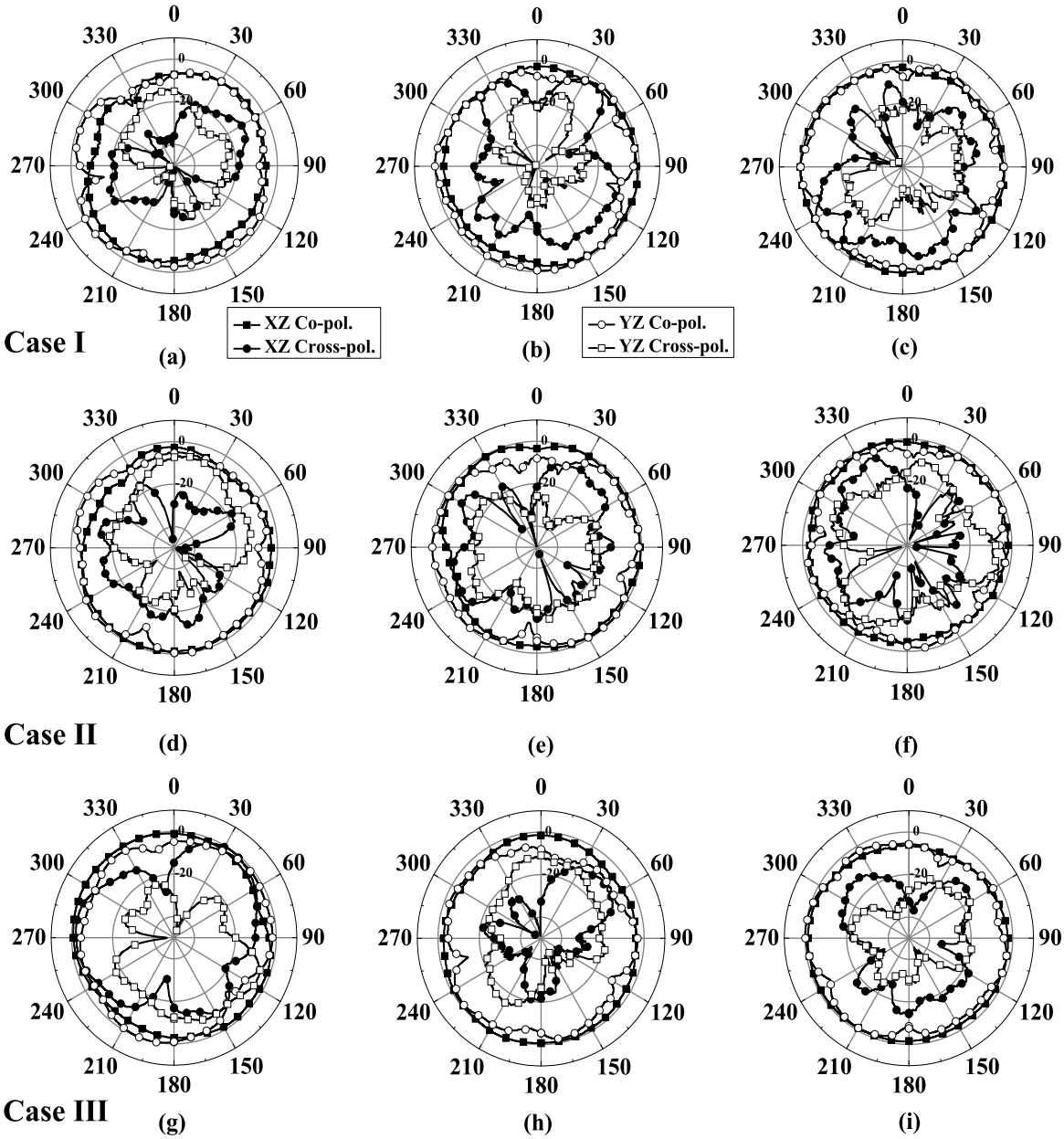

Figure 4.11: Measured radiation patterns for figs (a) at 3.2 GHz (b) at 3.9 GHz (c) at 4.4 GH, figs (d) at 2.2 GHz (e) at 2.8 GHz (f) at 3.4 GHz , figs (g) at 2.0 GHz (h) at 3.0 GHz (i) at 4.0 GHz.

Figure 4.11 shows the measured E- and H- planes radiation patterns for all the three cases. The proposed antenna radiation patterns are monopole like, which is almost omnidirectional in XZ (Co-pol. and Cross-pol.) and YZ (Co-pol. and Cross-pol.) planes at all the frequencies. While taking radiation pattern measurement in an anechoic chamber, the lithium battery is used to control PIN diodes as necessary.

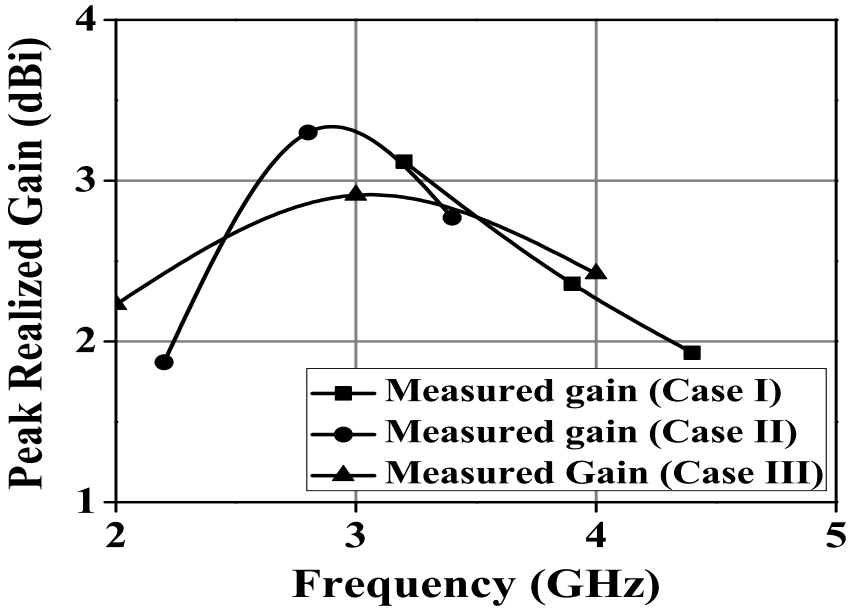

Figure 4.12: Gain curves of the proposed frequency reconfigurable Koch snowflake fractal monopole antenna for case I, case II & case III.

For case I, the measured radiation patterns are observed at frequency 3.2 GHz, 3.9 GHz and 4.4 GHz. Also for case II and case III the measured radiation pattern are found at 2.2 GHz, 2.8 GHz & 3.4 GHz and 2.0 GHz, 3.0 GHz & 3.0 GHz respectively. The measured results are showing acceptable omni-directional agreement for all the three cases. The peak gains in the boresight direction of the proposed Koch snowflake antenna is shown in Figure 4.12. In all the cases gain lies between 1.7-1.34 dB with the maximum of value 3.30 dBi.

4.3 Summary

A wideband frequency reconfigurable fractal monopole antenna is designed and experimentally verified in this chapter. Frequency reconfigurability is achieved by Koch snowflake fractal antenna. The RF PIN diodes and other lumped elements (capacitor, inductor and resistor) are used to achieve frequency reconfigurability. The proposed antenna provides three configurations for wide impedance bandwidth. An impedance bandwidth of 30% (3.34-4.52 GHz) is obtained for case I. Similiary in cases II and III, the impedance bandwidths are 43% (2.2-3.4 GHz) and 95.49% (1.45-4.1 GHz) respec-

tively. Thus the antenna provides continuous coverage of 100 % of bandwidth over 1.5-4.5 GHz. It is concluded that the proposed antenna is useful as a multi-function wideband operations for different wireless communication applications.

CHAPTER 5

Fractal Antenna for UWB Applications

5.1 Introduction

In the previous chapter, frequency reconfigurable monopole antenna was investigated. The proposed design was based on Koch snowflake fractal geometry. It has provided continuous coverage of 100 % impedance bandwidth from 1.5-4.5 GHz. In this chapter, a fractal geometry based Sierpinski square monopole antenna is investigated for UWB (3.1-10.6 GHz) application with band-notched characteristics.

UWB technology has unique features and promising applications in communications. For example, in wireless communications, the extremely wide operating bandwidth has the potential for high data-rate connections. However, the very low emission level has limited the wireless connection range to a few meters. As a result, the UWB radio technology is more likely to be applied in consumer electronics such as handset/laptop-centric and home networks which require short range but high data-rate wireless solutions. UWB systems will coexist with other traditional communication systems in the same frequency band by using low power levels. The Federal Communications Commission (FCC) has designated the 3.1 to 10.6 GHz band with an effective isotropic radiated power (EIRP) below -41.3 dBm/MHz for UWB communications.

UWB technology has received an impetus attracted academia and industrial attenuation in wider range of applications including ground plane penetrating radars, high data rate short range WLAN networks, communication systems for military purposes etc. As an important component of the UWB system the UWB antenna with simple

structure, wide impedance bandwidth, linear phase delay, stable radiation pattern and constant gain in desired direction is required even for degradation of radiated pulses.

In this chapter, modified square Sierpinski monopole fractal (MSSF) antenna is developed which is suitable for use in short range, low power indoor UWB radio systems, and outdoor base station communications. In addition effects of slot & feed geometry on the antenna performance are studied.

This chapter is organized as follows. Section 5.2 is on UWB square Sierpinski fractal monopole antenna. Subsections 5.2.1, 5.2.2 and 5.2.3 describes the antenna geometry, band-notch characteristics and transfer function characteristics, respectively. Finally, conclusions and summary are in Section 5.3.

5.2 UWB Square Sierpinski Monopole Antenna

In this Section, the microstrip line fed modified Sierpinski square fractal (MSSF) antenna for UWB with band notch characteristics has been studied. The UWB (3.1-10.6 GHz) is achieved by increasing the number of iterations and rectangular grooved ground plane. The band rejection characteristic is realized by an $\bigcap$-slot in feed line. The proposed antenna consists of volume 34×34×1.6 mm^3 with square shape structure and shows omni-directional radiation patterns. The measurement results indicate that the antenna offers impedance bandwidth of 110% for (UWB 3.1-10.6 GHz) and a notched at 5.5 GHz (5-6 GHz) for wireless local area network (WLAN) band.

Table 5.1: Dimensions of proposed MSSF antenna

L	W	W_f	L_f	W_g	L_g	x
34 mm	34 mm	3.8 mm	13.5 mm	34 mm	13 mm	20 mm
l	w_s	l_s	t_s	t_w	t_l	
22 mm	2.8 mm	4.4 mm	0.2 mm	2 mm	7.4 mm	

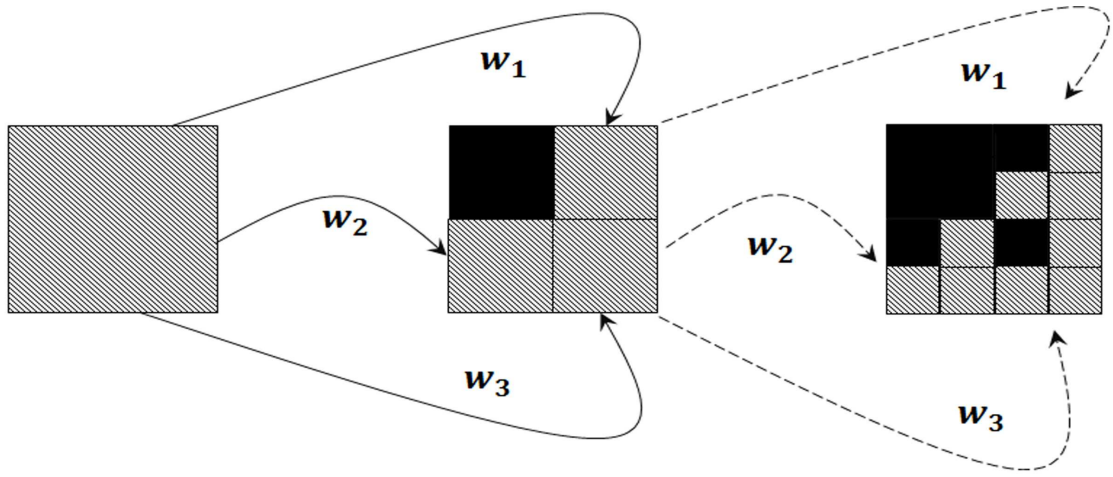

Figure 5.1: Stages of the IFS that generates the square Sierpinski.

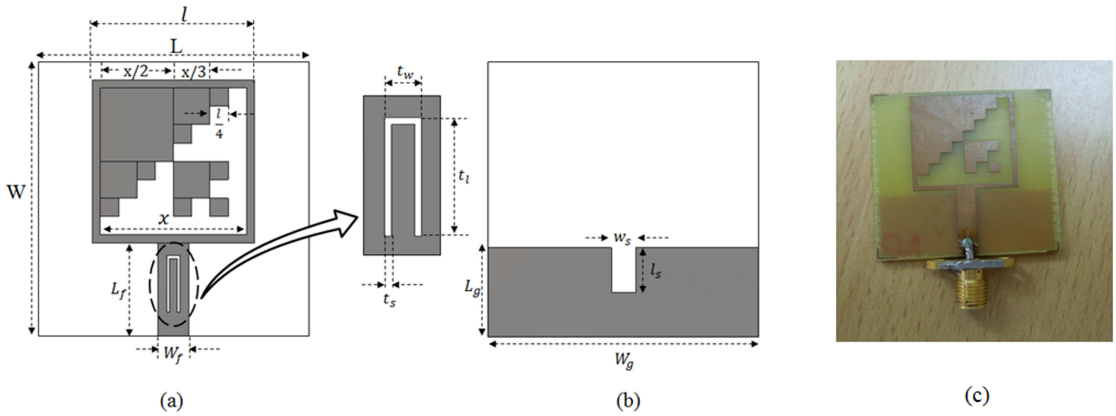

Figure 5.2: Geometry of proposed MSSF antenna (a) Front view (b) Rear view (c) Photograph.

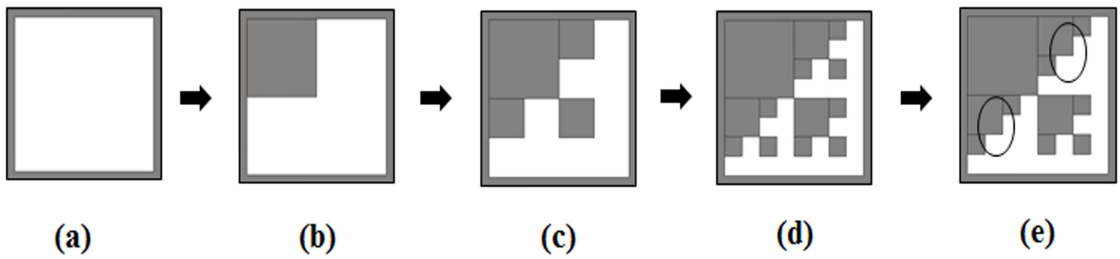

Figure 5.3: MSSF geometry and its different stages (a) Basic geometry (b) First iteration (c) Second iteration (d) Third iteration (e) Modified geometry.

5.2.1 Antenna geometry and simulation results

The recursive procedure for square Sierpinski geometry is shown in Figure 5.1. The proposed geometry is based on IFS model (Section 1.2). IFS generates the Sierpinski

square fractal gasket. It is unruffled of three similar transformations.

$$w_1(x,y) = \begin{pmatrix} 1/2 & 0 \\ 0 & 1/2 \end{pmatrix} \begin{pmatrix} x \\ y \end{pmatrix} + \begin{pmatrix} 1/4 \\ 0 \end{pmatrix} \tag{5.1}$$

$$w_2(x,y) = \begin{pmatrix} 1/2 & 0 \\ 0 & 1/2 \end{pmatrix} \begin{pmatrix} x \\ y \end{pmatrix} + \begin{pmatrix} -1/4 \\ 0 \end{pmatrix} \tag{5.2}$$

$$w_3(x,y) = \begin{pmatrix} 1/2 & 0 \\ 0 & 1/2 \end{pmatrix} \begin{pmatrix} x \\ y \end{pmatrix} + \begin{pmatrix} 0 \\ 1/2 \end{pmatrix} \tag{5.3}$$

Geometry of proposed modified square Sierpinski fractal (MSSF) antenna for UWB operation is illustrated in Figure 5.2 and corresponding optimized parameters are listed in Table 5.1. The antenna is implemented on standard FR-4 substrate $W \times L$ with relative permittivity ϵ_r=4.4, thickness h =1.58 mm and loss tangent $\tan(\delta)$ = 0.005. A 50 Ω microstrip transmission line with a strip width W_f and length L_f is used to feed the antenna with a matching section over rectangular ground plane. The radiating element is placed on one side of the substrate and grooved ground plane of size $W_g \times L_g$ is located on other side of the substrate. It is noted that the grooved area of size $w_s \times l_s$ is located on top of the ground plane. The proposed MSSF antenna consists of two parts. In first part, the fractal geometries are generated from an original square slot x, and iterated by generator method. The square slot is divided into four portions with the same physical size as shown in Figure 5.3. The first iteration is achieved when the upper left portion is filled with metal. Then, the same generator method is applied on the remaining portion. Repeating this generator method continuously, we can generate the n^{th} order Sierpinski square slot geometry with self-similar characteristics. Figure 5.3 (e) shows the modification after 3^{rd} iteration of proposed model. This model provides a UWB performance in the range of 3.1-10.6 GHz. In second part, an $\bigcap$-slot with height t_l and width t_s & t_w has been placed on microstrip feed line. A deep band notch at 5.5 GHz is provided using the $\bigcap$-slot. This slot prevents the interface between WLAN and UWB bands; meanwhile, the patterns and impedance bandwidth of the antenna are not affected using the $\bigcap$-slot.

Figure 5.4 shows the simulated reflection coefficient characteristics for different iteration stages of MSSF antenna. The resonance frequency of MSSF antenna decreases and bandwidth increases with increase in the number of iterations. Figure 5.5 shows simulated reflection coefficients for different length l_s and width w_s of grooved rectangular slot in ground plane. The values of length l_s and width w_s are varying from 2.8 mm to 3.8 mm and 3.6 mm to 5.2 mm, respectively. The operating bandwidth of MSSF antenna is improved for length, l_s=4.4 mm and width, w_s=2.8 mm. From this observation, it is clear that the reflection coefficients can be controlled by changing the value of rectangular slot l_s and w_s in top of the ground plane.

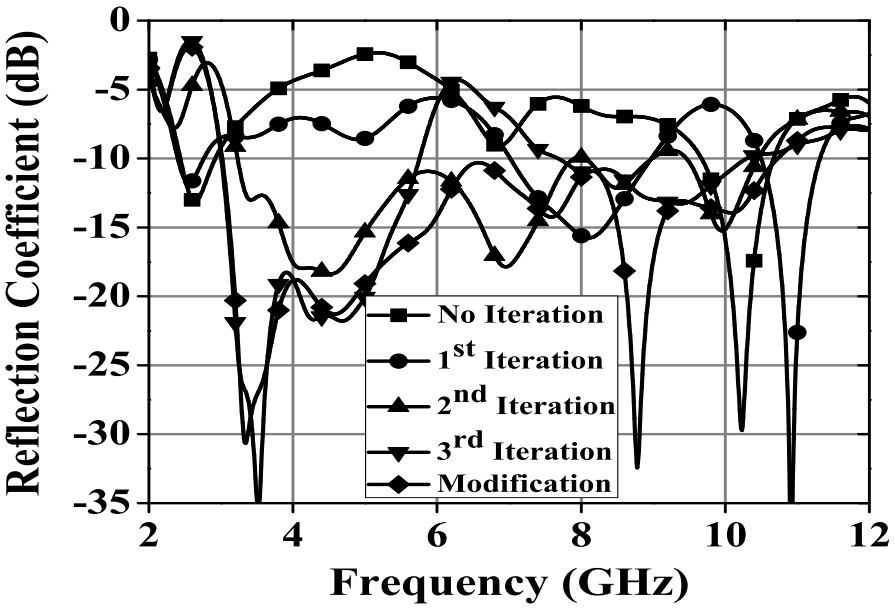

Figure 5.4: Simulated reflection coefficients of proposed MSSF antenna for different iterations.

A modification can be made to the above designed antenna for achieving the bandstop function to avoid possible interference to other existing WLAN systems. A very narrow $\bigcap$-slot is cut away from the feed line as shown in Figure 5.2 (a). It acts as a filter element to make the antenna non-responsive at the bandstop frequency. For perfect band-rejection performance of UWB antenna, the reflection coefficient of the stop-band notch should be almost 1.0. However, in the band-stop antenna design, reflection coefficient -2.1 dB is observed. The $\bigcap$-slot filter element dimensions will

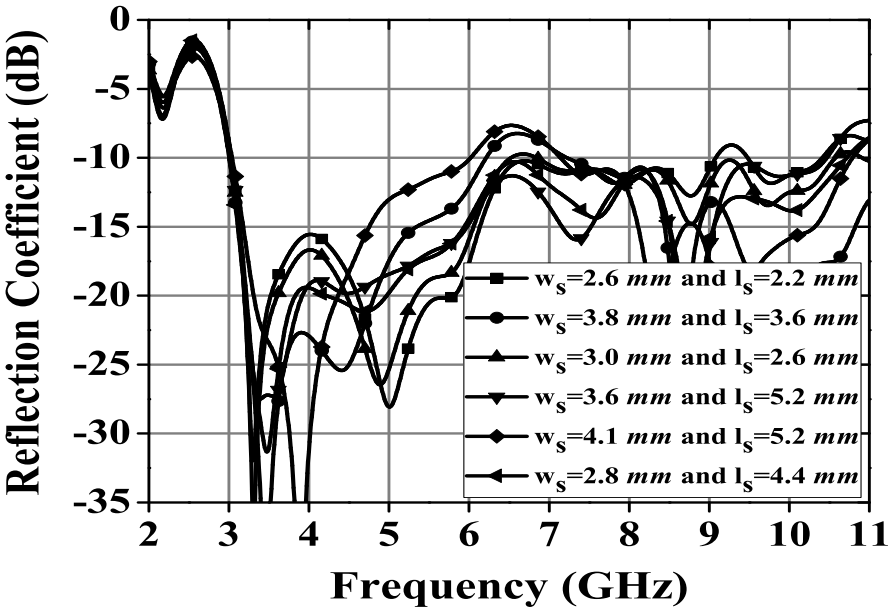

Figure 5.5: Simulated reflection coefficients of proposed MSSF antenna for different configuration of grooved ground plane.

control both the bandstop frequency f_{notch} and the rejection bandwidth of the band-notched filter BW_{notch}. The $\bigcap$-shaped slot filter of height t_l and widths t_s & t_w is placed on microstrip feed line. Figure 5.6 shows the simulated reflection coefficients of the MSSF antenna for different values of slot length t_l keeping other parameters fixed. It can be seen from Figure 5.6 that the length t_l of $\bigcap$-slot has an effect on resonance frequency of the notch band. Therefore, the resonance frequency can be adjusted by optimizing the length of $\bigcap$-slot. It is found that the resonant frequency of the notched band decreases with increase in the value of t_l. The simulated reflection coefficient curves with different values of t_s are plotted in Figure 5.7. As the t_s increases from 0.2 mm to 0.5 mm keeping other parameters fixed, the upper notched band edge remains unchanged and only the lower notched band shifted with variation of reflection coefficient value. Figure 5.8 shows the simulated reflection coefficient results for MSSF antenna in terms of width t_w. It can be noticed that tuning width t_w may be shifted to the upper notched band edge, while the lower notched band remains almost unchanged. Based on the above analysis, the resonance mechanism and parametric study on $\bigcap$-slot, the notched frequency (f_{notch}) can be empirically

approximated and given by (5.4)

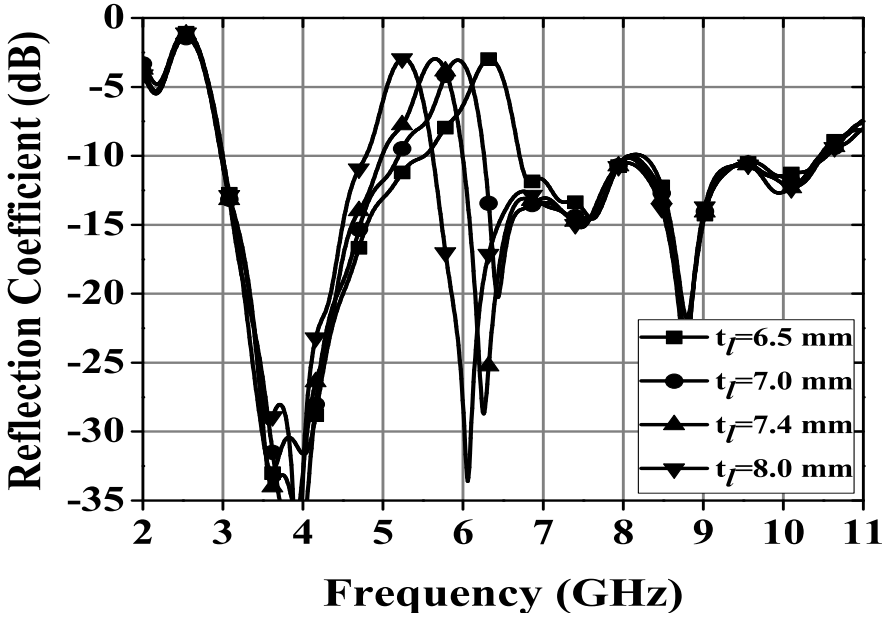

Figure 5.6: Simulated reflection coefficients of proposed MSSF antenna for length t_l of band notch slot.

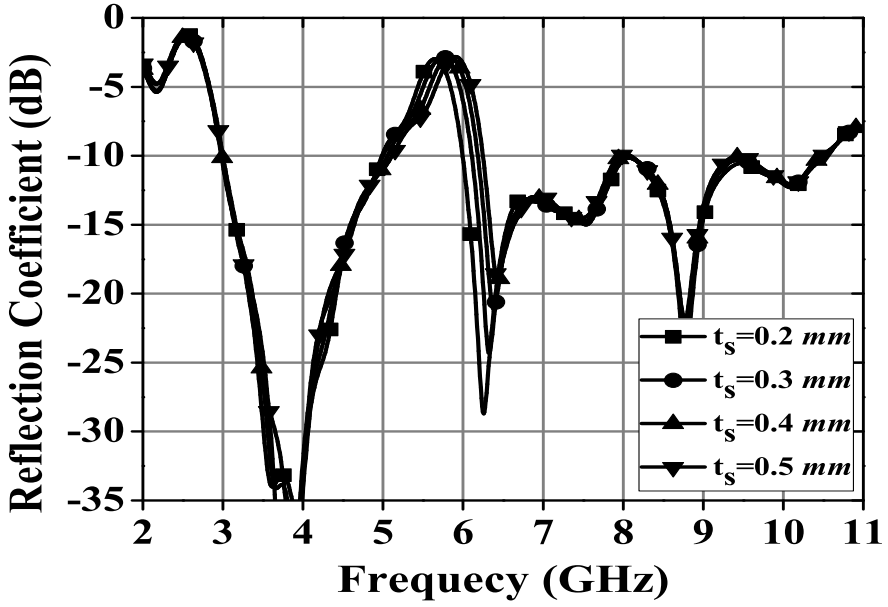

Figure 5.7: Simulated reflection coefficients of proposed MSSF antenna for width t_s of band notch slot.

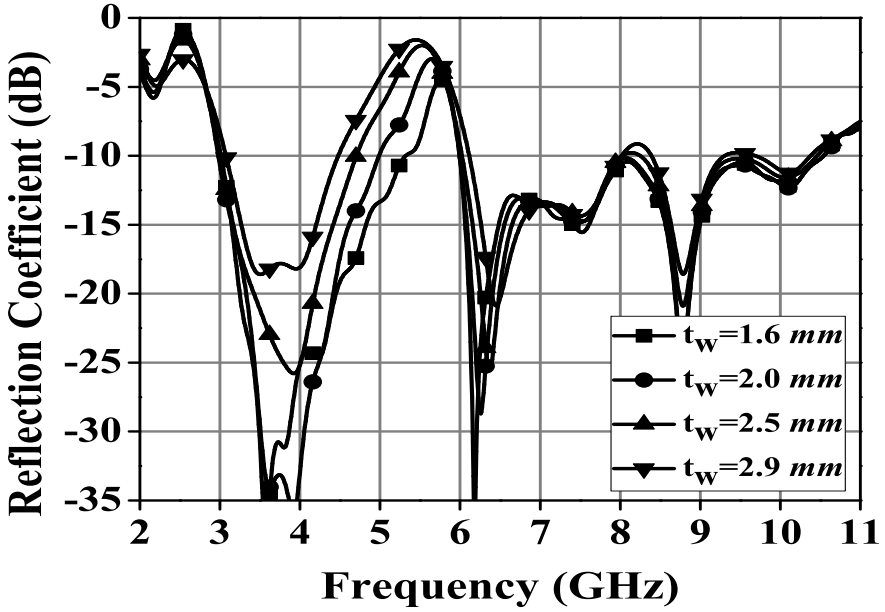

Figure 5.8: Simulated reflection coefficients of proposed MSSF antenna for width t_w of band notch slot.

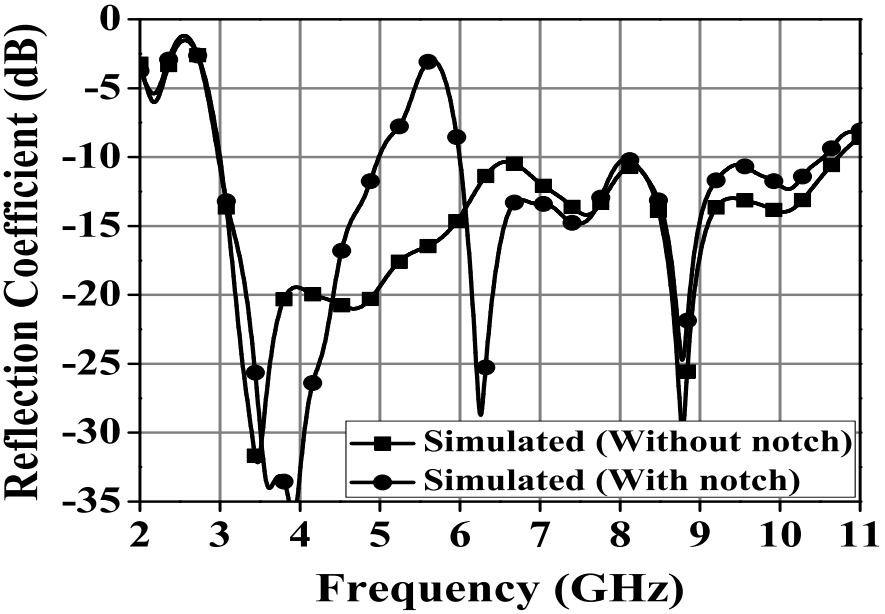

Figure 5.9: Simulated reflection coefficients of proposed MSSF antenna for with and without notch

$$slot\ length \approx \frac{c}{2f_{notch}} \left\{ \frac{\sqrt{\epsilon_r + 1}}{2} \right\}^{-1} \tag{5.4}$$

where c is the speed of light and ϵ_r is the relative permittivity.

Figure 5.9 plots the simulated reflection coefficients of antenna with and without the $\bigcap$-slot. It is clear that the antenna resonances remain unaffected due to the presence of the $\bigcap$-slot excluding the frequency band 5-6 GHz.

Figure 5.10 shows the simulated 3D radiation patterns and surface current distributions of the proposed MSSF antenna at 4 GHz, 5.5 GHz, 6.2 GHz and 8.7 GHz. It can be observed that the gain of the proposed antenna at all the frequencies is more than 2 dBi. 3D patterns are omnidirectional towards the lower frequency band and nearly omni-directional with multiple lobes towards the higher frequency band. The distribution of current in lower frequency is on lower side of the radiating element. Further, at higher frequency, the current moves towards the tip of the radiating element. In addition, at 5.5 GHz the 3D stronger current distribution mainly concentrated at the area of $\bigcap$-slot. It causes the antenna to be non-responsive at that frequency. The impedance changes making large reflection at the desired notched frequency. Table 5.2 provides the simulated gain, measured gain and simulated total antenna efficiency for UWB antenna. From the table, some discrepancy exists between measured and simulated gains. This is not consistent in nature. However, simulated total antenna efficiency is more than 75 % throughout UWB.

Table 5.2: Simulated gain, measured gain and simulated total antenna efficiency of MSSF antenna

Antenna Type	Frequency (GHz)	Simulated Gain (dBi)	Measured Gain (dBi)	Total Antenna Efficiency (%)
UWB MSSF antenna with $\bigcap$-slot	4	3.32	3.34	92.9
	5.5	4.11	4.17	83.82
	7	4.78	4.33	84.81
	9	3.78	3.26	75.14
UWB MSSF antenna without $\bigcap$-slot	4	3.10	3.39	91.5
	5.5	-4.15	-4.32	22.30
	7	4.12	4.39	81.47
	9	3.58	3.12	74.05

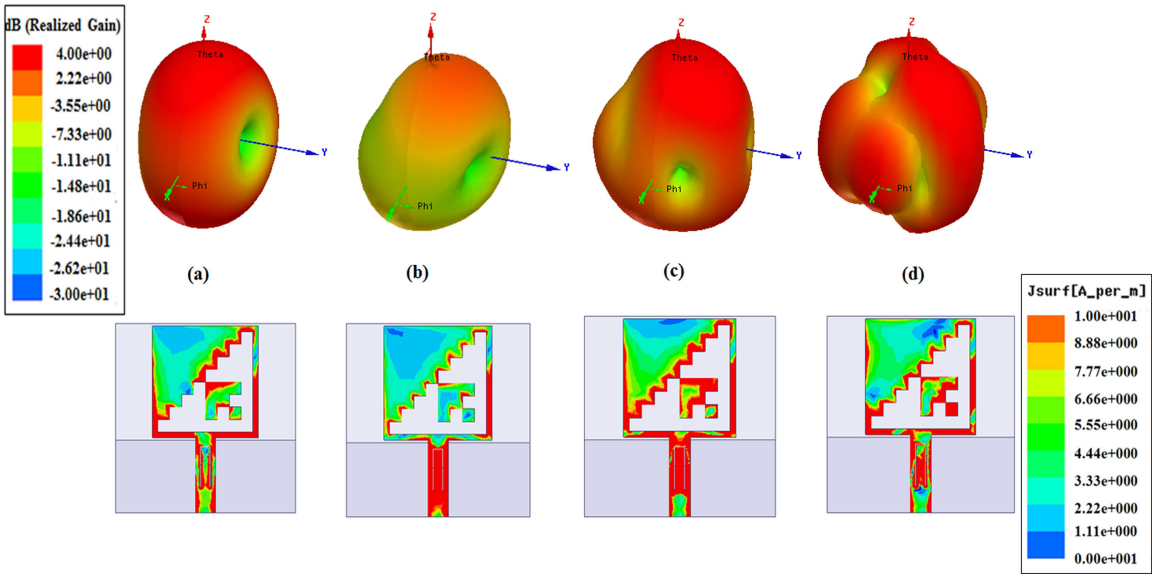

Figure 5.10: Simulated 3D radiation patterns for proposed MSSF antenna at (a) 4 GHz (b) 5.5 GHz (c) 6.2 GHz (d) 8.7 GHz

5.2.2 Experimental verification

Photographs of proposed MSSF antenna is shows in Figure 5.2 (c). The measurement has been carried out using Agilent vector network analyzer (model no.E863B) and radiation patterns are measured in an anechoic chamber in Space Applications Centre (SAC), Ahmadabad, India. Figure 5.11 and Figure 5.12 show the measured and simulated reflection coefficients with and without ⋂-slot in feed line. These results exhibit reasonable agreement although there is a frequency shift that can be attributed to reflection from SMA connector and some uncertainty in the electrical properties of the substrate. The impedance bandwidth of MSSF antenna is 110% covering UWB frequency band 3.1-10.6 GHz including the notched band of WLAN at 5.5 GHz (5-6 GHz).

Figure 5.13 shows the measured radiation patterns for XZ (Co-pol. and Cross-pol.) and YZ (Co-pol. and Cross-pol.) cut at 4 GHz, 5.5 GHz, 6.2 GHz, & 8.7 GHz. As can be seen from Figure 5.13 that, at lower frequency, the pattern is onmi-directional but at higher frequency it is nearly omnidirectional. The measured gain is plotted in Figure 5.14. The measured peak gain in boresight direction of proposed MSSF antenna without band notch varies between 0.2-3.0 dB with maximum peak gain of

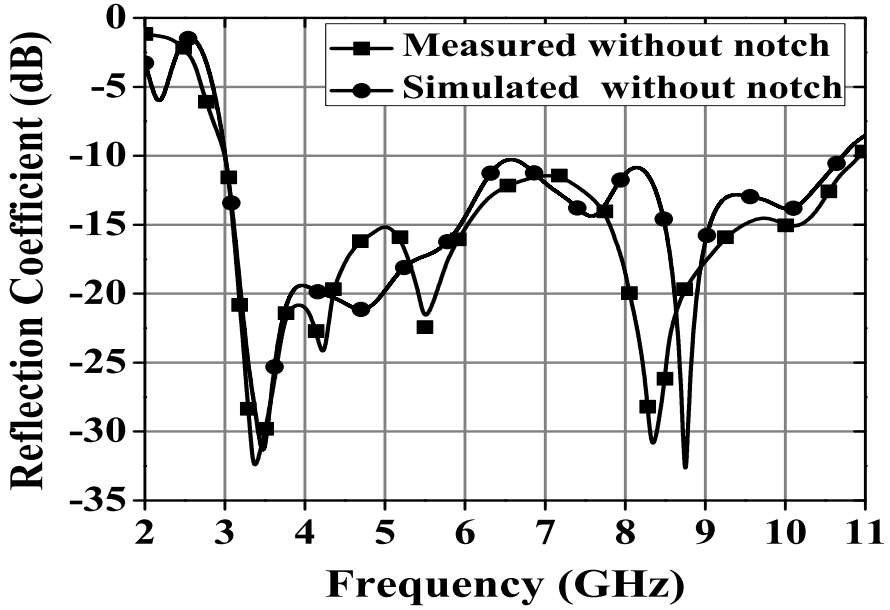

Figure 5.11: Simulated and measured reflection coefficients of proposed UWB MSSF antenna (a) Without band-notch (b) With band-notch characteristics.

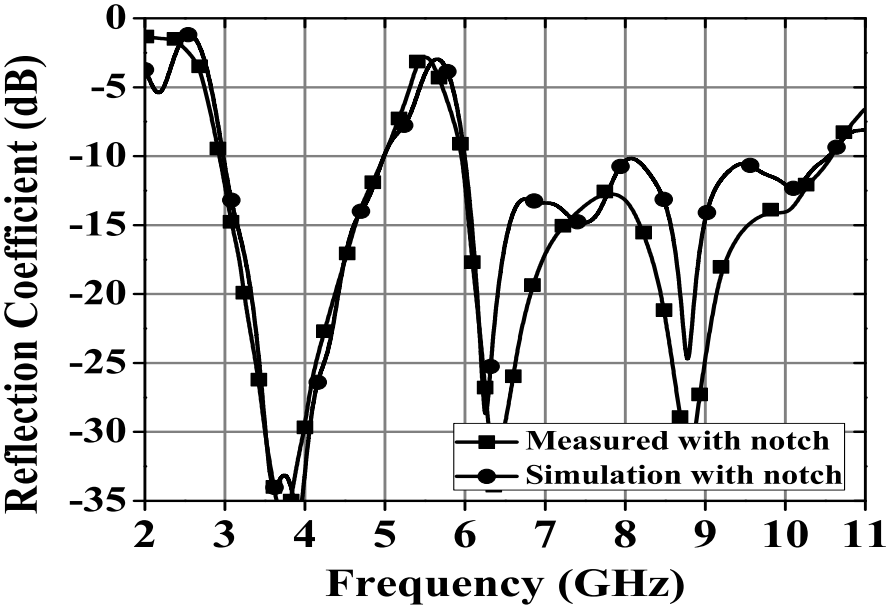

Figure 5.12: Simulated and measured reflection coefficients of proposed UWB MSSF antenna (a) Without band-notch (b) With band-notch characteristics.

4.75 dBi. The antenna gain decreases to 4 dBi in 5-6 GHz frequency due to the effect of band notch.

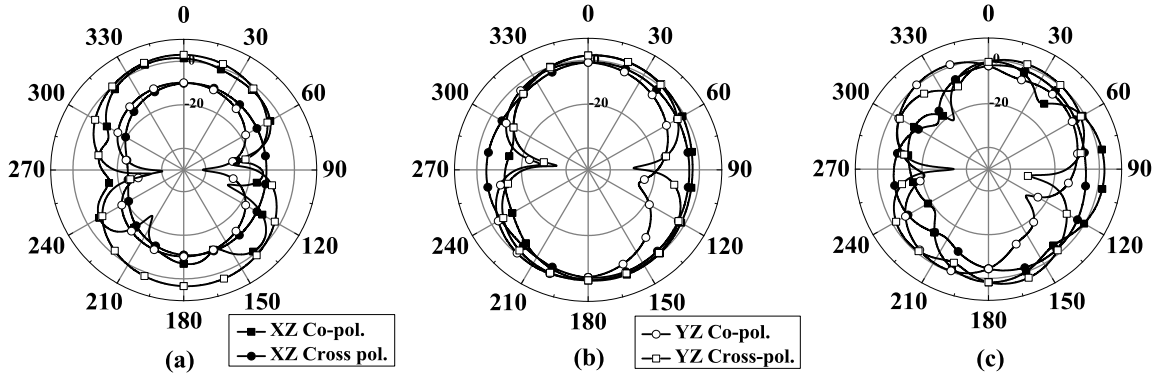

Figure 5.13: Measured radiation pattern of proposed MSSF antenna (a) at 4 GHz (XZ and YZ Co- and Cross- pol.), (b) at 6.2 GHz (XZ and YZ Co- and Cross- pol.), (c) 8.7 GHz (XZ and YZ Co- and Cross- pol.).

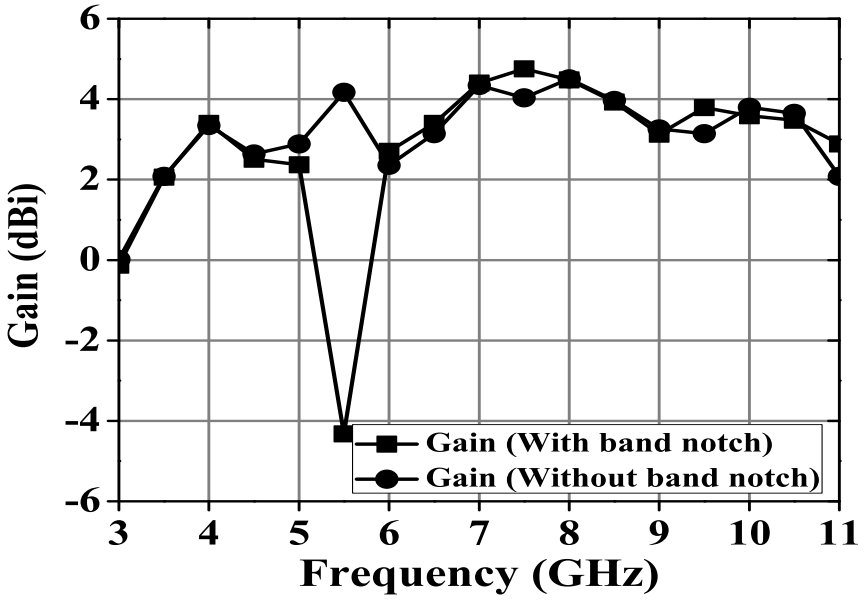

Figure 5.14: Measured peak realized gain of proposed UWB MSSF antenna with and without band notch

To examine the antenna performance in time domain, the phases of transmission response and waveform distortion in the operating frequency region are discussed. Here, time domain integration is used to carry out the above simulation. Two identical antennas are placed in the face to face orientation with a distance of 0.3 m [200]. Figure 5.15 (a) and (b) show the phase response of reference and band notch antenna. It is observed that the phase response is generally linear for reference antenna and

few ripples are found in band notch antenna at 5.5 GHz. The group delay $\tau_g(\omega)$ of an antenna characterizes the frequency dependence of the time delay and is defined in frequency domain as in equation (5.5)

$$\tau_g(\omega) = \frac{d\phi(\omega)}{d\omega} = -\frac{d\varphi(f)}{2\pi df} \tag{5.5}$$

where $\varphi(f)$ is the frequency dependent phase of the radiated signal. The group delay is the delay that a portion of the spectral energy at a given angular frequency ω encounters when transmitted through a filter. For minimum distortion, the group delay should be constant within the frequency band of interest, in which case the phase increases linearly with frequency. The magnitudes of transfer function and group delay are discussed in Figure 5.16. It shows sharp decreases in the magnitude of transfer function S_{21} and group delay in band notch. The low variation in magnitude as well as in the transfer function and nearly constant group delay imply that the proposed antenna exhibits phase linearity at designed UWB frequency band. Hence, it shows superior pulse handling capabilities as demanded by modern communication system.

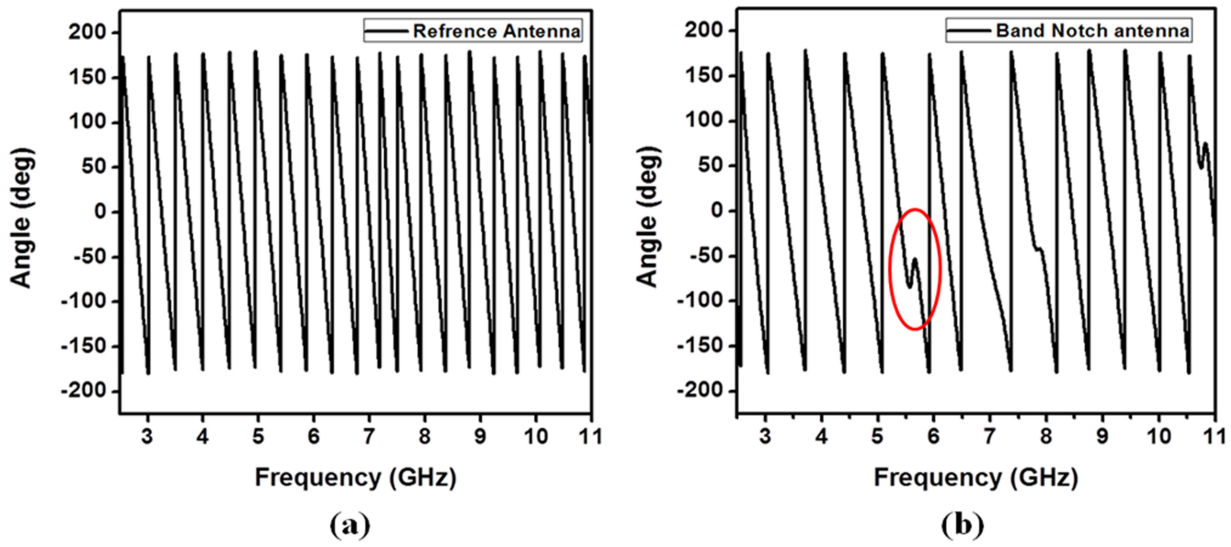

Figure 5.15: Phase responses for different identical pairs (a) Reference antenna (b) Band-notch antenna

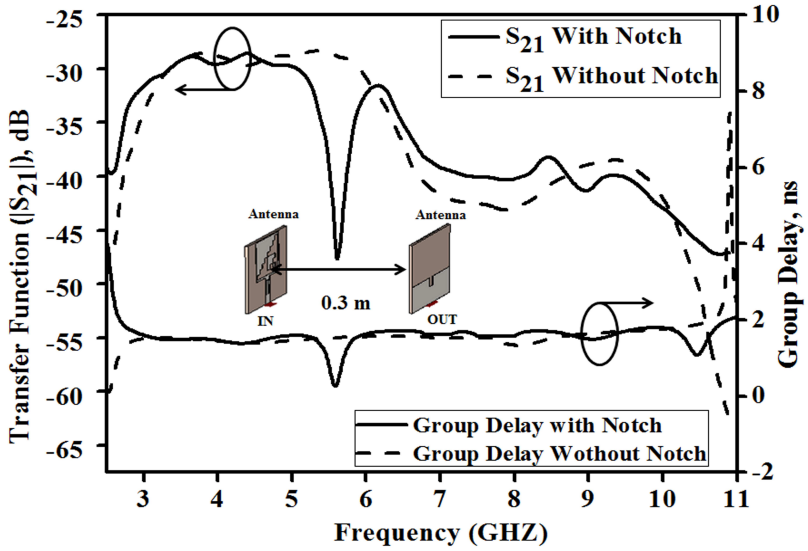

Figure 5.16: Transmission characteristics and group delay of proposed MSSF antenna

5.3 Summary

For UWB application, a modified square Sierpinski fractal (MSSF) antenna is designed. The proposed MSSF antenna is useful for UWB application (3.1-10.6 GHz) with band notch characteristics at 5.5 GHz (5-6 GHz). The band rejection is achieved by using $\bigcap$-slot in microstrip feed line. The measured radiation patterns are stable throughout the operating band. The gain of MSSF antenna is 2-5 dB in UWB frequency range and decreases in band rejection frequency. Therefore, the proposed antenna can be a candidate for low profile and low cost UWB wireless communication systems.

CHAPTER 6

Fractal Antenna Array for MIMO Environment

6.1 Introduction

In the previous chapter, a fractal geometry based Sierpinski square monopole antenna was studied for UWB application with band-notched characteristics. In this chapter, fractal antenna arrays for MIMO environment are investigated. Here, some of the fractal antenna designs are used from previous chapters to obtained the arrays.

New generation of mobile communication system devices, such as the current 3G-4G networks and the provision of multimedia services, have exponentially increased the number of mobile users demanding for higher data rate. This fact has aroused the interest in studying possible solutions to improve system performance without making use of new frequency band allocations. In this chapter, we discuss about wireless communication systems with Multiple-Inputs and Multiple-Outputs (MIMO) in which many antennas (2-element and 4-element) are used for transmission and reception. In addition to this, design of wideband feed network based on modifying Wilkinson power divider is also introduced. A linear antenna array is good candidate to achieve a higher gain and directivity for certain applications. Here, microstrip printed 2-element and 4-element linear antenna arrays for wideband applications using modified Wilkinson power divider are proposed. EM simulation is used to tune their physical dimensions.

This chapter is organized as follows. Section 4.2 shows the 2-element and 4-element hybrid fractal shape antenna with MIMO implementation for hand-held devices. The proposed antenna geometry is based on previously designed (chapter 3) hybrid fractal antenna. Section 4.3 presents the results for wideband feed network based modified 3-

section 2-ways Wilkinson power divider. Section 4.5 focuses on the design of 2-element and 4-element wideband sectoral linear antenna arrays by exploiting the previously designed antenna elements (chapter 3). Finally, Section 4.7 summarizes the chapter.

6.2 Hybrid Fractal Antenna with MIMO Implementation

Mobile communication using MIMO processing has emerged as a breakthrough for wireless systems of revolutionary importance. All wireless technologies face the challenges of signal fading, multi-path, increasing interference and limited spectrum. MIMO technology exploits multi-path to provide higher data throughput, and simultaneous increase in range and reliability without need of additional radio frequency. Early studies indicate that increase in capacity is possible by using MIMO systems. A lot of wideband/UWB antennas and MIMO antennas have already been reported in literature.

This section deals with multiband/wideband MIMO antennas for hand-held devices. It presents the defined objectives and consequently the approaches to achieve these goal. The analysis and evaluation of performances of these proposed designs are considered taking special parameters into account which are necessary to characterize multiband MIMO antennas. Finally, solution to enhance isolation with reduced antenna size, envelope correlation coefficient and capacity loss are presented.

6.2.1 2-Element Hybrid Fractal Antenna

This section is uses previously designed hybrid fractal (chapter 3) shape monopole antenna. It coverage of multiple wireless communication bands for hand-held mobile devices with MIMO implementation. The proposed antenna is a combination of Minkowski island curve [58] and Koch curve fractals [54, 55]. It is placed with edge to edge separation of 0.16 λ_0 at 1.75 GHz. The T-shape strip is inserted and rectangular slot is etched at top side of ground plane, in order to improve the impedance matching and isolation between the antennas. The measured impedance bandwidths of the proposed antenna ($S_{11} \leq 10dB$) are 14% from 1.65 GHz-1.9 GHz for the band

1 and 80% from 2.68 GHz-6.25 GHz for the band 2.

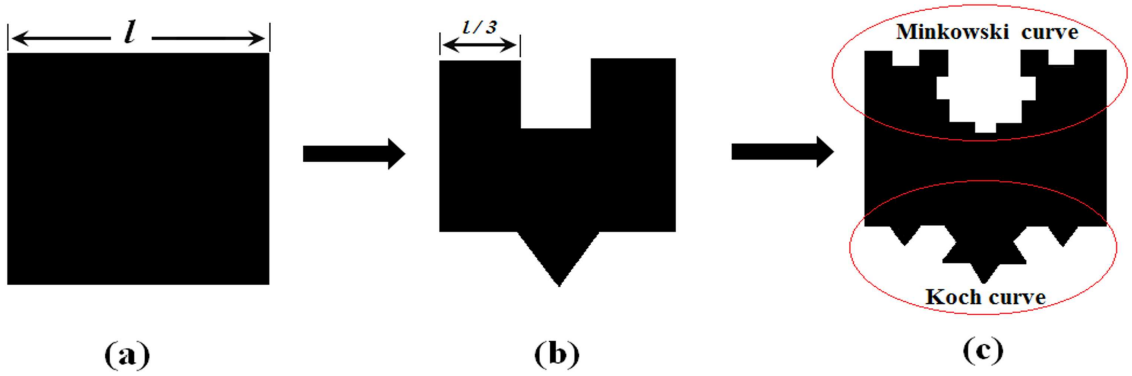

Figure 6.1: Recursive procedure if the hybrid fractal antenna (a) Initial geometry (b) First iteration (c) Second iteration

Antenna geometry and simulation results

To obtain the self-similarity dimensions, the geometry is divided using downscaling approach, but identical copies of itself. If there are 'n' such copies of original geometry scaled down by a function S, the similarity dimension 'D' is defined as in equation (6.1).

$$D = \frac{logn}{\log \frac{1}{S}} \tag{6.1}$$

The recursive procedure of the hybrid fractal antenna is shown in Figure 6.1. It is observed that the square can be divided into four copies of 1/2 scale, nine copies of 1/3 scale, 16 copies of 1/4 scale, or n^2 copies of $1/n$ scale. Substituting in the above formula, the dimension of the geometry is ascertained to be 2. This approach can be followed in determining the dimension of fractal geometries.

For construction of Koch and Minkowski curve fractals (Figure 6.1), one can start with a straight-line (l) called initiator and it is divided into three equal parts ($l/3$). In case of Koch curve, the middle segment is divided and replaced with two other segments of the same length. Besides, in case of the Minkowski island curve, the middle segment is replaced by two horizontal and a vertical segment of equal lengths. This is the first iterated version of the geometry and is called 'generator' for higher iterations, as shown in Figure 6.1. This procedure may be iterated recursively to

result in self-similar fractal geometries.

Table 6.1: Dimensions of 2-element hybrid fractal MIMO antenna

L	W	L_t	W_t	L_s	W_s	h
10 mm	10 mm	17 mm	20 mm	6 mm	20 mm	1.54 mm

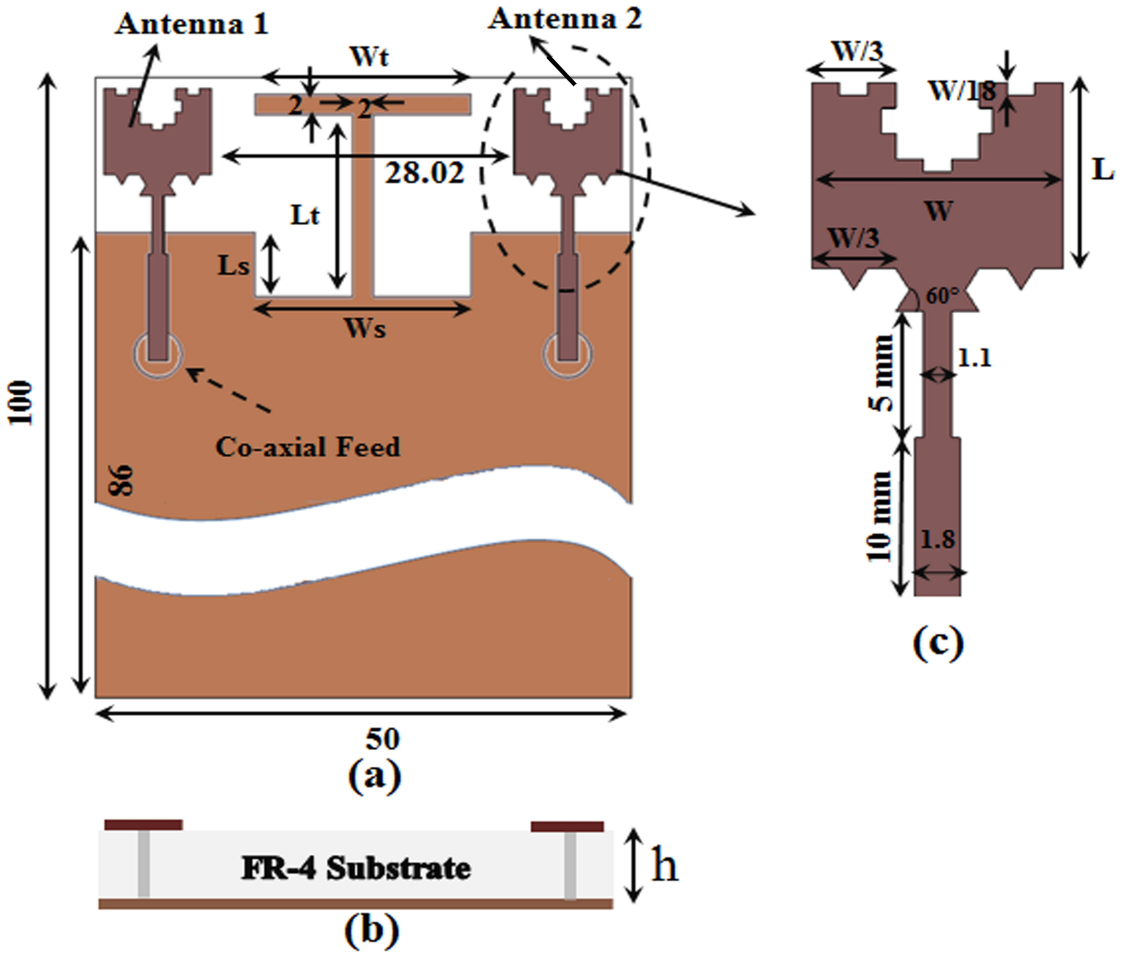

Figure 6.2: Geometry of 2-element hybrid fractal antenna (a) Front view (b) Top view (c) Hybrid fractal design dimensions

The geometry of the proposed hybrid fractal antenna with MIMO implementation is shown in Figure 6.2 with its final dimensions listed in Table 6.1. Koch curve and Minkowski island curve fractals are applied to the edges of the square patch up to the second iteration. Its dimensions are also indicated in Figure 6.2 (c). The motivation of such geometry is to improve space filling, a feature that translates into reduced antenna physical size and for increased number of resonant frequency bands. The

antenna is fed through the 50Ω SMA coaxial probe connected to the microstrip line with matching section over the grooved ground plane. As shown in Figure 6.2, MIMO antenna consists of the edge-to-edge separation of 28.02 mm (0.16 λ_0 at 1.75 GHz) between the two symmetrical hybrid fractal radiating elements. The FR-4 ($\epsilon_r = 4.4$) substrate of size 100×50 mm^2 with height 'h' is used. Here, the radiating elements are placed on one side of the substrate and grooved ground plane of size 86×50 mm^2 is located on the other side. It should be noted that the grooved areas L_s and W_s are located on top of the ground plane with T-shape strip (W_t and L_t); the widths of 2 mm is fixed for T-shape strip. It is introduced to improve the impedance matching and isolation between the radiating elements.

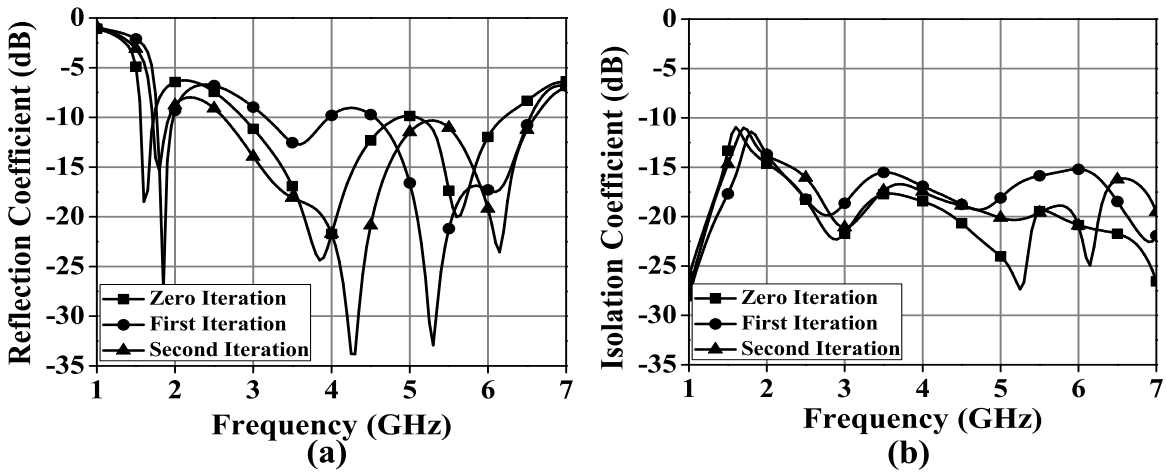

Figure 6.3: Simulated reflection and isolation coefficients of proposed hybrid fractal antenna with different iterations

As the number of iterations increase, the average electrical length of the monopole also increases which consequently, lowers the operating frequency of the proposed antenna and leads to effective antenna miniaturization. The simulated reflection coefficients (S_{11}, S_{22}) and isolation coefficients (S_{21}, S_{12}) of the proposed antenna are shown in Figure 6.3, which are computed using the Ansys High frequency structure simulator (HFSS) v 14. It is observed from Figure 6.3 (a) that when the number of iterations increase, the fractional matching bandwidth ((S_{11}, S_{22})= -10 dB) of the antenna also increases. There are several visible multiple resonances within the bandwidth. For the iteration 2, impedance bandwidths are 14 % from 1.65-1.9 GHz for

the band 1 and 80 % from 2.68-6.45 GHz for the band 2, which covers LTE band (1.7-1.9 GHz) and several wireless communication bands like WiFi/WiMAX/WLAN bands (2.68-6.45 GHz). In addition, the isolation coefficients (S_{21}, S_{12}) are below -10 dB and -15 dB for the band 1 and band 2, respectively are shown in Figure 6.3 (b).

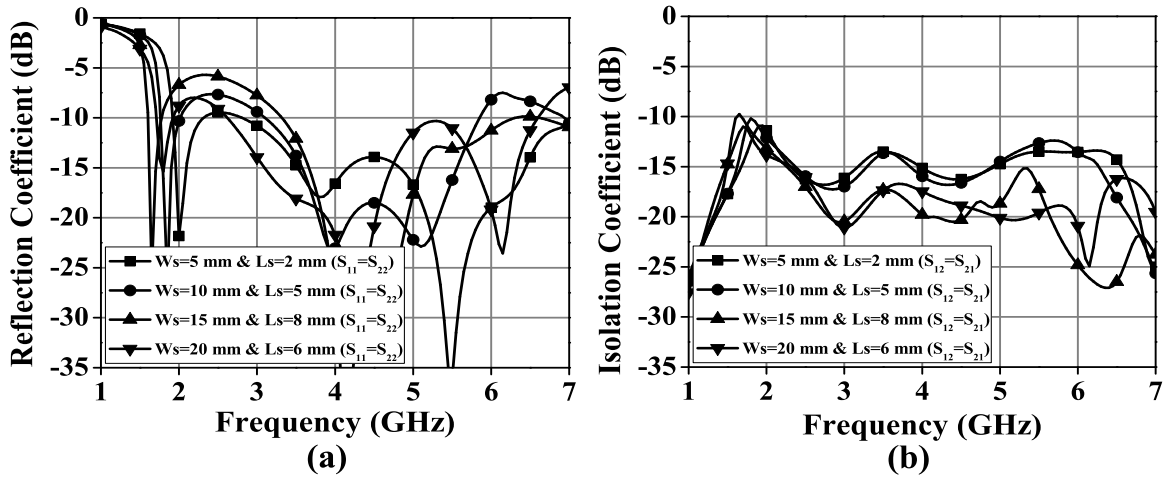

Figure 6.4: Simulated reflection and isolation coefficients of proposed hybrid fractal antenna with different configuration of grooved area.

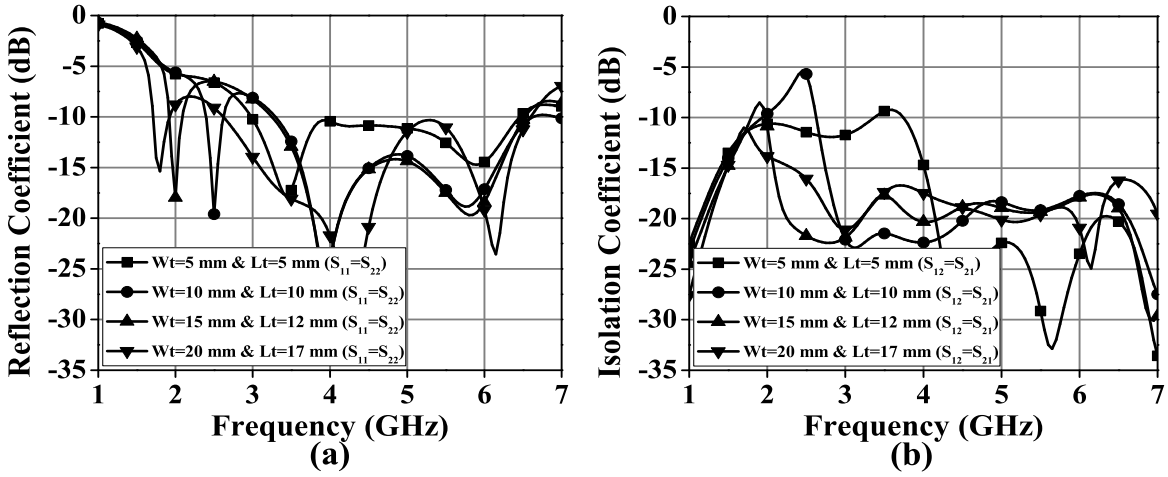

Figure 6.5: Simulated reflection and isolation coefficients of proposed hybrid fractal antenna with different configuration of T-shape strip.

Figures 6.4 shows the simulated reflection coefficients S_{11}, S_{22} and isolation coefficients S_{21}, S_{12} of the proposed monopole antenna for grooved ground plane in different cases. In case I, the grooved rectangular slots W_s= 5 mm and L_s= 2 mm are present. It is observed that the reflection coefficients of S_{11}, S_{22} and isolation coefficients

S_{21}, S_{12} are not good enough for the desired frequency bands (LTE/WiFi/WiMAX /WLAN). In case II, W_s= 10 mm and L_s= 5 mm, it is perceived that S_{11}, S_{22} and S_{21}, S_{12} are not well below -10 dB for our desired operating bands. In case III, W_s= 15 mm and L_s= 8 mm, it is noticed that S_{21}, S_{12} are well below -10 dB for our desired operating bands whereas the S_{11}, S_{22} are not matching with band 1. In case IV, $W_s = 15mm$ and $L_s = 8mm$, it is noticed that the S_{11}, S_{22} and S_{21}, S_{12} are well below the acceptable criteria for our desired operating bands. Thus, the proposed structure provides satisfactory performance in case IV for the band 1 and band 2. Similiary, S_{11}, S_{22} and S_{21}, S_{12} of proposed antenna for different values of T-shape strip W_t, L_t are shown in Figure 6.5. It is observed that the mutual coupling between antenna 1 and antenna 2 is greatly improved. For W_t= 20 mm and L_t= 17 mm, the values of S_{11}, S_{22} and S_{21}, S_{12} are well below the acceptable criteria for our desired operating bands.

Figure 6.6 shows the surface current distributions at 1.75 GHz and 4.5 GHz for the proposed MIMO antenna. As can be seen, when antenna 1 is excited, the antenna 2 is terminated in 50 Ω load, and vice versa. The surface current flows in the feed line as well as in T-shape strip, at both the frequencies. It can be noticed that there is negligible current on the second radiator due to the presence of T-shape strip, thereby improving isolation between the antennas. This tends to decouple the current on antenna 2 and hence it enhances the isolation between two radiators efficiently at 1.75 GHz and 4.5 GHz.

Figures 6.7 shows the simulated 3D radiation patterns for the antenna 1 and antenna 2 at 1.75 GHz, 3 GHz, 4.5 GHz and 6 GHz. It can be noticed that the gain of the proposed monopole antenna at all the frequencies within the bands are more than 2 dBi. The 3D radiation patterns are omni-directional towards the lower frequency band and becomes nearly omni-directional with multiple lobes towards the higher frequency band. These patterns are ideal for hand-held wireless devices.

Experimental Verifications

The proposed hybrid fractal MIMO antenna is milled on the copper side of FR-4 substrate using LPKF-42 Protomat milling machine. Photographs of fabricated

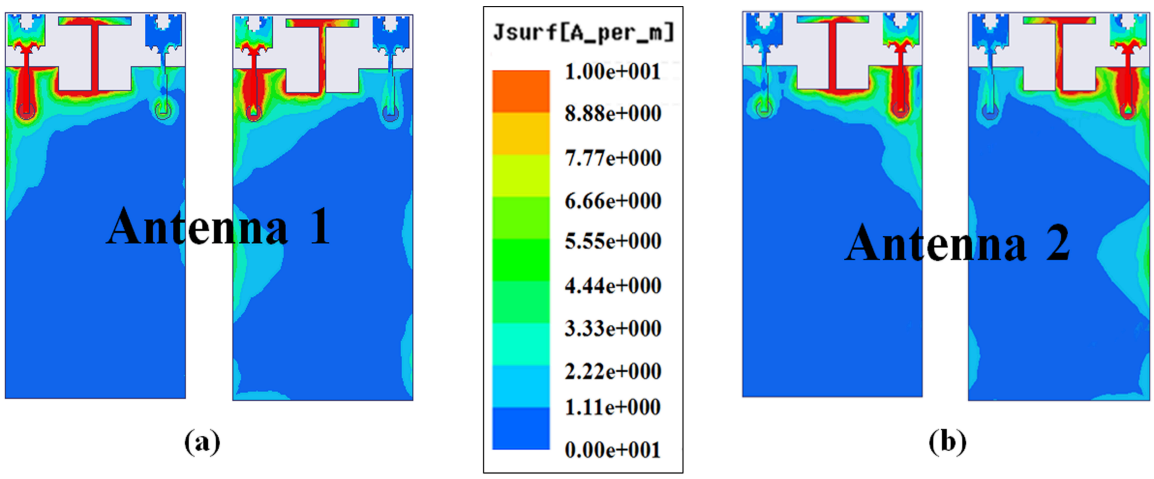

Figure 6.6: Simulated surface current distribution of the MIMO antenna (a) Antenna 1 at 1.75 GHz and 4.5 GHz (b) Antenna 2 at 1.75 GHz and 4.5 GHz.

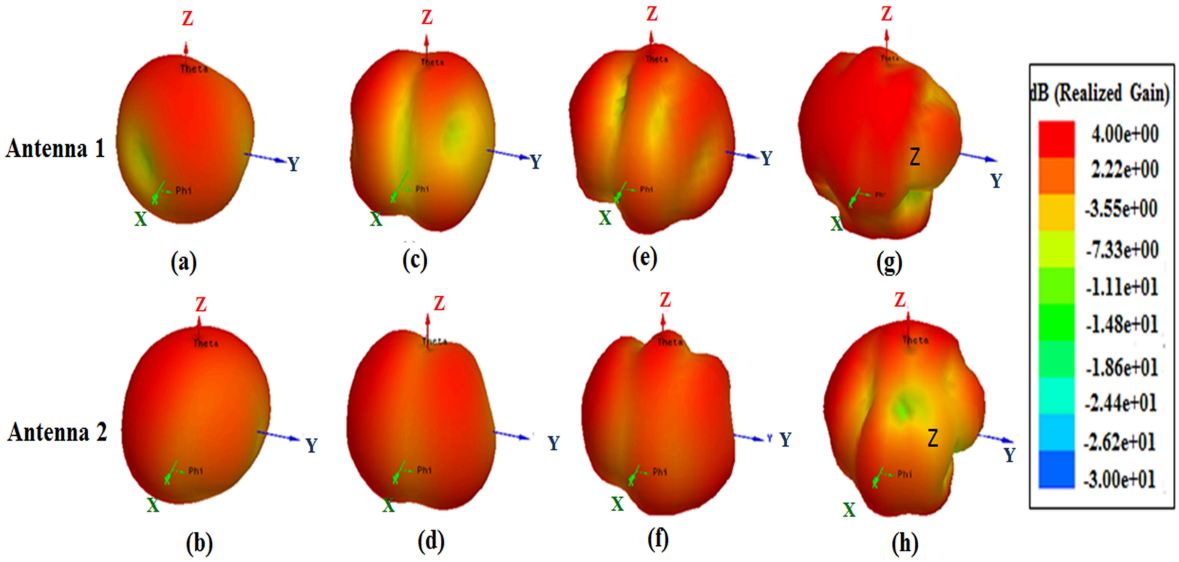

Figure 6.7: Simulated 3D gain radiation patterns for the antenna 1 & antenna 2; Figs. (a) and (b) are at 1.75 GHz , Figs. (c) and (d) are at 3 GHz, Figs. (e) and (f) are at 4.5 GHz, and finally, Figs. (g) and (h) are at 6 GHz.

antenna are shown in Figure 6.8. The antenna is measured using Anritsu (model 37486D) vector network analyzer (VNA) for impedance matching. The radiation patterns are measured in an anechoic chamber, both available at the Antenna and Microwave Laboratory (AML) SDSU, CA, USA. Measured and simulated values of the reflection coefficients (S_{11}, S_{22}) and isolation coefficients (S_{21}, S_{12}) are plotted in Figures 6.9 (a) and 6.9 (b), respectively. These results exhibit reasonable agreement

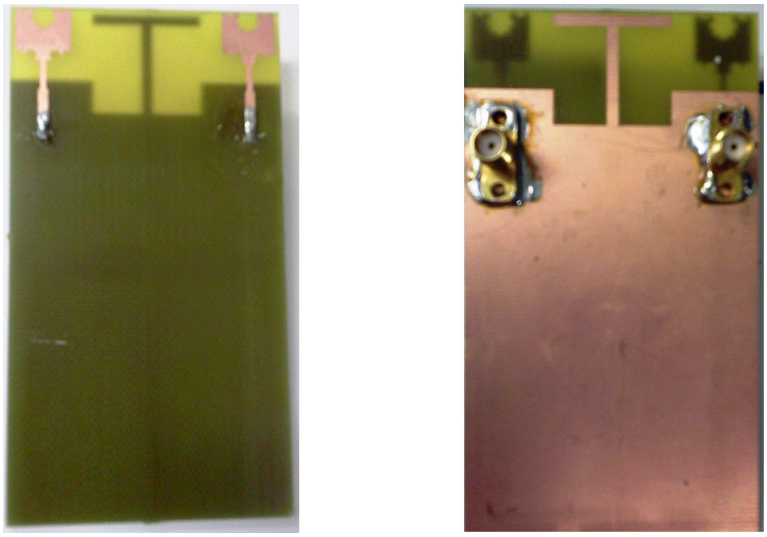

Figure 6.8: Photographs of the fabricated hybrid fractal MIMO antenna (a) Front view (b) Rear view.

although there is a frequency shift that can be attributed to reflection from SMA connector and other uncertainties. As can be seen, measured impedance bandwidths are 14 % from 1.65-1.9 GHz for band 1 and 80 % from 2.68-6.25 GHz for band 2. The achieved bandwidth covers the requirement of LTE/WiFi/WiMAX/WLAN communication applications. The isolation between the two antennas is below -10 dB and -15 dB for the lower and higher frequency bands respectively.

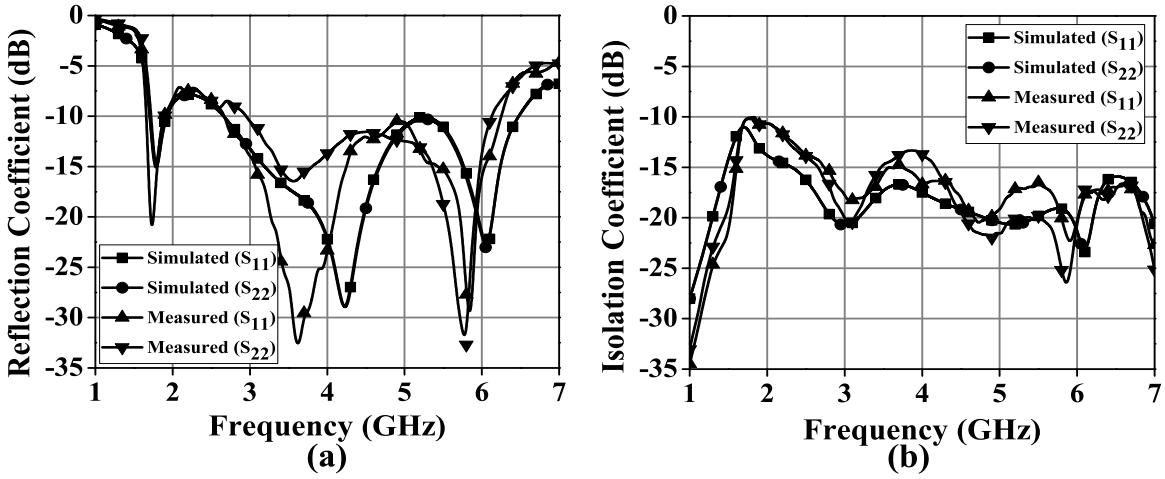

Figure 6.9: Simulated and measured reflection and isolation coefficients of proposed hybrid fractal antenna

The correlation coefficient is a parameter of great importance for MIMO systems

providing diversity. The signals received in the diversity systems can be correlated to some extent. The correlation coefficient is a statistical tool that measures the degree of similarity among the received signals. Its modulus varies from 0 to 1. Ideally, diversity systems require a correlation coefficient of zero or low by default. This parameter can be viewed by three ways: complex, envelope and power correlation coefficients. Complex correlation coefficient gives the complex measure of correlation between received signals at the antennas. It can be given as [201]

$$\rho_c = \frac{\int_0^{2\pi}\int_0^{\pi}\left(XPRE_{\theta k}\left(\theta,\varphi\right)E_{\theta l}^{*}\left(\theta,\varphi\right)P_{\theta}\left(\theta,\varphi\right)+E_{\varphi k}\left(\theta,\varphi\right)E_{\varphi l}^{*}\left(\theta,\varphi\right)P_{\varphi}\left(\theta,\varphi\right)\right)\sin\theta d\theta d\varphi}{\sqrt{\sigma_k^2\sigma_l^2}} \tag{6.2}$$

where σ_k^2 and σ_l^2 represent the variances of k^{th} and l^{th} branches and can be written mathematically as

$$\rho_c = \int_0^{2\pi}\int_0^{\pi}\left(XPRG_{\theta k}\left(\theta,\varphi\right)P_{\theta}\left(\theta,\varphi\right)+G_{\varphi k}\left(\theta,\varphi\right)P_{\varphi}\left(\theta,\varphi\right)\right) \tag{6.3}$$

also

$$G_{\theta k}\left(\theta,\varphi\right) = E_{\theta k}\left(\theta,\varphi\right)E_{\theta l}^{*}\left(\theta,\varphi\right) \tag{6.4}$$

$$G_{\varphi k}\left(\theta,\varphi\right) = E_{\varphi k}\left(\theta,\varphi\right)E_{\varphi l}^{*}\left(\theta,\varphi\right) \tag{6.5}$$

where 'XPR' is the cross polarization ratio, $E_{\theta k}$ and $E_{\varphi l}$ are complex electric fields in the directions θ and φ respectively for the k^{th} antenna. Similar expressions are valid for l^{th} antenna. Usually, the envelope correlation is presented to evaluate the diversity capabilities of MIMO systems [202]. This parameter is always real and by definition gives the correlation among the amplitudes of the signals at antennas. For Rayleigh fading channel, the envelope correlation can be given as follows:

$$\rho_c = \left|\rho_c\right|^2 \tag{6.6}$$

It is clear that Envelope Correlation Coefficient (ECC) should be preferably computed from 3D radiation patterns but it becomes tedious. However, assuming that the diversity system will operate in a uniform multi-path environment, the ECC can

be calculated from S-parameters using the following equation (6.7) [[181, 203].

$$\rho_c = \frac{|S_{11}^* S_{12} + S_{21}^* S_{22}|}{\left(1 - |S_{11}|^2 - |S_{12}|^2\right)\left(1 - |S_{11}|^2 - |S_{12}|^2\right)} \tag{6.7}$$

Figure 6.10 (a) shows the simulated and measured ECC across the desired frequency band. As can be seen, the value of ECC is well below the practical threshold value of 0.5 for both the bands 1 & 2. Similarly, capacity loss (bits/Hz) is another performance parameter which characterizes quality of a MIMO antenna system. Channel capacity is the tightest upper bound on the rate of information that can be reliably transmitted over a communications channel. This can be defined using the correlation matrix given in [204], and is calculated by using the following equation (6.8) [179, 205].

$$C_{loss} = -\log_2 det\left(\Psi^R\right) \tag{6.8}$$

where Ψ^R is the receiving antenna correlation matrix that is given by:

$$\Psi^R = \begin{pmatrix} \rho_{11} & \rho_{12} \\ \rho_{21} & \rho_{22} \end{pmatrix}$$

$\rho_{ii} = 1 - \left(|S_{ii}|^2 - |S_{ij}|^2\right),\ and\ \rho_{ij} = -\left(|S_{ii}^* S_{ij} + S_{ji}^* S_{ij}|\right)$

Figure 6.10 (b) shows the comparison of measured and simulated capacity loss values of the proposed MIMO antenna. It can be observed that the capacity loss does not exceed 0.3 bits/Hz and is well below the threshold value 0.4 bits/Hz for both the bands 1 & 2.

Figure 6.11 shows the measured radiation patterns at the bands 1 & 2 for XZ (Co-pol. and Cross-pol.) and YZ (Co-pol. and Cross-pol.) cut planes. During the measurement, only antenna 1 is excited while antenna 2 is terminated with a 50 Ω broadband load. It can be seen from Figure 6.11 (a-h) that at band 1, patterns are omni-directional but it is nearly omni-directional with some multiple lobe toward the higher frequency band. In the proposed MIMO antenna, the radiators are placed symmetrically, therefore, it will provide complementary or diversity patterns when one antenna is excited at a time and the other one is match terminated. Table 6.2 provides the measured gain, simulated total antenna efficiency at the band 1 & 2. The

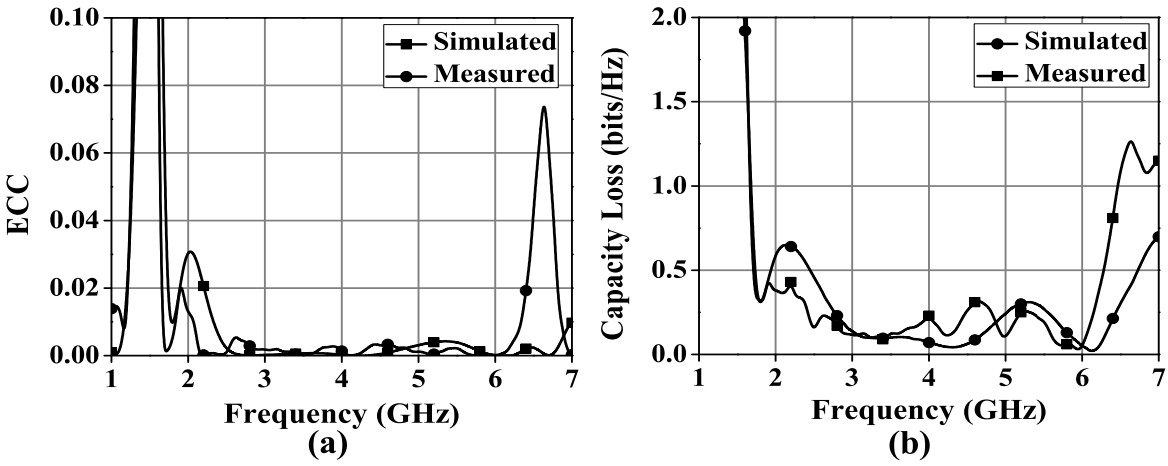

Figure 6.10: Simulated and measured (a) Envelope correlation coefficient (ECC) (b) Capacity loss of the proposed MIMO antenna.

simulated total antenna efficiency is found to be more than 80 % throughout the bands 1 & 2. The measured peak gain is varying between 0-2.5 dB with a maximum gain of around 2 dBi for the band 1. Similarly, for the band 2, it is varying between 2.5-4.85 dB with a maximum gain of 6.78 dBi. Due to symmetry of the antenna structure and their common fabrication tolerances; the gain values of the two radiators are almost the same. Therefore, only the gain of the antenna 1 is presented, when the antenna 2 is terminated in a 50Ω matched load.

Table 6.2: Gain and simulated total antenna efficiency of 2-element MIMO antenna

	Frequency (GHz)	Measured peak realized gain (dBi)	Simulated total antenna efficiency (%)
Band 1	1.75	1.67	82
Band 2	3.0	3.29	83
	4.5	5.25	93
	6.0	6.78	97

6.2.2 4-Element Hybrid Fractal Antenna

This section based on a previously designed 2-element hybrid fractal shape planar monopole antenna covering multiple wireless communication bands for hand-held mobile devices. The proposed MIMO antenna is having 4 symmetrical elements as radiators. It is also placed with edge to edge separation of 0.16 λ_0 at 1.75 GHz. The

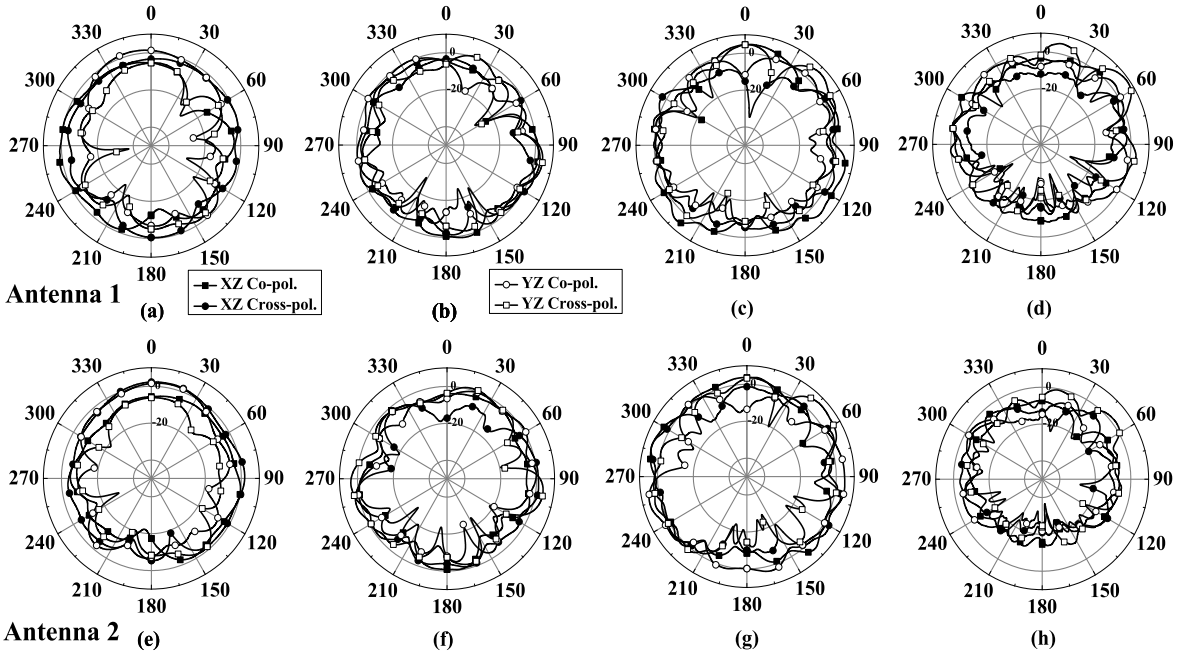

Figure 6.11: Measured radiation pattern for the antenna 1 and antenna 2; Figs. (a) and (e) at 1.75 GHz, Figs. (b) and (f) at 3 GHz, Figs. (c) and (g) at 4.5 GHz, and finally, Figs. (d) and (h) at 6 GHz.

T-shape strip is inserted and rectangular slot is etched at top and bottom side of ground plane, respectively, to improve the impedance matching and isolation between the antennas. Measured impedance bandwidths of 18 % (1.6-1.92 GHz) for the band 1 and 83.7 % from (2.58-6.3 GHz) for the band 2 are found.

Antenna Geometry and Simulation Results

The geometry of the proposed 4-element hybrid fractal MIMO antenna is shown in Figure 6.12. The motivation behind of 4-elements hybrid fractal geometry is to improve radiation characteristics, gain, efficiency and spatial or pattern diversity to increase data capacity in MIMO system for hand-held devices. The antenna is fed through the 50Ω SMA coaxial probe connected to the microstrip line with matching section over the grooved ground plane. The FR-4 ($\epsilon_r = 4.4$) substrate of size 100×50 mm^2 with height h is used. The proposed antenna consists of four symmetrical element antennas (element #1, element #2, element #3 & element #4) and the edge-to-edge separation of the elements is about 28.02 mm (0.16 λ_0) at 1.75 GHz. The length and width of the radiating element are W and L, respectively. The radiating

elements are placed on one side of the substrate and grooved ground plane of size 67×50 mm^2 is located on the other side. It should be noted that the grooved area $L_s \times W_s$ is located on top and bottom of the ground plane with T-shape strip ($W_t \times L_t$). T-shape strip is introduced for isolation and grooved area is for impedance matching between the radiating elements.

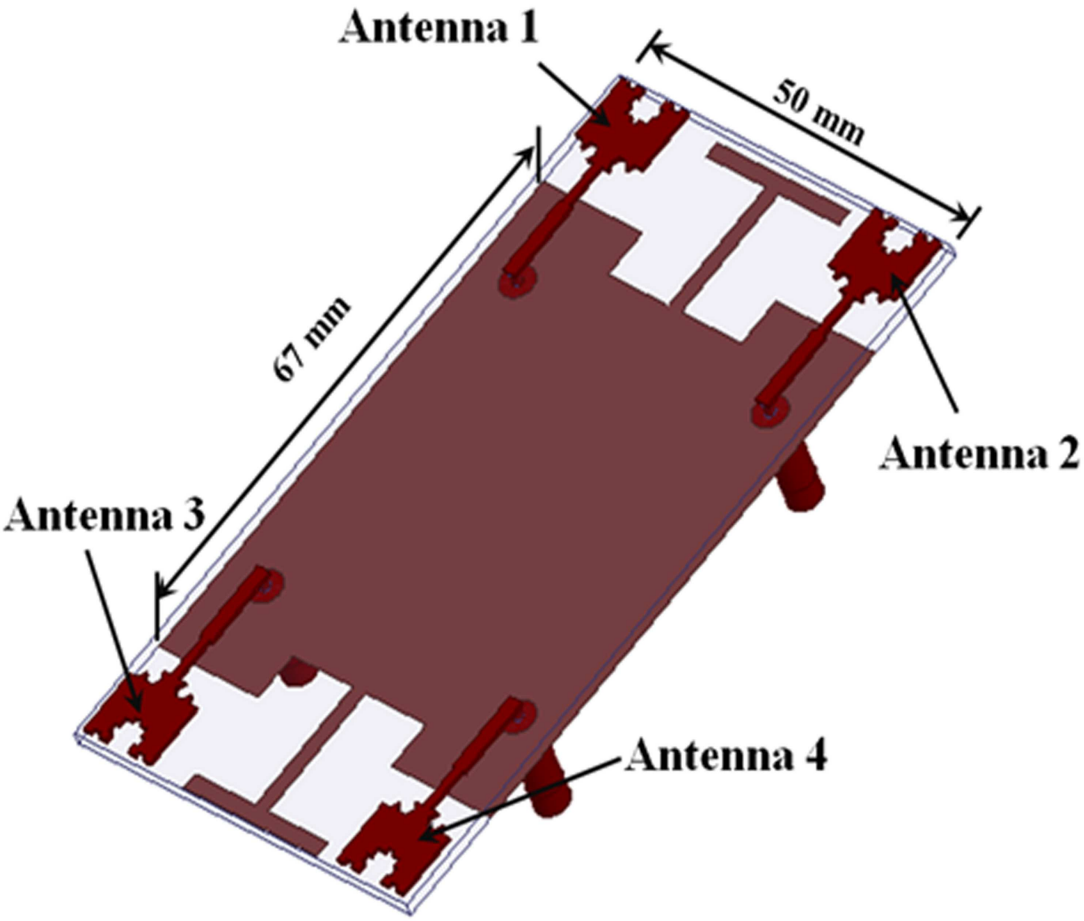

Figure 6.12: Geometry of proposed 4-element hybrid fractal antenna.

The proposed MIMO antenna has a symmetric configuration of four antenna elements. Therefore, only S_{11}, S_{12}, S_{13} and S_{14} are studied. S_{11} denotes the reflection coefficients of element #1 and S_{12}, S_{13}, S_{14} present mutual coupling/isolation between elements #1 and #2, #3, #4. Figure 6.13 shows the simulated reflection coefficient and isolation coefficient curves for 4-element MIMO antenna. It is observed from the Figure 6.13 (a) that the values of S_{11}, S_{22}, S_{33} and S_{44} for all 4 antennas are well below -10 dB. The reflection coefficients are overlapped. Strong coupling between the

ports is not desired which will be manifested in crosstalk. Besides, the Figure 6.13 (b) shows the isolation coefficients S_{12}, S_{13} and S_{14} for the antenna. It is observed that in case of S_{12} and S_{13}, the value of reflection coefficient is well below -10 dB whereas in case of S_{14}, it is below -20 dB for band 1 and band 2. It is concluded from the above observation that the proposed antenna is a good candidate for 4-element antenna. The proposed antenna covers impedance bandwidth of 1.66-1.92 GHz for the band 1 and 2.9-6.5 GHz for the band 2.

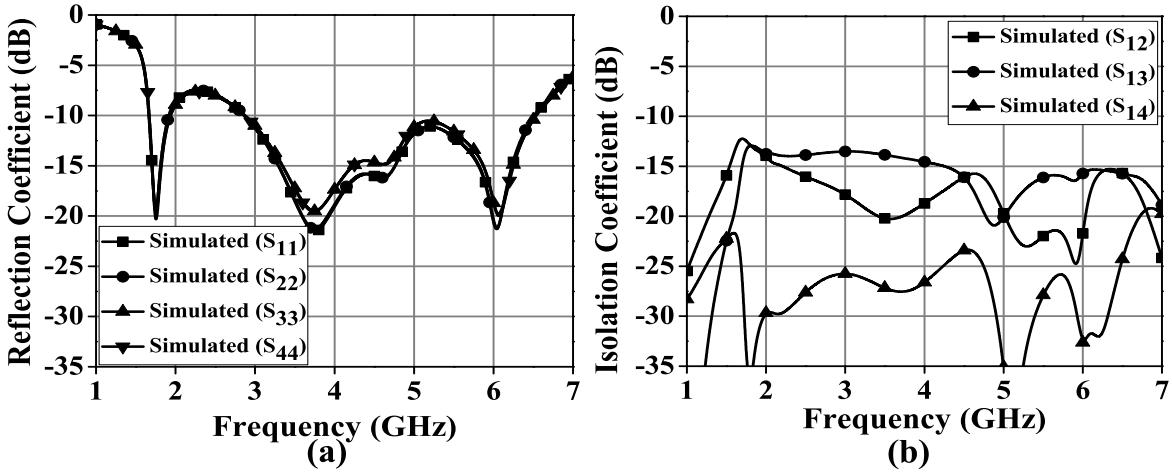

Figure 6.13: Simulated reflection and isolation coefficients of proposed 4-element antenna.

Figures 6.14 shows the surface current distribution at 1.75 GHz and 4.5 GHz for the proposed 4-element MIMO antenna. As can be seen, when antenna 1 is excited and antennas 2, 3 & 4 are terminated with 50Ω load, the surface current flows in the feed line as well as in T-shape strip at both the resonance frequencies. It can be noticed that there is negligible current on the antennas 2, 3 & 4 due to the presence of T-shape strip, thereby improving isolation between the antennas. This tends to decouple the current on antenna 2, 3 & 4 and hence it enhances the isolation between the radiators efficiently at 1.75 GHz and 4.5 GHz. Similiary the excitation of antennas are applicable for all the radiators.

Figures 6.15 shows the simulated 3D radiation patterns for the antenna 1, 2, 3 & 4 at 1.75 GHz, 3.0 GHz, 4.5 GHz and 6.0 GHz respectively. It can be noticed that the gain of the proposed monopole antenna at all the frequencies within the bands are

more than 2 dBi. The 3D patterns are omni-directional towards the lower frequency band and becomes nearly omni-directional with multiple lobes towards the higher frequency band.

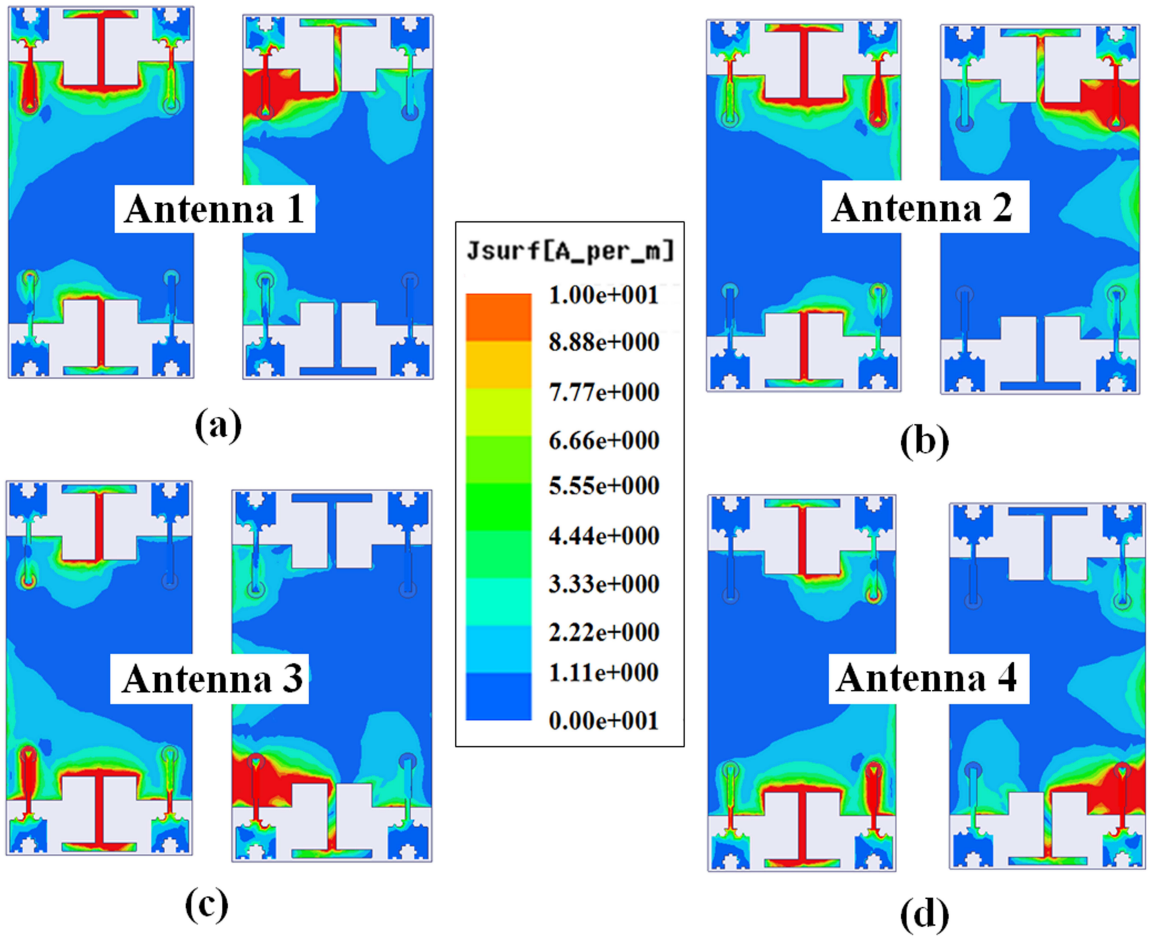

Figure 6.14: Simulated surface current distribution of the MIMO antenna (a) Antenna 1 at 1.75 GHz and 4.5 GHz (b) Antenna 2 at 1.75 GHz and 4.5 GHz (c) Antenna 1 at 1.75 GHz and 4.5 GHz (d) Antenna 2 at 1.75 GHz and 4.5 GHz

Experimental Verifications

The proposed 4-element hybrid fractal MIMO antenna is also milled on the copper side of FR-4 substrate. Photographs of fabricated antenna are shown in Figure 6.16. All the measurements are carried out using Agilent vector network analyzer (Model no. N5230A) and radiation patterns are measured in an anechoic chamber in Microwave Lab, IISc Bangalore, India. The Measured values of the reflection coefficients (S_{11}, S_{22}, S_{33}, S_{44}) and isolation coefficients (S_{12}, S_{13}, S_{13}) are plotted in Figures. 6.17

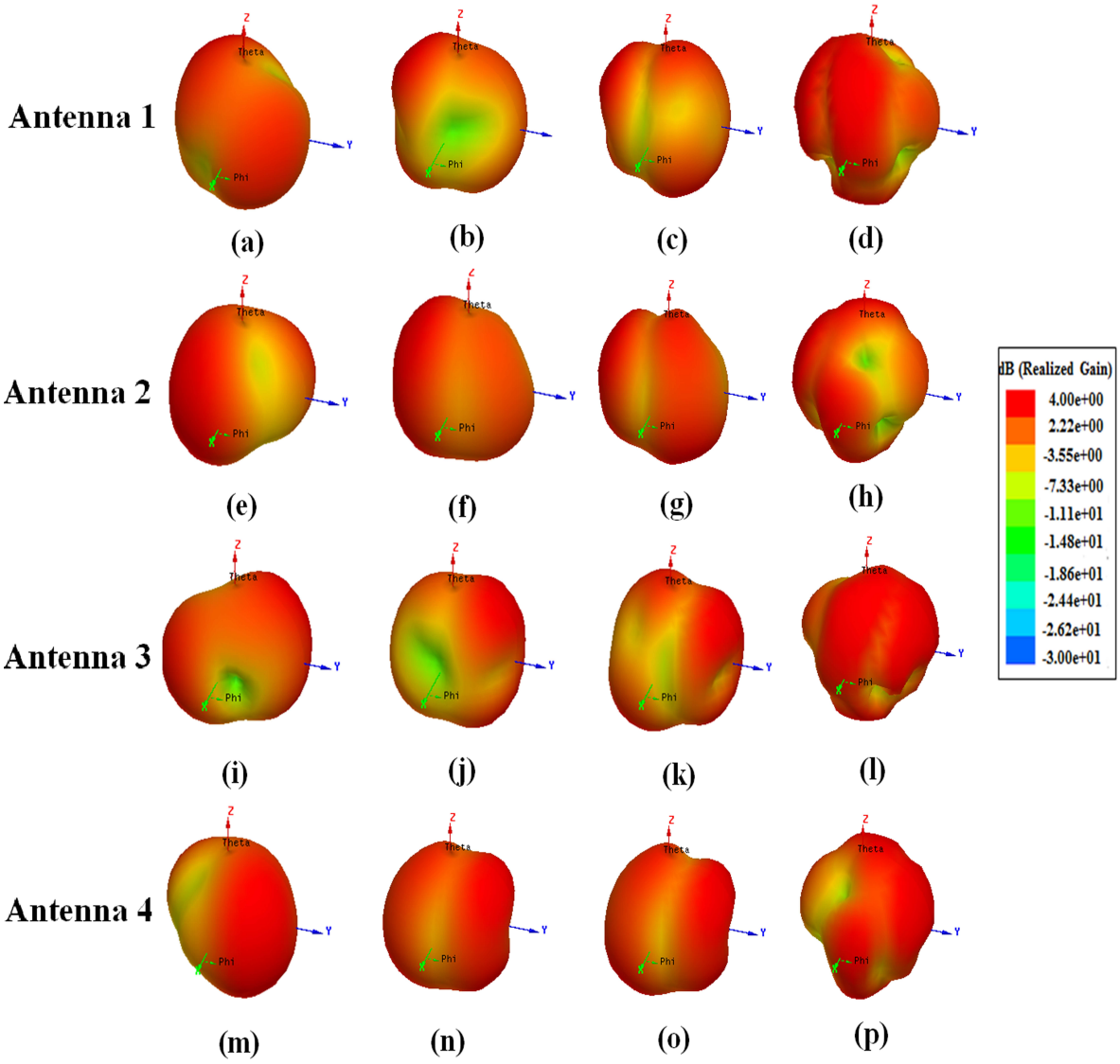

Figure 6.15: Simulated 3D radiation patterns for the antenna 1, 2, 3 & 4; Figs. (a),(e),(i) and (m) at 1.75 GHz, Figs. (b),(f),(j) and (n) at 3 GHz, Figs. (c),(g),(k) and (o) at 4.5 GHz, and finally, Figs. (d),(h),(l) and (p) at 6 GHz.

(a) and 6.17 (b), respectively. As can be seen, measured impedance bandwidths are 18.18 % from 1.6-1.92 GHz for band 1 and 83.7 % from 2.58-6.3 GHz for band 2. The proposed antenna bandwidth covers the requirement of LTE/WiFi/WiMAX/WLAN frequency bands. The isolation between the two antennas is below -10 dB and -20 dB for the lower and higher frequency bands, respectively.

Figure 6.18 (a) shows the simulated and measured ECC across the desired frequency band. It is calculated between antennas i and j in the (N, N) MIMO antenna

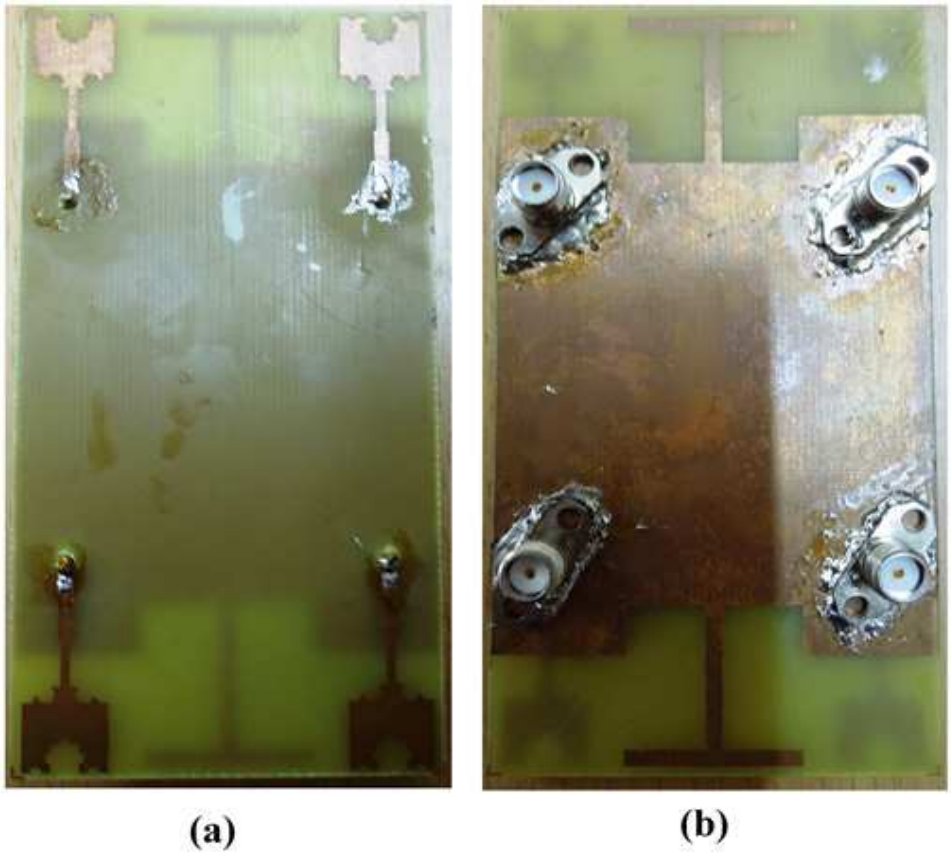

Figure 6.16: Photographs of the fabricated hybrid fractal MIMO antennas (a) Front view (b) Rear view.

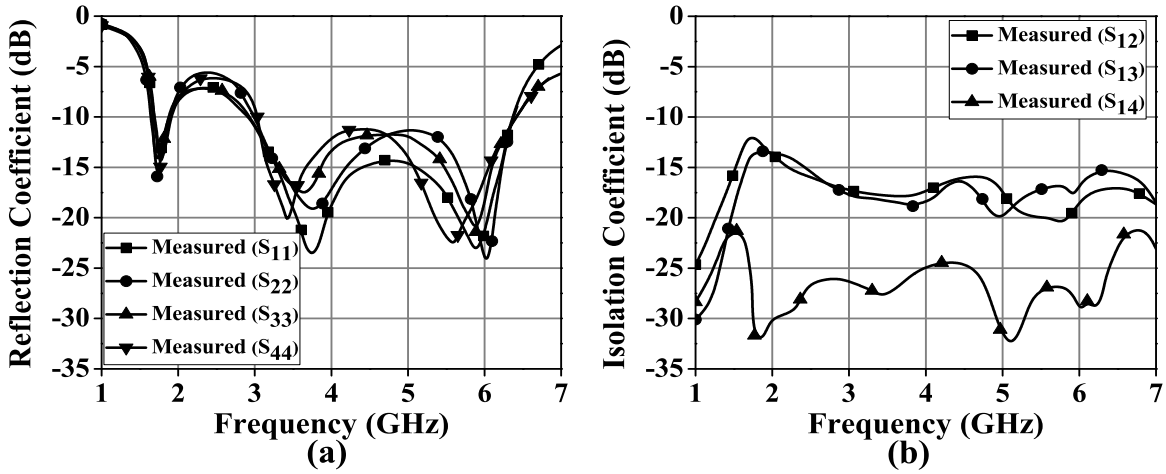

Figure 6.17: Measured reflection and isolation coefficients of proposed 4-element hybrid fractal antenna

system. In case of the proposed 4-element hybrid fractal antenna MIMO system, with $N = 4$, antennas are placed at the ends. The envelope correlation between antennas,

can be calculated as given in (4.10).

$$\rho_{1,2,3,4} = \frac{|S_{11}^* S_{12} + S_{12}^* S_{22} + S_{13}^* S_{32} + S_{14}^* S_{42}|^2}{\left(1 - \left(|S_{11}|^2 + |S_{21}|^2 + S_{31}|^2 + |S_{41}|^2\right)\right)\left(1 - \left(|S_{11}|^2 + |S_{22}|^2 + |S_{32}|^2 + |S_{42}|^2\right)\right)} \tag{6.10}$$

As can be seen, the value of ECC is well below the practical threshold value of 0.5 for both the bands 1 & 2. Similarly, capacity loss (bits/Hz) is another performance parameter which characterizes quality of a MIMO antenna system. Figure 6.18 (b) shows the capacity loss of proposed 4-element MIMO system. It is found to be below 0.3 bits/Hz and calculated using the equation (6.8) can be written as.

$$\Psi^R = \begin{pmatrix} \rho_{ii} & \rho_{ij} \\ \rho_{ji} & \rho_{jj} \end{pmatrix}$$

$$\rho_{ii} = 1 - \left(|S_{ii}|^2 - |S_{ij}|^2\right), \; and \; \rho_{ij} = -\left(|S_{ii}^* S_{ij} + S_{ji}^* S_{ij}|\right), \; for \text{ i,j= } 1, 2, 3 \; or \; 4$$

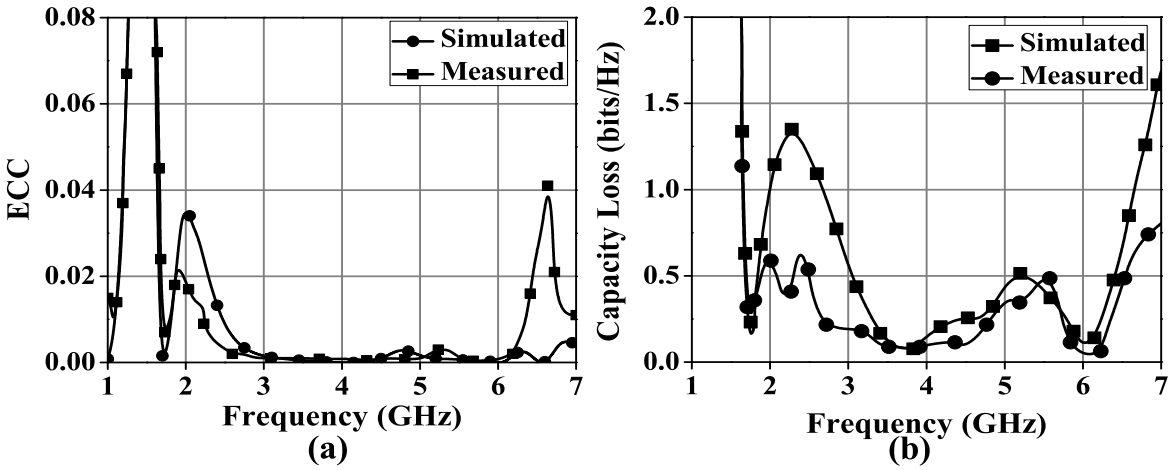

Figure 6.18: Measured and simulated envelope correlation coefficient (ECC) and capacity loss of 4-element MIMO antenna (a) Envelope correlation Coefficient (ECC) (b) Capacity loss.

Figure 6.19 shows the measured radiation patterns at the band 1 and band 2 for XZ (Co-pol. and Cross-pol.) and YZ (Co-pol. and Cross-pol.) planes. During the measurement, only antenna 1 is excited while antenna 2, 3 & 4 are terminated with a 50Ω matched load. It can be seen from Figure 6.19 (a-p) that at band 1, patterns are omni-directional but are nearly omni-directional with some multiple lobes

towards the higher frequency for band 2. Table 6.3 provides measured gain, simulated total antenna efficiency at the band 1 & 2. The simulated total antenna efficiency is obtained as more than 80 % throughout the bands. The measured maximum peak realized gain is 7.88 dBi. Due to symmetry of the antenna structure and their common fabrication tolerances; the gain values of the four radiators are almost the same. Therefore, only the gain of the antenna 1 is presented, when the antenna 2, 3 & 4 are terminated in a 50Ω matched load.

Table 6.3: Gain and simulated total antenna efficiency of 4-element MIMO antenna

	Frequency (GHz)	Measured peak realized gain (dBi)	Simulated total antenna efficiency (%)
Band 1	1.75	2.38	80
Band 2	3.0	4.05	82
	4.5	5.10	87
	6.0	7.88	95

Table 6.4: Comparison of 2-element & 4-element MIMO antenna

Parameters		**2-Element hybrid fractal antenna**	**4-Element hybrid fractal antenna**
Dimensions (mm^3)		100×50×1.58	100×50×1.58
10 dB RL Bandwidth		(Dual Band), 1.65-1.9, 2.68-6.25	(Dual Band), 1.6-1.92, 2.58-6.3
10 dB RL Bandwidth (%)		14%, 80%	18.18%, 83.7%
Peak Realized gain		6.78dBi	7.88dBi
Efficiency		> 80%	> 80%
ECC	1.75GHz	0.0003	0.0001
	3.0GHz	0.0008	0.0007
	4.5GHz	0.0029	0.0009
	6.0GHz	0.0011	0.0012
Capacity Loss	1.75GHz	0.33	0.09
	3.0GHz	0.11	0.31
	4.5GHz	0.26	0.13
	6.0GHz	0.03	0.05

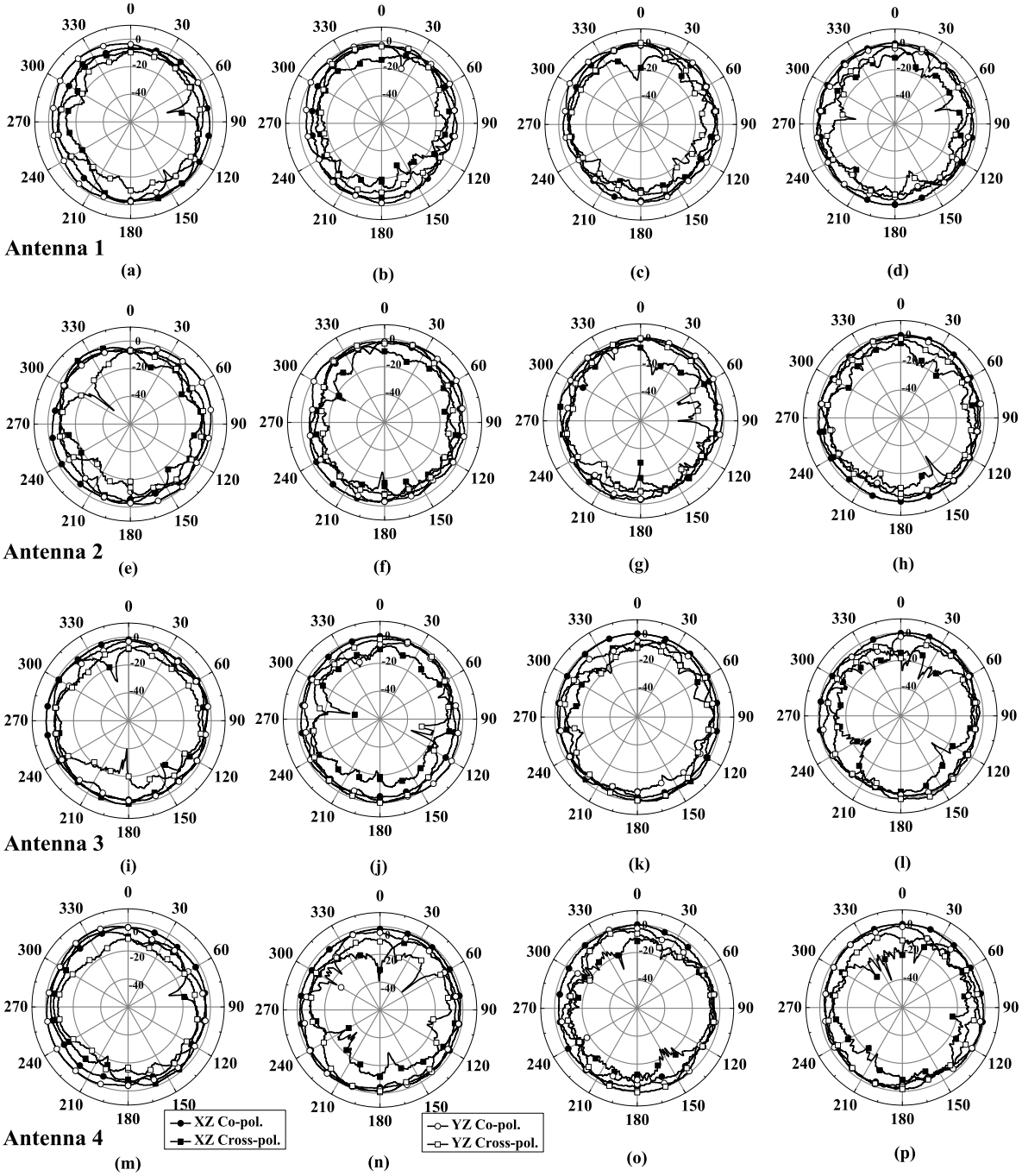

Figure 6.19: Measured radiation patterns for the antennas 1, 2, 3 & 4; Figs. (a),(e),(i) and (m) at 1.75 GHz, Figs. (b),(f),(j) and (n) at 3 GHz, Figs. (c),(g),(k) and (o) at 4.5 GHz, and finally, Figs. (d),(h),(l) and (p) at 6 GHz.

6.3 Modified 3-Section 2-way Wilkinson power divider

This section deals with the modified 3-section 2-way Wilkinson power divider for wide range of frequency. The parameters of the feed network are optimized by using full-wave analysis to achieve the desired performance. Both simulated and measured results show that the proposed feed networks has almost equal power splitted in all branches. This feed network has low insertion loss and good reflection coefficient at all ports. The isolation between the two output ports are found to be better than -10 dB which makes these feed networks as good as dividers and/or combiners at the same time.

6.3.1 Circuit structure and Design

The original power divider developed by Wilkinson [206] consists of two quarter-wavelength line operating in a single band. Here, a new coupled line Wilkinson power divider is designed. This circuit has 3-section 2-way coupled line and three isolation resistors. Since all the inherent separated space of coupled lines makes resistor placement more convenient. Meanwhile, practical layout can be very small, leading to miniaturized wideband power divider.

Figure 6.20 shows the configuration of coupled line power divider. It consists of 3-section of Wilkinson power divider with three isolation resistors. The source at port#1 has internal input impedance Z_1 while the loads at output port#2 and port#3 have the same internal impedance, Z_2. The coupled lines with characteristic impedances Z_{ie} (even mode), Z_{io} (odd mode) and electrical length θ_i, where i= 1, 2 & 3 are not for impedance matching but also to make the total circuit of this divider compact. Moreover, the lumped resistors R_1, R_2 and R_3 play an important role in enhancing the isolation and matching performance of the output port.

In the proposed structure (Figure 6.20), for even mode, there is no current flow through the plane of symmetry, which means the middle of the power divider is open circuit as shown in Figure 6.21 (a). Therefore the resistors are omitted and the impedance at the port#1 is doubled i.e $2Z_1$. Impedances are given [207,208] in (6.12,

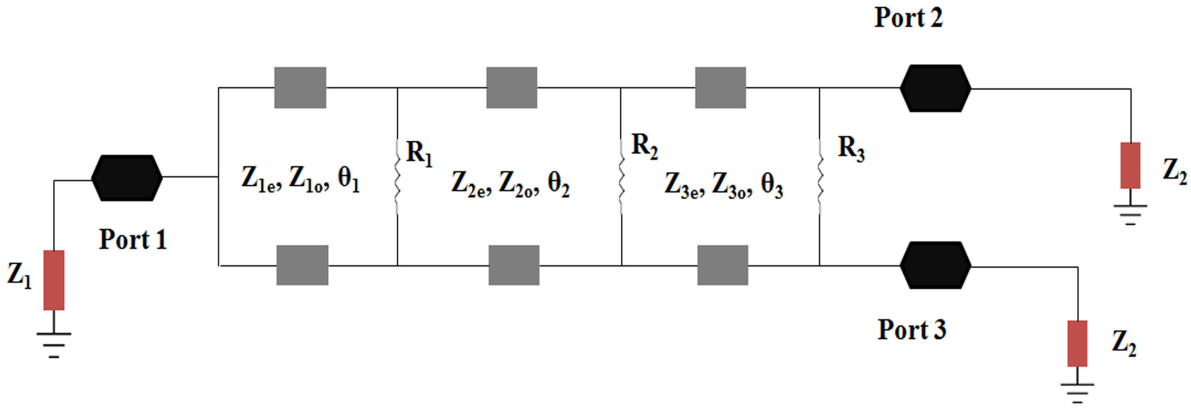

Figure 6.20: Coupled line Wilkinson power divider

6.13 & 6.14).

$$2Z_1 = Z_{1e}\frac{Z_{in1} + jZ_{1e} + tan(\theta_1)}{Z_{1e} + jZ_{in1} + tan(\theta_1)} \tag{6.12}$$

$$Z_{in1} = Z_{2e}\frac{Z_{in2} + jZ_{2e} + tan(\theta_2)}{Z_{2e} + jZ_{in2} + tan(\theta_2)} \tag{6.13}$$

$$Z_{in2} = Z_2\frac{Z_{in2} + jZ_{3e} + tan(\theta_3)}{Z_{3e} + jZ_{in3} + tan(\theta_3)} \tag{6.14}$$

Similarly, in case of odd-mode, there is a voltage null along the plane of symmetry, which means the middle of the divider is short circuit (SC) as shown in Figure 6.21 (b). Therefore, the resistors are grounded and the impedances at port#2 can be derived as [207] given in equations (6.15, 6.16, 6.17 & 6.18).

$$Z_{in3} = \frac{jR_1Z_{1o}tan(\theta_1)}{R_1 + j2Z_{1o}tan(\theta_1)} \tag{6.15}$$

$$Z_{in4} = Z_{2o}\frac{Z_{in3} + jZ_{2o}tan(\theta_2)}{Z_{2o} + jZ_{in2}tan(\theta_2)} \tag{6.16}$$

$$Z_{in5} = Z_{3o}\frac{jR_2Z_{3o}tan(\theta_3)}{R_2 + j2Z_{3o}tan(\theta_3)} \tag{6.17}$$

$$Z_{in5} = \frac{R_3Z_{in5}}{R_3 + 2Z_{in5}} \tag{6.18}$$

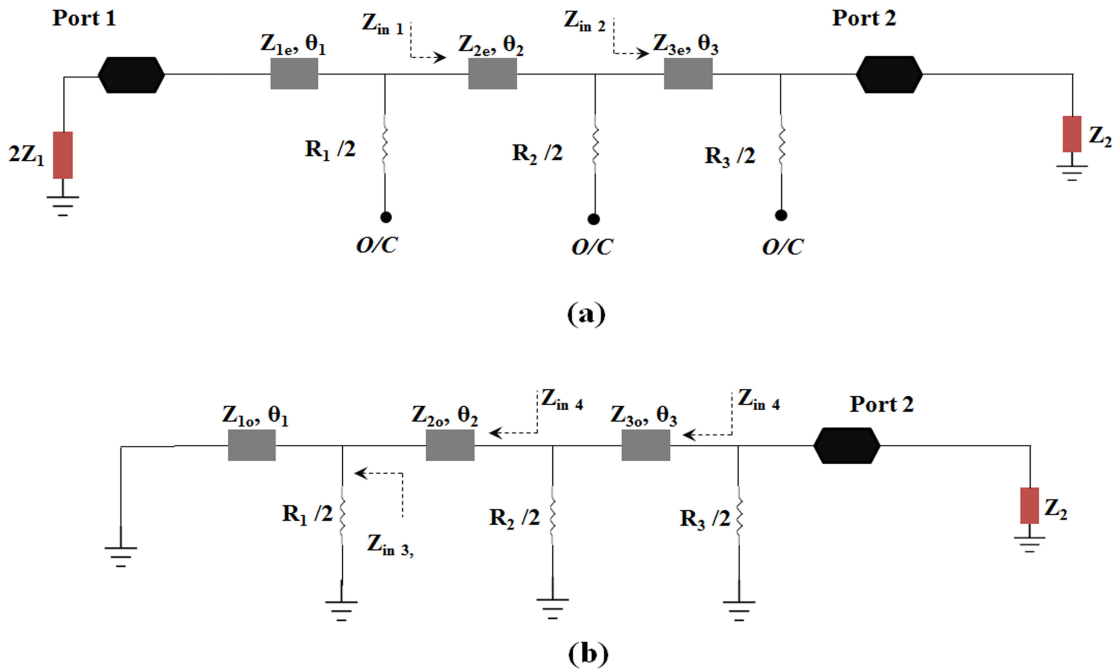

Figure 6.21: Simplified equivalent circuit of the Wilkinson power divider (a) even- (b) odd-mode excitations

A modified 3-section 2-way Wilkinson power divider for wideband application is chosen as a feeding network for the antenna array [188]. The geometry of the proposed wideband power divider is shown in Figure 6.22. It consists of a modified 3-section 2-way Wilkinson power divider. To validate the proposed design, a prototype is fabricated and experimentally verified. Measured results show good performance within the wideband frequency range. The three chip resistors R_1=110Ω , R_2=220Ω and R_3=390Ω have been placed between the two output ports with an area of 2.2 mm^2 for good isolation. The proposed power divider is printed on FR-4 substrate 30×40×1.58 mm^3, ϵ_r=4.4 with loss tangent, $\tan\delta$=0.005. The proposed wideband power divider feeds the two optimized wideband printed monopole antenna elements with equal phase and amplitude wideband signals. The optimized design parameters are listed in Table 6.5. The simulated reflection coefficients and group delay of the chosen divider are plotted in Figure 6.23. It can be noticed from Figure 6.23 (a) that the S-parameters at input and output ports S_{11}, S_{22}, and S_{33} are lower than -15 dB over the whole wideband frequency range. Also, good isolation S_{32} (better than -10dB) between two output ports is observed for the entire frequency range. The

power is splitted equally between the two output ports, i.e.,S_{21}=S_{12}=S_{13}=S_{31}=-3dB. In addition, Figure 6.23 (b) shows the simulated group delay. It is almost constant and less than 0.30 ns, which shows good linearity within the wide-frequency range. Figure 6.24 shows the measured S-parameters for wide frequency band and it is measured using Agilent vector network analyzer (Model no. N5230A). It is thus concluded that there is good agreement in simulated reflection coefficient, insertion loss and isolation between output ports for wide frequency band.

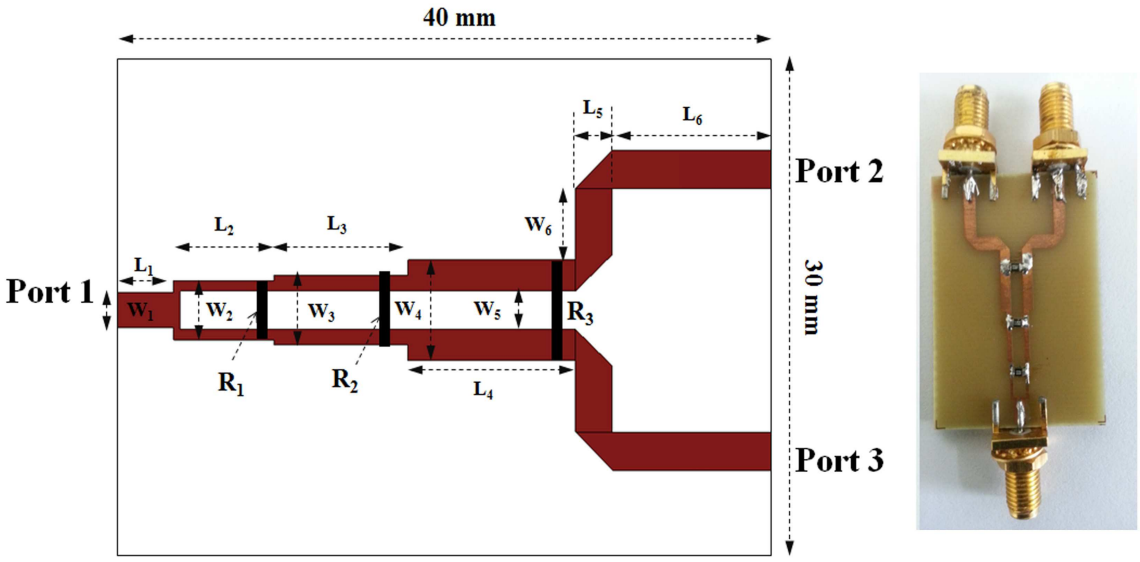

Figure 6.22: Geometry of modified Wilkinson power divider.

Table 6.5: Dimensions of modified Wilkinson power divider

L_1	L_2	L_3	L_4	L_5	L_6
4 mm	6 mm	8 mm	10 mm	2.2 mm	9.8 mm
W_1	W_2	W_3	W_4	W_5	W_6
2.2 mm	3.4 mm	4 mm	5.8 mm	2.2 mm	4.1 mm

6.4 Wideband Sectoral Fractal Linear Antenna Array

The 2-element and 4-element wideband linear antenna arrays are constructed using previously designed sectoral fractal monopole antenna (chapter 3) and wideband feed network (Section 6.3). The geometry and photograph of the proposed 2-element and

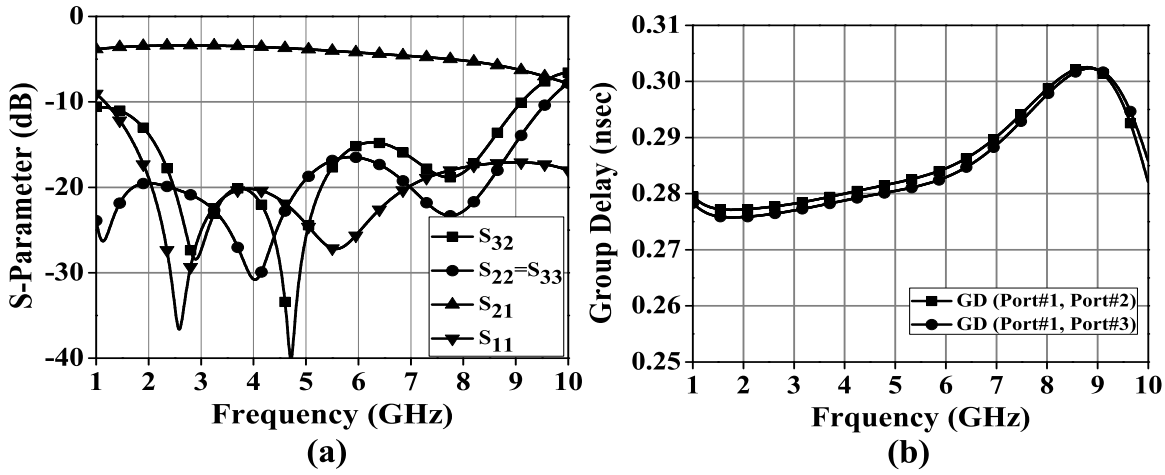

Figure 6.23: Simulated results of proposed modified Wilkinson power divider (a) Reflection coefficients (b) Group delay.

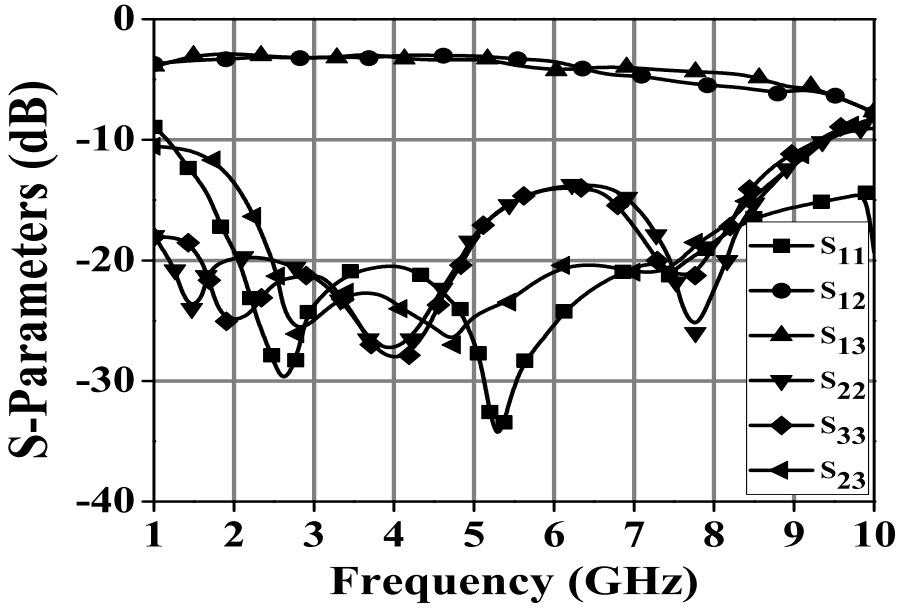

Figure 6.24: Measured S-parameters of modified Wilkinson power divider.

4-element linear antenna array are shown in the next section. The inter-element spacing between the antenna elements has a great effect on the overall performance of the array. It is chosen as a half wavelength at the higher frequency of the impedance bandwidth. In addition, the effect of different design parameters on the array performance, extensive parametric studies are carried out using full-wave analysis of the arrays. The target is to design 2-element and 4-element linear antenna arrays for good impedance

matching characteristics across the desired wideband frequency range. Moreover, the designed arrays should attain higher gain, stable radiation pattern characteristics throughout the desired frequency band of interest.

6.4.1 2-Element sectoral fractal antenna array

A 2-element sectoral fractal linear antenna array is shown in Figure 6.25. which is constructed by feeding two optimized antenna elements with the designed wideband power divider. The optimized parameters are listed in Table 6.6. The optimized inter-spacing distance between antenna elements is chosen as a half wavelength for the higher frequency of the impedance bandwidth of the patch element, yielding a value 'D'. The proposed antenna array is fabricated on FR-4 ($\epsilon_r = 4.4$) substrate of size L×W with height h. The array elements are placed on one side of the substrate and common grooved ground plane of size $L_g \times W$ is located on the other side. It should be noted that the grooved area $L_s \times W_s$ is located on top of the ground plane and a good performance has been observed. It is introduced to improve the impedance matching and reduce the effect of mutual coupling between antenna elements. The optimized values for the rectangular cut in the ground plane are: W_s and L_s. Figure 6.26 shows the reflection coefficients for different values of grooved areas. It is observed that in case of W_s= 19 mm and L_s= 14.5 mm the reflection coefficient is less than -10dB for the desired frequency band.

Table 6.6: Dimensions of proposed 2-element linear antenna array

L	W	L_s	W_s	L_g	D	h
65 mm	50 mm	14.5 mm	19 mm	48.5 mm	31.5 mm	1.58 mm

The optimized inter-spacing center-to-center distance between antenna elements are chosen as for D = 31.5 mm. However, the distance between two antenna elements is higher than the minimum requirement to avoid grating lobes. Figure 6.27 shows the simulated 3D radiation patterns and corresponding surface current distribution at 3.5 GHz, 5.5 GHz and 6.5 GHz. As seen from surface current, it is mainly distributed to the conductor edges of the radiator and grooved ground plane, which gives an indication about the dependence of antenna geometry on the resonant frequencies. It

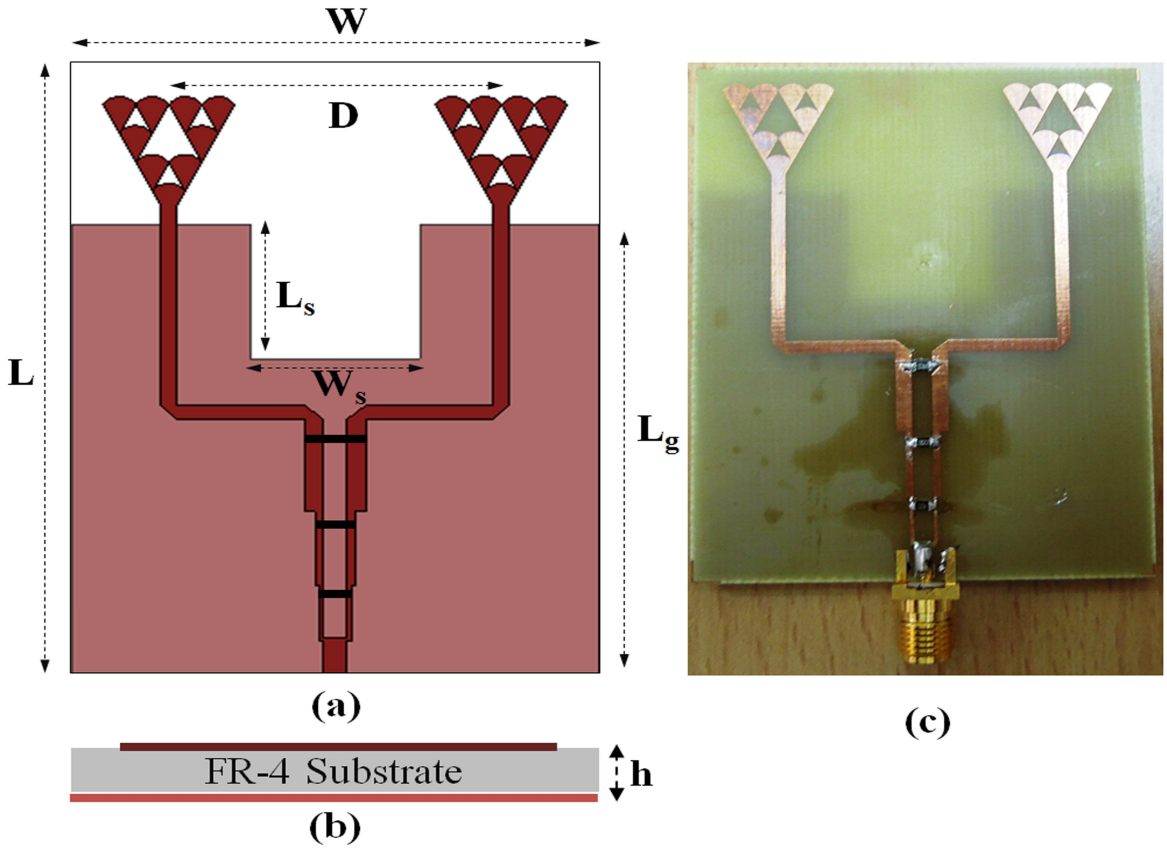

Figure 6.25: Geometry of proposed 2-element linear antenna array (a) Front view (b) Top view (c) Photograph of fabricated antenna

is further noticed that the current distribution is more dense in grooved area, which indicates that it is responsible for mutual coupling between elements. Animations at 5.5 GHz shows that the current is traveling along the feed line and in the grooved area, whereas oscillating at the top edges. The radiation patterns also appear to lose its omnidirectional property in the XY plane at 5.5 GHz and 6.5 GHz. It can be concluded that the radiation patterns are omnidirectional at the lower resonant frequency whereas deteriorates at higher frequencies.

Experimental Verifications

Photographs of proposed fabricated antenna is shown in Figure 6.25 (c). The measurement has been carried out using Agilent vector network analyzer (Model no. N5230A) and radiation patterns are measured in an anechoic chamber in Microwave Lab, IISc Bangalore, India. Measured and simulated values of the reflection coefficients are

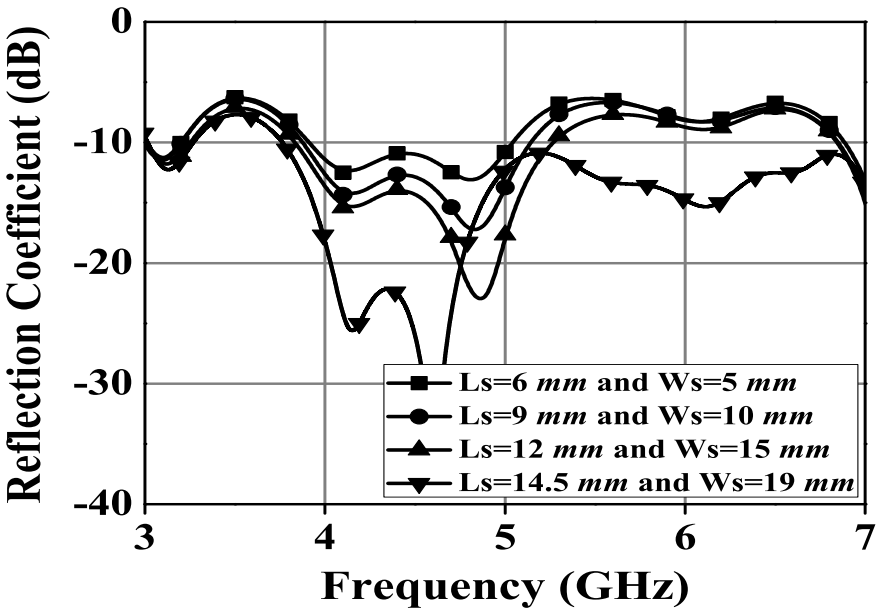

Figure 6.26: Simulated reflection coefficients of proposed 2-element linear antenna array for different grooved areas in ground plane

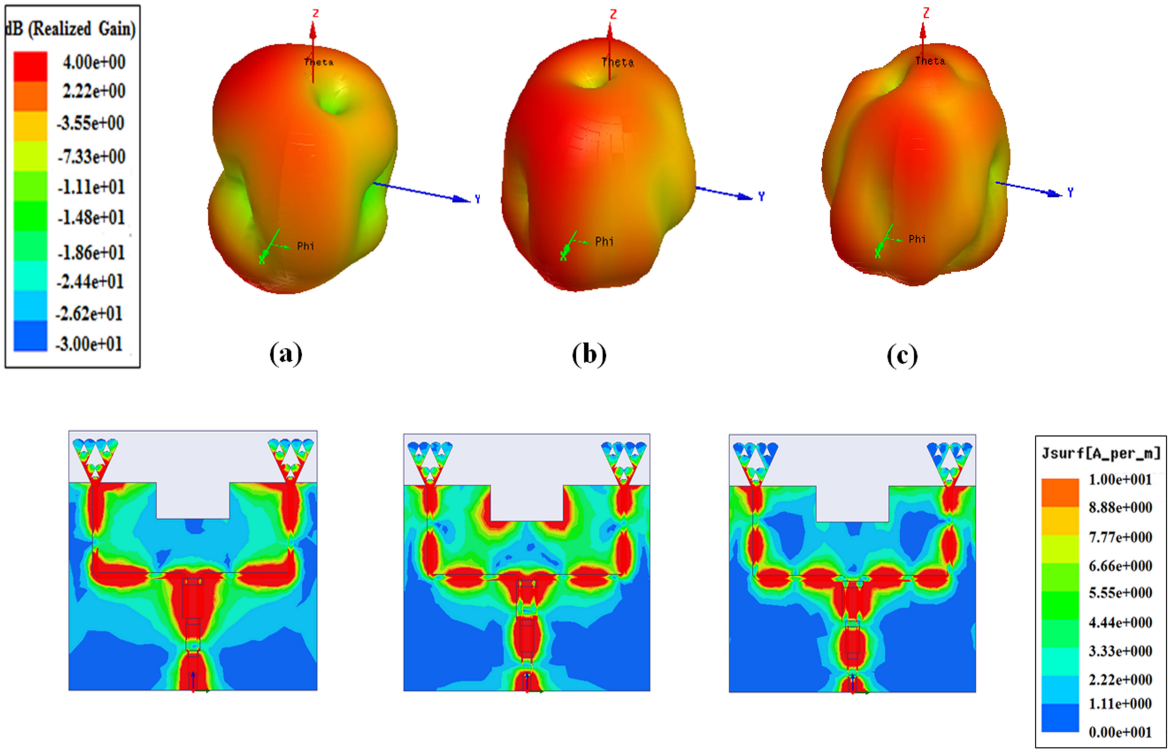

Figure 6.27: Simulated 3D radiation patterns and surface current distribution at (a) 3.5 GHz (b) 5.5 GHz (c) 6.5 GHz.

plotted in Figures 6.28. As can be seen, measured impedance bandwidth is 76.28 % from 3.1-6.8 GHz.

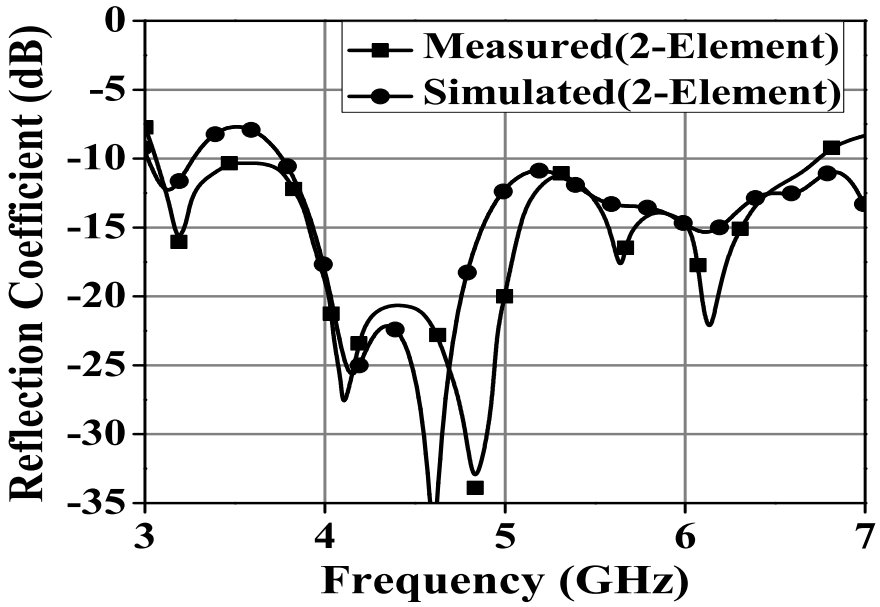

Figure 6.28: Simulated and measured reflection coefficients of proposed 2-element linear antenna array.

The measured radiation patterns for three resonant frequencies of 3.5 GHz, 5.5 GHz and 6.5 GHz are shown in Figure 6.29. These are normalized results with monopole like radiation pattern behavior. In addition, the radiation patterns give a similar trend due to a small deviation between each frequency. It is observed that the radiation patterns are approximately omnidirectional in XZ (Co-pol. and Cross-pol.) and YZ (Co-pol. and Cross-pol.) planes. There are differences of about 10 dB or more between co-polarized and cross-polarized ones in most of the angular region. In some angular regions cross-polarized compensate for co-polarized components to enable the total field to be more uniform. In fact, the measurement of the cross-polarized cases need to be more accurate because positioning effect due to feeding cable is more vulnerable to the measurement error. Table 6.7 shows the measured gain and total efficiency at different frequencies. The peak gains in the boresight direction of the 2-element antenna array is 7.98 dBi and 4 dBi higher than that of the single element. The simulated total antenna efficiency is found to be more than 70 %

throughout the band.

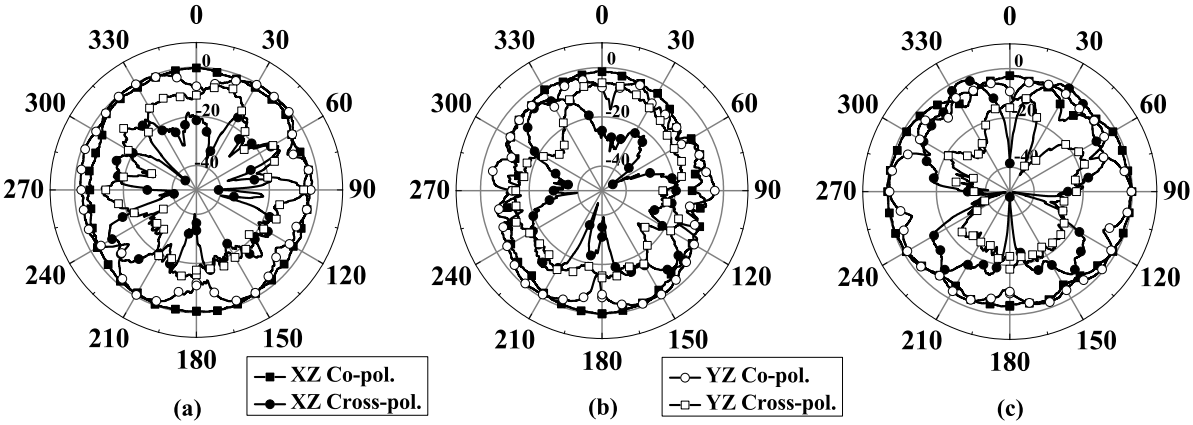

Figure 6.29: Measured radiation patterns of proposed 2-element linear antenna array at (a) 3.5 GHz (b) 5.5 GHz (c) 6.5 GHz.

Table 6.7: Measured gain and simulated total antenna efficiency of proposed 2-element linear antenna array.

Frequency (GHz)	3.0	3.5	4.0	4.5	5.0	5.5	6.0	6.5	7.0
Gain (dBi)	4.9	5.23	6.36	6.71	7.77	7.89	6.39	6.52	4.68
Efficiency (%)	71.52	67.53	80.60	81.12	73.70	73.46	71.32	72.30	65.27

6.4.2 4-Element sectoral fractal antenna array

Figure 6.30 shows a 4-element sectoral fractal monopole linear antenna array constructed by feeding network, which is composed of three modified Wilkinson power dividers. The optimized parameters are listed in Table 6.8. The proposed antenna is having four optimized antenna elements as radiators. The optimized inter-spacing distance between antenna elements is chosen as a half wavelength for the higher frequency of the impedance bandwidth of the patch element, yielding a value D_1, D_2 and D_3. The proposed antenna array is also fabricated on FR-4 ($\epsilon_r = 4.4$) substrate of size L×W with height h is used. The array elements are placed on one side of the substrate and common grooved ground plane of size $L_g \times W$ is located on the other side. A good 4-element array performance has been achieved by means of using a rectangular grooved area on the ground plane with certain dimensions. It is introduced to improve the impedance matching and reduce the effect of mutual coupling

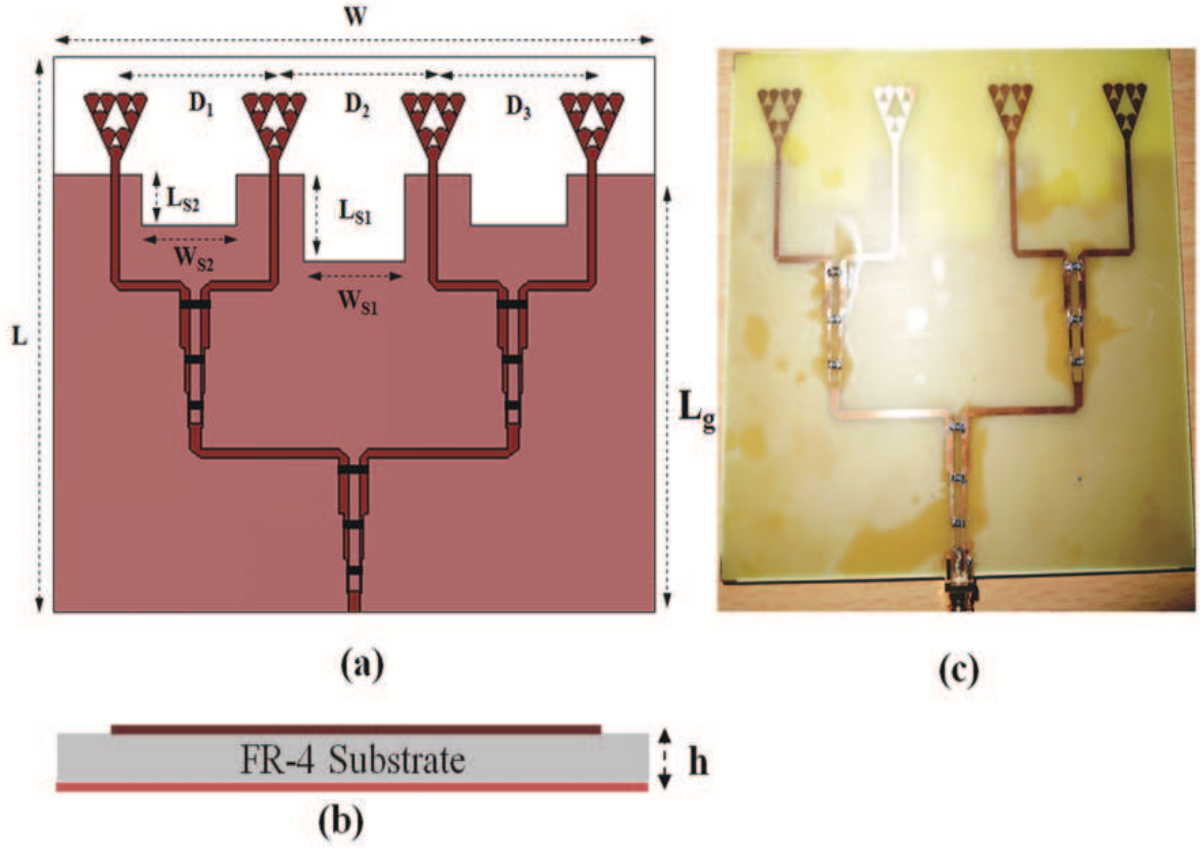

Figure 6.30: Geometry of proposed 4-element linear antenna array (a) Front view (b) Rear view (c) Photograph of fabricated antenna

between antenna elements. The optimized values for the rectangular grooved area on the ground plane are: W_{s1} and L_{s1}, W_{s2} and L_{s2}. Figure 6.31 shows the reflection coefficients for different values of grooved areas. It is observed that in case of W_{s1}=20 mm and L_{s1}=15.5 mm, W_{s2}= 20 mm and L_{s2}= 9 mm the reflection coefficient is well below the desired frequency band.

Table 6.8: Dimensions of proposed 4-element linear antenna arrays

L	W	L_{s1}	W_{s1}	L_{s2}	W_{s2}
100 mm	120 mm	15.5 mm	20 mm	9.0 mm	20 mm
D_1	D_2	D_3	h	L_g	
31.5 mm	31.5 mm	31.5 mm	1.58 mm	78 mm	

The optimized inter-spacing center-to-center distance distance between antenna elements is chosen as D_1=D_2=D_3= 31.5 mm. Figure 6.32 shows the simulated 3D radiation patterns and corresponding surface current distribution at 3.5 GHz, 5.5 GHz

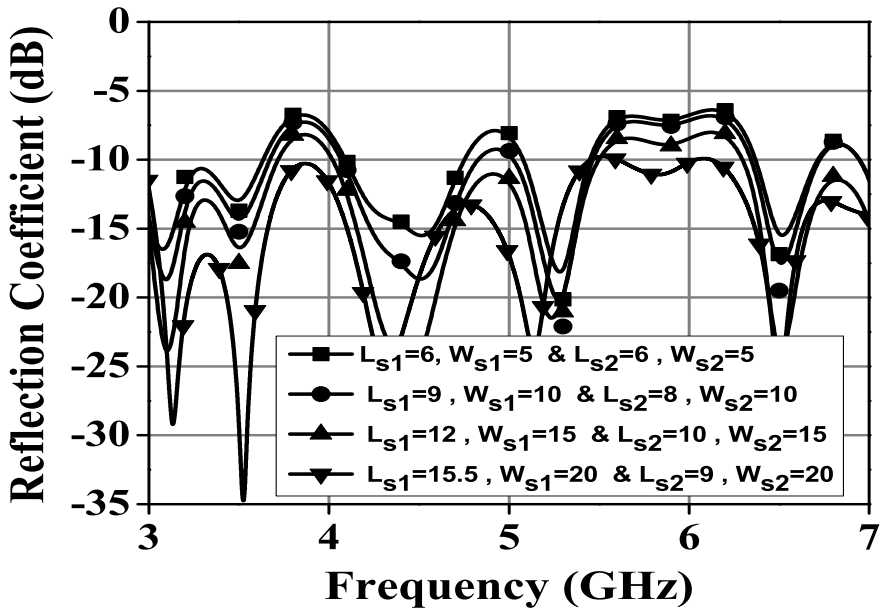

Figure 6.31: Simulated reflection coefficients of proposed 4-element linear antenna array for different grooved area in ground plane.

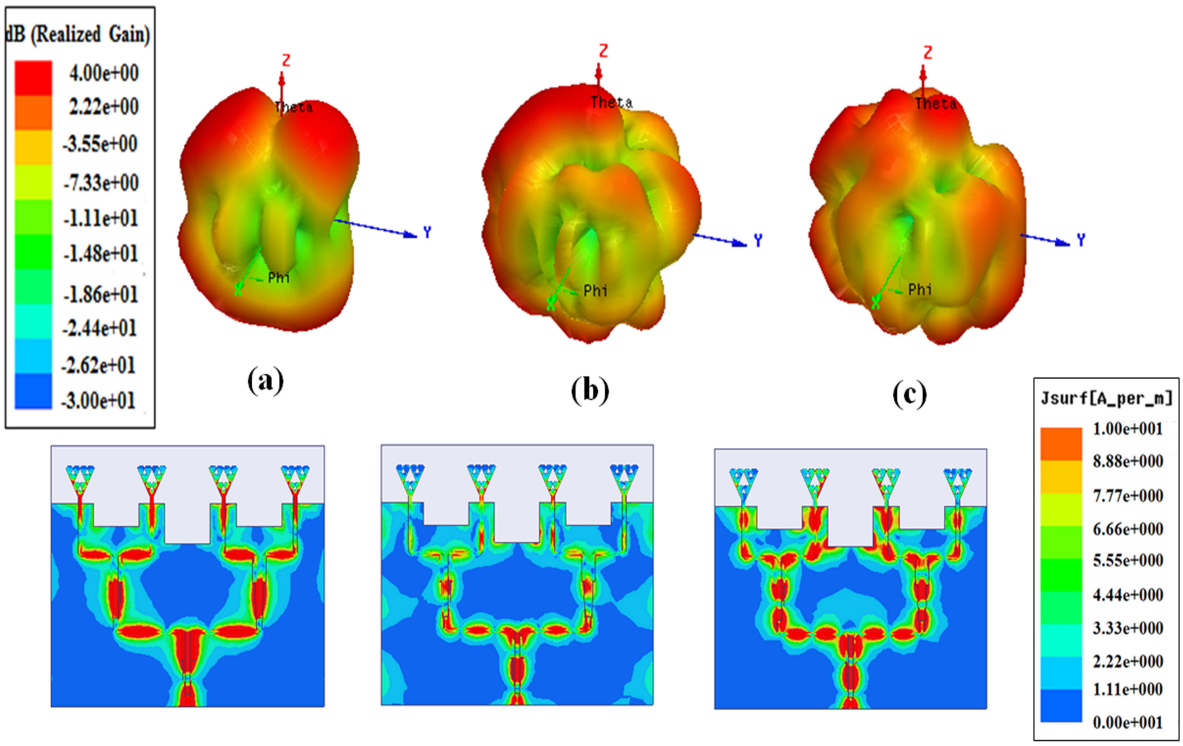

Figure 6.32: Simulated 3D radiation patterns and surface current distribution at (a) 3.5 GHz (b) 5.5 GHz (c) 6.5 GHz.

and 6.5 GHz. As seen from surface current, it is mainly distributed on the grooved ground plane at higher frequency which is responsible for mutual coupling between the elements. In addition, the surface current is also travelling along the feed line and grooved area, whereas oscillating at the top edges. The simulated 3D radiation patterns also appear to loose its omnidirectional property in the XY plane. The gain is more than 4 dBi at desired frequency band. It is observed that the radiation patterns are omnidirectional at the lower resonant frequency whereas deteriorates at higher frequencies.

Experimental Verifications

Photographs of proposed fabricated antenna is shown in Figure 6.30 (c). Measured and simulated values of the reflection coefficients are plotted in Figures 6.33. The measured impedance bandwidth is found to be 77.22 % from 3.1-7.0 GHz. It is noticed that the measured reflection coefficients are well matched with simulated ones.

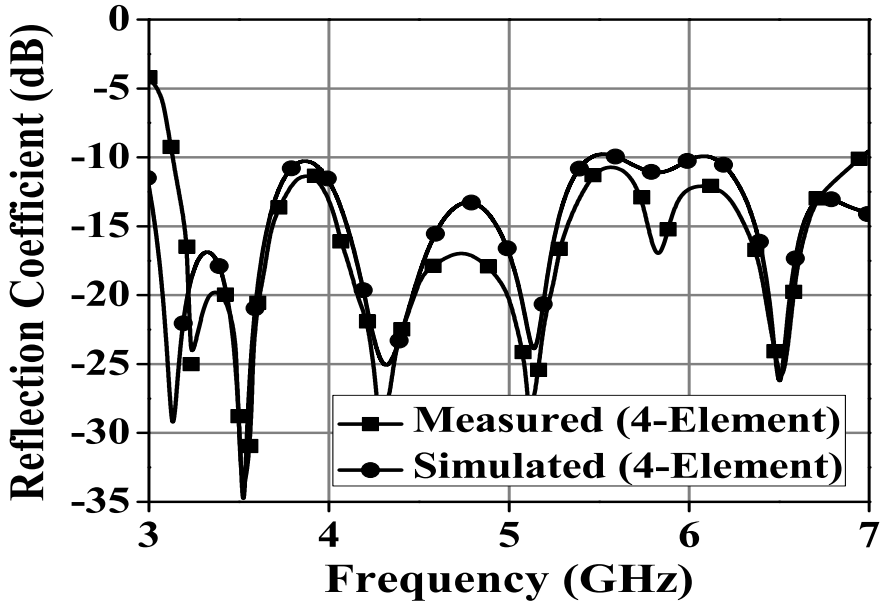

Figure 6.33: Simulated and measured reflection coefficients of proposed 4-element linear antenna array

Figure 6.34 shows the measured E- and H- plane radiation patterns at 3.5 GHz, 5.5 GHz and 6.5 GHz. The radiation patterns of the proposed antenna are also stable

monopole like, which is almost omnidirectional in XZ (Co-pol. and Cross-pol.) and YZ (Co-pol. and Cross-pol.) planes and same as those of 2-element. Table 6.9 shows the measured gain and total efficiency at different frequencies. The peak gains in the boresight direction of the 4-element antenna array is 10.68 dBi and it is 7 dBi higher than that of the single element. The simulated total antenna efficiency is obtained as more than 65 % throughout the band.

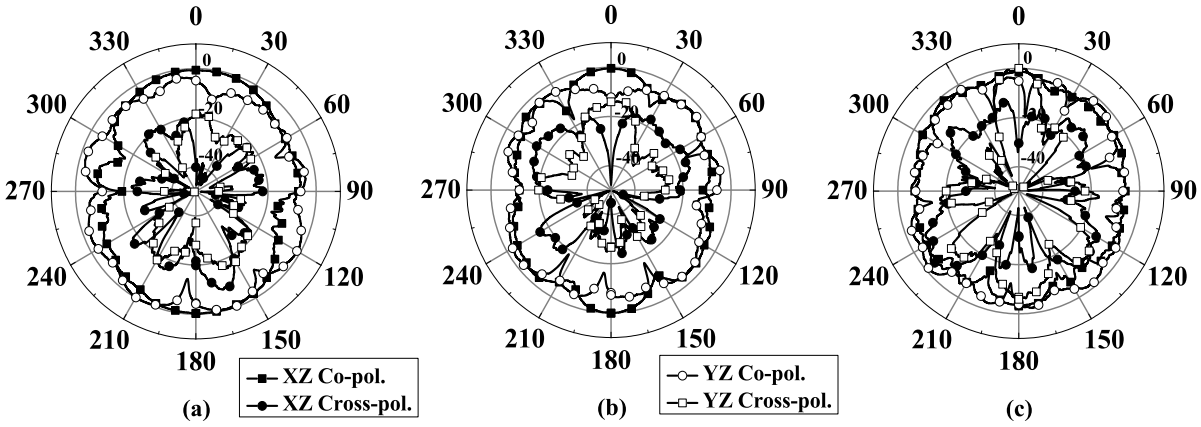

Figure 6.34: Measured radiation patterns of proposed 4-element linear antenna array at (a) 3.5 GHz (b) 5.5 GHz (c) 6.5 GHz

Table 6.9: Measured gain and simulated total antenna efficiency of proposed 4-element linear antenna array.

Frequency (GHz)	3.0	3.5	4.0	4.5	5.0	5.5	6.0	6.5	7.0
Gain (dBi)	6.79	8.32	8.78	9.21	10.68	9.11	7.90	8.10	7.52
Efficiency (%)	67.38	73.69	65.35	66.82	64.44	69.38	68.23	71.10	54.22

6.5 Summary

In this chapter, initially, 2-element MIMO is designed for hand-held mobile devices. The proposed MIMO antenna provides a dual wideband responses for band 1 (1.65-1.9 GHz) and for band 2 (2.68-6.45 GHz). From simulation results explanations are derived for the reflection coefficient, peak realized gain, total antenna efficiency, envelope correlation coefficients, 3D radiation patterns and current distributions of the proposed MIMO antenna. The measured results are reasonably matched with simulated ones. It has a nearly omnidirectional property in all bands. Furthermore,

Table 6.10: Comparison of 2-element and 4-element linear antenna array with single element

Parameters	**Single-Element antenna array (Section 3.3)**	**2-Element antenna array**	**4-Element antenna array**
Dimensions (mm)	25×37×1.58	65×50×1.58	100×120×1.58
10dB RL bandwidth (GHz)	3.2-6.5	3.1-6.8	3.1-7.0
10dB RL bandwidth (%)	68.04 %	76.28 %	77.22 %
Maximum peak realized gain (dB)	4.42 dBi, (3.11-4.42) ± 1.8	7.89 dBi, (6.28-7.89) ± 1.6	10.68 dBi, (6.79-10.68) ±1.94
Efficiency (%)	> 70 %	> 70 %	> 65 %

a 4-element MIMO antenna is simulated and experimentally verified. Four radiating elements and coaxial feed are used on same ground plane as in case of 2-element. The design goals are to achieve lower correlation values and capacity loss, higher gain, and high efficiency over operating bands. As expected, measured results are well matched with simulated results. The radiation patterns are same as 2-element MIMO antenna. A comparison between 2-and 4- element MIMO antenna prototypes is summarized in Table 6.4

In linear antenna arrays, sectoral fractal antenna is used as radiating element. A compact modified Wilkinson power divider prototype is introduced for high gain applications. It is fabricated and tested for wideband frequency operations. Both measured and simulated results show the proposed wideband network have acceptable reflection coefficients, insertion loss and isolation coefficients for all ports. Based on this feeding network, 2- and 4- element linear monopole antennas are designed fabricated and experimentally verified. Both the antenna arrays have acceptable reflection coefficients, gain, radiation patterns for wideband frequency rage. The maximum peak gain of 2-element array has 7.98 dBi and 4 dBi higher than of the

single element. Similiary, for a 4-element array, maximum peak gain of 10.68 dBi is observed which is 7 dBi higher than that of the single element. A comparison between 2-and 4- element monopole linear antenna prototypes is summarized in Table 6.10

CHAPTER 7

Conclusions and Future Work

This thesis has presented the results and procedure of the endeavour of the author towards contribution to compact wideband fractal antenna systems. It contains **SEVEN** chapters, including this as the last chapter.

This thesis presents the design methodology and results of fractal antenna elements and arrays. Several wideband/dual wideband antennas have been designed, fabricated and experimentally verified seeking for better wireless communication systems. In addition, this research work has addressed the effectiveness of fractal geometries in antenna and to bring-out the true advantages of their in antenna engineering.

7.1 Conclusions

The **FIRST** chapter describes the motivation factor for carrying out this work. It outlines requirements of antenna in the present and future communication systems. The **SECOND** chapter presents the literature review of wideband planar monopole antennas. It is started by describing the introduction about wideband technology and its advantages over present and future wireless communication systems.

The **THIRD** chapter of this thesis concludes the development of different wideband fractal monopole antennas to achieve low profile and ease of integration. The main aim is to develop such fractal monopole antennas to improve space filling feature, reduce physical antenna size and increase number of band as well as impedance bandwidth. Koch fractal and Hybrid fractal monopole antennas are investigated for wideband range. In case of Koch fractal, the antenna covers impedance bandwidth of 100.7% (2.6-7.88 GHz). Its measured maximum peak realized gain is 4.42 dBi and

simulated antenna efficiency of 95 %. For hybrid fractal monopole antenna, the two fractal geometries are used in simple rectangular patch. It is found that the measured impedance bandwidth of 72.37 % from 1.6-3.4 GHz frequency band. The measured maximum peak realized gain of the proposed antenna is 4.35 dBi. A new sectoral fractal monopole antenna is designed for wideband wireless applications. It covers the impedance bandwidth of 68.04 % from 3.22-6.55 GHz. The peak gain of 4.42 dBi is achieved with a simulated antenna efficiency of 80 %. Furthermore, modified sectoral and semi circle fractal antennas are investigated for dual wideband operations. The modified sectoral fractal antenna is covering 76.37 % impedance bandwidth for band 1 (1.51-3.39 GHz) and 17.3 % impedance bandwidth for band 2 (5.31-6.32). The semi circle fractal antenna is constructed using a Descartes Circle (DC) theorem. Its impedance bandwidth of 33.3 % for band 1 (2.2-2.45 GHz) and 39.28 % for band 2 (4.5-6.6 GHz) are observed.

The parametric studies have been carried out to observe the effect of some antenna parameters. For understanding the behavior of the proposed antennas, surface current distributions and 3D radiation patterns are presented. Experimental as well as the simulated results confirm that the proposed antennas have nearly stable omnidirectional radiation properties over the entire frequency band of interest. These features make them attractive for present and future communication systems.

The design procedure and implementation of frequency reconfigurable antenna is developed in **FOURTH** chapter. Frequency reconfigurability is found in Koch snowflake fractal antenna. Koch snowflake fractal is modified and used as an array element. The RF PIN diodes and other lumped elements (capacitor, inductor and resistor) are used to achieve frequency reconfigurability. The proposed antenna provides three configuration of measured impedance bandwidth. The impedance bandwidth of 30% (3.34-4.52 GHz) is obtained for case I. Similiary in case II and case III the impedance bandwidths are 43% (2.2-3.4 GHz) and 95.49% (1.45-4.1 GHz). Thus the antenna provides continuous coverage of 100% (1.5-4.5 GHz) impedance bandwidth. Its measured maximum peak realized gain is 2.71 dBi.

In **FIFTH** chapter, UWB modified square Sierpinski fractal antennas is designed

with band notched characteristics. The proposed antenna is useful for UWB applications (3.1-10.6 GHz) with band notch characteristics at 5.5 GHz (5-6 GHz). The UWB is achieved by increasing the number of iterations and rectangular grooved ground plane. The band rejection characteristic is realized using $\bigcap$-slot in microstrip feed line. The gain of the proposed antenna varies from 2-5 dB in UWB frequency range and decreases in band notched frequency upto 4 dBi. Therefore, the proposed antenna is feasible for using as a low profile and low cost UWB antenna for wireless communication systems.

The **SIXTH** chapter describes, 2- and 4- element antenna array with MIMO environment for hand held devices and high gain applications. In MIMO antenna, a hybrid fractal (combination of Koch and Minkowski curve fractals) is used as a radiating element. Initially, 2-element MIMO is designed for hand-held mobile devices. The proposed MIMO antenna provides a dual wideband responses for band 1 (1.65-1.9 GHz) and for band 2 (2.68-6.45 GHz). The simulation results produce the reflection coefficient, peak realized gain, total antenna efficiency, envelope correlation coefficients, 3D radiation patterns and current distributions. The measured results are well matched with simulated ones. Furthermore, a 4-element MIMO antenna is simulated and experimentally verified. Four radiating elements and feed are used on same ground plane as 2-element. The design goals of lower correlation values & capacity loss, higher gain and high efficiency over operating bands. As expected, measured results are well matched with simulated results. The radiation patterns are omnidirectional in nature for both 2- and 4- element antennas.

In linear antenna array, a sectoral fractal antenna is used as a radiating element. Wideband feed networks are necessary for high gain applications. For this purpose, a compact modified Wilkinson power divider prototype is introduced. Initially, 2-element monopole linear antenna array is designed and experimentally verified. The inter spacing distance between antenna elements is chosen as a half wavelength for higher frequency. The measure impedance bandwidth of 76.28 % (3.1-6.8 GHz) is found. The measured radiation patterns are monopole like and omnidirectional in nature. Its measured peak realized gain is 7.98 dBi which is 4 dBi higher than that

of single element. Furthermore, a 4-element monopole linear antenna is simulated, fabricated and experimentally verified. The design goal of such antenna is to improve the gain and efficiency. The measured impedance bandwidth of 72.22 % (3.1-7.0 GHz) is achieved. The radiation patters are same as 2-element is observed. Its measured peak realized gain is 10.68 dBi which 7 dBi higher than that of the single element. For all the designed antennas, measurement of total antenna efficiency could not be possible due to lack of sophisticated equipments.

7.2 Suggestion for Future Work

In this thesis different types of compact fractal antennas are investigated for wideband operations. Based on this work many future research works may be performed. Some of these are outlined in the following task:

- The effect of material properties on fractal antenna performance such as gain, efficiency, radiation patterns, bandwidth etc. can be studied.
- Investigation of new techniques to reduce the size and enhancing bandwidth of fractal wideband monopole antennas for use in mobile and portable devices.
- Design of different types of fractal shapes and techniques for wideband microwave components such as transitions, hybrid couplers and phase shifters with better performance in the wideband of frequency range.
- Detail study and design of different frequency reconfigurable fractal antennas for wideband operation and to tune its resonant frequency electronically.
- The direct time domain performance may be performed in future, for UWB antenna involving a nano-sec pulse generator and wide digital storage oscilloscope. Also, antenna integration with low-noise amplifier may be investigated in future.
- The designed fractal antennas in this thesis have been printed on lossy substrates. Those can be designed on low temperature co-fired ceramic (LTCC)

substrates in future. It will have the advantages of direct integration with monolithic microwave integrated circuits (MICs).

APPENDIX A

Design Methodology

A.1 Introduction

This Section deals with the techniques used for the design, fabrication and measurement of antennas. The design and simulations are performed using the CST MW Studio v12 and HFSS v14 packages. The antennas are fabricated using photolithographic method and milling machine techniques.Vector Network Analyzer (VNA) is used to measure antenna characteristics such as S-parameters, gain, radiation patterns etc.

A.1.1 Numerical and Analytical approaches

Scientists and engineers use several techniques in solving continuum of electromagnetic field problems. The following methods are commonly used in electromagnetic (EM) theory.

Analytical method (exact solution)

1. Separation of variables
2. Series expansion
3. Conformal mapping
4. Integral solution, e.g. Laplace and Fourier transformation
5. Perturbation methods

Numerical methods (approximate solutions)

1. Finite difference method
2. Moment method
3. Finite element method
4. Transmission-line modeling

The principles of EM fields and waves are very important for the design and development of antennas as key elements of any wireless communication system. The need for numerical solutions of electromagnetic problems is the best expressed by Paris and Hurd [209]; "***Most problems that can be solved formally (analytically) have been solved.***" Until 1940s, the most EM problems were solved using well known Maxwell's equations. These equations describe all electromagnetic phenomena of different structures and configurations. They can be expressed in their either differential or integral forms as given in equations (A.1 to A.8) [210].

Differential form

$$\nabla.\vec{D} = \rho_v \tag{A.1}$$

$$\nabla.\vec{B} = 0 \tag{A.2}$$

$$\nabla \times \vec{E} = -\frac{\partial \vec{B}}{\partial \vec{t}} - \vec{M} \tag{A.3}$$

$$\nabla \times \vec{H} = \vec{J} + \frac{\partial \vec{D}}{\partial t} \tag{A.4}$$

Integral form

$$\oiint \vec{D}.d\vec{s} = Q_{enc} \tag{A.5}$$

$$\oiint \vec{B}.d\vec{s} = 0 \tag{A.6}$$

$$\oint \vec{E}.d\vec{l} = -\frac{\partial \phi_B}{\partial t} \tag{A.7}$$

$$\oint \vec{H}.d\vec{l} = i_{enc} + \epsilon \frac{\partial \phi_E}{\partial t} \tag{A.8}$$

where the vectors $\vec{E}$ and $\vec{H}$ are the electric and magnetic field intensities and are measured in units of [V/m] and [A/m], respectively. The vectors quantities $\vec{D}$ and $\vec{B}$ are the electric and magnetic flux densities and are in units of [C/m^2] and [Wb/m^2]. The scalar quantities $\phi_E = \iint \vec{D}.d\vec{S}$ and $\phi_B = \iint \vec{B}.d\vec{S}$ are the electric and magnetic fluxes and are in units of [C] and [Wb], respectively.

When the EM field problem is complex, an exact solution in a closed form may be difficult to obtain and hence we should solve them by applying numerical techniques. In this thesis, all proposed antenna structures are complex. Hence they can be modeled using commercial simulation software programs which enable us to design, simulate, tune and optimize structure's physical parameters to reach the best design before fabricating prototypes. Currently, there are several numerical techniques that can be used to solve the EM problems, such as the Finite Element (FE) method [211], the Method of Moments (MoM) [212], the Finite Difference Time Domain (FDTD) [213] and the Finite Integration Technique (FIT) [214] etc. The first two methods solve the EM problems in the frequency domain while the other two methods use the time domain.

A.1.2 Finite Element Method using Ansoft HFSS

The first simulation software program is Ansoft High Frequency Structure Simulator (HFSS) [18]. Ansoft HFSS is currently considered to be one of the top industry-standard software programs and a powerful EM field simulation tool for many years. It is based on a three-dimensional (3D) full-wave finite element (FE) method which is a frequency-domain numerical technique for solving Maxwell's equations. Because of its high accuracy and performance, Ansoft HFSS can be used by engineers in industry or researchers and scientists in academia to analyze and design different complex structures for high-frequency applications.

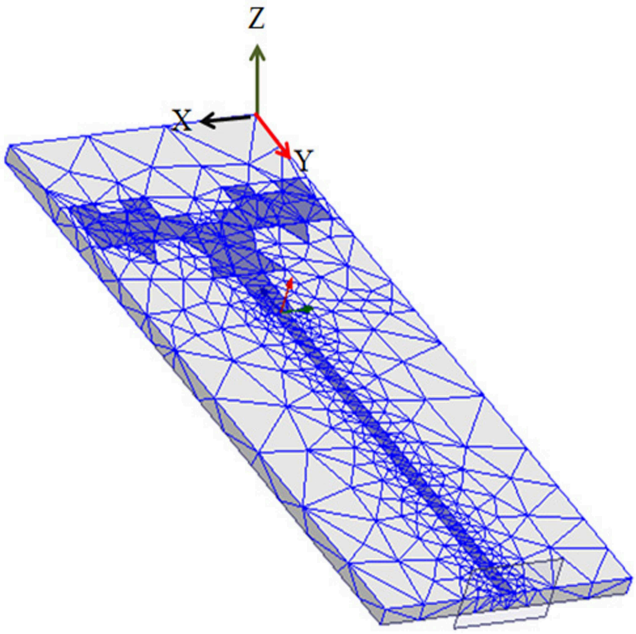

Figure A.1: Meshing of an antenna structure in Ansoft HFSS.

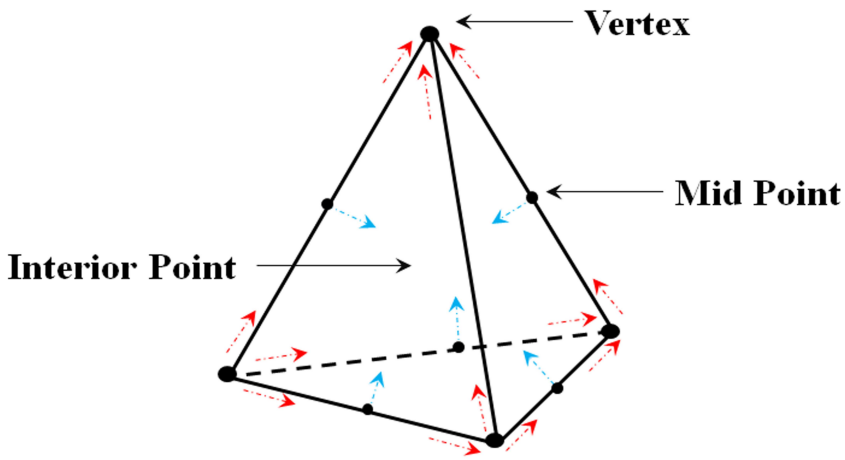

Figure A.2: A single mesh shape used in Ansoft HFSS

Ansoft HFSS uses the FE numerical technique in order to generate an EM field solution for different 3D problems. At first, the finite element technique is based on dividing the whole big problem space into small regions or sub-regions called elements. Then the fields in each finite element are formulated by local functions. Ansoft HFSS automatically converts the whole problem structure into a finite element mesh which consists of a large number of very small 3D tetrahedral shapes as shown in Figure

A.1. Each single tetrahedron is a four-sided pyramid as presented in Figure A.2. It can be noticed that the meshing or discretization operation done by Ansoft HFSS is very coarse in almost the whole structure while it is very fine at some regions which need more accuracy such as near wave port, metallic edges or discontinuities. After finalizing the mesh operation of the whole structure, the solution process starts with two-dimensional (2D) port solutions as the structure excitation then followed by the field solution of the full 3D problem including fields at all vertices, midpoints and interior points as in Figure A.2. The program exploits the computed 2D fields on ports to be used as boundary conditions to solve the 3D fields of the whole structure.

During the numerical iterative solution, Ansoft HFSS solves the electric field for a given problem based on the following matrix equation (for a lossless case) [18]:

$$[A]\overline{x} + K_0^2[B] = c \tag{A.9}$$

where [A] and [B] are square matrices and their sizes depend on the geometry of the problem and the size of the mesh, $\overline{x}$ is the electric field vector, K_0 is wave number in free space and c is the value of the source or excitation defined for the given problem. Then the magnetic field solution is calculated from the following relationship with the electric field:

$$\vec{H} = -\frac{1}{j\omega\mu}\nabla \times \vec{E} \tag{A.10}$$

A.1.3 Finite Integration Technique using CST

The other simulation software program is called Computer Simulation Technologies Microwave Studio (CST MWS) [17]. CST MWS is a tool for fast and accurate 3D EM simulation of high frequency problems. Currently, it is considered to be industry-standard software programs and a powerful 3D EM field simulation tool. CST MWS is based on the Finite Integration Technique (FIT) [215] which is equivalent to FDTD. Unlike the FE method, FIT is a time-domain numerical technique for solving Maxwell's equations. Using the function of parametric study in both Ansoft HFSS and CST MWS simulation programs, we can tune and optimize the structure

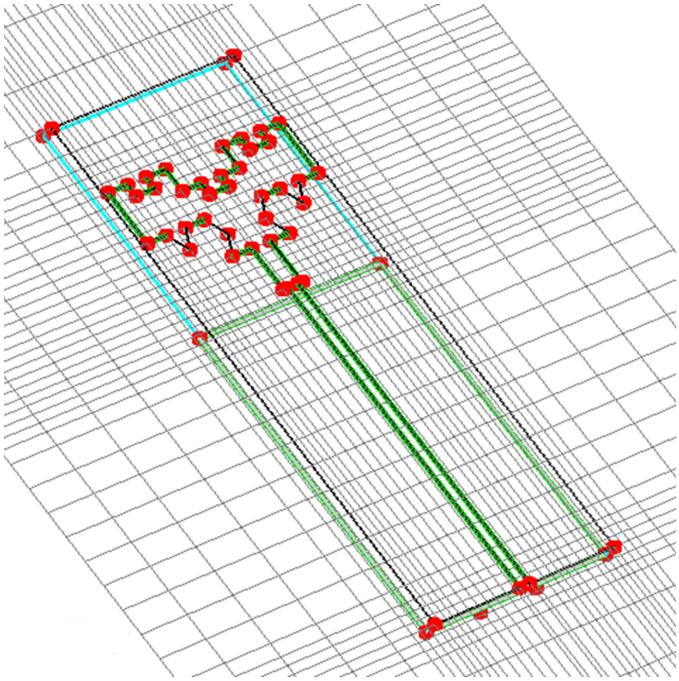

Figure A.3: A single (a) hexahedral, (b) tetrahedral and (c) surface mesh element used in CST MW Studio

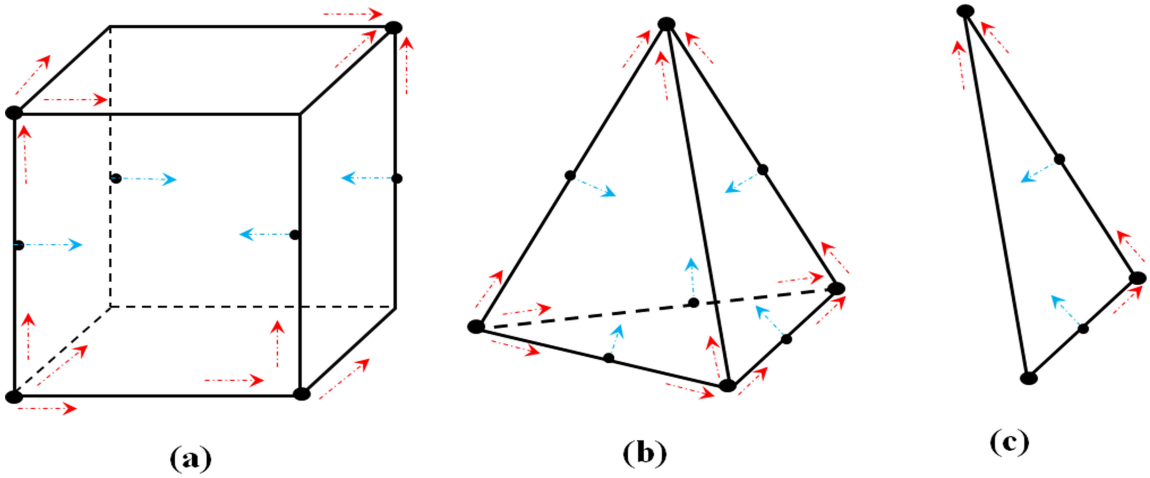

Figure A.4: Meshing of an antenna structure in CST MW studio.

physical parameters to obtain the best design before going to the fabrication process. CST MWS has different kind of solvers not only a transient solver but also a frequency domain solver, an eigen mode solver and an integral equation solver.

In a transient or time-domain solver, the value of the vector electric $\vec{E}$ or magnetic $\vec{H}$ field quantities are computed through time at discrete spatial locations and at discrete time samples. The maximum time step Δt used in the simulation program

depends on the minimum mesh step size which can be determined by the density of the mesh used in the meshing process of the whole structure. Therefore the program takes more time to run simulation if the mesh is dense. Once the spatial mesh or discretization is performed by the CST program, the finite integration method is employed. CST has two different mesh types available, i.e. hexahedral and tetrahedral meshes. Another type of mesh used by the Integral Equation (IE) solver is called surface mesh. Figure A.3 shows a single hexahedral tetrahedral and surface mesh element used in CST program. For complex structures, CST uses a hexahedral mesh in meshing or discretization because it is considered to be very robust. Other solvers use a tetrahedral or surface mesh method. Figure A.4 shows the meshing based on hexahedral shapes of an antenna structure in CST.

The finite integration technique converts the well-known Maxwell equations in their integral form into set of discrete matrix equations called Maxwell grid equations (MGE) as follows [215]:

Integral form ⇒ Matrix form

$$\oiint \vec{D}.d\vec{A} = \iiint_{v} \rho_v d\vec{V} \Longrightarrow [\tilde{S}] = q \tag{A.11}$$

$$\oiint \vec{B}.d\vec{A} = 0 \Longrightarrow [S]b = 0 \tag{A.12}$$

$$\oint \vec{E}.d\vec{l} = -\iiint_{A} \frac{\partial \vec{B}}{\partial t} d\vec{A} \Longrightarrow [C]e = -\frac{d}{dt}b \tag{A.13}$$

$$\oint \vec{H}.d\vec{l} = -\iint_{A} \left[\frac{\partial \vec{A}}{\partial t} + J\right] d\vec{A} \Longrightarrow [\tilde{C}]h = -\frac{d}{dt}d + j \tag{A.14}$$

where $[\tilde{C}]$,[C],[S] and $[\tilde{C}]$ are square matrices represent the discrete curl and divergence operators, respectively and their sizes depend on the problem geometry. 'e' and 'h' represent the electric and magnetic grid voltages and they are related to the electric and magnetic fields according to $e = \int_{\partial A} \vec{E}.d\vec{l}$ and $h = \int_{\partial \tilde{C}} \vec{H}.d\vec{l}$ d and b are the electric and magnetic facet flux vectors over the mesh cell.

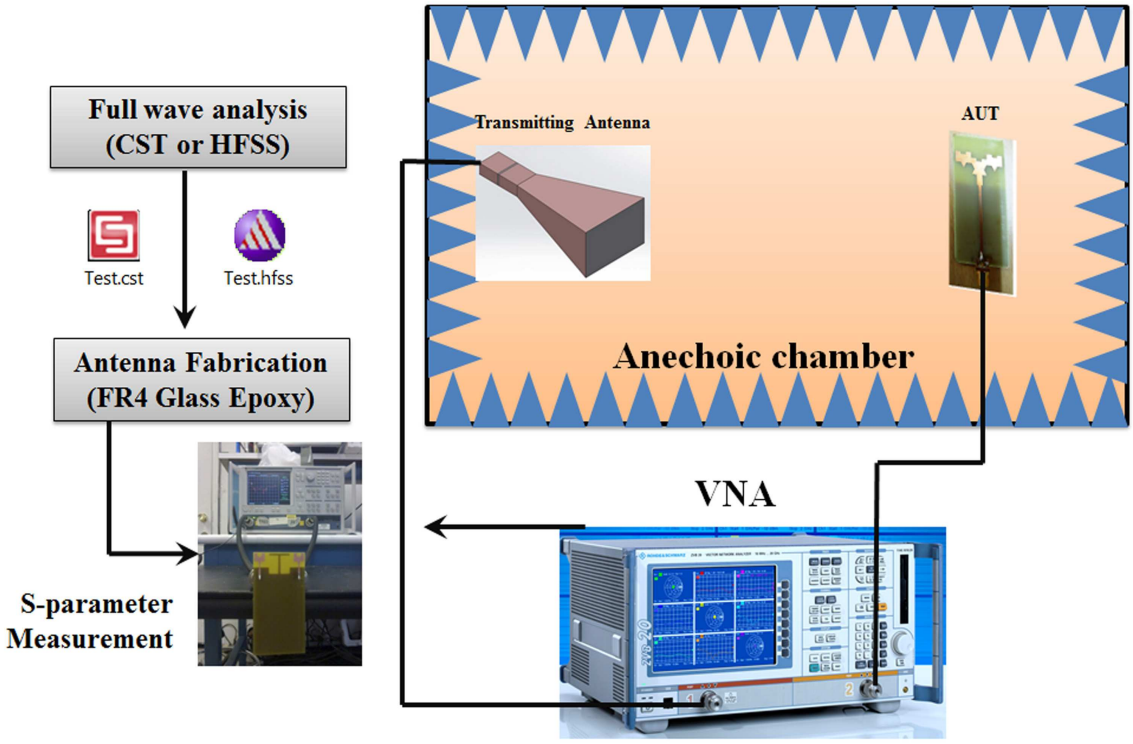

Figure A.5: Setup for measurement of reflection coefficients and radiation patterns.

A.1.4 Antenna Fabrication

All the antennas investigated in the thesis are fabricated using the photolithographic technique and milling machine techniques. The photolithographic technique is a chemical etching process by which the unwanted metal regions of the metallic layer are removed so that the intended design is obtained. The milling machine technique refers to the removal of metal from the work piece using a tool which has several cutting points and is rotating about its axis. Thus each cutting point removes a little bit of the metal but since there are multiple such points and the tool is rotating at a fast speed, the overall removal is quite brisk. Depending upon the design of the antenna, biplanar or uniplanar, dual or single side substrates are used. The selection of a proper substrate material is the essential part in antenna design.

A.1.5 S-Parameter Measurement

The S-parameter characteristics of the antenna are measured using the network analyzer ports (S_{11} or S_{22} mode) as shown in Figure A.5. The specific port of the

analyzer should be calibrated for the frequency range of interest using the standard open, short and matched load, prior to the measurement. The S_{11} values of the antenna in the entire frequency band are stored on a computer. The frequency at which the S-parameter value is taken minimum, as the resonant frequency of the antenna. The range of frequency for which the S-parameter value within the -10dB points is usually treated as the band width of the antenna.

The frequency bandwidth of an antenna can be expressed in terms of either the absolute bandwidth (ABW) or the fractional bandwidth (FBW). Assuming that the antenna bandwidth has a lower edge frequency of f_L, an upper edge frequency of f_U and a center frequency of f_c. The ABW is defined as the difference between the upper and the lower edge frequencies of operation while the FBW can be defined as the percentage of the ratio between the absolute bandwidth and the center frequency as given in equation (A.15) and equation (A.16), respectively:

$$AWB = f_U - f_L \tag{A.15}$$

$$FBW = AWB/f_c = (f_U - f_L)/f_c \tag{A.16}$$

where the center frequency f_c=(f_U+f_L)/2. Another definition for the bandwidth in case of broadband antennas which is the ratio of the upper edge frequency f_U to the lower edge frequency f_L, as given in equation (A.17):

$$BW = (f_U/f_L) \tag{A.17}$$

The band width of the antenna, usually expressed as the percentage of bandwidth as given in equation (A.18).

$$\%BW = 2\left[\frac{f_U - f_L}{f_U + f_L}\right] \times 100\% \tag{A.18}$$

A.1.6 Anechoic Chamber

The measurement setup in anechoic chamber is shown in Figure A.5. The anechoic chamber provides a quite zone and used to measure the antenna characteristics accurately. All the antenna characterizations are done in an anechoic chamber to avoid

reflections from nearby objects. The absorbers fixed on the walls are highly lossy at microwave frequencies. They have tapered shapes to achieve good impedance matching for the microwave power impinges upon it. The chamber is made free from the surrounding EM interferences by covering all the walls and the roof with aluminum sheet.

A.1.7 Radiation pattern Measurement

The radiation pattern measurement is carried out in the anechoic chamber with the help of VNA. The antenna under test (AUT) is mounted on a turntable assembly in the anechoic chamber and connected to one port of the network analyzer configured in the receiver mode. The other port of the network analyzer is connected to a wideband horn which acts as the transmitter. The network analyzer and the turntable controller are interfaced to a computer which runs the measurement automation software. The measurement automation software requires the measurement band, angular step size and file name as input. The system automatically undergoes through calibration prior to the measurement and performs the transmission measurement for each step angle and records the angular transmission characteristics in a data file specified by the file name.

A.1.8 Antenna Gain Measurement

Gain transfer method is employed to measure the gain of the antenna. The experimental setup for determining the gain is similar to the radiation pattern measurement setup. The gain of the AUT is measured relative to the power levels detected by a standard gain antenna. In order to measure the gain of AUT, the standard gain antenna is mounted on the turntable and a thorough calibration is performed at boresight direction. The AUT is carefully mounted over the turntable and extreme care is taken for the exact alignment. The relative power level is obtained from the analyzer and this provides the gain with respect to the standard antenna. The gain of the standard antenna is added to the relative gain to obtain the gain of the AUT. The gain measurement method basically based on Friis transmission formula as given by equation (A.19) [216].

$$(G_t + G_r)_{dB} = 20\log_{10}\left(\frac{4\pi R}{\lambda} + 10\log_{10}\left(\frac{P_r}{P_t}\right)\right) \tag{A.19}$$

where,

$(G_t)_{dB}$= gain of the transmitting antenna (dB)

$(G_r)_{dB}$= gain of the receiving antenna (dB)

P_r= received power (W)

P_t= transmitted power (W)

R= antenna separation (m)

λ= operating wavelength (m)

If transmitting and receiving antennas are identical ($(G_t)_{dB}$=$(G_r)_{dB}$). So, the equation can be written as

$$(G_t + G_r)_{dB} = (G_r)_{dB} = 20\log_{10}\left(\frac{4\pi R}{\lambda} + 10\log_{10}\left(\frac{P_r}{P_t}\right)\right) \tag{A.20}$$

By measuring R, λ and P_r/P_t, the gain of the antenna cab be calculated using the equation (A.20).

Bibliography

[1] J. C. Maxwell, "A Treatise on Electricity and Magnetism," tech. rep., Oxford University Press, London, UK, 1873-1904.

[2] K. Fujimoto and J. James, *Mobile Antenna Systems Handbook*. Artech House, 1994.

[3] W. Beynon, "Marconi, Radio waves and the Ionosphere," *Radio Science*, vol. vol.10, no. 7, pp. 657–664, July, 1975.

[4] T. S. Rappaport, *Wireless Communications, Principles and Practice*. Prentice Hall, 1996.

[5] K. Hirasawa and M. Haneishi, "Analysis, Design and Measurement of Small and Low-profile Antennas," *Boston, London: Artech House Antennas and Propagation Library*, 1992.

[6] K. Fujimoto, "Small Antennas," *England, Research Studies Press*, 1993.

[7] K. L. Wong, *Compact and Broadband Microstrip Antennas*. Wiley-Interscience, John Wiley & Sons, 2002.

[8] D. B. Miron, *Small Antenna Design*. Communications Engineering Series, Newnes, 2006.

[9] James S. McLean, "A re-examination of the fundamental limits on the radiation Q of electrically small antennas ," *IEEE Transactions on Aantenna and Propagation*, vol. 44, no. 5, pp. 672–676, 1996.

[10] H. Morishita, Y. Kim, and K. Fujimoto, "Design Concept Of Antennas For Small Mobile Terminals And The Future Perspective," *IEEE Antennas and Propagation Magazine,*, vol. 44, no. 5, pp. 30–43, 2002.

[11] K. L. Wong, *Planar Antennas for Wireless Communications*. Wiley-Interscience, 2000.

[12] A. F. Peterson, S. L. Ray, and R. Mittra, *Computational Methods for Electromagnetics*. IEEE Press Series on Electromagnetic Wave Theory, 1997.

[13] E. K. Miller, L. Medgyesi Mitschang, and E. H. Newman, *Computational Electromagnetics: Frequency-Domain Method of Moments*. IEEE Press, 1992.

[14] W. C. Chew, J. Jin, E. Michielssen, and J. Song, *Fast and Efficient Algorithms in Computational Electromagnetics*. Artech House, 2001.

[15] *IE3D User Manual*. Zeland Sofware Inc, 2003.

[16] *FEKO User's Manual, Suite 5.1.* EM Software & Systems, South Africa.

[17] *User Manual for the CST.* IMST GmbH, Germany, 2004.

[18] *User Manual for HFSS.* Ansoft Corporation Pittsburg, PA, USA., 2000.

[19] E. K. P. Chong and S. H. Zak, *An Introduction to Optimization.* Wiley-Interscience Series in Discrete Mathematics and Optimization, 2001.

[20] J. Robinson and Y. Rahmat-Samii, "Particle Swarm Optimization In Electromagnetics," *IEEE Transactions on Antennas and Propagation*, vol. 52, no. 2, pp. 397–407, 2004.

[21] C. G. Christodoulou, M. Georgioipoulos, and A. H. E. Zooghby, *Applications of Neural Networks in Smart Antennas for Mobile Communications.* Applied Computational Intelligence, CRC Press, LLC, 2000.

[22] C. Christodoulou, M. Georgiopoulos, and C. Christopoulos, *Applications of Neural Networks in Electromagnetics.* Artech House, 2001.

[23] Y. Rahmat-Samii and E. Michielssen, *Electromagnetic Optimization by Genetic Algorithms.* New York: John Wiley & Sons, 1999.

[24] D. S. Linden, *Automated Design and Optimization of Wire Antennas Using Genetic Algorithms.* PhD thesis, Massachusetts Institute of Technology, Department of Electrical Engineering and Computer Science, 1997.

[25] D. T. Pham, A. Ghanbarzadeh, E. Koç, S. Otri, S. Rahim, and M. Zaidi, "The Bees Algorithm: A Novel Tool for Complex Optimisation Problems," in *Proc. 2nd Int. Virtual Conf. on Intelligent Production Machines and Systems (IPROMS 2006)*, 2006.

[26] D. Werner and S. Ganguly, "An overview of fractal antenna engineering research," *IEEE Antennas and Propagation Magazine,*, vol. 45, no. 1, pp. 38–57, 2003.

[27] K. Vinoy, *Fractal shaped antenna elements for wideband and multi band wireless applications.* Ph.d. dissertation, The Pennsylvania StateUniversity, 2002.

[28] C. Puente, J. Romeu, R. Pous, X. Garcia, and F. Benitez, "Fractal Multiband Antenna Based On The Sierpinski Gasket," *Electronics Letters*, vol. 32, no. 1, pp. 1–2, 1996.

[29] C. Puente-Baliarda, J. Romeu, R. Pous, and A. Cardama, "On The Behavior Of The Sierpinski Multiband Fractal Antenna," *IEEE Transactions on Antennas and Propagation*, vol. 46, no. 4, pp. 517–524, 1998.

[30] N. Cohen, "Fractal antenna applications in wireless telecommunications," in *Professional Program Proceedings Electronics Industries Forum of New England*, pp. 43–49, 1997.

[31] C. Puente, J. Romeu, R. Pous, J. Ramis, and A. Hijazo, "Small but long Koch fractal monopole," *Electronics Letters*, vol. 34, no. 1, pp. 9–10, 1998.

[32] B. B. Mandlebrot, *The Fractal Geometry of Nature.* W.H.Freeman and Company, 1983.

[33] J. Anguera, *Fractal and Broadband Techniques on Miniature, Multifrequency, and High-Directivity Microstrip Patch Antennas*. PhD thesis, Department of Signal Theory and Communications, Universitat Politecnica de Catalunya, Spain, 2003.

[34] H.O. Peitgen, H. Jurgens and D. Saupe, *Chaos and Fractals. New Frontiers of Science*. Springer-Verlag, 1990.

[35] Y. Kim and D. Jaggard, "The fractal random array," *Proceedings of the IEEE*, vol. 74, no. 9, pp. 1278–1280, 1986.

[36] C. Puente-Baliarda and R. Pous, "Fractal Design of Multiband and Low Side-Lobe Arrays," *IEEE Transactions on Antennas and Propagation,*, vol. 44, no. 5, pp. 730–739, 1996.

[37] G. J. Walker and J. James, "Fractal Volume Antennas," *Electronics Letters*, vol. 34, no. 16, pp. 1536–1537, 1998.

[38] C. Borja, C. Puente, and A. Medina, "Iterative Network Model To Predict The Behaviour Of A Sierpinski Fractal Network [antennas]," *Electronics Letters*, vol. 34, no. 15, pp. 1443–1445, 1998.

[39] C. T. P. Song, P. Hall, H. Ghafouri-Shiraz, and D. Wake, "Fractal Stacked Monopole With Very Wide Bandwidth," *Electronics Letters*, vol. 35, no. 12, pp. 945–946, 1999.

[40] C. Baliarda, C. Borau, M. Rodero, and J. Robert, "An Iterative Model for Fractal antennas: Application to the Sierpinski Gasket Antenna," *IEEE Transactions on Antennas and Propagation,*, vol. 48, no. 5, pp. 713–719, 2000.

[41] D. Werner, P. Werner, and K. Church, "Genetically Engineered Multiband Fractal Antennas," *Electronics Letters*, vol. 37, no. 19, pp. 1150–1151, 2001.

[42] C. T. P. Song, P. Hall, H. Ghafouri-Shiraz, and I. Henning, "Shorted fractal sierpinski monopole antenna," *Electronics Letters*, vol. 37, no. 16, pp. 1000–1001, 2001.

[43] S. Best, "operating Band Comparison Of The Perturbed Sierpinski And Modified Parany Gasket Antennas," *IEEE Antennas and Wireless Propagation Letters*, vol. 1, no. 1, pp. 35–38, 2002.

[44] S. Best, "On The Radiation Pattern Characteristics Of The Sierpinski And Modified Parany Gasket Antennas," *IEEE Antennas and Wireless Propagation Letters*, vol. 1, no. 1, pp. 39–42, 2002.

[45] S. Best, "A Multiband Conical Monopole Antenna Derived From A Modified Sierpinski Gasket," *IEEE Antennas and Wireless Propagation Letters*, vol. 2, no. 1, pp. 205–207, 2003.

[46] G. Tsachtsiris, C. Soras, M. Karaboikis, and V. Makios, "Analysis Of A Modified Sierpinski Gasket Monopole Antenna Printed On Dual Band Wireless Devices," *IEEE Transactions on Antennas and Propagation*, vol. 52, no. 10, pp. 2571–2579, 2004.

[47] J. Anguera, E. Martinez, C. Puente, C. Borja, and J. Soler, "Broad-band Dual-frequency Microstrip Patch Antenna With Modified Sierpinski Fractal Geometry," *IEEE Transactions on Antennas and Propagation,*, vol. 52, no. 1, pp. 66–73, 2004.

[48] J. Vemagiri, M. Balachandran, M. Agarwal, and K. Varahramyan, "Development Of Compact Half-sierpinski Fractal Antenna For RFID Applications," *Electronics Letters*, vol. 43, no. 22, pp. –, 2007.

[49] W. Krzysztofik, "Modified Sierpinski Fractal Monopole for ISM-Bands Handset Applications," *IEEE Transactions on Antennas and Propagation*, vol. 57, no. 3, pp. 606–615, 2009.

[50] K. Hwang, "Dual-wideband Monopole Antenna Using A Modified Half-sierpinski Fractal Gasket," *Electronics Letters*, vol. 45, no. 10, pp. 487–489, 2009.

[51] J. S. Castany, J. R. Robert, , and C. Puente, "Mod-P Sierpinski Fractal Multi-Band Antenna," in *Proc. Millennium Conference on Antennas and Propagation*, April 2000.

[52] Y. Sung, "Bandwidth Enhancement of a Wide Slot Using Fractal-Shaped Sierpinski," *IEEE Transactions on Antennas and Propagation*, vol. 59, no. 8, pp. 3076–3079, 2011.

[53] C. Borja, G. Font, S. Blanch, and J. Romeu, "High Directivity Fractal Boundary Microstrip Patch Antenna," *Electronics Letters*, vol. 36, no. 9, pp. 778–779, 2000.

[54] S. Best, "On The Performance Properties Of The Koch Fractal And Other Bent Wire Monopoles," *IEEE Transactions on Antennas and Propagation,*, vol. 51, no. 6, pp. 1292–1300, 2003.

[55] C. Borja and J. Romeu, "On The Behavior Of Koch Island Fractal Boundary Microstrip Patch Antenna," *IEEE Transactions on Antennas and Propagation*, vol. 51, no. 6, pp. 1281–1291, 2003.

[56] D. Li and J.-F. Mao, "A Koch-Like Sided Fractal Bow-Tie Dipole Antenna," *IEEE Transactions on Antennas and Propagation*, vol. 60, no. 5, pp. 2242–2251, 2012.

[57] C. Baliarda, J. Romeu, and A. Cardama, "The Koch Monopole: A Small Fractal Antenna," *IEEE Transactions on Antennas and Propagation,*, vol. 48, no. 11, pp. 1773–1781, 2000.

[58] S. Behera and K. J. Vinoy, "Multi-Port Network Approach for the Analysis of Dual Band Fractal Microstrip Antennas," *IEEE Transactions on Antennas and Propagation,*, vol. 60, no. 11, pp. 5100–5106, 2012.

[59] D. Oloumi, S. Ebadi, A. Kordzadeh, A. Semnani, P. Mousavi, and X. Gong, "Miniaturized Reflectarray Unit Cell Using Fractal-Shaped Patch-Slot Configuration," *IEEE Antennas and Wireless Propagation Letters*, vol. 11, pp. 10–13, 2012.

[60] J. Gianvittorio and Y. Rahmat-Samii, "Fractal Antennas: A Novel Antenna Miniaturization Technique, And Applications," *IEEE Antennas and Propagation Magazine,*, vol. 44, no. 1, pp. 20–36, 2002.

[61] S. Sinha and M. Jain, "A Self-Affine Fractal Multiband Antenna," *IEEE Antennas and Wireless Propagation Letters,*, vol. 6, pp. 110–112, 2007.

[62] D.-C. Chang, B.-H. Zeng, and J.-C. Liu, "CPW-Fed Circular Fractal Slot Antenna Design for Dual-Band Applications," *IEEE Transactions on Antennas and Propagation*, vol. 56, no. 12, pp. 3630–3636, 2008.

[63] M. Naghshvarian-Jahromi, "Novel Wideband Planar Fractal Monopole Antenna," *IEEE Transactions on Antennas and Propagation*, vol. 56, no. 12, pp. 3844–3849, 2008.

[64] W.-L. Chen, G.-M. Wang, and C. xin Zhang, "Bandwidth Enhancement of a Microstrip-Line-Fed Printed Wide-Slot Antenna With a Fractal-Shaped Slot," *IEEE Transactions on Antennas and Propagation*, vol. 57, no. 7, pp. 2176–2179, 2009.

[65] J. Pourahmadazar, C. Ghobadi, J. Nourinia, and H. Shirzad, "Multiband Ring Fractal Monopole Antenna for Mobile Devices," *IEEE Antennas and Wireless Propagation Letters*, vol. 9, pp. 863–866, 2010.

[66] W. Lui, C. Cheng, and H. Zhu, "Compact Frequency Notched UWB Fractal Printed Slot Antenna," *IEEE Microwave and Wireless Components Letters*, vol. 16, no. 4, pp. 224–226, 2006.

[67] W.-L. Chen, G.-M. Wang, and C. xin Zhang, "Small-Size Microstrip Patch Antennas Combining Koch and Sierpinski Fractal-Shapes," *IEEE Antennas and Wireless Propagation Letters,*, vol. 7, pp. 738–741, 2008.

[68] R. Azaro, L. Debiasi, E. Zeni, M. Benedetti, P. Rocca, and A. Massa, "A Hybrid Prefractal Three-Band Antenna for Multistandard Mobile Wireless Applications," *IEEE Antennas and Wireless Propagation Letters*, vol. 8, pp. 905–908, 2009.

[69] H. Oraizi and S. Hedayati, "Miniaturized UWB Monopole Microstrip Antenna Design by the Combination of Giusepe Peano and Sierpinski Carpet Fractals," *IEEE Antennas and Wireless Propagation Letters,*, vol. 10, pp. 67–70, 2011.

[70] N. Bayatmaku, P. Lotfi, M. Azarmanesh, and S. Soltani, "Design of Simple Multiband Patch Antenna for Mobile Communication Applications Using New E-Shape Fractal," *IEEE Antennas and Wireless Propagation Letters*, vol. 10, pp. 873–875, 2011.

[71] H. Oraizi and S. Hedayati, "Miniaturization of Microstrip Antennas by the Novel Application of the Giuseppe Peano Fractal Geometries," *IEEE Transactions on Antennas and Propagation,*, vol. 60, no. 8, pp. 3559–3567, 2012.

[72] H. Oraizi and S. Hedayati, "Circularly Polarized Multiband Microstrip Antenna Using the Square and Giuseppe Peano Fractals," *IEEE Transactions on Antennas and Propagation*, vol. 60, no. 7, pp. 3466–3470, 2012.

[73] *Very High-frequency Techniques*, ch. 1, pp. 1–25. Radio Research Laboratory (U.S.), McGraw Hill, New York, 1947.

[74] J. Dyson, "The Equiangular Spiral Antenna," *IRE Transactions on Antennas and Propagation*, vol. 7, no. 2, pp. 181–187, 1959.

[75] R. H. Duhamel, *Dual Polarized Sinuous Antennas.* No. 4,658,262, U. S. Patent, 1987.

[76] W. L. Stutzman and G. Thiele, *Antenna Theory and Design 2nd edition.* John Wiley & Sons, New York, 1998.

[77] S. Honda, M. Ito, H. Seki, and Y. Jinbo, "A Disc Monopole Antenna With 1:8 Impedance Bandwidth And Omni-directional Radiation Pattern," in *Proc. ISAP 92*, (Sapporo, Japan), pp. 1145–1148, Sep. 1992.

[78] M. Hammoud, P. Poey, and F. Colombel, "Matching The Input Impedance Of A Broadband Disc Monopole," *Electronics Letters*, vol. 29, no. 4, pp. 406–407, 1993.

[79] N. Agrawall, G. Kumar, and K. P. Ray, "Wide-band Planar Monopole Antennas," *IEEE Transactions on Antennas and Propagation*, vol. 46, no. 2, pp. 294–295, 1998.

[80] J. A. Evans and M. Amunann, "Planar Trapezoidal And Pentagonal Monopoles With Impedance Bandwidths In Excess Of 10:1," in *IEEE Antennas and Propagation Society International Symposium,*, vol. 3, pp. 1558–1561 vol.3, 1999.

[81] R. Taylor, "A Broadband Omnidirectional Antenna," in *AP-S. Digest Antennas and Propagation Society International Symposium*, vol. 2, pp. 1294–1297 vol.2, 1994.

[82] M. Sindou, G. Ablart, and C. Sourdois, "Multiband And Wideband Properties Of Printed Fractal Branched Antennas," *Electronics Letters*, vol. 35, no. 3, pp. 181–182, 1999.

[83] E. Lee, P. Hall, and P. Gardner, "Compact Wideband Planar Monopole Antenna," *Electronics Letters*, vol. 35, no. 25, pp. 2157–2158, 1999.

[84] A. Bhobe, C. Holloway, M. Piket-May, and R. Hall, "Coplanar Waveguide Fed Wideband Slot Antenna," *Electronics Letters*, vol. 36, no. 16, pp. 1340–1342, 2000.

[85] F. Yang, X.-X. Zhang, X. Ye, and Y. Rahmat-Samii, "Wide-band E-shaped patch antennas for wireless communications," *IEEE Transactions on Antennas and Propagation*, vol. 49, no. 7, pp. 1094–1100, 2001.

[86] N. Behdad and K. Sarabandi, "Wideband Double-element Ring Slot Antenna," *Electronics Letters*, vol. 40, no. 7, pp. 408–409, 2004.

[87] D.-U. Sim, J.-I. Moon, and S.-O. Park, "A Wideband Monopole Antenna For PCS/IMT-2000/Bluetooth Applications," *IEEE Antennas and Wireless Propagation Letters*, vol. 3, no. 1, pp. 45–47, 2004.

[88] T. Sudha, T. S. Vedavathy, and N. Bhat, "Wideband Single-fed Circularly Polarised Patch Antenna," *Electronics Letters*, vol. 40, no. 11, pp. 648–649, 2004.

[89] M. Joseph, B. Paul, R. Raj, and P. Mohanan, "Compact Wideband Antenna For 2.4 Ghz Wlan Applications," *Electronics Letters*, vol. 40, no. 23, pp. 1460–1461, 2004.

[90] S. Tanaka, S. Hayashida, H. Morishita, and Y. Atsumi, "Wideband And Compact Folded Loop Antenna," *Electronics Letters*, vol. 41, no. 17, pp. 945–946, 2005.

[91] J. Y. Jan and T.-M. Kuo, "CPW-fed Wideband Planar Monopole Antenna For Operations In DCS, PCS, 3G, And Bluetooth Bands," *Electronics Letters*, vol. 41, no. 18, pp. 991–993, 2005.

[92] J.-S. Row and S.-H. Chen, "Wideband Monopolar Square-Rring Patch Antenna," *IEEE Transactions on Antennas and Propagation*, vol. 54, no. 4, pp. 1335–1339, 2006.

[93] J. Y. Jan and C. Y. Hsiang, "Wideband CPW-fed Slot Antenna For DCS, PCS, 3G and Bluetooth Bands," *Electronics Letters*, vol. 42, no. 24, pp. 1377–1378, 2006.

[94] S.-H. Wi, Y.-S. Lee, and J.-G. Yook, "Wideband Microstrip Patch Antenna With U-Shaped Parasitic Elements," *IEEE Transactions on Antennas and Propagation*, vol. 55, no. 4, pp. 1196–1199, 2007.

[95] Y. Ruan, Y. Guo, K.-W. Khoo, and X.-Q. Shi, "Compact Wideband Antenna For Wireless Communications," *IET Microwaves, Antennas Propagation*, vol. 1, no. 3, pp. 556–560, 2007.

[96] T. Wong, C. Lau, K.-M. Luk, and K.-F. Lee, "Wideband Fractal Vertical Patch Antenna," *IEEE Antennas and Wireless Propagation Letters*, vol. 6, pp. 5–6, 2007.

[97] B. Mirzapour and H. Hassani, "Size Reduction And Bandwidth Enhancement Of Snowflake Fractal Antenna," *IET Microwaves, Antennas Propagation*, vol. 2, no. 2, pp. 180–187, 2008.

[98] D. Krishna, M. Gopikrishna, C. K. Anandan, P. Mohanan, and K. Vasudevan, "CPW-Fed Koch Fractal Slot Antenna for WLAN/WiMAX Applications," *IEEE Antennas and Wireless Propagation Letters*, vol. 7, pp. 389–392, 2008.

[99] M. Naghshvarian-Jahromi, "Novel Wideband Planar Fractal Monopole Antenna," *IEEE Transactions on Antennas and Propagation*, vol. 56, no. 12, pp. 3844–3849, 2008.

[100] D. D. Krishna, M. Gopikrishna, C. K. Aanandan, P. Mohanan, and K. Vasudevan, "Compact Wideband Koch Fractal Printed Slot Antenna," *IET Microwaves, Antennas Propagation*, vol. 3, no. 5, pp. 782–789, 2009.

[101] R. Guo, X. Chen, and K. Huang, "A Novel Wideband Microstrip Fractal Antenna Based on the Fractal Binary Tree," *Electromagnetics*, vol. 29, no. 4, pp. 283–290, 2009.

[102] G.-M. Zhang, J.-S. Hong, B.-Z. Wang, G. Song, and P. Zhang, "Compact Wideband Unidirectional Antenna With a Reflector Connected to the Ground Using a Stub," *IEEE Antennas and Wireless Propagation Letters*, vol. 10, pp. 1186–1189, 2011.

[103] S. W. Lee and Y. T. Lo, *Antenna Handbook, Theory, Applications, and Design*. Van Nostrand Reinhold, New York, 1988.

[104] J. R. Harrington, *Time Harmonic Electromagnetic Fields*. McGraw-Hill, New York, 1961.

[105] E. Brown, "RF-MEMS Switches For Reconfigurable Integrated Circuits," *IEEE Transactions on Microwave Theory and Techniques*, vol. 46, no. 11, pp. 1868–1880, 1998.

[106] Y. Qian, B. C. C. Chang, M. F. Chang, and T. Itoh, "Reconfigurable Leaky-mode/multifunction Patch Antenna Structure," *Electronics Letters*, vol. 35, no. 2, pp. 104–105, 1999.

[107] F. Yang and Y. Rahmat-Samii, "A reconfigurable patch antenna using switchable slots for circular polarization diversity," *IEEE Microwave and Wireless Components Letters*, vol. 12, no. 3, pp. 96–98, 2002.

[108] J. Petko and D. Werner, "Miniature Reconfigurable Three-dimensional Fractal Tree Antennas," *IEEE Transactions on Antennas and Propagation*, vol. 52, no. 8, pp. 1945–1956, 2004.

[109] D. Peroulis, K. Sarabandi, and L. P. B. Katehi, "Design Of Reconfigurable Slot Antennas," *IEEE Transactions on Antennas and Propagation*, vol. 53, no. 2, pp. 645–654, 2005.

[110] N. Jin, F. Yang, and Y. Rahmat-Samii, "A Novel Patch Antenna With Switchable Slot (PASS): Dual-frequency Operation With Reversed Circular Polarizations," *IEEE Transactions on Antennas and Propagation*, vol. 54, no. 3, pp. 1031–1034, 2006.

[111] B. Z. Wang, S. Xiao, and J. Wang, "Reconfigurable patch-antenna design for wideband wireless communication systems," *IET Microwaves, Antennas Propagation*, vol. 1, no. 2, pp. 414–419, 2007.

[112] Y.-Y. Yang and Q.-X. Chu, "Planar 4-element uwb antenna array and time domain characterization," *Microwave and Optical Technology Letters*, vol. 50, no. 12, pp. 3118–3123, 2008.

[113] W. Kang, J. Park, and Y. Yoon, "Simple Reconfigurable Antenna With Radiation Pattern," *Electronics Letters*, vol. 44, no. 3, pp. 182–183, 2008.

[114] S.-J. Wu and T.-G. Ma, "A Wideband Slotted Bow-Tie Antenna With Reconfigurable CPW-to-Slotline Transition for Pattern Diversity," *IEEE Transactions on Antennas and Propagation*, vol. 56, no. 2, pp. 327–334, 2008.

[115] Y. Tawk and C. Christodoulou, "A New Reconfigurable Antenna Design for Cognitive Radio," *IEEE Antennas and Wireless Propagation Letters*, vol. 8, pp. 1378–1381, 2009.

[116] H. Li, J. Xiong, Y. Yu, and S. He, "A Simple Compact Reconfigurable Slot Antenna With a Very Wide Tuning Range," *IEEE Transactions on Antennas and Propagation*, vol. 58, no. 11, pp. 3725–3728, 2010.

[117] P.-Y. Qin, A. Weily, Y. Guo, and C.-H. Liang, "Polarization Reconfigurable U-Slot Patch Antenna," *IEEE Transactions on Antennas and Propagation*, vol. 58, no. 10, pp. 3383–3388, 2010.

[118] J.-H. Lim, G.-T. Back, Y.-I. Ko, C.-W. Song, and T.-Y. Yun, "A Reconfigurable PIFA Using a Switchable PIN-Diode and a Fine-Tuning Varactor for USPCS/WCDMA/m-WiMAX/WLAN," *IEEE Transactions on Antennas and Propagation*, vol. 58, no. 7, pp. 2404–2411, 2010.

[119] Y. Li, Z. Zhang, J. Zheng, and Z. Feng, "Compact Heptaband Reconfigurable Loop Antenna for Mobile Handset," *IEEE Antennas and Wireless Propagation Letters*, vol. 10, pp. 1162–1165, 2011.

[120] Y. K. Park and Y. Sung, "A Reconfigurable Antenna for Quad-Band Mobile Handset Applications," *IEEE Transactions on Antennas and Propagation,*, vol. 60, no. 6, pp. 3003–3006, 2012.

[121] H. AbuTarboush, R. Nilavalan, S. W. Cheung, K. Nasr, T. Peter, D. Budimir, and H. Al-Raweshidy, "A Reconfigurable Wideband and Multiband Antenna Using Dual-Patch Elements for Compact Wireless Devices," *IEEE Transactions on Antennas and Propagation,*, vol. 60, no. 1, pp. 36–43, 2012.

[122] J. Rayno and S. Sharma, "Wideband Frequency-Reconfigurable Spirograph Planar Monopole Antenna (SPMA) Operating in the UHF Band," *IEEE Antennas and Wireless Propagation Letters*, vol. 11, pp. 1537–1540, 2012.

[123] E. Erfani, J. Nourinia, C. Ghobadi, M. Niroo-Jazi, and T. Denidni, "Design and Implementation of an Integrated UWB/Reconfigurable-Slot Antenna for Cognitive Radio Applications," *IEEE Antennas and Wireless Propagation Letters*, vol. 11, pp. 77–80, 2012.

[124] FCC, "First report and order, revision of part 15 of the commission's rules regarding ultra-wideband transmission systems fcc," tech. rep., 2002.

[125] W. T. Barrett, "History of Ultra Wideband Communications and Radar: Part 1, UWB Communications," *Microwave Journal*, Jan. 2001.

[126] A. Boryssenko, "Time Domain Studies Of Ultra-wide Band Antennas," in *IEEE Canadian Conference on Electrical and Computer Engineering,*, vol. 1, pp. 95–100 vol.1, 1999.

[127] E. Guillanton, J. Y. Dauvignac, C. Pichot, and J. Cashman, "A New Design Tapered Slot Antenna For Ultra-wideband Applications," *Microwave and Optical Technology Letters*, vol. 19, no. 4, pp. 286–289, 1998.

[128] K. Chung, J. Kim, and J. Choi, "Wideband Microstrip-fed Monopole Antenna having Frequency Band-Notch Function," *IEEE Microwave and Wireless Components Letters,*, vol. 15, no. 11, pp. 766–768, 2005.

[129] H. Schantz, G. Wolenec, and I. Myszka, E.M., "Frequency Notched UWB Antennas," in *IEEE Conference on Ultra Wideband Systems and Technologies,*, pp. 214–218, 2003.

[130] Y. Kim and D.-H. Kwon, "Cpw-fed Planar Uwb Antenna Having A Frequency Band Notch Function," *Electronics Letters*, vol. 40, no. 7, pp. 403–405, 2004.

[131] S.-W. Su, K.-L. Wong, and F.-S. Chang, "Compact Printed Ultra-Wideband Slot Antenna With A Band-notched Operation," *Microwave and Optical Technology Letters*, vol. 45, no. 2, pp. 128–130, 2005.

[132] W. Choi, K. Chung, J. Jung, and J. Choi, "Compact Uwb Printed Antenna With Band-rejection Characteristic," *Electronics Letters*, vol. 41, no. 18, pp. 990–991, 2005.

[133] Y. Kim and D.-H. Kwon, "Planar Ultra Wide Band Slot Antenna With Frequency Band Notch Function," in *IEEE Antennas and Propagation Society International Symposium*, vol. 2, pp. 1788–1791 Vol.2, 2004.

[134] H. Yoon, H. Kim, K. Chang, Y.-J. Yoon, and Y. hwan Kim, "A Study On The UWB Antenna With Band-rejection Characteristic," in *IEEE Antennas and Propagation Society International Symposium*, vol. 2, pp. 1784–1787 Vol.2, 2004.

[135] S.-Y. Suh, W. Stutzman, W. A. Davis, A. Waltho, K. Skeba, and J. Schiffer, "A UWB Antenna With A Stop-band Notch In The 5-ghz Wlan Band," in *IEEE/ACES International Conference on Wireless Communications and Applied Computational Electromagnetics,*, pp. 203–207, 2005.

[136] W. Lui, C. Cheng, Y. Cheng, and H. Zhu, "Frequency Notched Ultra-wideband Microstrip Slot Antenna With Fractal Tuning Stub," *Electronics Letters*, vol. 41, no. 6, pp. 294–296, 2005.

[137] K.-H. Kim, Y. Cho, S. Hwang, and S.-O. Park, "Band-notched UWB planar monopole antenna with two parasitic patches," *Electronics Letters*, vol. 41, no. 14, pp. 783–785, 2005.

[138] W. Lui, C. Cheng, and H. Zhu, "Frequency Notched Printed Slot Antenna With Parasitic Open-circuit Stub," *Electronics Letters*, vol. 41, no. 20, pp. 1094–1095, 2005.

[139] Y.-J. Cho, K.-H. Kim, D. H. Choi, S.-S. Lee, and S.-O. Park, "A Miniature Uwb Planar Monopole Antenna With 5-ghz Band-rejection Filter And The Time-domain Characteristics," *IEEE Transactions on Antennas and Propagation,*, vol. 54, no. 5, pp. 1453–1460, 2006.

[140] S.-Y. Chen, P.-H. Wang, and P. Hsu, "Uniplanar Log-Periodic Slot Antenna Fed by a CPW for UWB Applications," *IEEE Antennas and Wireless Propagation Letters*, vol. 5, no. 1, pp. 256–259, 2006.

[141] S.-W. Qu, J.-L. Li, and Q. Xue, "A Band-Notched Ultrawideband Printed Monopole Antenna," *IEEE Antennas and Wireless Propagation Letters,*, vol. 5, no. 1, pp. 495–498, 2006.

[142] T.-G. Ma and C.-H. Tseng, "An UWB coplanar waveguide-fed tapered ring slot antenna," *IEEE Transactions on Antennas and Propagation*, vol. 54, no. 4, pp. 1105–1110, 2006.

[143] K. Bahadori and Y. Rahmat-Samii, "A Miniaturized Elliptic-Card UWB Antenna With WLAN Band Rejection for Wireless Communications," *IEEE Transactions on Antennas and Propagation,*, vol. 55, no. 11, pp. 3326–3332, 2007.

[144] C.-Y. Hong, C.-W. Ling, I.-Y. Tarn, and S.-J. Chung, "Design of a Planar Ultrawideband Antenna With a New Band-Notch Structure," *IEEE Transactions on Antennas and Propagation*, vol. 55, no. 12, pp. 3391–3397, 2007.

[145] K. P. Ray and Y. Ranga, "Ultrawideband Printed Elliptical Monopole Antennas," *IEEE Transactions on Antennas and Propagation*, vol. 55, no. 4, pp. 1189–1192, 2007.

[146] M. Bialkowski and A. Abbosh, "Design of UWB Planar Antenna With Improved Cut-Off at the Out-of-Band Frequencies," *IEEE Antennas and Wireless Propagation Letters*, vol. 7, pp. 408–410, 2008.

[147] O. Ahmed and A. Sebak, "A Printed Monopole Antenna With Two Steps and a Circular Slot for UWB Applications," *IEEE Antennas and Wireless Propagation Letters*, vol. 7, pp. 411–413, 2008.

[148] J.-W. Jang and H.-Y. Hwang, "An Improved Band-Rejection UWB Antenna With Resonant Patches and a Slot," *IEEE Antennas and Wireless Propagation Letters*, vol. 8, pp. 299–302, 2009.

[149] N. Choi, C. Jung, J. Byun, F. Harackiewicz, M.-J. Park, Y.-S. Chung, T. Kim, and B. Lee, "Compact UWB Antenna With I-Shaped Band-Notch Parasitic Element for Laptop Applications," *IEEE Antennas and Wireless Propagation Letters*, vol. 8, pp. 580–582, 2009.

[150] M. Ojaroudi, C. Ghobadi, and J. Nourinia, "Small Square Monopole Antenna With Inverted T-shaped Notch In The Ground Plane For UWB Application," *IEEE Antennas and Wireless Propagation Letters*, vol. 8, pp. 728–731, 2009.

[151] H.-W. Liu, C.-H. Ku, T.-S. Wang, and C.-F. Yang, "Compact Monopole Antenna With Band-Notched Characteristic for UWB Applications," *IEEE Antennas and Wireless Propagation Letters*, vol. 9, pp. 397–400, 2010.

[152] H.-W. Liu and C.-F. Yang, "Miniature hook-shaped monopole antenna for UWB applications," *Electronics Letters*, vol. 46, no. 4, pp. 265–266, 2010.

[153] K. Shambavi and Z. Alex, "Printed Dipole Antenna With Band Rejection Characteristics for UWB Applications," *IEEE Antennas and Wireless Propagation Letters*, vol. 9, pp. 1029–1032, 2010.

[154] R. Azim, M. Islam, and N. Misran, "Compact Tapered-Shape Slot Antenna for UWB Applications," *IEEE Antennas and Wireless Propagation Letters*, vol. 10, pp. 1190–1193, 2011.

[155] Q. X. Chu and T. G. Huang, "Compact UWB antenna with sharp band-notched characteristics for lower WLAN band," *Electronics Letters*, vol. 47, no. 15, pp. 838–839, 2011.

[156] A. Nouri and G. DadashZadeh, "A Compact UWB Band-Notched Printed Monopole Antenna With Defected Ground Structure," *IEEE Antennas and Wireless Propagation Letters*, vol. 10, pp. 1178–1181, 2011.

[157] T. Li, H. Zhai, L. Li, C. Liang, and Y. Han, "Compact UWB Antenna With Tunable Band-Notched Characteristic Based on Microstrip Open-Loop Resonator," *IEEE Antennas and Wireless Propagation Letters*, vol. 11, pp. 1584–1587, 2012.

[158] Y. S. Seo, J. W. Jung, H. J. Lee, and Y. S. Lim, "Design Of Trapezoid Monopole Antenna With Band-notched Performance For UWB," *Electronics Letters*, vol. 48, no. 12, pp. 673–674, 2012.

[159] J.-H. Lu and C.-H. Yeh, "Planar Broadband Arc-Shaped Monopole Antenna for UWB System," *IEEE Transactions on Antennas and Propagation*, vol. 60, no. 7, pp. 3091–3095, 2012.

[160] A. Gautam, S. Yadav, and B. Kanaujia, "A CPW-Fed Compact UWB Microstrip Antenna," *IEEE Antennas and Wireless Propagation Letters*, vol. 12, pp. 151–154, 2013.

[161] A. Kaye and D. George, "Transmission of Multiplexed PAM Signals Over Multiple Channel and Diversity Systems," *IEEE Transactions on Communication Technology*, vol. 18, no. 5, pp. 520–526, 1970.

[162] W. Van Etten, "Maximum Likelihood Receiver for Multiple Channel Transmission Systems," *IEEE Transactions on Communications*, vol. 24, no. 2, pp. 276–283, 1976.

[163] J. Winters, "On the Capacity of Radio Communication Systems with Diversity in a Rayleigh Fading Environment," *IEEE Journal on Selected Areas in Communications*, vol. 5, no. 5, pp. 871–878, 1987.

[164] T. K. Arogyaswami J. Paulraj, *Increasing capacity in wireless broadcast systems using distributed transmission/directional reception [DTDR].* No. 5,34,599, U. S. Patent, 1994.

[165] G. J. Foschini and M. J. Gans, "On Limits Of Wireless Communications In A Fading Environment When Using Multiple Antennas," *Wireless Personal Communications*, vol. 6, pp. 311–335, 1998.

[166] T.-Y. Wu, S.-T. Fang, and K.-L. Wong, "Printed diversity monopole antenna for WLAN operation," *Electronics Letters*, vol. 38, no. 25, pp. 1625–1626, 2002.

[167] K.-L. Wong, S.-W. Su, and Y.-L. Kuo, "A Printed Ultra-wideband Diversity Monopole Antenna," *Microwave and Optical Technology Letters*, vol. 38, no. 4, pp. 257–259, 2003.

[168] S. Blanch, J. Romeu, and I. Corbella, "Exact Representation Of Antenna System Diversity Performance From Input Parameter Description," *Electronics Letters*, vol. 39, no. 9, pp. 705–707, 2003.

[169] M. Jensen and J. Wallace, "A Review Of Antennas And Propagation For MIMO Wireless Communications," *IEEE Transactions on Antennas and Propagation*, vol. 52, no. 11, pp. 2810–2824, 2004.

[170] G. Chi, B. Li, and D. Qi, "Dual-band Printed Diversity Antenna For 2.4/5.2-GHz Wlan Application," *Microwave and Optical Technology Letters*, vol. 45, no. 6, pp. 561–563, 2005.

[171] J. Thaysen and K. B. Jakobsen, "Envelope Correlation in (nxn) MIMO Antenna Array from Scattering Parameters," *Microwave and Optical Technology Letters*, vol. 48, no. 5, pp. 832–834, 2006.

[172] D. Yuan, Z. Du, K. Gong, and Z. Feng, "A Novel Dual-Band Printed Diversity Antenna for Mobile Terminals," *IEEE Transactions on Antennas and Propagation*, vol. 55, no. 7, pp. 2088–2096, 2007.

[173] S. Hong, K. Chung, J. Lee, S. Jung, S.-S. Lee, and J. Choi, "Design Of A Diversity Antenna With Stubs For UWB Applications," *Microwave and Optical Technology Letters*, vol. 50, no. 5, pp. 1352–1356, 2008.

[174] R.-A. Bhatti, J.-H. Choi, and S.-O. Park, "Quad-Band MIMO Antenna Array for Portable Wireless Communications Terminals," *IEEE Antennas and Wireless Propagation Letters*, vol. 8, pp. 129–132, 2009.

[175] S. Zhang, Z. Ying, J. Xiong, and S. He, "Ultrawideband MIMO/Diversity Antennas With a Tree-Like Structure to Enhance Wideband Isolation," *IEEE Antennas and Wireless Propagation Letters*, vol. 8, pp. 1279–1282, 2009.

[176] S.-W. Su, "High-Gain Dual-Loop Antennas for MIMO Access Points in the 2.4/5.2/5.8 GHz Bands," *IEEE Transactions on Antennas and Propagation*, vol. 58, no. 7, pp. 2412–2419, 2010.

[177] S. Cui, Y. Liu, W. Jiang, and S. X. Gong, "Compact Dual-band Monopole Antennas With High Port Isolation," *Electronics Letters*, vol. 47, no. 10, pp. 579–580, 2011.

[178] J.-F. Li, Q.-X. Chu, and G. X.-X., "Tri-band Four-element MIMO Antenna With High Isolation," *Progress In Electromagnetics Research C*, vol. 24, pp. 235–249, 2011.

[179] C. H. See, R. Abd-Alhameed, Z. Abidin, N. McEwan, and P. Excell, "Wideband Printed MIMO/Diversity Monopole Antenna for WiFi/WiMAX Applications," *IEEE Transactions on Antennas and Propagation*, vol. 60, no. 4, pp. 2028–2035, 2012.

[180] Q. Zeng, Y. Yao, S. L. abd Junsheng Yu, P. Xie, and X. Chen, "Tetraband Small-Size Printed Strip MIMO Antenna for Mobile Handset Application," *International Journal of Antennas and Propagation*, vol. 2012, p. 8, 2012.

[181] A. Kulkarni and S. Sharma, "Frequency Reconfigurable Microstrip Loop Antenna Covering LTE Bands With MIMO Implementation and Wideband Microstrip Slot Antenna all for Portable Wireless DTV Media Player," *IEEE Transactions on Antennas and Propagation*, vol. 61, no. 2, pp. 964–968, 2013.

[182] A. A. Eldek, A. Z. Elsherbeni, and C. E. Smith, "Wideband 2d array of microstrip fed rectangular-slot antennas for radar applications," *Microwave and Optical Technology Letters*, vol. 46, no. 1, pp. 36–40, 2005.

[183] H.-Z. Liu, J. C. Coetzee, and K. Mouthaan, "Uwb antenna array for wireless transmission along corridors," *Microwave and Optical Technology Letters*, vol. 50, no. 4, pp. 886–890, 2008.

[184] P. Li, J. Liang, X. Chen, and C. Parini, "A 4-element ultra-wideband tapered-slot-fed antenna array," in *Antennas and Propagation Society International Symposium 2006, IEEE*, pp. 4475–4478, 2006.

[185] D. Guha and Y. M. M. Antar, "Four-element cylindrical dielectric resonator antenna for wideband monopole-like radiation," *Antennas and Propagation, IEEE Transactions on*, vol. 54, no. 9, pp. 2657–2662, 2006.

[186] H. Wang, X. B. Huang, and D.-G. Fang, "A single layer wideband u-slot microstrip patch antenna array," *Antennas and Wireless Propagation Letters, IEEE*, vol. 7, pp. 9–12, 2008.

[187] Y. Ito, M. Ameya, M. Yamamoto, and T. Nojima, "Unidirectional uwb array antenna using leaf-shaped bowtie elements and flat reflector," *Electronics Letters*, vol. 44, no. 1, pp. 9–11, 2008.

[188] O. M. H. Ahmed and A.-R. Sebak, "Planar ultrawideband antenna array for short-range wireless communications," *Microwave and Optical Technology Letters*, vol. 52, no. 5, pp. 1061–1066, 2010.

[189] C.-H. Weng, H.-W. Liu, C.-H. Ku, and C.-F. Yang, "Dual circular polarisation microstrip array antenna for wlan/wimax applications," *Electronics Letters*, vol. 46, no. 9, pp. 609–611, 2010.

[190] R. Mishra, S. Dash, P. Patra, and S. Pattnaik, "A three element planner antenna array in golden ratio with 2 x2236;1 corporate feeding," in *A Workshop on Advanced Antenna Technology, 2010 Indian Antenna Week*, pp. 1–3, 2010.

[191] Z. Ma, V. Volski, and G. Vandenbosch, "Optimized design of a compact low-cost 4 element microstrip antenna array for wlan," in *Electromagnetic Theory (EMTS), 2010 URSI International Symposium on*, pp. 573–576, 2010.

[192] R. Bayderkhani and H. Hassani, "Very-low-sidelobe printed tapered arc-shaped wide-slot antenna array," *Microwaves, Antennas Propagation, IET*, vol. 5, no. 10, pp. 1143–1147, 2011.

[193] V. Deepu, R. Raj, M. Joseph, S. M.N, and P. Mohanan, "Compact Asymmetric Coplanar Strip Fed Monopole Antenna for Multiband Applications," *IEEE Transactions on Antennas and Propagation*, vol. 55, no. 8, pp. 2351–2357, 2007.

[194] F. Shao-jun and B.-S. Wang, "Analysis of Asymmetric Coplanar Waveguide with Conductor Backing," *IEEE Transactions on Microwave Theory and Techniques,*, vol. 47, no. 2, pp. 238–240, 1999.

[195] Y. Choukiker and S. Behera, "Design of Planar Monopole Antenna for 2.4 GHz WLAN," in *International Conference on Computational Intelligence and Communication Networks (CICN)*, pp. 16–19, 2010.

[196] L. Desclos, "Size reduction of planar patch antenna by means of slot insertion," *Microwave and Optical Technology Letters*, vol. 25, no. 2, pp. 111–113, 2000.

[197] S. Reed, L. Desclos, C. Terret, and S. Toutain, "Patch antenna size reduction by means of inductive slots," *Microwave and Optical Technology Letters*, vol. 29, no. 2, pp. 79–81, 2001.

[198] R. Mishra, R. Ghatak, and D. Poddar, "Design Formula for Sierpinski Gasket Pre-Fractal Planar-Monopole Antennas [Antenna Designer's Notebook]," *IEEE Antennas and Propagation Magazine,*, vol. 50, no. 3, pp. 104–107, 2008.

[199] C. Jeffrey and A. Mallows, C.L.. and. Wilks, "Beyond the Descartes circle theorem," *Mathematical Association of America*, vol. 109, pp. 338–361, 2002.

[200] J. Qiu, Z. Du, J. Lu, and K. Gong, "A Planar Monopole Antenna Design With Band-notched Characteristic," *IEEE Transactions on Antennas and Propagation*, vol. 54, no. 1, pp. 288–292, 2006.

[201] G. Pedersen and J. Andersen, "Handset Antennas For Mobile Communications: Integration, Diversity, and Performance," *Review of Science Radio*, pp. 119–138., Wiley IEEE Press 1999.

[202] A. N. Kulkarni and S. K. Sharma, "A Multiband Antenna With MIMO Implementation For Usb Dongle Size Wireless Devices," *Microwave and Optical Technology Letters*, vol. 54, pp. 1990–1994, 2012.

[203] A. Kulkarni and S. Sharma, "Frequency Reconfigurable Microstrip Loop Antenna Covering LTE Bands With MIMO Implementation and Wideband Microstrip Slot Antenna all for Portable Wireless DTV Media Player," *IEEE Transactions on Antennas and Propagation*, vol. 61, no. 2, pp. 964–968, 2013.

[204] D. Valderas, P. Crespo, and C. Ling, "UWB portable printed monopole array design for MIMO communications," *Microwave and Optical Technology Letters*, vol. 52, no. 4, pp. 889–895, 2010.

[205] H. Shin and J. H. Lee, "Capacity Of Multiple-antenna Fading Channels: Spatial Fading Correlation, Double Scattering, And Keyhole," *IEEE Transactions on Information Theory*, vol. 49, no. 10, pp. 2636–2647, 2003.

[206] E. Wilkinson, "An N-Way Hybrid Power Divider," *IRE Transactions on Microwave Theory and Techniques*, vol. 8, no. 1, pp. 116–118, 1960.

[207] Y. Wu, Y. Liu, and Q. Xue, "An Analytical Approach for a Novel Coupled-Line Dual-Band Wilkinson Power Divider," *IEEE Transactions on Microwave Theory and Techniques*, vol. 59, no. 2, pp. 286–294, 2011.

[208] S. B. Cohn, "A Class of Broadband Three-Port TEM-Mode Hybrids," *IEEE Transactions on Microwave Theory and Techniques*, vol. 16, no. 2, pp. 110–116, 1968.

[209] D. Paris and F. Hurd, *Basic Elctromagnetics Theory*. McGraw-Hill, Newyork, 1969.

[210] D. Pozar, *Microwave Engineering, 3rd edition*. Wiley, New York, 2005.

[211] N. Bastos, J. P. A.and Sadowski, *Electromagnetic Modeling by Finite Element Methods*. New York: Marcel Dekker, Inc, 2003.

[212] W. C. Gibson, *The Method of Moments in Electromagnetics, Chapman & Hall/CRC, Taylor & Francis Group 2008,*. Chapman & Hall/CRC, Taylor & Francis Group, 2008.

[213] A. Taflove and S. C. Hagness, *Computational Electrodynamics: The Finite-Difference Time-Domain Method, Third Edition, Artech House, 2005.* Artech House, 2005.

[214] D. Swason, *Microwave Circuit Modeling using Electromagnetic Field Simulation*. ARTECH House, 2003.

[215] M. Clements and T. Weiland, "Discrete Electromagnetism with the Finite Integration Technique," *Progress In Electromagnetics Research*, vol. 32, pp. 65–87, 2001.

[216] C. A. Balanis, *Antenna Theory: Analysis and Design*. Wiley-Interscience, 1997.

Disseminations

Journal papers Published/Accepted

1. **Yogesh K Choukiker**, S K Behera , R Jyoti, "Modified Sectoral Shape Fractal Antenna for Wireless LAN Application", *International Journal of RF and Microwave Computer Aided Engineering (Wiley) USA, 22(1):68-74 2012*

2. **Yogesh K Choukiker** and S K Behera, "ACS-Fed Koch Fractal Shape Antenna for Wideband Application", *International Journal of Signal and Imaging Systems Engineering, 6(1):9-15. 2012.*

3. **Yogesh K Choukiker** and S K Behera "Sierpinski Square Fractal Antenna for UWB application with a band notch characteristic", *IET Microwave and Antenna Propagation,.8: 1-7. 2013*

4. **Yogesh K Choukiker**, S K Sharma and S K Behera, "Hybrid Fractal Shape Planar Monopole Antenna Covering Multiband Wireless Communications with MIMO Implementation for Handheld Mobile Devices", *IEEE Transactions on Antennas Propagation, 68(3): 1483-1488, 2014.*

5. **Yogesh K Choukiker** and S K Behera, "Compact Sectoral Fractal Planar Monopole Antenna for Wideband Wireless Applications", *Microwave and Optical Technology Letters, 56(3): 1073-1076, 2014.*

Conference papers Published/Accepted

1. **Yogesh K Choukiker** and S K Behera, "Microstrip Line-Fed Modified Sierpinski Fractal Monopole Antenna for Dual wideband Applications", *IEEE International Conference on communication Control and Computing Technologies, page 17-20, Tamilnadu, India, April 2011.*

2. **Yogesh K Choukiker** and S K Behera, "CPW-Fed Compact Multiband Sierpinski Triangle Antenna", *Annual IEEE India Conference (INDICON), pp 1-3, Kolkata, India, Dec 2010.*

3. **Yogesh K Choukiker** and S K Behera, "Compact ACS-Fed Koch Fractal Shape Antenna for Wideband Application", *Procc. On International Conference on Electronic System, page 247-251, NIT Rourkela, India, Jan 2011.*

4. **Yogesh K Choukiker**, S Rai and S K Behera, "Modified Half-Circle Fractal Antenna Using DC Theorem for 2.4/5.2 GHz WLAN Application", *IEEE National Conference on Communication , pp 1-4, IISc, Bangalore, India, Jan 2011.*

5. **Yogesh K Choukiker** and S K Behera, "Modified Fractal Shape Antenna for Wideband Application", *IEEE International Conference on Device and Communication, pp 1-3, BIT Ranchi, February 2011.*

6. **Yogesh K Choukiker** and S K Behera, "Design of Wideband Fractal Antenna with Combination of Fractal Geometries", *IEEE Eighth International Conference on Information, Communications, and Signal Processing, Singapore, December, 2011.*

7. **Yogesh K Choukiker** S K Behera and S K Sharma, "Hybrid Fractal shape planar monopole antenna with MIMO implementation covering multiband wireless communication for handheld devices", *International Symposium on Antennas and Propagation (APS 2013), Florida, USA, 7-13, July, 2013.*

8. **Yogesh K Choukiker**, S K Behera and S K Sharma "Two and Four-Element Wideband Sectoral Fractal Array Antennas with Omni-Directional Radiation Patterns" *Applied Electromagnetic Conference (AEMC-2013), Bhubaneswar, Dec. 2013.*

Journal papers Communicated/To be communicated

1. **Yogesh K Choukiker** and S K Behera, "Compact hybrid fractal planar monopole antenna for wideband wireless application", *IEEE, Electronics Letter.* (Under review Manuscript ID: ELL-2013-2921.R1)

2. **Yogesh K Choukiker** and S K Behera, "A CPW-Fed Half Circle Fractal Slot Antenna for Wideband Wireless Applications", *Journal of Electromagnetic Waves and Applications.* (Under review Manuscript ID:TEWA-2013-0728)

3. **Yogesh K Choukiker** S K Behera and S K Sharma "Two and Four-Element Wideband Sectoral Fractal Array Antennas with Omni-Directional Radiation Patterns", *IET Microwave and Antenna Propagation.* (To be communicated)

4. **Yogesh K Choukiker** S K Behera and S K Sharma "Frequency Reconfigurable Koch fractal antenna for Wideband Applications", *Microwave and Optical Technology Letters.* (To be communicated)